2nd Annual Workshop Proceedings of the Collaborative Project "Redox Phenomena Controlling Systems" (7th EC FP CP RECOSY)

Gunnar Buckau, Bernhard Kienzler, Lara Duro, Mireia Grivé, Vanessa Montoya (eds.)

KIT Scientific Publishing

Gunnar Buckau, Bernhard Kienzler, Lara Duro, Mireia Grivé,
Vanessa Montoya

**2nd Annual Workshop Proceedings of the Collaborative Project
"Redox Phenomena Controlling Systems" (7th EC FP CP RECOSY)**

Karlsruhe Institute of Technology

KIT SCIENTIFIC REPORTS 7557

2nd Annual Workshop Proceedings of the Collaborative Project "Redox Phenomena Controlling Systems" (7th EC FP CP RECOSY)

Gunnar Buckau

Bernhard Kienzler

Lara Duro

Mireia Grivé

Vanessa Montoya

(eds.)

KIT Scientific Publishing

FOREWORD

The present document is the proceedings of the 2nd Annual Workshop of the EURATOM FP7 Collaborative Project ReCosy (Redox Phenomena Controlling System). The Workshop was hosted by University of Cyprus (UCYPRUS) and held in Larnaca (Cyprus) 16th – 19th March 2010. The project started April 2008 and has four years duration. It has 32 Contractors and presently 6 Associated Groups. Annual workshops bring together, Beneficiaries/Contractors, Associated Groups and external interested groups. The present proceedings will be followed by two additional proceedings corresponding to the forthcoming annual workshops to be held in 2011 and 2012, respectively. The 3rd Annual Workshop will be held in France 22nd – 25th March 2011, organized by Bernd Grambow (ARMINES/SUBATECH) and Laurent Charlet (CNRS). The 4th and final one will be held in Karlsruhe, Germany, March 2010, hosted by KIT-INE.

The proceedings serve several purposes. The key purpose is to document and make available to a broad scientific community the outcome of the RECOSY project. For this purpose, a considerable part of the project activity reporting is done through the proceedings, together with the outcome of a large number of scientific-technical contributions and Topical Sessions on different topics which could be important for the development of the project. In the 2nd Annual Workshop this topic focused on redox determination by thermodynamic methods and the associated databases. Additional purposes of the proceedings are to ensure ongoing documentation of the project outcome, promote systematic scientific-technical development throughout the project, and to allow thorough review of the project progress.

The proceedings give only very brief information about the project structure and the different activities around the project, such as training measures and dissemination of knowledge. Such information about the project can be found in detail under www.recosy.eu

TABLE OF CONTENTS

THE PROJECT

The EURATOM 7th EC Framework Program Collaborative Project REdox phenomena Controlling SYstems (RECOSY) started in April 2008 and extends over 4 years. The project is based on problems identified within studies related to national nuclear waste disposal implementation programs. Main objectives of RECOSY are the sound understanding of redox phenomena controlling the long-term release/retention of radionuclides in nuclear waste disposal, providing tools to apply the result to Performance Assessment/Safety Case, training of next generation, and documentation and communication of the results. To this aim, the project set up a consortium of 32 Beneficiaries/Contractors and presently 6 Associated Groups. The consortium includes key European Research Institutes, Universities, National Waste Management Agencies and SMEs, from 13 EURATOM signatory states, Russia, Japan, Korea, USA and one European Joint Research Centre. The ReCosy concept is innovative in the scientific approach to the redox phenomena. It includes i) advanced analytical tools, ii) investigations of processes responsible for redox control (thermodynamically and kinetically controlled processes, surface reactions and microbial processes, ..), iii) provision of required data on redox controlling processes, and iv) response to disturbances in disposal systems. The work program is structured along six RTD workpackages (WP1-6). They cover near-field and far field aspects as well as all relevant host-rocks considered in Europe. In WP1, the scientific state-of-the-art and its application to Performance Assessment/Safety Case is documented and regularly up-dated. WP2 focuses on development of redox determination methods. WP3 focuses on redox response of defined and near-natural systems. WP4 studies the redox reactions of radionuclides. WP5 focuses on Redox processes in radionuclide transport and WP6 deals with redox reactions affecting the spent fuel source-term. Specific workpackages on knowledge management, education and training (WP7) and administrative management issues (WP8) are also included in the project

The present proceedings document the outcome of the 2nd Annual Project Workshop and give an overview of the outcome of the 2nd project year.

THE SECOND ANNUAL WORKSHOP

The 2nd Annual Project Workshop was held in Larnaca (Cyprus) 16th – 19th March 2010. The Workshop was hosted by the University of Cyprus (UCYPRUS). There were 65 attendees at the workshop, representing Beneficiaries/Contractors, Associated Groups, the European Commission, the End-User Consultancy Group, and project external organizations. The workshop was organized in four days of oral presentations on results obtained within the project, two poster sessions, and a topical session on thermodynamic databases.

Objectives

The Workshop combines different activities and meetings with the following objectives:

- Informing about the scientific progress

- Informing about the administrative status

- Informing/agreeing upon forthcoming reporting

- Discussing various topics of interest for the consortium

- Agreeing upon the forthcoming work program

Emphasis was on scientific-technical topics with administrative issues kept to the minimum necessary.

RTD sessions

Individual workpackage internal meetings were held in parallel during the 1st day of the annual workshop (16th March). The following days of the workshop included plenary sessions where the results from the different work packages were presented. Next to an overview of the achievements within the respective WP, scientific highlights were presented. The following presentations were given within the project

WP2 session:

- Dörte Steinbrük. Fiber-optic chemical sensing – recent developments

- Evelyn Krawczyk-Bärsch, Thuro Arnold, Dörte Steinbrück, Michael Kumke. Electrochemical and fiber-optic oxygen sensor measurements in uranium contaminated biofilms - a collaboration with UPPC

- Tina Scharge, Barbara P. Bischofer, Sven Hagemann, Dagmar Schönwiese. Spectrophotometric and potentiometric determination of the redox potential in solutions of high ionic strength

- David Fellhauer, V. Neck, M. Altmaier, J. Runke, Th. Fanghänel. Redox chemistry of Np(V)

- Edit Marosits, B. Kuczewski, K. Wenzl. Iodine sorption on kaolinite and humic acid.

- N. Gebala, C. Bailly, C. Landesman, B. Grambow. Redox state determination in hyperalcaline solutions by speciation of selenium

- Stephanie Betelu, Christophe Tournassat, Ioanis Ignatiadis. Multi-electrodes redox potential measurements versus geochemical modelling

- Marcus Altmaier. Outcome of Inter Comparison Exercise (ICE)

WP3 session:

- María J. Gimeno, Luis F. Auqué, Patricia Acero, Javier B. Gómez, M. Pilar Asta. Distribution of redox elements and speciation solubility results as a first approach to the general characterisation of the redox systems in the Swedish candidate sites for deep disposal of nuclear waste

- K. Lazar, J. Megyeri and Z. Mathe. Limited redox response in minerals of Boda Claystone

- L. Charlet, S. Chakraborty, A., F. Bardelli, F.Molton. Se and U redox chemistry in presence of Fe(II)-rich clays and carbonates

- I. Ignatiadis, F. Chainet, S. Betelu, E. Gaucher, C. Tournassat. Interest in chemical and electrochemical approaches to investigate abiotic pyrite reactivity versus nitrate

- D. Arcos, L. Richard, I. Rojo, F. Clarens, J. De Pablo. Kinetics of pyrrhotite oxidation

WP4 session

- Stellan Holgersson. Investigations on U(IV) / U(VI) redox chemistry – Work at Chalmers University of technology

- Michel Perdicakis. In situ characterization of pyrite interaction with atmospheric oxygen and iodine species using scanning reference electrode (SRET) and dielectric techniques

- Jan Tits, Xavier Gaona, Eric Wieland. Influence of oxidation state on Neptunium uptake by calciumsilicate-hydrates and cement

- Evelyn Krawczyk-Baersch, Thuro Arnold. Determination of redox processes in biofilms from acidic waters

- Benedikta Lukŝienė. Effect of micro-organisms on Plutonium oxidation states. Plutonium oxidation state distribution in natural clays

- R. Hallam, S. Aldridge, N. Evans, P. Warwick. Effect of EDTA and Picolinate on Tc in a UK Intermediate-Level Radioactive Waste

WP5 session

- <u>Thorsten Schäfer</u>. Status of the work on actinide and Tc interaction with fracture filling material, clay and magnetite nanoparticles

- Susanna Salminen, <u>Juhani Suksi</u>. Investigation of redox-state of U deposited on rock.

- Fanos Papanicolaou, Stella Antoniou, <u>Ioannis Paschalidis</u>. Redox Chemistry of Sulfate and Uranium in a Phosphogypsum Stack

- Karoly Lazar. Retarded diffusion of uranyl ions through Boda Claystone samples

- <u>Sébastien Savoye</u>, Bernard Grenut. Diffusive behaviour of iodide through Callovo-Oxfordian argillite: Can experimental artefacts explain its retardation?

WP6 session

- <u>Detlef Wegen</u>, A. Seibert. Studies on Spent Fuel in Presence of Corroding Fe and on Thin Film Model Systems

- <u>Paul Carbol</u>, P. Fors, S. Van Winckel,K. Spahiu. Corrosion of Spent Fuel in Presence of H_2

- <u>Mats Jonsson</u>, martin Trummer. Combined Effect of Metallic Inclusions and Rare Earth Doping on the Oxidative Dissolution of UO_2

- <u>Detlef Wegen</u>, Bernhard Kienzler, Andreas Loida. Reductive Trapping of Actinides in Container Corrosion Products during Spent Nuclear Fuel (SNF) Corrosion (WP 6)

- <u>K. Spahiu</u>, <u>P. Carbol</u>, D. Cui. Np-Pu Immobilization on Iron Surface at Simulated HLW Repository Conditions

- <u>David Dobrev</u>, R. Červinka, A. Vokál. The Effect of Iron Corrosion on Redox Potential

Poster presentations

- The following posters were presented during the 2nd annual Workshop

- Scherbina, N., Perminova I. V., Novikpv A. P., Kalmykov, S. N, Marquardt C. M., Walther C, Buckau, G., Kumke M. Eidner S. Redox properties of hydroquinone-enriched humic subtances

- Altmaier, M., Fellhauer, D., Neck, V., Lützenkirchen, J. and Fanghänel, Th. Actinide(IV) chemistry in reducing alkaline $CaCl_2$ solutions and the formation of ternary $Ca_4[An(OH)_8]^{4+}$ complexes

- M. Altmaier, V. Brendler, S. Gester, S. Hagemann, H.-J. Herbert, C.M. Marquardt, H.C. Moog, V. Neck, A. Richter, T. Scharge, W. Voigt, S. Wilhelm. THEREDA – Thermodynamic Reference Database.

- Memorial workshop for Volker Neck

- Huber F., Schäfer T., Gamazo P., Dentz M., Saaltink M..Colloid mediated radionuclide transport under simulated glacial melt-water intrusion in fractured rocks (Äspö, Sweden)

- Mirek Icker, Clemens Walther, Volker Neck, Marcus Altmaier, Sebastien Büchner. The redox potential of Pu containing acidic solutions and the fate of "Pu(IV)-colloids": direct measurement versus optical absorption spectroscopy

- Hadi, J., Chainet, F., Betelu, C., Tournassat, C., Charlet, L. Ignatiadis, I. Redox potential of Fe(II)/Fe(III) couple in clays

- Grivé, M., Riba, O., Montoya, V. and Duro, L. The effect of $H_2(g)$ on the dissolution of unirradiated $UO_2(s)$ under alkaline to hyperalkaline conditions

- Buckau, G., Duro L. Recosy training and mobility measures

- S. Stumpf, A. Seibert, T. Gouder, F. Huber, T. Petersmann, th. Fanghanel. Corrosion mechanism of spent nuclear fuel model.

- Fellhauer,D., Altmaier, M., Neck, V., Rumke, J. and Fanghänel, Th. Kinetics aspects of Np(V) redox chemistry

- Xavier Gaona, Jan Tits, Regina Kirsch, David Fellhauer, Erich Wieland. Recosy ICE: Comparison of Experimental, Reference and Thermodynamic Eh Values.

- X. Gaona, M. Altmaier, V. Petrov, D. Fellhauer, J. Tits, E. Wieland, S. Kalmykov, Th. Fanghänel. Aqueous Speciation ans Solubility of Np(V/VI) in Hyperalkaline Systems: a KIT-INE / PSI-LES / JRC-ITU / MSU Joint Project.

- Kuczewski B., Dully C., dittrich T., Marosits E. Speciation of iodine with CE-DAD for the investigation in redox phenomena in natural groundwaters

- Alejandro Fernandez-Martinez, Fabrizio Bardelli, Florian Molton, Gaston Garbarino, Laurent Charlet. Synthesis and reactivity of mackinawite towards radionuclides and low activity waste

- Michel Perdicakis and Carine Streiff. Some considerations on the validity of the experimental determinations of redox potentials

- Michel Perdicakis and Yuliang Xu, Károly Lázár. Voltammetric characterization of Boda Albitic Claystone: Comparison with Mössbauer spectroscopy data

- K. Lazar, J. Megyeri and Z. Mathe. Lack of redox responses in certain cases on Boda Claystone samples as reflected in the Fe^{2+}/Fe^{3+} ratios in minerals

- K. Lazar, J. Megyeri, Z. Mathe. Retarded diffusion of uranyl ions in Boda Claystone samples

- Pedersen, K. Eriksson, S. Hallbeck, L. The effect of microbial activity and hydrogen on redox potential under in situ conditions 450 m underground in the Äspö Hard Rock Laboratory.

- K. Bateman, P. Coombs, H.M. Harrison, J.F. Harrington, A. Lacinska, A.E. Milodowski, D.J. Noy, G.H. Turner, D. Wagner and J.M. West. Studies of the impact of microbes in subsurface environments and their effects on the fluid transport

- Donald T. Reed, Juliet S. Swanson, Marian Borkowski, Jean Francois Lucchini, Hnin Khaing, Michael K. Richmann and David Ams. Plutonium Redox Control in the subsurface: WIPP approach

Topical session

The Topical Sessions aim at covering the key areas of redox determination methods along with the project. The Topical Session focuses on Redox determination by thermodynamic methods and the associated databases

Presentations within this topic were:

- Bernd Grambow. Assessment of kinetic contraints on the establishment of redox sensitive solubility equilibria

- Tara Beattie. Current Status of the HATCHES Thermodynamic Database to Support Safety Case Development of a UK Geological Disposal Facility

- Lara Duro. The development of Thermochimie, the ANDRA database

- Vincenz Brendler. THEREDA - a thermodynamic reference database for radwaste repositories in Germany

Structure of the proceedings

The proceedings are divided into the following sections:

- WP activity overviews, with summaries of the Research, Technology and Development Components

- Individual Scientific and Technical Contributions, containing reviewed scientific and technical manuscripts

- Additional contributions giving topics of general interest, especially in the context of the present workshop

Scientific-technical contributions submitted by Contractors were reviewed by the EUCG members (End-User Consultancy Group).

SUMMARY OF WP ACTIVITIES

WORKPACKAGE 2:
DEVELOPMENT OF REDOX DETERMINATION METHODS

D. Steinbrück[1], M.U. Kumke[1], M. Altmaier[2], V. Neck[2], D. Fellhauer[2], J. Runke[2], Bernd Grambow[3], Catherine Landesman [3], Solange Ribet[3], Evelyn Krawczyk-Bärsch[4], Michel Perdicakis[5], BRGM[6], GRS[7], TUG[8]

[1]Institute of Chemistry, University of Potsdam, Karl-Liebknechtstr. 24-25, 14476 Potsdam, Germany

[2] Institut für Nukleare Entsorgung, KIT, Campus Nord, Herrmann-von-Helmholtz-Platz 1, 76344 Eggenstein-Leopoldshafen, Germany

[3] SUBATECH (Ecole des Mines, University of Nantes, IN2P3/CNRS (FRANCE)

[4]Forschungszentrum Dresden-Rossendorf, Germany

[5]Laboratoire de Chimie Physique et Microbiologie pour l'Environnement

Nancy-Université, CNRS -54600 VILLERS-LES-NANCY France

[6]Environnement Industriel et Procédés Innovants, BRGM, 3 avenue Claude Guillemin, 6009, 45 060, Orléans Cedex 2, France

[7]Gesellschaft für Anlagen und Reaktorsicherheit (GRS) mbH, (GER)

[8]Graz University of Technology, Technikerstrasse 4, 8010 Graz, Austria

Introduction

The objective of WP2 is the development and testing of redox determination methods using different type of electrodes as well as optodes (optical sensors) in order to provide a broad and solid scientific-technical basis for the application of such. In combination with chemical analysis and associated thermodynamic modeling the redox state of systems (relevant for nuclear waste repositories) is assessed. The overall goals are (i) redox determination methods specifically designed for environmental applications, and (ii) a broader information base for interpretation of system conditions. The first point reflects the limitations of existing determination methods and models (and new developments) due to poisoning of electrode material, diffusion potentials in electrode bridges, drift through catalytic reactions on electrode material, drift through changes in electrolytes via diffusion, analytical difficulties in determining concentrations of redox sensitive system components or state of involved solids/minerals, and insufficient/inadequate thermodynamic data for calculation of the redox state.

In the following paragraphs a summary of work performed during the second project year is given by each partner.

Work performed by partners

In order to investigate whether there is a well-defined redox potential or pe value (pe = 16.9 E_h at 25°C) for the reduction of NpO_2^+(aq), the redox behaviour of $3.5 \cdot 10^{-5}$ M Np(V) solutions in 0.1 M NaCl was studied by **KIT-INE** at pH = 5 - 10 under Ar atmosphere. To cover a wide range of chemically different reducing systems, including homogeneous solutions and heterogeneous suspensions, several different inorganic and organic reducing agents were used. The reduction process was monitored spectroscopically and by the decrease of the aqueous Np(V) concentration determined after removal of colloidal Np(IV) by 10 kD ultrafiltration. As presented before, a "borderline" (E_h = 0.01 ± 0.02 V; pe = 0.15 ± 0.40) for Np(V) reduction has been identified. Above this line, samples with initially Np(V) are not reduced, samples falling below this line do show Np(V) reduction.

Extending this work (also reported in the first Annual Management and Activity report) and largely retaining the experimental setup and chemical boundary conditions, the kinetic influence on the redox reactions has been investigated. Most importantly, the Np(V) reduction in several series containing anthraquinone / anthrahydroquinone (2,6)-disulfonate (AQDS, AH_2QDS) buffer was analysed systematically over an extended period of time.

Independent of homogenous system or heterogeneous suspensions and the kind of chemical used to fix redox conditions, a general trend is apparent as shown in Figure 1. The more negative the measured redox potential in the system, the faster the Np(V) reduction takes place. The pe measured in the solutions obviously corresponds to some thermodynamic driving force controlling the reduction kinetics.
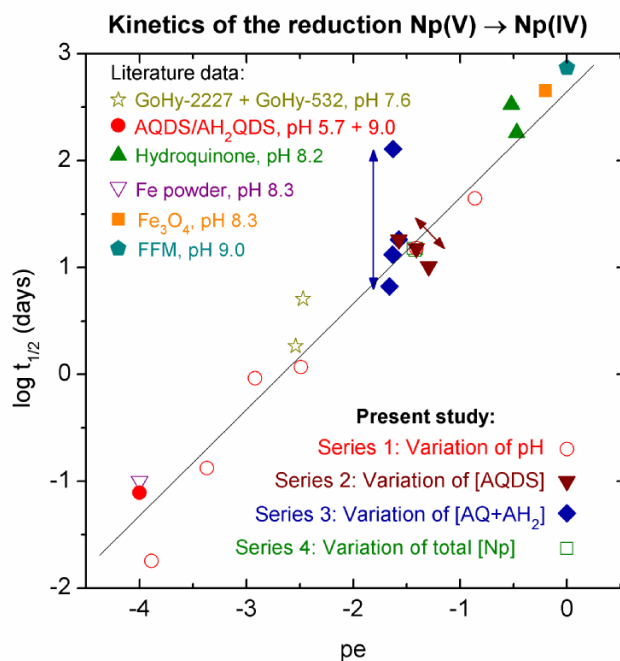
Figure 1: *Dependence of the half-life (log $t_{1/2}$) of Np(V) reduction on the redox potential pe.*

In one set of experiments containing anthraquinone / anthrahydroquinone (2,6)-disulfonate ([AQDS] = [AH$_2$QDS]) buffer (Series 3 in Fig. 1), a dependence of the half-life of reduction on the concentration of reducing chemicals was observed. When keeping pe and pH constant (pH = 5.73 ± 0.04, pe = -1.62 ± 0.04) and varying only the concentration of the redox buffer (from 6.7·10^{-5} M to 1.2·10^{-3} M), a direct dependence of reduction kinetics on the redox buffer concentration *at the same pe* is observed. By increasing the buffer concentration by a factor of 10 the half-life of reduction is decreased by a factor of 10. This indicates that pH and pe alone are not sufficient to characterise reduction kinetics and more elaborate chemical models are required.

ARMINES continued in the development of a methodology for redox determination in hyperalkaline systems based on Se speciation. Selenium is a redox sensitive element existing in aqueous solutions in the redox states –II (organic and inorganic forms), IV, VI and as polyselenide ion in mixed (-II/0) oxidation states and in the solid state as well as Se(0). Polyselenide species play a large role under alkaline conditions will strongly reduce the stability field for Se(0). Se speciation can only be deduced directly form Eh measurements with Pt electrodes and geochemical equilibrium calculations if reversibility is attained. Hence, Se redox speciation must be measured and compared with Eh measurements to show under which conditions reversibility is assured. For this purpose, advanced analytical techniques for Se speciation are indispensable.

Se(-II) has been produced by electrochemical reduction of either Se(0) or Se(IV) in an inert-gas box. The problem re-oxidation by migration of Se(-II) to anode was resolved using a cation exchange membrane separating anodic and cathodic space (Nafion perfluorinated membrane, used for fuel cells). When starting from Se(-IV) in NaOH the electrochemical reduction produced HSe$^-$ as verified by UV spectra. In contrast, when starting from floating Se(0) in NaOH some weakly soluble white crystals were formed which where later identified by XRD as Na$_2$Se·9H$_2$O. The sodium selenide hydrate crystals where stable against re-oxidation in the inert-gas box for more than 5 month, as shown by XPS analyses, but few seconds of exposure of the solid to air resulted in strong oxidation to Se(0). It shall be mentioned, that transfer from the inert-gas box to the XPS was assured by a special air-tight transport cask and assuring absence of oxygen traces in the entry system of the XPS. In order to increase dissolved Se concentrations for studying polyselenide formation, NaOH was replaced by KOH. In this case no solid phase was formed.

In order to study speciation equilibrium states in the Se(-II) to Se(0) range we added differents quantities of Se(0) to a 0.01 M Se(-II) solution to achieve Se(0)/Se(-II) ratios of 1, 2 and 2.8. The solution became red indicating polyselenide formation. UV-Vis analyses in 4 M KOH (Figure 2) showed disappearance of Se^{-2} and appearance of Se$_2^{-2}$ and Se$_3^{-2}$ with increasing Se(0) additions. First signs of Se$_4^{-2}$ formation were indicated for highest reaction progress. The behavior in 0.5 M KOH is largely similar to 4 M KOH but as expected from geochemical calculations, Se$_2^{-2}$ formation is less important compared to the higher polyselenide species in 0.5 M than in 4 M KOH. The measured Eh(SHE) followed the oxidation state mass ratio as already reported in literature (Licht et al. 1998). Geochemical modeling using the NEA-TDB database

indicated close agreement between calculated and measured Eh values when polyselenide formation was taken into account.

These observations are a clear indication for the fact that Se(0) is readily available for reaction under reducing alkaline conditions. In other words, Se(0) is not stable under strongly reducing conditions in hyperalkaline conditions, such as might be expected in a repository where hydrogen formation occurs due to container corrosion. Se(0) dissolves both under electrochemical conditions and as well in presence of a reductant (Se-II). The polymer species are formed fast and needs to be included in the redox state assessment. All our data show that reversibility is attained under reducing conditions, and in contrast to the Se(IV)/Se(VI) system, thermodynamic equilibrium might be expected under reducing conditions with Se(0) and Se(-II). Se retention under reducing conditions relies more than ever on the role of precipitation in Fe rich phases.

Effect of Se(0) addition to Se(-II) solution
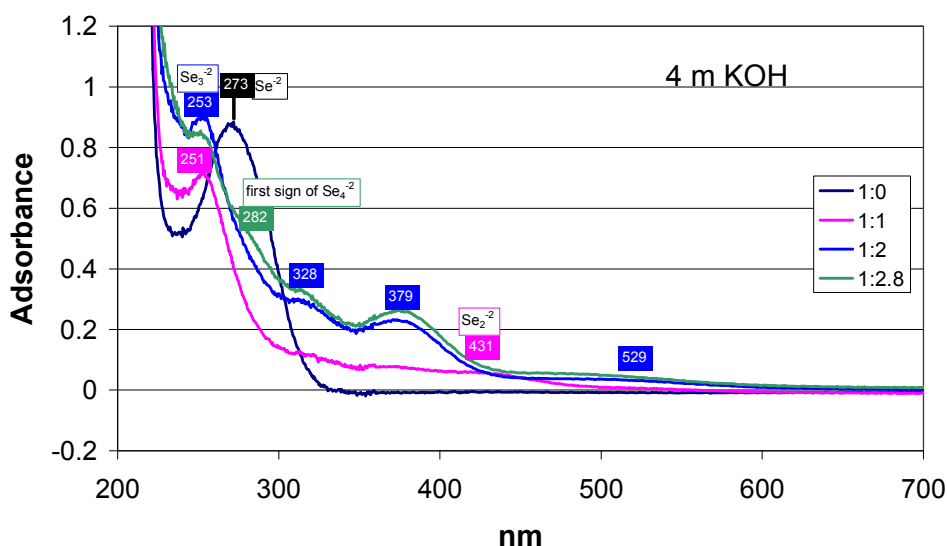
Figure 2: UV-Vis analyses of Se speciation in 4 M KOH under reducing conditions. Effect of addition of Se(0) to 0.01 M Se(-II) solutions.

One of the major objectives in 2009 for **BRGM** was to carry out robust geochemical (Eh-pH) sensor concepts being able to be devoted (after adaptation or development and/or implementation) to the observation and monitoring of the underground components of a nuclear waste storage. These sensors must answer precise specifications related to the requirements and constraints of observation and monitoring of the storage components (geological environment and associated phenomenology). In addition to the technical aspects, the major constraint seems to be the operation life, which will have to be based on the robustness and the perseverance of the principle of the sensors. Among the geochemical parameters to be followed, the most significant are temperature, pH, conductivity, redox potential, the speciation of certain elements, and measurement of H_2, O_2, CO_2 and H_2S. The inventory and the assessment of the currently available methodologies and tools for these parameters indicate that today there are not suitable geochemical sensors for monitoring nuclear waste storing systems. Based on this report, **BRGM** proposes some realistic pathways of research and

development to be initiated to mitigate the lack of geochemical sensors dedicated to the underground storage of nuclear waste. For that purpose, R&D pathways will be the development and manufacture of geochemical sensors made of robust and unalterable material (gold, platinum, glassy carbon). They must possess active principles everlasting, or protected or restored easily.

Moreover, solid-state sensors fabricated with a few components of the argillaceous formations (raw Callovo-Oxfordian argillite (COx) or purified argillite K119, or pyrite) for measuring pH and redox potential can be designed for use. Response characteristics of these sensors must be tested in aqueous samples with compositions similar to those present inside an underground repository and results were compared with those obtained with commercial electrodes obtaining a good agreement between commercial and the sensors. Electrochemical methods will be in the base of the sensors assessments. These approaches will be consisted in the continuous or semi-continuous analysis of large surface electrodes (pyrite, argillite,…) immersed in solutions with or without oxidant (nitrate, selenate and selenite) or reducer (sulfide, Fe^{2+},…). The electrochemical behavior of these electrodes was compared to those of known inert and un-attackable electrodes (Pt, Au, glassy carbon) positioned in the same operating conditions. Measurements realized by voltammetry (at open circuit potential and cyclic voltammetry), by Tafel polarization analysis and by electrochemical impedance spectroscopy (EIS) were used to identify, monitor and compare the electrochemical reactions and kinetics occurring during immersion, both in solution and on the surface of electrodes. The combination of chemical and electrochemical approaches appears to be an appropriate method to investigate the redox reactivity of COx components versus predicted redox perturbations.
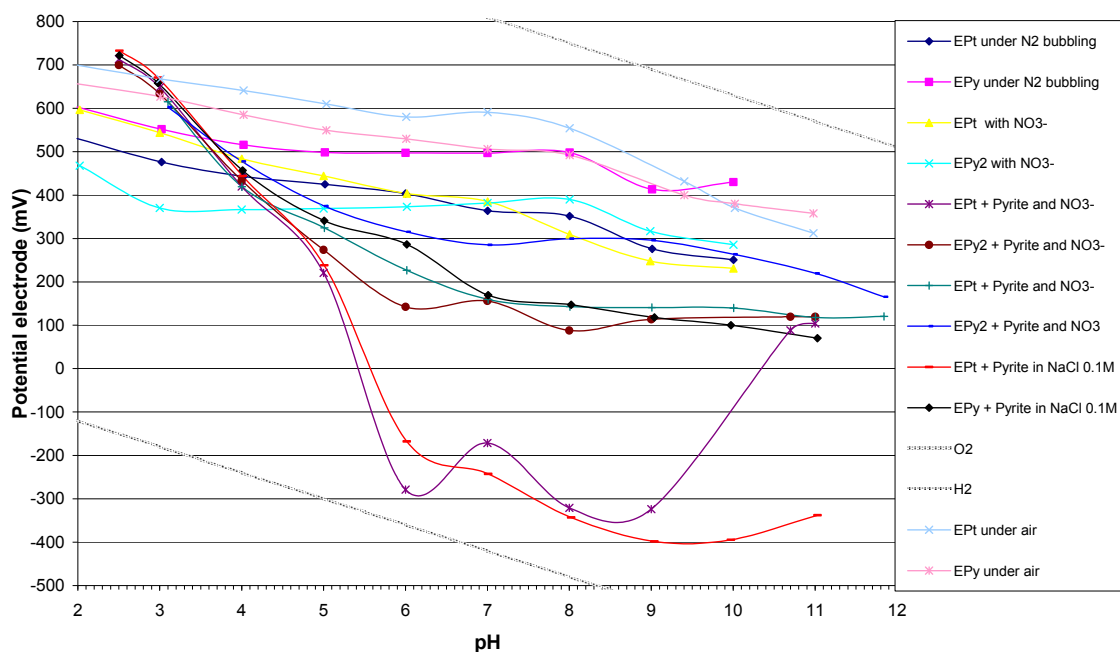
Figure 3: *Measurement of free electrode potential of Pyrite and Platinum electrodes immersed in different media (different pH, and presence or absence of nitrate and or pyrite in grains).*

As example, Figure 3 presents the measurements of electrode potentials (versus KCl-Saturated Calomel Electrode, SCE) for Pyrite and Platinum electrodes immersed in different media (different pH and composition). With responses in potential of this type, it is obvious that it will be possible to manufacture systems of solid and robust electrodes where the reference electrode is unnecessary. It will be also possible, provided that the potential difference is known, to deduce the pH of the solution, as it is demonstrated in Figure 4.
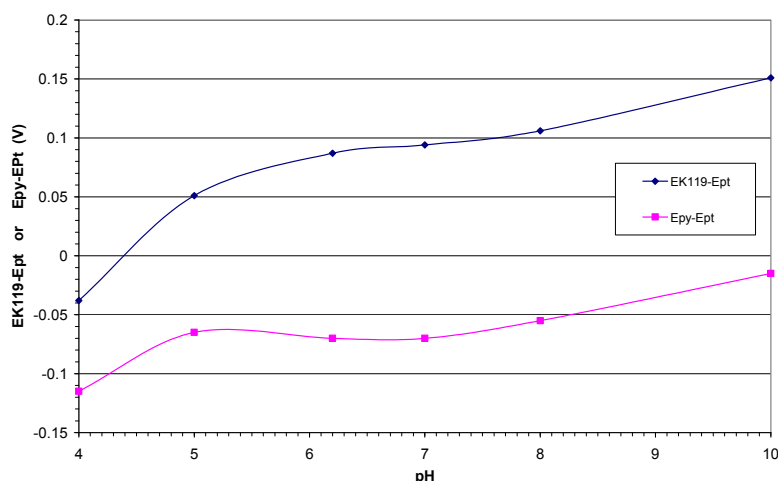
Figure 4.   *Measurement of the difference of free electrode potential between two couples of electrodes (purified COx and Pyrite versus Platinum electrode) as a function of pH.*

At **BRGM** in WP2 another major objective in 2009 was the determination of the redox potential using complementary approaches: geochemical modelling and continuous potential measurements on multi-electrodes. Among other experiments, the ICE was an occasion to put this complementary approach into practice.

Background and objectives: Redox potential value E_h versus Normal Hydrogen Electrode (NHE) is generally approached by voltage measurement between an inert indicator electrode and a reference electrode. Indicator electrodes, that ideally acts as a site for reactions occurring in the local environment by functioning as a source or a sink of electrons without undergoing chemical changes itself, therefore adopts a potential that is determined by the electron demand or availability at its interface with the surrounding solution (Stumm *et al.* 1983). In practice, however, numerous problems can arise. Those related to the voltage measurement fall into two categories, (i) those related to the non-ideal behaviour of electrode materials and (ii) those associated to redox species and reactions (Whitfield 1969, Whitfield 1971, Aller 1982, Stumm *et al.* 1983).

Problems related to the non-ideal behaviour of electrode materials: Inert indicator electrodes such as gold (Au), platinum (Pt) or glassy carbon (GC) have been favoured for redox potential measurements but their respective responses depend on both the electrode nature and surface properties. Measurement difficulties associated with indicator electrodes can nevertheless be partly addressed by ensuring suitable electrode preparation (polishing, cleaning, conditioning…), and calibration before use (Peter *at al.* 1998). Concerning reference electrodes, Ag/AgCl/KCl_sat saturated by

AgCl$_{(s)}$ or Saturated Calomel, they often remain suitable for laboratory work with the appropriate maintenance.

Problems related to Redox species and reactions: Two or more redox couples frequently occur in solution, in equilibrium or not. Redox species that are not in equilibrium each other give rise to "mixed potential" measurement. Species involved in irreversible and kinetically slow reactions do not participate in the redox measurement. Those involved in reversible but kinetically slow reactions are responsible for weak and unstable potential signals (Grenthe *et al.* 1992, Stumm *at al.* 1996). It is thus rarely possible to relate the measured E$_h$ to the activities of reduced and oxidised species present for most actual systems by a single measurement.

The purpose of the study was (i) to investigate the semi-continuous monitoring of the redox potential with multi electrodes (Au, Pt and GC electrodes) and (ii) to compare the acquired results with those obtained by geochemical modeling.

Experimental approach: The multi-electrode and continuous measurement approaches were considered in order to examine both the stability of the signal and the convergence of various electrode responses in order to be sure that an equilibrium of the system as a whole was obtained. The acquired results were compared to those obtained by geochemical modelling in order to identify the redox reactions that could control the measured potential and to test different hypotheses in order to reconcile, if needed, measured and theoretical values. The robustness of the complementary approaches was investigated in no organic matter content samples, at different ionic strength, where the iron redox-active species dominated the redox reactions. All aliquots were taken from the Ar inert gas glove-box and transferred to the workbench. Transfer, that took less than one minute, was ensured in hermetically closed electrochemical cells ensuring minimum perturbation generated by atmospheric O$_2$ and CO$_2$. Electrochemical cells were placed under Ar bubbling for 3 min before incorporating any electrode. Electrodes immersion was performed under argon bubbling. All measurements were then conducted under gently and continuous stirring with a magnetic stirrer and under argon atmosphere without bubbling to avoid CO$_2$ depletion from the samples. pH and temperature were followed by a SenTix 41 pH-electrode from WTW (Germany) with automatic temperature compensation. Potentiometric measurements were performed by a 10 mm-disk shaped Pt electrode (78.54 mm²), 2 mm-disk shaped Au electrode (3.14 mm²) and a 2 mm-disk shaped Gc electrode (3.14 mm²). Each electrode was successively polished with diamond pastes (3 µm and 1 µm), rinsed with milli-Q water and dried before use. Potentials were measured versus SCE, which consisted in a commercial SCE protected with a KCl 3 mol L^{-1} junction. Three SCE reference electrodes, that were stored in KCl 3 mol L^{-1} when not used, were used during experiments: two for the experimental analyses; the third one served as a reference in order to check the drift of the others. The two first electrodes were checked once a day versus the first one. No drift was observed over the four days of experiments. All indicator-electrode potentials were checked at the beginning of each experiment with a redox buffer solution (190 mV/NHE at 23.9°C). Nevertheless, it is worth noting that a problem with the use of such standards reference solutions could be their high poise. As they produce such a stable potential they are probably not capable of distinguishing between small differences in the indicator electrodes performance, such as might arise due to adsorption of chemicals onto the surface of the electrode or the formation of surface oxide layers. Such effects could however have influence the measured potential. Potentiometric measurements were recorded continuously with a data acquisition

system (Keithley instruments, 2700 data acquisition system) for 25 minutes at least. PHREEQC geochemical code was used to determine E_h and aqueous speciation by thermodynamic methods with the appropriate associated Thermodynamic database (THERMODEM® thermodynamic database generated by **BRGM**). Redox potential calculated values were obtained by speciation measurements given by INE. Redox potential calculated values were obtained from the initials conditions given by INE or speciation measurements, when they were given by PSI. Only two reference solutions are discussed here, *Ref 01 (II/III) b and Ref 02 Na c.*

Result and discussion: The influence of the ionic strength was investigated in NaCl samples in acidic media (pH fixed to 2), in which processes controlling the concentration of the redox sensitive elements are kinetically fast reactions, and thus in which shorter stabilization times should have been encountered. Figure 5 presents the experimental measurements versus time obtained in *Ref 01 (II/III) b and Ref 02 Na c* samples. Table 1 summarizes pH, temperature, Fe speciation measurement as well as equilibrium (E_h) and calculated (by geochemical modeling) potentials from the given samples. It is worth noting that no Pitzer database was available at **BRGM** with Fe(III); activity coefficient correction was not possible. Consequently, thermodynamic calculation was not achieved for *Ref 02 Na c*.

Potential voltages obtained by the others partners who investigated measurements into the glove box are also given. All potential values are expressed in Volt (V) with respect to the NHE.
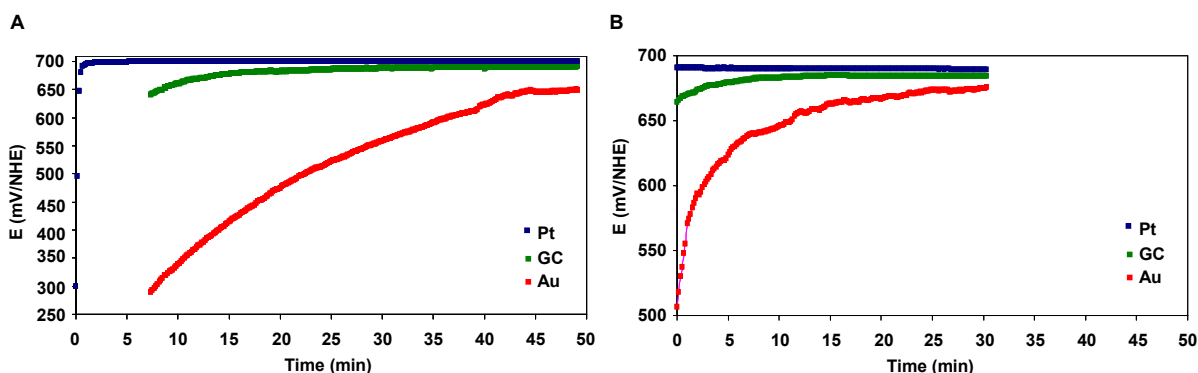
Figure 5: *Ref 01 (II/III) NaCl (0.1 mol L^{-1}) and Ref 02 Na c (5 mol L^{-1}) multi-electrode potential voltage (Eh (V/NHE)) versus time.*

As expected, potential stabilization times fluctuated as a function of electrode nature and sample composition. In comparison with Au or GC electrodes, Pt electrode stabilization time was generally faster. Indeed, platinum has the higher exchange current density (10 mA/cm² in comparison to 0.3 mA/cm² for Au), leading to a reasonable response time. Moreover, the higher the conductivity, the faster the stabilization time is. During the experiments, the general convergence of the stabilisation potential of all the immersed inert electrodes demonstrated (i) the outcome of an equilibrium state under the experimental conditions and (ii) the interest in using multiple inert electrodes in order to ensure measurement reliability. It is worth noting that the equilibrium potential was not or little influenced by NaCl concentration. Potential voltages were comparable to those obtained by other partners (see table 1). Potential voltages are in a good agreement with the geochemical modelling: Fe(II) and Fe(III) concentrations were controlled by equilibrium between aqueous Fe(II) and Fe(III) species. Measurements,

geochemical modeling as well as "speciation measurements" (concentrations in solution, identification of precipitated solid etc…) are necessary for redox determination and interpretation. The interest in continuous monitoring of voltage measurements using multiple redox electrodes have clearly been demonstrated in order to ensure reliable qualitative measurement.

Table 1: *Initial conditions as well as experimental and geochemical data*

Initial conditions

Ref 01 (II/III) b: NaCl 0.1 mol L^{-1}; FeCl$_2$ 10^{-4} mol L^{-1}; FeCl$_3$ 4.10^{-4} mol L^{-1}, pH fixed with HCl (2)

Ref 02 Na c: NaCl 5 mol L^{-1}; FeCl$_2$ 10^{-4} mol L^{-1}; FeCl$_3$ 4.10^{-4} mol L^{-1}, pH fixed with HCl (2)

Experimental measurements

	Ref 01 (II/III) b		**Ref 02 Na c**	
T (°C)	23.4		23.9	
pH	2.18		1.1	
Fe(II) (mol L^{-1})*	1 10^{-4}			
Fe(III) (mol L^{-1})*	5.6 10^{-5}			
	E (mV/NHE)	Equilibration time	E (mV/NHE)	Equilibration time
E Pt	697.0 ± 0.1	30 s	690.0 ± 0.4	0
E GC	688 ± 3	12 min	683 ± 2	3 MIN
E Au	647 ± 1	30 min	666 ± 1	10 MIN
E$_h$*	690.00 ± 0.05			

GEOCHEMICAL MODELLING

E$_h$ (mV/NHE)	700		-	

* Results coming from LWM: Laboratory for waste management, PSI, Switzerland

Within **FZD** research work in collaboration with **UPPC** it was shown that the application of electrochemical and laser-based fiber-optic oxygen microsensors to biological systems, e.g. multispecies biofilms grown in the laboratory and exposed to environmentally relevant uranium concentration, offer two methods that allow the measurements of oxygen with comparable good results. Both sensor methods showed almost identical curve progressions within the absolute error from the top to a biofilm depth of approximately 680 μm and 480 μm, respectively (see Figure 6). At this depth the electrochemical sensor measurements had to be stopped in order to avoid the destruction of the very fragile sensor tip when reaching the solid microscope glass slide on the bottom of the biofilm. Due to the high stability of the optodes against

consolidated materials, laser-based microsensor measurements were continued over an additional range of approximately 1 mm down to the biofilm/solid glass slide interface within the same biofilms. Thus, additional information of the oxygen concentration of the lower zone was obtained and showed that the oxygen concentration within the biofilm exposed to uranium decreased rapidly. With our aim to use microsensors for field-measurement in radionuclide contaminated environments, e.g. former uranium mining sites, to verify redox processes in in-situ biofilms, the improved miniaturized laser-based fiber-optic oxygen microsensor equipments proved to be very suitable.
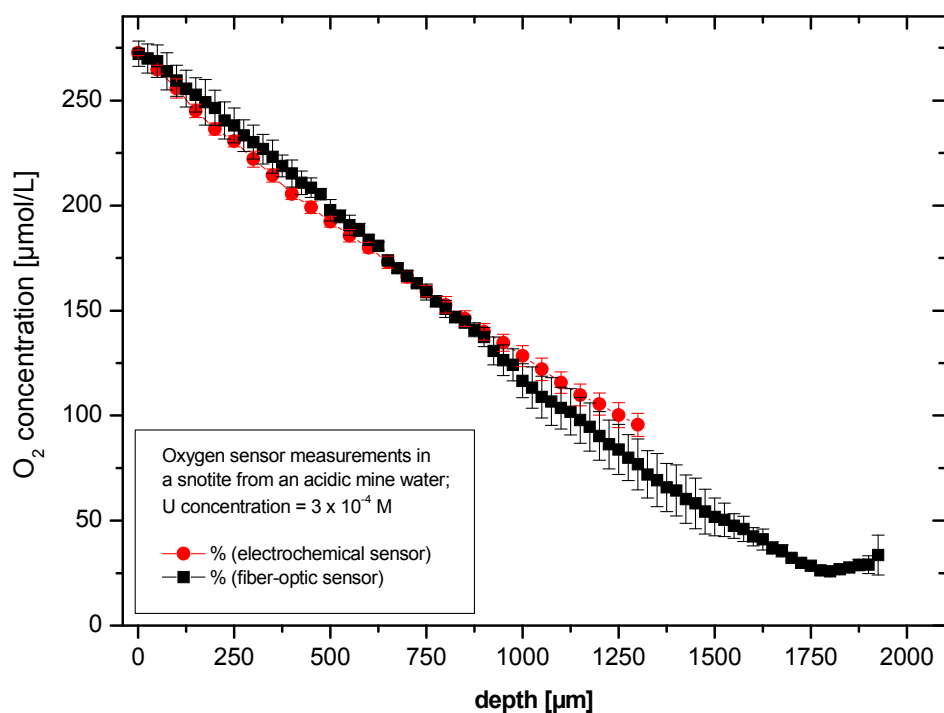
Figure 6: Oxygen concentration profiles in a stalactite-like biofilm from the uranium mine Königstein (Germany), exposed to a uranium concentration of 3×10^{-4} mol/L U(VI) in the bulk solution. The data were obtained by electrochemical and fiber-optic microsensor measurements. The error bars represent one standard deviation. The vertical increments of each microelectrode movement during the measurements were 20μm.

First comparative studies have been carried out in stalactite-like biofilms from the uranium mine Königstein (Germany), where the mining activities had been stopped in 1990 and the uranium mine has been partially flooded for remediation. In the acidic, sulphate-rich waters with high concentration of heavy metals and radionuclides (uranium) as contamminants, biofilms are formed and occur as gelatinous filaments, and as stalactite-like snotites. The analyses of the bacterial diversity of these biofilms showed a dominance of *Ferrovum myxofaciens*, an acidophilic, autotrophic, iron oxidizing bacteria, which belongs to the *Betaproteobacteria*. Ferrous iron is oxidized strongly catalyzed by Fe(II)-oxidizing bacteria with the consequence of producing oxidizing conditions within the biofilm with high oxygen concentration. Fiber-optic oxgyen microprofiles, carried out in these snotites are in a good agreement with

electrochemical measurements. The oxygen concentration is decreasing slowly from the edge versus center of the snotite biofilm.

In the last year the **GRS** continued the development of two methods for redox potential determination in saline media and tested them on solutions with low and high ionic strength. The first method, the potentiometric method, is based on redox measurements with a combined Pt ring electrode in different chlorine and sulfate media with a constant H^+ concentration and a constant Fe(II)/Fe(III) ratio. The results showed that sulfate media have a greater effect on the measured potential (up to 110 mV) than chlorides (up to 60 mV). Concerning the cations a constant order was observed: potassium had the strongest impact on the redox signal followed by sodium and magnesium. Correction functions (ΔRx) for the medium induced bias in saline solutions could be developed based on these measurements and by using geochemical modeling tools with Pitzer ion interactions coefficients (see Figure 7). The correction functions take into account the varying liquid junction potential in saline solutions. With ΔRx the difference between the measured potential E and an iron specific redox potential Rx_0 can be calculated.

$$Rx_0 = E - \Delta Rx = E^0 - 0.059 \log \frac{a_{Fe^{2+}} a_{Cl^-}^2}{a_{Fe^{3+}} a_{Cl^-}^3}$$

In case of the second method, the spectrophotometric method, the redox potential Rx_0 is achieved by iron species analysis. For this the influence of saline media on iron species analysis with UV/VIS-spectrometry was investigated. As complexing agents phenanthroline and thiocyanate were used. It could be shown that phenanthroline can be used for determining Fe^{2+} and Fe_{tot} in saline solutions with conventional cuvettes in a two beam UV/VIS spectrometer. Application of a 5 m long pass flow cell resulted in good analyses only for Fe(II) species. Determinations of Fe_{tot} and Fe(III) were not possible with the capillary spectrometer due to effects emerging by the use of a long pass flow cell. The thiocyanate method for determining Fe(III) showed influence upon time, pH, SCN^- concentration and sulfate anions. Thus, the thiocyanate method is not applicable for natural saline samples.

The comparison between the two methods, the potentiometric and spectrophotometric method, during the Interlaboratory Comparison Exercise of the ReCosy Project resulted in a good agreement of the determined redox values which suggest that both methods give reliable results. Furthermore a comparison between apparent potential E and the Rx_0 values demonstrated clearly that the apparent redox potential in saline solutions is not synonymous with the Eh in non saline solutions. For the determination of the redox potential in brines correction functions for media effects have to be applied.
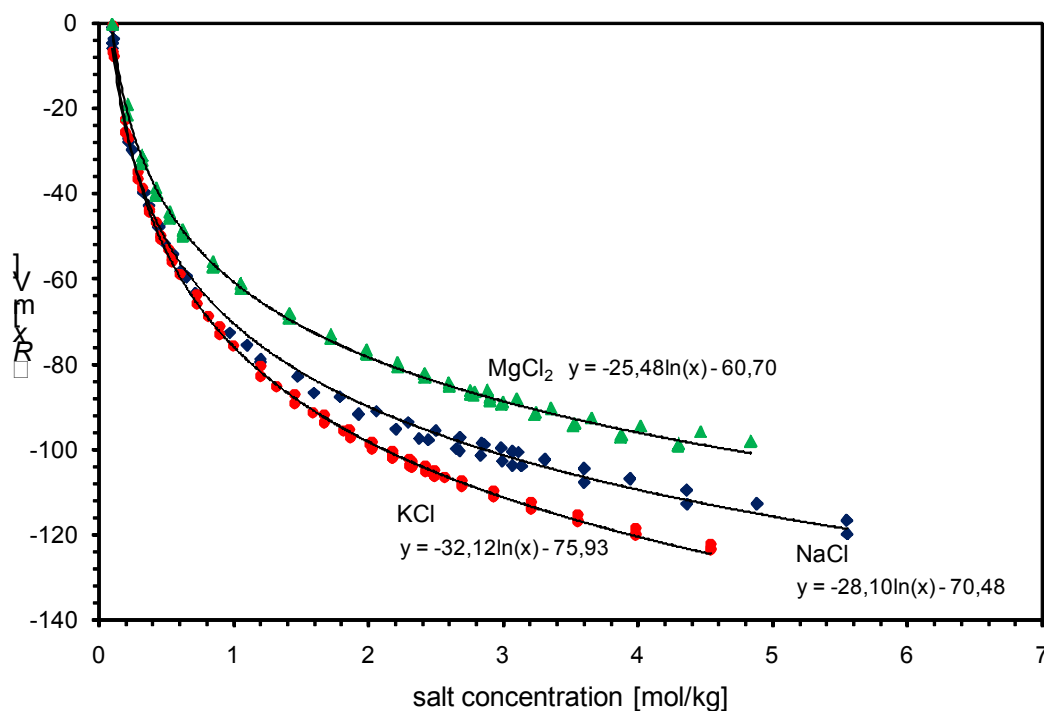
Figure 7: *Development of the correction functions ΔRx for the medium induced bias in case of chloride solutions*

Both methods were tested on acidified solutions for which a disturbance of hydroxo complexes could be excluded. For solutions with H+ concentrations higher than 0.01 mol/l hydroxo or mixed hydroxo chloro complexes are expected. For these species there are no adequate interaction parameters so far. That leads to a strong limited area of application for the second method. Therefore we are developing at the moment a mathematical model valid for solutions with a higher pH. This model will be based on redox and UV measurements in saline solution with varied pH. With this we should be able to apply the spectrophotometric method till a lower limit of the H+ concentration of 10-4 mol/l. The potentiometric method is valid independently of the pH and furthermore, is very simple practicable.

Within the framework of batch experiments **TUG** examined the sorption behaviour of iodine species from $NaClO_4$-solution by the well known KGa-1b kaolinite and humic acid (HS, Sigma Aldrich). Samples in the pH range of 2-10 were prepared with a kaolinite concentration of 4 g/L. After the pre-equilibration time (2 weeks) the solutions were spiked with iodine species (iodide or iodate) for concentration of 10 mg/L. After a contact time of 14 days the iodine species content remaining in the solutions were measured by ICPMS.
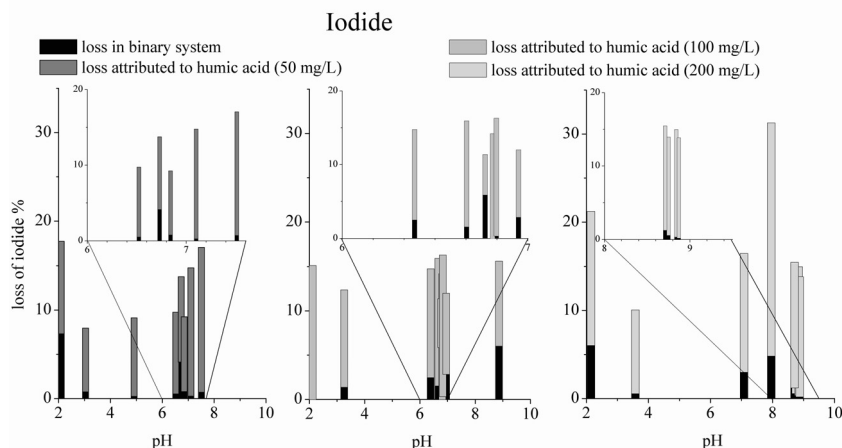
Figure 8: *Iodide systems*

Both iodide and iodate had a low sorption capacity on kaolinite below 8% and 21% respectively (see Figure 8 and Figure 9). The pH of the solutions had an effect on the adsorbability of the species only at pH < 4.

After measuring the loss of iodine species from the solutions attributed to sorption on kaolinite, the ternary systems were examined by adding different amounts of HS to the already equilibrated iodine species - kaolinite systems (concentrations of 50, 100, 200 mg/L).
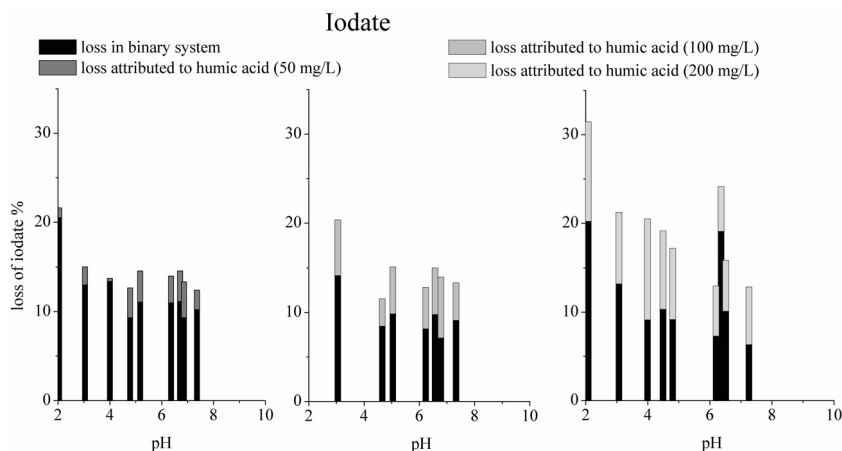
Figure 9: *Iodate systems*

Compared to the binary systems an additional loss of iodine species from the solutions attributed to reactions with humic acid was observed for both species which was higher for iodide (up to 26%) than for iodate (<14%). Further investigations with methods for structure examination like XPS or EXAFS could provide more detailed information about the sorption mechanism of iodine species in ternary systems.

UPPC research was focused on i) the implementation of an improved dual-phase modulation-based fiber optode for the determination of oxygen concentrations in the sub-ppm range and ii) the development of a luminescence decay time based pH-senor. The challenges of these research topics are highly different. The development of the

optode for trace level oxygen measurements requires an optical sensor with a very long luminescence decay time in order to have a sufficient dynamic range at low oxygen concentrations. Technical requirements such as sensitivity of the detection system, adaption of the modulation frequencies and polymer matrix used for immobilisation are major aspects that need to be considered in the development. Moreover, for pH measurements the luminescence probes available show mostly spectral alterations, have fluorescence decay times in the nanosecond range (hence require a completely different electronics for light modulation and detection) and show only limited pH sensitivity when immobilized in a polymer matrix.

A novel luminescence probe with a luminescence decay time of several hundred µs was implemented for improved oxygen detection using fiber-optical two-modulation luminescence detection. The novel probe has a very high dynamic range with respect to the decay time change due to the presence of oxygen (gain of a factor of 10!) compared to the previously established oxygen sensor. For the implementation of the novel probe a thorough calibration in the ppm concentration range is indispensible and turned out to be a demanding task. In a first step **UPPC** has carried out calibration experiments in the low vol% range. The first results are very promising and it can be envisioned that the optical detection of oxygen at the very low ppm range (or even less) is in reach.

In the development of multiparameter FOCS the determination of pH was investigated with emphasis on a time-resolved detection scheme using dual frequency phase modulation spectroscopy. **UPPC** tested different pH-sensitive dyes and the 6-Carboxyfluorescein showed promising results for the implementation in a decay-time-based optical sensor. It has the comparable spectroscopic properties to BCECF, but it is less expensive. The hardware setup for the fast phase modulation spectroscopy in the MHz range, which is necessary for the detection of fluorescence decays an a nanosecond time scale, is up and running. Novel modulation as well as detection moduls were built and implemented. The measurements with the pH sensitive dye 6-Carboxyfluorescein in aqueous solutions were performed as a reference in order to test the performance of the new setup (see Figure 10).

The embedding of the pH-sensitive dyee in the polymers, results in more or less unfavourable changes in the spectroscopic pH-response of the dyes. For example, the absorption is unchanged compared to solution condition and showed the expected pH dependency, but with respect to the fluorescence pH-response in the most cases the dependency on the pH is less pronounced, especially the fluorescence decay time is in the immobilized samples only weakly dependent on the activity of the protons. An exception is the nafion-membrane, in which preliminary results indicate that the pH-sensitivity of the fluorescence decay time is preserved. However, here the fast leaching of the dye into the solution is a problem, that need to be solved (e.g., for a better immobilisation it is necessary to enclose the membrane with another water permeable polymer or a covalent bonding between the nafion membrane and the dye may be solutions of the leaching problem).
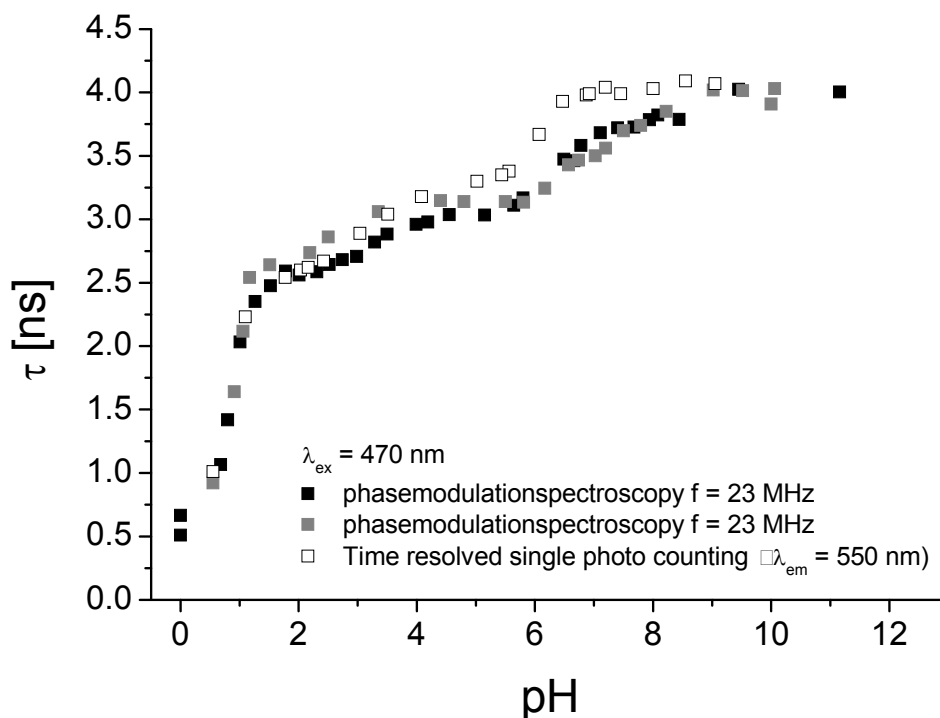
Figure 10: 6-Carboxyfluorescein in solutions with different pH, comparison of two methods of determination the fluorescence lifetime.

Contribution of **LQC** was essentially advisory to various other partners on issue in which the principal investigator in LQC has direct experience. These include:

- *oxygen sensing technologies*, notably, operation of Ocean Optics and TauTheta sensor systems utilizing phase shift measurement of fluorescence of ruthenium phenantroline and platinum phthalocyanine dyes in silica sol-gel matrix. Extended communications were exchanged with partners **CTM** and **SKB** that were instrumental in selecting suitable sensor systems getting their newly acquired equipment to perform.

- *redox sensing technologies*. **LQC** provided information to partner UP on redox sensitive dyes developed and characterized by centers such as the Photochemistry unit in the Department of Chemistry of the University of Bologna, Italy. Experimental setups were conceived and contacts were established with potential suppliers of suitable instrumentation, chemicals, and sensors. Furthermore, communications on methods and instrumentation suitable for electrochemical determination of pH and redox potential in poorly buffered media were held with various partners, as follow-up to the oral presentation given in the course of the 1st annual workshop of Recosy in Barcelona in the year 2009.

- *hydrolysis studies and data processing*. Constructive discussions were held with partner **KIT-INE** following discovery of inaccuracies in the evaluation of past experimental data in project FUNMIG. In particular, Am phosphate complexation constants previously calculated were found to be in error by about one order of magnitude due to incorrect selection of hydrolysis constant data. Resulting corrections,

if applied in Recosy and future literature, may improve the quality of models for speciation and transport of actinides in neutral and alkaline environments.

References

Aller R.C. (1982). Animal-Sediment Relations. The Biogenic Alteration of Sediments in: P. McCall, M.J.S. Tevesz (Eds.), Ch. 2, Plenum Press, New York, p. 53.

Grenthe I., Stumm W., Laaksuharju M., Nilsson A-C., Wikberg P. (1992). Redox potentials and redox reactions in deep groundwater systems. Chem. Geol. Vol. 98, 131.

Teasdale P.R., Minett A.I., Dixon K., Lewis T.W., Batley G.E. (1998). Practical improvements for redox potential (E_H) measurements and the application of a multiple-electrode redox probe (MERP) for characterising sediment in situ, Analytica Chimica Acta, Vol. 367, 201.

Stumm W., Morgan J.J. (1983). Aquatic Chemistry. Chemical Equilibria and Rates in Natural Waters, Ch. 7, 2nd ed., Wiley, New York, p. 418.

Stumm W., Morgan J.J. (1996). Aquatic Chemistry. Chemical Equilibria and Rates in Natural Waters, 3rd ed., Wiley, New York, Ch. 8, p. 425.

Whitfield M. (1971). Ion Selective Electrodes for the Analysis of Natural Waters, Ch. 9, Australian Marines Sciences Association, Sydney, p. 101.

Whitfield M. (1969). Eh as an operational parameter in estuarine studies. Limnol. Oceanogr. 14, 547-558.

WORK PACKAGE 3:
REDOX RESPONSE OF DEFINED AND NEAR NATURAL SYSTEMS

Laurent Charlet

(CNRS)-Laboratoire de Géophysique Interne et tectonophysique LGIT- (UMR 5559)
Rue de la Piscine, 1381
38041/19 Grenoble
France

Introduction

The "Redox processes of defined and near-natural system" WP3 group has in Year 2 performed work on (i) Field data, (ii) Field samples, (iii) Microbiology, (iv) Sorption experiments, (v) Redox experiments and (vi) Conceptual Model. This work is summarized below.

Work performed by partners

KIT-INE (Partner 1, rep. Thorsten Schäffer) has worked on redox reactions induced by irradiation on clay rock microtomes. A mapping of Fe oxidation state on these microtome by µXANES is planned but has not been yet measured.

Other work involves the uptake and reduction of U(VI) by nanohematite; U.J. Ilton described by XPS the formation of U(V) in this system, but this could not be, to date, reproduced by INE.

BRGM (Partner 3, rep. Ioannis Ignatiadis) investigated the oxidation of pyrite by nitrate, thanks to pyrite electrodes. The same work is going on with Cox. However the Cox electrodes being in the process to be patented, this part of the work will be reported next year in 3AWS.

CTM (Partner 6, rep. Frederic Laren) and **AMPHOS** (Partner 7, rep. David Arcos) have continued investigating the reducing capacity of natural pyrrhotite through thermodynamic and kinetic experiments with natural pyrrhotite in 0.1M $NaClO_4$ media. DRX indicates that the rock is composed mainly of pyrrhotite (identified as Fe_7S_8) and quartz, with some minor impurities like clays (chlorite and kaolinite), phylosilicates and calcite. Thermodynamic studies (TD) focused on the response to pH increase (10.5) and sulfate addition at two concentration level (5.10^{-5} and 1.10^{-3} M). On the other hand, kinetic experiments (EC) focused on the maximum oxygen uptake capacity by

experiments conducted at different initial oxygen concentration and repeated cycles. DO was continuously monitored by optical sensor.

SEM images and EDX measurements show Fe-rich secondary phases formed that have grown homogeneously on both kinds of experiments, which lead to an incongruent dissolution between Fe and S. This is specially enhanced in kinetic studies, where even is possible to observe the precipitation of three different layers according to the number of cycles used. The masking effect of Fe secondary phase scavenger the DRX peaks characteristics for pyrrhotite measured at the end of the experiments.

Within TD experiments no effect on the iron concentration in solution was observed at low sulfate level. However, a 50-fold increase was observed at high sulfate level. The oxygen uptake in EC experiments has been postulated (see report from partner 7) to correspond to 1) the oxidation of the S^{2-} to SO_4^{2-} and 2) the oxidation of Fe(II) to Fe(III). Congruently with the precipitation of iron secondary phases, the oxygen uptake rates are higher than the rate of iron released ($r_{o2,\ uptake} \sim 10^{-9}$-$10^{-10}$ mol $m^{-2} s^{-1}$, $r_{Fe,\ release} \sim 10^{-11}$ mol $m^{-2} s^{-1}$). In all cases more rapid response of platinum versus gold electrodes has been observed, but without significant difference in measures.

TUG (Partner 14, rep. Edit Marosits) worked on the analytical iodine concentration measurement.

CNRS (Partner 16) The immobilization by calcite of Fe(II) (to be released by canister corrosion) and Se(IV) (to be released as ^{79}Se) has been investigated. The sorption and coprecipitation of each individual ion was first studied individually, with wet chemistry, and for Se, by neutron diffraction (ND), Extended X-ray Fine Structure spectroscopy (EXAFS) and ab initio modeling using the Vienna Ab-initio Simulation Package (VASP) code. Then the reaction of Se(IV) added to an Fe(II)-rich calcite suspension was investigated by X-ray Absorption Near Edge (XANES) spectroscopy.

The interaction of Fe(II) with calcite was investigated experimentally under anoxic conditions (O2 < 1 ppmv). Fe(II) sorption isotherm depicts the S-shape curve typical of a continuum between adsorption and co-precipitation processes (Wersin et al., 1989). A Langmuir type adsorption predominates at low Fe(II) aqueous concentrations, while a surface coprecipitation process dominates at higher concentration. The incorporated Fe(II) could not after one week be remobilized by a strong complexing agent but the dissolution of surface layers of calcite particles with carbonic acid allowed its recovery. Through dynamic dissolution/reprecipitation processes, the Fe(II) ion has been incorporated in the calcite 25 nm surface layer, characterized by an Fe:Ca ratio equal to 0.04.

The coprecipitation of Se(IV) with calcite was shown to occur by substitution of the carbonate ion by the selenite oxyanion. Neutron diffraction experiments, EXAFS spectroscopy, and theoretical modeling of the crystallographic structure using VASP show the calcite unit cell volume to increase linearly with Se content in the structure. EXAFS spectroscopy, in combination with our theoretical model of the local structure surrounding the Se atom, confirms that quasi-isomorphic substitution of carbonate ions by selenite ions offer tremendous storage facilities for selenite in the various calcite-rich materials consider for the confinement of ^{79}Se rich nuclear waste.

Finally the reaction of Se(IV) with Fe(II)-rich calcite was investigated under anoxic conditions (O_2 < 1 ppmv) using XANES. The Se(IV) sorption on calcite increased in the presence of sorbed Fe(II) compared to that of Fe-free pure calcite. XANES spectra of Se K-edge show that nearly half of the total sorbed Se(IV) is reduced to Se(0) by Fe(II) freshly adsorbed on calcite. The extent of reduction decreases with increasing equilibration time of calcite with Fe(II) solution, before Se(IV) addition. The combined results of Field Emission Scanning Electron Microscopy (FESEM) and X-Ray Diffraction (XRD) have shown that needle shaped red monoclinic elemental Se with diameters of 30-50 nm and lengths of up to 100 nm, is precipitated on the calcite surface. In contrast, Fe(II) coprecipitated calcite does not contribute to Se(IV) reduction within 72 h. Therefore, the reduction capacity of Fe(II) linked to calcite critically depends on its location (either on the surface or in the bulk solid), and less extensively on the pre-equilibration time of calcite with Fe(II) solution. Such understanding is important to predict the transport, transformation, and attenuation of Se in subsurface and in nuclear waste repositories.

Bernd Granbow indicated that the shit in XPS spectra attributed to the U(VI) reduction could be due to different U(VI) complex with silica and attributed to U(IV)-like spectra Froideval et al. Journal of Colloid and Interface Science 266 (2003) 221–235)

Two series of samples from the Boda Siltstone Formation (BSF) which have been previously characterized by Mössbauer spectroscopy (II-HAS) were characterized electrochemically in order to specify the redox status of iron using 'Voltammetry of MicroParticles' (VMP). We adopted the more favourable experimental conditions for the voltammetric analysis i.e. various acidic media complexing or not complexing. The analysis of the voltammograms recorded allowed us to identify the different constituents of the clays and to visualize the release in solution of iron species. The results are in agreement with those obtained by Mössbauer spectroscopy, as regards the species present. On the other hand, we noticed an extreme sensitivity of the clays towards atmospheric oxygen, whereas one among the conclusions of the Mössbauer study was their high stability against oxidation.

The electrochemical characterization of the Callovo-Oxfordian argillite (Cox) has been performed in various conditions and a new voltammetric signal was pointed out. It is located at very negative potentials (~-0.85 V) is well-detected only at pH 2. Therefore, the voltammograms Cox exhibit three main signals: two are in relation with the presence of pyrite (oxidation and reduction of FeS_2) and the third one at ~-0.85 V is under identification.

In collaboration with the "Laboratoire de Géologie et Gestion des Ressources Minérales et Energétiques (G2R)", UMR 7566 CNRS Nancy-Université, humic and fulvic acids have been synthesised and their reactivity towards iodide ion has been investigated in acidic and alkaline media with UV-Visible Spectroscopy and Fluorimetry. The exploitation of the experimental results is in progress

UNIZAR (Partner 17). Swedish granite system groundwaters is investigated through thermodynamic equilibrium computations. The top 500 m (xher Cl-concentration varies from 300 to 6àà mg/L, as a result from Litorina sea highlysaline water infiltration) are at equilibrium with oyrrhotite (or mackinawite), siderite ($FeCO_3$) and rhodocrosite ($MnCO_3$).   The carbonate solid phases have not till know been

inditified in cores. At 200 m depth exist an Eh buffer (between -150band -275 m). At greater depth salinity increases (former seawater), and water become undersaturated with respect to the three above mentioned solid phases.

For these great variety of waters, there exist a very good agreement between the measured Eh and the one calculated from the SO42-/S2-, SO4/FeS; CO2/CH4 CO2/CH4, but a poor agreement with values computed from Fe2°/Fe(III) solid, the latter being critically depending on the nature of Fe(OH)3 phase.

II-HAS (Partner 19, rep. Karoly Lazar) investigated the response of Boda Claystone samples for redox disturbances was investigated. Both contain albite (30%) and illite (30%) Two types of samples were selected ,formed either in oxic (arid, alkaline and oxidizing environment (Fe(III) dominance, as 9% hematite) or anoxic (Fe(II) dominance, as 10% chlorite) environment, found now at 900m depth. The anoxic sample was exposed to oxidizing treatments in aqueous media by treatments with perchlorate, hydrogen peroxide and hypochlorite, in amounts of 3-fold stiochiometric excess, for ten days, respectively, but no influence of the oxidizing treatments was detected by Mössbauer spectroscopie (no change in shape of spectra. The oxic sample was exposed to reducing treatments with hydroxylamine hydrochloride, hydrazine, formaldehyde and sodium dithionite. The first three treatment did not result in any change in the shape of spectra. There was one exception with reductants: the treatment with dithionite resulted in two effects: (i) in the reductive dissolution of hematite, i.e. a significant portion of the hematite was dissolved and went into the solution in form of ferrous iron, and unexpectedly,(ii) a part of this dissolved ferrous iron was relocated again in the clay structure, as the appearance of a novel ferrous component indicated in the respective Mössbauer spectra.

UNICYPRUS (Partner 20, rep. Ioannis) has during the first project year collected phosphogypsum samples from different areas of the phosphogypsum stack. The solid samples have been contacted with de-ionized water and the sulfide and sulfate concentrations in these solutions has been determined by potentiometric titration using ion selective electrode and Hg(II) standard solution, and ion chromatography, respectively. Similar experiments have been also performed with phosphogypsum samples in contact with aqueous solutions containing natural organic matter under nitrogen atmosphere.

Based on previous data and the data obtained after the second project year's investigation about the phosphogypsum stack at a coastal area in Cyprus, the redox conditions existing in the open stack are oxic/aerobic (400 mV $<$ E$_H$ $<$ 600 mV), whereas after application of a vegetative cover the redox conditions become suboxic (-200 mV $<$ E$_H$ $<$ 100 mV). These results indicate that sulfate and uranium(VI) under oxic and sulfide and uranium(IV) under sub-oxic conditions will be the predominant redox species.

MICANS (Partner 24, rep. Karsten Pedersen) Has done 20 boreholes in the underground Aspö laboratory. The water was collected and transported under pressure (25 bars) to crushed granite columns. Hydrogen(1 or 10 mM; while GW hydrogen

concentration was 0.1 mM) , acetate or lactate was introduced, and Eh, gas and solute concentrations followed.

WORK PACKAGE 4:
REDOX REACTIONS OF RADIONUCLIDES

WP 4.1.

Chemical and redox behaviour of the investigated radionuclides in the different systems

[1]Perdicakis, M., [2]Allard, S., [2]Holgersson, S., [3]Brian, N., [4]Baltrunas, D.,[4]Lujaniene, G., [5]Schäfer, Th., [5]Marquardt, Ch., [6]Evans, N.,[6]Hallam, R., [7]Grivé, M., [8]Gaona, X., [8]Tits, J., [8]Wieland, E.

[1]Laboratoire de Chimie Physique et Microbiologie pour l'Environnement, Nancy-Université, CNRS -54600 VILLERS-LES-NANCY France

[2]Chalmers University of Technology, SE-412 96 Gothenburg, Sweden

[3]University of Manchester, Centre for Radiochemistry Research, School of Chemistry, , Manchester M13 9PL, (UK)

[4]Institute of Physics of Lithuania, LT-02300 Vilnius, Lithuania

[5]Karlsruhe Institute of Technology, Institute for Nuclear Waste Disposal, Karlsruhe, Germany

[6]Loughborough University ' Department of Chemistry, Loughborough, Leics, LE11 3TU, UK

[7]AMPHOS XXI Consulting, S.L., E08019 Barcelona, Spain

[8]Paul Scherrer Institut, Laboratory for Waste Management, CH-5232 Villigen-PSI, Switzerland

* Corresponding author: jan.tits@psi.ch

Introduction

The goal of the activities within this work package is to provide fundamental process understanding of the redox behavior of radionuclides, including the question of equilibrium / disequilibrium with the system redox conditions. The objectives of this work package result from gaps in the knowledge identified from previous projects dealing with redox processes involving radionuclides

The activities within WP4.1 can broadly be divided in three main topics:

1. Interactions of radionuclides with pyrite

2. Interactions of radionuclides with far-field solids

3. Redox processes under hyperalkaline conditions

Work performed by partners

Interactions of radionuclides with pyrite
CNRS/LCPME no response

Interactions of radionuclides with far-field solids

The work performed within this topic is focused on obtaining fundamental process understanding of the interaction of redox sensitive radionuclides such as Tc, U, Np and Pu with various far-field minerals.

Chalmers University of Technology **(CTH)** will investigate redox reactions and states of selected redox sensitive elements with relevance to a crystalline rock environment (Äspö, Sweden).

The investigations are basically divided into two parts:

1. Bulk water measurements
2. Groundwater with minerals measurements

In both parts we intend to look into aspects of the E_h agreement between the redox couple Fe(II)/Fe(III) and e.g. Tc(IV)/Tc(VII), U(IV)/U(VI), Np(IV)/Np(V), Pu(III)/Pu(IV)/Pu(VI) in ionic media of varying type with ionic strength < 0.1, including natural Äspö groundwater. Our aim is to perform these studies under both oxic and anoxic conditions.

Measurements with commercial redox electrodes as well as analysis and quantification of elemental oxidation states will be examined over time and discrepancies between these will be looked into.

Geological material and groundwater recipe are taken from the Äspö LTDE-project (Long Term Diffusion Experiment) where results for in-situ adsorption of radionuclides onto rock surface, both for transport in fractures and fracture zones, and in-diffusion into the rock matrix is compared with laboratory results with crushed material.

During 2009 scoping experiments have been made for:

1) Production of U(IV) from U(VI) by catalytic reduction with H_2/Pt.
2) Spectroscopic measurement of purity of solutions of U(IV) from U(VI) and its stability over time.
3) Separation of U(IV) from U(VI) by solvent extraction, using Thenoyltrifluoroacetone or Acetylacetone for the purpose of quantification of ^{233}U in tracer amounts.

The scoping experiments looks promising but a final method for rapidly determining the oxidation states of U have yet to be devised. The intention is to use ^{233}U as tracer addition to the aqueous system of interest and then, after a period of time, take samples for extraction and measurements with Liquid Scintillation Counting for determining the concentration of U(IV) and U(VI).

University of Manchester **(UMANCH)** is investigating the interactions between surfaces, humic acids (HA) and redox sensitive radionuclides in ternary systems, with the aim of predicting radionuclide chemistry and solid/solution partition.

The experiments

During the second year of the Recosy project a series of batch experiments were performed at room temperature in order to study the effect of HA on actinide sorption on quartz sand. The solid to solution ratio was 500 g·L^{-1}. The amounts of actinide adsorbed were determined from the concentrations in the supernatant after a given time. Known amounts of actinide, added as a small amount of a concentrated stock solution, were added to electrolyte solutions containing concentrations of humic in the range 0 – 200 ppm. The actinide and humic were allowed to equilibrate for 24 hours before known masses of quartz sand were added to the system. At regular intervals, the solution phase was separated from the solid and the solution phase concentration was measured. For some systems, once (apparent) equilibrium was reached, the supernatant was separated from the mineral phase and replaced with a fresh electrolyte containing the same concentration of humic. The distribution of actinide between solid and solution was then monitored as before with time.

During the development phase, experiments used UO$_2^{2+}$ and Th^{4+} ions as analogues for redox sensitive actinides (e.g. Th(IV) for U(IV) or Pu(IV)). Also, the initial experiments were conducted in an ambient atmosphere (air, pCO$_2$ = 10$^{-3.5}$ atm), but later experiments used carefully controlled CO$_2$ and O$_2$ free conditions. Most recently, some experiments have used the redox sensitive U(IV) ion.

Some example Results

Figure 1 shows the effect of humic concentration on the sorption of Th(IV) onto quartz sand. In many ways, this system displays fairly simple ternary system behaviour. As the concentration of the humic increases, the amount of Th(IV) sorbed to the mineral surface decreases. Hence, in this system, the main effect of the humic is to act as a competing solution phase ligand, which holds the actinide in solution. These results suggest that the presence of HA could increase Th(IV) mobility, since even the lower concentrations of HA (e.g. 10 ppm), which could be found at a real site can increase Th(IV) solubility.
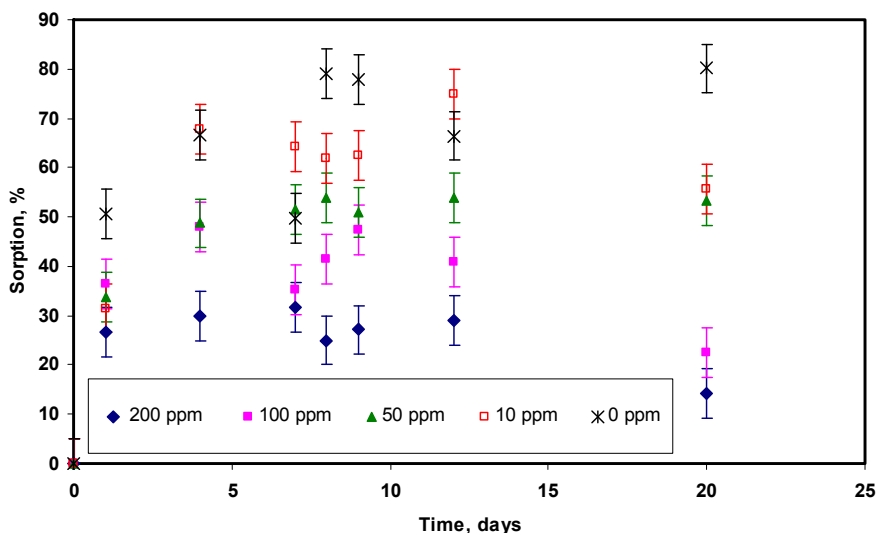
Figure 1: *Sorption of Th(IV) onto 500 g·L⁻¹ quartz sand at pH=6.0 and I=0. 1 M ([Th_T]=47 mBq/ml) as a function of total (sorbed plus free) humic concentration.*

Figure 2 shows the equivalent results for the uranyl system. In this case, the effect of the humic is more subtle. First, the humic has less of an effect on the distribution of uranium. The difference in the final amounts sorbed is only 15% across the whole concentration range (0 – 200 ppm). Secondly, the presence of the humic actually increases the sorption of uranyl. This can happen in systems where the interaction of the metal ion with the mineral surface is weak compared to that with the humic. In that case, ternary complex formation is particularly favourable for the uranium and the presence of humic enhances sorption. The importance of the humic to the distribution of uranium in this system is shown by the results of the experiment where the fresh humic was added to the system (Figure 3). In Figure 3 the points plotted at 0 days represent the amount of U sorbed prior to the removal of the supernatant and its replacement with fresh solution of the same free humic concentration. Immediately after this point, the solution was exchanged. For the system without humic, there is no significant change in sorption. However, for the humic containing systems, there is a significant drop in sorption after fresh humic is added. It seems that the fresh humic is removing uranium from the surface by competition. With time, the amount of uranium sorbed does increase, and this probably represents slow exchange between solution and sorbed humic species, which results in a return of U to the surface as a ternary complex. Experiments such as this provide useful information, because at a contaminated site there would be a constant supply of fresh humic.
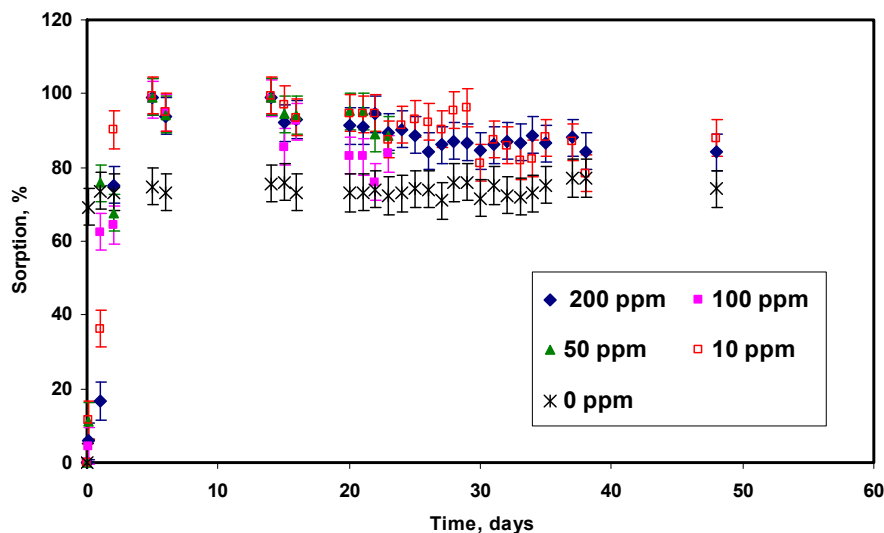
Figure 2: Sorption of U(VI) onto 500 g·L⁻¹ quartz sand at pH=6.0 and I=0. 1 M ([U$_T$]=100 Bq/ml) as a function of total (sorbed plus free) humic concentration..

The data in Figures 2 and 3 suggest that although humic may promote sorption in a static system, in one where there is flow of groundwater introducing fresh material, competition may result in a resuspension of uranium. Whether this would result in increased mobility would depend upon the relative magnitudes of the time taken for re-adsorption and the residence time of the groundwater in the contaminated region.

In the last few weeks, we have extended our experiments to U(IV) systems. Some preliminary batch kinetic uptake results are shown in Figure 4.
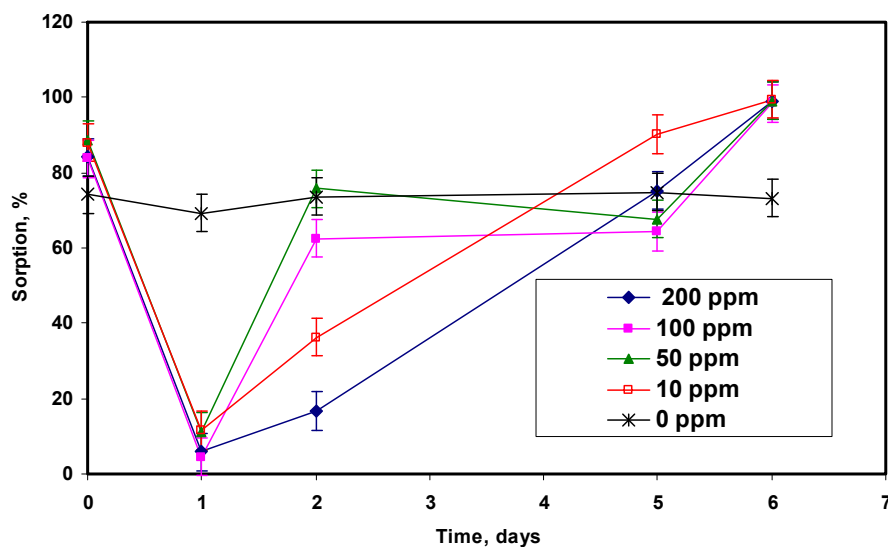
Figure 3: Effect of the addition of fresh humic to U(VI)/sand/HA ternary system (same system details as Fig. 1 and 2).
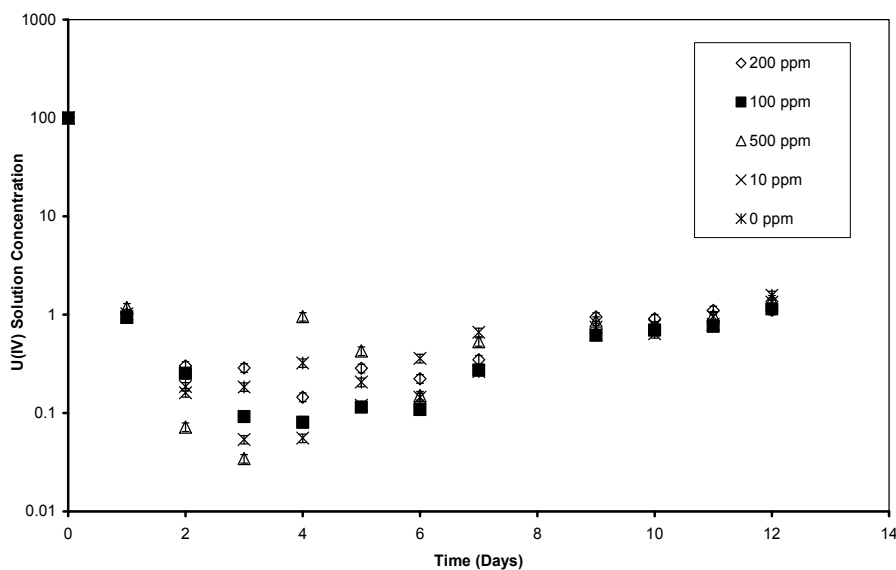
Figure 4: *Simple sorption experiment for U(IV) in presence of humic acid, various concentrations.*

IPL studies the sorption of Pu to natural clays with naturally present iron oxide coatings. Samples of a Triassic clay from a site mined for industrial exploitation known as the Šaltiškiai (North Lithuania) quarry were taken for laboratory investigations. This clay is selected for the engineered barrier at the Lithuanian near surface repository. The compositions of this clay material was presented in the 1st Recosy Annual Workshop Proceedings (Tits, 2009)**.**

Sorption of Pu(IV) and Am(III) was studied under argon atmosphere using $0.1 \; mol \cdot L^{-1}$ NaNO$_3$ solutions and experiments were based on the standard method for measuring laboratory batch K_d values. Initial concentrations of the Pu isotope mixture and [241]Am were $1.0 \cdot 10^{-10}$ and $2.50 \cdot 10^{-11} \; mol \cdot L^{-1}$, respectively. Measurements of pH were conducted before and after sorption experiments under continuous Ar flow using WTW SenTix 41 or SenTix 81 pH-electrodes, calibrated with standard buffers DIN 19266 (pH values 4.006, 6.865, 9.180) and a WTW inoLab Multi Level 1 meter. In all experiments ACS reagent grade or higher grade chemicals were used. All solutions were freshly prepared using Milli - Q (Millipore Milli - Q Synthesis A - 10) water with TOC < 10 ppb. Dissolved oxygen concentration in solutions was measured using a WTW OxiCal - SL probe and a WTW inoLab Multi Level 1 meter. Suspensions were shaken for desirable time and the solid-phase was then separated from the liquid-phase by centrifugation for twenty minutes at 10,000 – 20,000 g. Pu and Am in the solution and the solid-phase were determined after separation using the UTEVA and TRU resins (Eichrom Industries), concentrations were then measured by alpha spectrometry or ICP-MS (Finnigan Mat Element 2). A combined standard uncertainty was not higher than 10% at the lowest concentration. [242]Pu and [243]Am were used as tracers in the separation procedure.

Oxidation state distribution was determined using an ultrafiltration/solvent extraction technique, TTA, HDEHP and DBM. [241]Am(III), [228]Th(IV), [237]Np(V) and [232]U(VI) as oxidation state analogues for Pu(III), (IV), (V) and (VI) as well as [242]Pu(IV), [236]Pu(III) were used to establish effective leaching conditions of Pu from the

solid-phase and to validate   oxidation state analyses procedure.   Results of these experiments indicated that Pu can be quantitatively desorbed (up to 96±6 %) from solids. Experiments performed using ^{242}Pu(IV), ^{236}Pu(III) indicated that Pu(III) and Pu(IV) remain stable during the desorption procedure using 3 mol·L^{-1} HCl.

Pu(IV) oxidation state distribution in the system of natural clay – 0.1 mol·L^{-1} NaNO$_3$ after 7-day contact time indicated comparatively high content (up to 75%) of Pu(III,IV) at pH 4.86 – 4.98 while polymeric species of Pu(IV) were found to be the dominant ones at pH 5.76 – 8.21 in the liquid-phase. Analyses of Pu oxidation state determination in the solid-phase were performed after the desorption step using 3 mol·L^{-1} HCl, and Pu(III,IV), Pu(V) and Pu(VI) as well as Pu(IV) at pH= 0 were analysed in parallel. The content of Pu(III) was calculated from balance. Pu(III) was not found in the system at pH (5.76 - 8.2) while 4.9% and 10.7% of Pu(III) were found at pH 4.86 ± 0.11 and 4.98 ± 0.08, respectively.

Iron-bearing minerals such as montmorillonite, siderite determined in the studied clay to a great extent account for 10.7 % of Pu(III) in solids because these minerals posses a reductive capacity and can cause the abiotic reductive transformation of plutonium. Oxidation state distribution at trace initial Pu concentrations in liquid- and solid-phase of the natural clay systems was studied. Existing solvent extraction techniques were verified with respect to determination of Pu(III) in the liquid- and solid-phase. Pu(III) was desorbed quantitatively from the solids, no oxidation of Pu(III) and Pu(IV) was observed during desorption procedure. The reduction of Pu(IV) by natural clay containing iron-bearing minerals in the pH range from 4.22 to 4.98 was found, however, no reduction was detected at the near-neutral and high pH.

KIT-INE has worked on three different research topics:

a) Rock powder of the COx or OPA claystone was equilibrated with synthetic porewater in an Ar glovebox containing 1% CO2 admixture for 1-2 weeks. After this period the experiments were started with different liquid to solid ratios ranging from 1:10 to 1:200 and a radionuclide concentration (Pu(V), Np(V) or Tc(VII)) of $1.2 \cdot 10^{-8}$ mol/L. Spectroscopic investigations will include UV-VIS, LSC, ICP-MS and capillary electrophoresis (CE)-ICP-MS as well as liquid-liquid extraction (PMBP, TTA) for redox speciation. pH/E$_h$ will be frequently measured. The long-term kinetic experiments have been started in January 2010 an Eh measurements have been performed in two month contacted samples. The preliminary results show that Pu, Np and Tc are mainly sorbed onto the OPA and COx clay assuming a reduction of Pu(V), Np(V) and Tc(VII) in both systems.

b) Pu(IV), Np(V), Tc(VII) and U(VI)) batch-type experiments in the presence of fracture filling material have been conducted. Monitoring included the contact time dependent evolution over one year of the pH and the Eh value. The measured plateau values for pH dropped from pH 9.6 originally found in the Grimsel groundwater to 9.3 ± 0.1 in the Grimsel FFM and Äspö FFM system. Meanwhile, the E$_h$ values dropped from ~50mV to ~0mV in the first two days and started to increase again to values ~50mV in the Grimsel FFM system, whereas in the Äspö FFM system a tendency to lower Eh values ~ -25mV could be observed. From a comparison of ultra-centrifuged (UC) with not ultra-centrifuged samples it is obvious that Tc-99, U-233 and Np-237 are not colloidal associated. The concentrations of Tc-99 and U-233 remain constant over the entire observation

period, indicating an absence of sorption to fracture filling material or reduction in both investigated systems. This observation is in good agreement with the thermodynamic calculations predicting a predominance of TcO_4^- and $UO_2(CO_3)_3^{4-}$ under the established pH/E$_h$ conditions. Np(V) concentration decreases after ~ 100h from $2\cdot10^{-6}$ mol/L to $1\cdot10^{-7}$ mol/L after one year in both investigated systems. This observation could either be explained by slow sorption kinetics to the fracture filling material or more plausible by a slow reduction to Np(IV). The borderline of Np reduction is around -60 mV (50% reduced Np), which is slightly lower than our measured Eh values of -25 mV for the Äspö system and +25 mV in the Grimsel system. Due to uncertainties in redox measurements these values are likely in the range of the borderline for reduction (see WP 2). In contrast, Pu introduced in the tetravalent oxidation state is clearly bentonite colloidal associated which again can be derived through a comparison between the UC and the not-UC samples. The differences in radionuclide concentration are 1-2 orders of magnitude which also reflect the effective separation of the colloids through the experimental procedure. Additional data on the radionuclide bentonite sorption reversibility over one year observation period were obtained (for details see S&T contribution Huber et al.).

c) Within the training activity of Dr. Natalia Shcherbina (MSU) carbon XANES analysis of Mayak sediments and isolated humic colloids from Lake Yrtyash and different hydroquinone enriched humic substances have been investigated at the soft X-ray spectromicroscopic beamline X1A at the National Synchrotron Light Source (NSLS), Brookhaven National Lab. (BNL). Additionally, it was attempted to identify redox functional groups in humic substances by a combination of time-resolved laser fluorescence spectroscopy (TRLFS) with change in the humic acid redox state by electrochemical means and titration with reducing and oxidizing agents. Quinone enriched humic acid is also studied for comparison with the findings with natural ones. For details concerning the TRLFS work see S&T contribution Shcherbina et al..

Redox processes under hyperalkaline conditions

The work performed within this topic aims to provide an understanding of the redox behaviour of redox-sensitive radionuclides such as Tc, U, Np under hyperalkaline conditions.

Loughborough University **(ULOUGH)** has performed experiments to investigate the complexation of Tc(IV) with 4 anthropogenic ligands, EDTA, NTA, ISA and picolinic acid.

All experiments were conducted in a Unilab MBraun Nitrogen Glove Box with O_2 levels kept below 1 ppm. All solutions were boiled and N_2 sparged. Solid Na_4EDTA and sodium picolinate were added to NaOH(aq) at pH 13.3, to give concentrations between 0.4 and 0.001 mol dm^{-3}. NH_4TcO_7 was added and reduction was achieved by pasting a voltage (5V) through the solution for at least 12 h. The activity in solution was measured by liquid scintillation counting using Canberra Packard TRI-Carb 2750TR/LL, indicating an aqueous concentration of Tc(IV) of around 4 x 10^{-9} mol dm^{-3}. 5 replicates were used. Control experiments without ligands showed that reducing

conditions were maintained for the required periods of time. To measure the stability constants for the reaction of Tc(IV) with EDTA, NTA, ISA and picolinic acid, the solubility product approach was used, as discussed by Warwick *et al.* [5].

Complexation of Tc(IV) with EDTA

Figure 5 shows the effect of increasing concentration of EDTA on Tc(IV) solubility, the aqueous concentration of Tc(IV) rising from $\sim 10^{-9}$ mol dm^{-3} to 10^{-7} mol dm^{-3}, albeit at high EDTA concentrations. The slope of close to unity in the log-log plot (1.18) indicates that the increase in solubility of Tc is being controlled by the formation of a 1:1 Tc(IV)-EDTA complex. This relationship allows the calculation of a conditional stability constant for this complex using the solubility product approach.
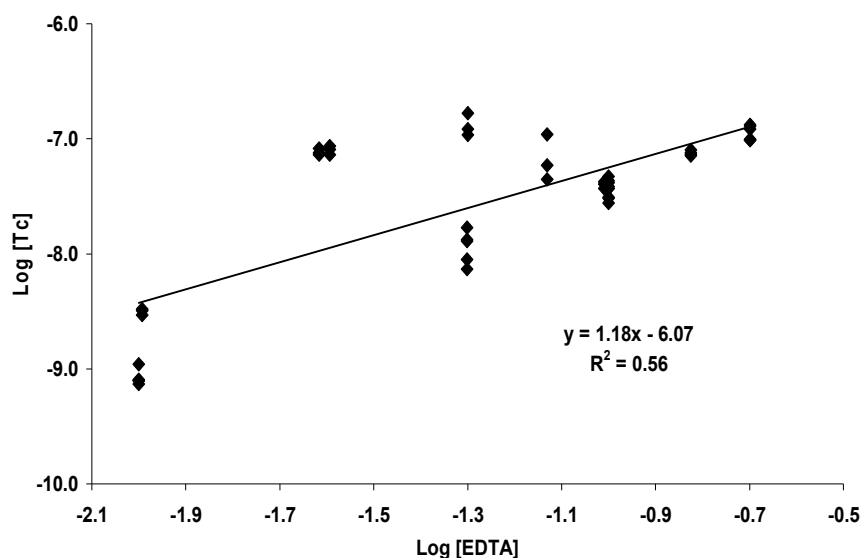
Figure 5: *Effect of concentration of EDTA on aqueous technetium concentration above TcO$_2$(am) at pH 13.3.*

The conditional stability constant for the Tc(IV)-EDTA complex was determined to be; $\beta_{Tc(IV)-EDTA} = 1.6 \times 10^{26}$ or log $\beta_{Tc(IV)-EDTA} = 25.9 \pm 0.6$.

Complexation of Tc(IV) with Picolinic Acid

Figure 6 shows the effect of increasing concentration of picolinic acid (PA) on Tc(IV) solubility, the aqueous concentration of Tc(IV) rising from $\sim 10^{-9}$ mol dm^{-3} to 10^{-6} mol dm^{-3} at high picolinate concentrations. The slope of close to unity in the log-log plot (1.05) indicates that the increase in solubility of Tc is being controlled by the formation of a 1:1 Tc(IV)-PA complex. This relationship allows the calculation of a conditional stability constant for this complex using the solubility product approach [5]. The conditional stability constant for the Tc(IV)-PA complex was determined to be, $\beta_{Tc(IV)-PA} = 8.65 \times 10^{26}$, or log $\beta_{Tc(IV)-PA} = 26.9 \pm 0.1$.
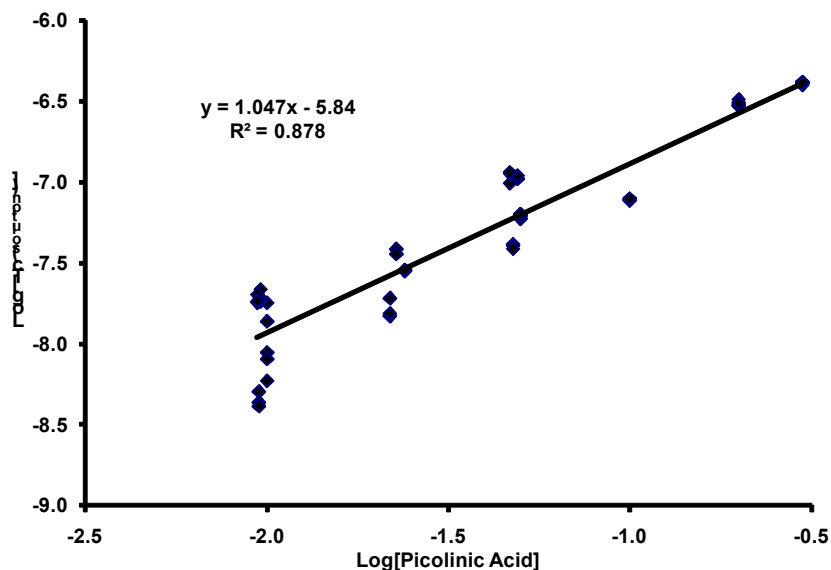
Figure 6: *Effect of concentration of picolinic acid on aqueous technetium concentration above TcO₂(am) at pH 13.3.*

Work has also been performed on NTA and ISA, but the results are as yet inconclusive and need repeating before publication.

AMPHOS aims to provide an understanding of redox behaviour of the uranium system under hyperalkaline conditions. During the first year preliminary UO_2 solubility experiments were performed under anoxic redox conditions into an autoclave batch reactor connected to a Time-resolved Laser-induced Fluorescence Spectrometer (TRLFS) and to a cell designed to measure pH and E_h online. The described experimental set up would characterise the aqueous uranium hydroxide species by TRLFS spectrometry in equilibrium with the solid phase $UO_2(s)$ at a defined pH and E_h making possible to solve the questionable existence of the anionic aqueous species of U(IV): $U(OH)_5^-$ and $U(OH)_6^{2-}$ (see Figure 7), which have been considered to contribute to the increase of solubility of UO_2 at hyperalkaline and reducing conditions. Such species were difficult to detect because of their stability at anoxic and hyperalkaline conditions which are very difficult conditions to maintain during sampling manipulation.

a   b
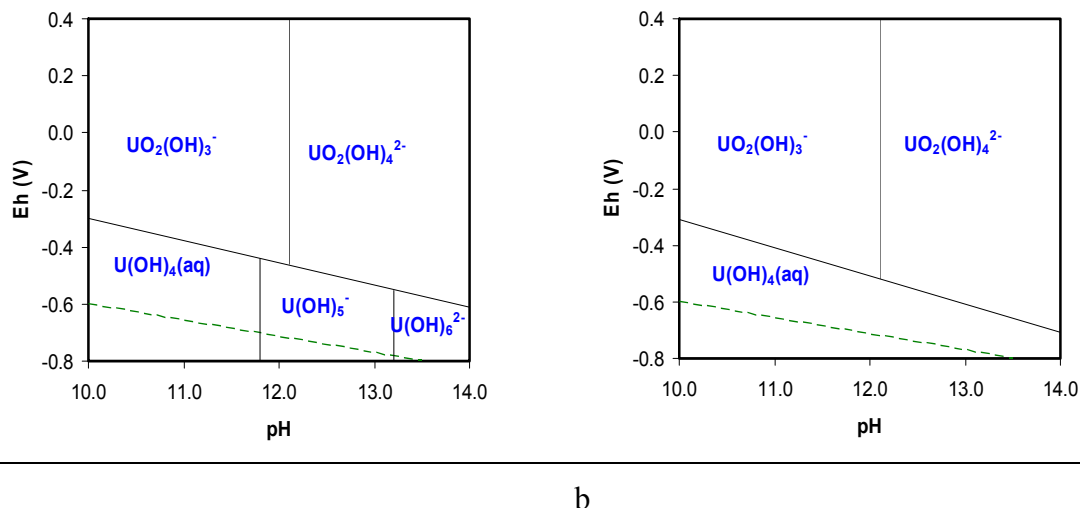
Figure 7: *Predominance diagram E_h vs pH of uranium aqueous species in pure water. $[U]_{Total} = 1\cdot10^{-7}$ M using thermodynamic data from a) Guillamount et al. (2003) and including the species $U(OH)_5^-$ and $U(OH)_6^{2-}$ from Fujiwara et al.(2005). b) Guillamount et al. (2003)*

In this second year of the project, experimental studies have been slightly refocused and new experiments have been designed to study the effect of different pressures of $H_2(g)$ on uranium oxide solubility (UO_2). The presence of hydrogen in the vicinity of the spent nuclear fuel (generated by the steel corrosion) produces very reducing conditions and high pH. Once the hydrogen pressure reaches a given value in the repository it diffuses away from the system, which will cause a drop in the hydrogen content. In these experiments we aim at simulating the diffusion of $H_2(g)$ out from the repository and its effect on the uranium solubility and speciation.

Solubility experiments

The surface of already existing UO_2 powder has been cleaned with acid in order to minimize the possibility of the presence of oxidized phases on the surface.

Both the experimental set up and the solubility experiments are performed in a glove box under N_2 atmosphere. The solid is contacted with an hyperalkaline solution (pH 11-13) and high hydrogen pressure (ca. 9 atm) into the autoclave shown in Figure 8 at 0.1 ionic strength. Samples are taken at given time intervals for pH, E_h and [U] determination. With every sample withdrawn, a drop in the hydrogen pressure takes place and the system is allowed to evolve both in terms of pH and E_h, i.e., pH will not be fixed. Hydrogen pressure, E_h, pH and [U] are determined at every sampling point.

Therefore, no effort is made to avoid the hydrogen pressure drop due to sampling, on the contrary, such a hydrogen pressure drop is wanted to allow simulation of the diffusion of $H_2(g)$ out from the repository and to know how it affects to the uranium solubility and its speciation.

Figure 8. *Autoclave used to perform the batch experiments.*

Once each experiment has been performed and in order to elucidate the dissolution mechanism, the solid phase will also be characterized with spectroscopic techniques (e.g. XANES, XPS, SEM-EDX and XRD).
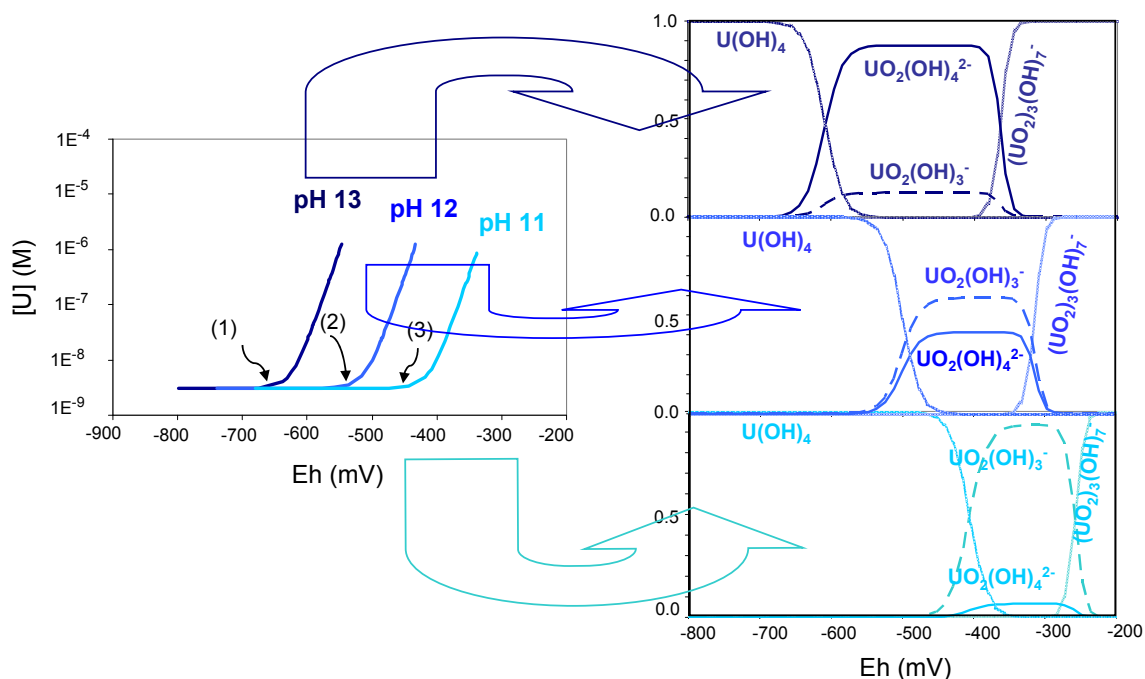
Figure 9. *Modeling results of [U] versus E_h at initial pH 13, 12 and 11 (left) together with the speciation diagrams of uranium aqueous species versus Eh at the corresponding pH, using thermodynamic data from Guillamount et al. (2003) (right). The numbers (1), (2) and (3) indicate the H_2 pressure at which the oxidation of $UO_2(am)$ starts taking place; (1) $PH_2 (bar) = 6E^{-4}$ bar, (2) $PH_2 (bar) = 3E^{-5}$ and (3) $PH_2(bar) = 1E^{-6}$.*

Preliminary models of the studied system at hyperalkaline conditions (pH 11, 12 and 13) considering an initial H_2 pressure = 9.6 bar together with the corresponding speciation diagrams are shown in Figure 9. The geochemical model indicates that as the pH decreases, the H_2 pressure at which the oxidation of UO_2(am) takes place decreases as well. This observation is directly related to the aqueous speciation scheme in equiblibrium with the solid phase; the increase in the uranium solubility is a consequence of the oxidation of U(IV) to U(VI) species and this process occurs at specific redox conditions (i.e. the H_2 pressure) at a given pH of the system.

Currently samples are taken at different reaction times from the UO_2(am) solubility experiment set up to an initial pH = 11. It is intended to compare the experimental data with the described thermodynamic model in the near future in order to discuss the chemical processes occurring in repository conditions.

The contribution of **PSI** to WP4 is focused on the influence of redox conditions on the immobilization of Neptunium in highly alkaline cementitious environments. In many sorption databases, sorption values for tetravalent actinides such as Np(IV), and Pu(IV) are often estimated based on their chemical analogy with Th(IV), an actinide for which sorption data are more easily experimentally accessible (Wieland and Van Loon, 2003). On the other hand, the sorption behaviour of Np(V) is expected to be similar to bi- or trivalent metal cations based on its effective charge of 2.3. In general, actinides sorption is influenced by the effective charge of the cations and by steric effects and sorption strength follows the same trend as complexation. The order of increasing complexation / sorption strength is: Na^+(+1) $<<Ca^{2+}$(+2) $< AnO_2^+$(+2.3) $< An^{3+}$ (+3) $< AnO_2^{2+}$ (+3.3) $< An^{4+}$(+4) (Choppin, 1983; Choppin, 2006).

The PSI contribution to WP4 aims at validating these assumptions.

During the first year of WP4, emphasis was mainly put on Neptunium speciation calculations under hyperalkaline conditions and the development of experimental procedures to control the redox conditions and measure the Np redox state during solubility and sorption experiments. Furthermore some preliminary Np solubility tests under anoxic and reducing conditions as well as a few Np(V) sorption tests on calcium silicate hydrates (C-S-H) phases, the main sorbing component of hardened cement paste, under anoxic conditions. During the second year of Recosy, more detailed Np(IV) and Np(V) solubility studies were carried out. In addition, detailed investigations of the sorption of Np(V) on C-S-H phases and hardened cement paste were started. Finally, a study on the complexation of Np(IV) with gluconate was started and the complexes obtained were compared with known Th(IV)-GLU complexes in an attempt to obtain more confidence in chemical analogy of Np(IV) and Th(IV) under hyperalkaline conditions.

Neptunium speciation under hyperalkaline conditions

Current thermodynamic databases such as the Nagra-PSI Chemical Thermodynamic Database (Hummel et al., 2002) do not include stability constants for the Np(VI) hydroxyl species, $NpO_2(OH)_3^-$ and $NpO_2(OH)_4^{2-}$ but only propose limiting values for these species. Speciation calculations in the absence of CO_2 using such thermodynamic databases show a relatively large stability field for the pentavalent redox state under alkaline conditions. Predominance diagrams for Np are shown in

Figure 10. The redox neutral line (redox potential of "redox-neutral" solutions in the absence of reducing or oxidizing agents) is represented by a red line.   Including estimates for the Np(VI) complexes $NpO_2(OH)_3^-$ and $NpO_2(OH)_4^{2-}$ based on the known stability constants for the corresponding U(VI) complexes (Hummel et al., 2002) results in a much narrower Np(V) stability field. Np predominance diagrams in the aqueous phase show that under redox conditions prevailing in a cementitious repository before closure (~200 mV<E_h<650mV versus standard hydrogen electrodes (SHE)), Np is either predominantly in the pentavalent state or in the hexavalent state depending on the choice of the Np(VI) complexes. Below a redox potential of roughly 0 mV, Np(IV) becomes the dominating redox species. In the solid phase, the Np(V) stability field might even disappear when it is assumed that the Np(VI) speciation is similar to U(VI) (Figure 10b).. On the other hand, the existence of Np(V) mixed solid phases under alkaline conditions, such as $Ca_{0.5}NpO_2(OH.)_2$ (Altmaier et al., 2007) might result in a stabilisation of the Np(V) redox state (not shown in Figure 10). The above discussion makes clear that a thorough knowledge of the redox behaviour of neptunium under alkaline conditions is a prerequisite for a proper understanding of the neptunium sorption on cementitious materials. Key data are still missing in this field.
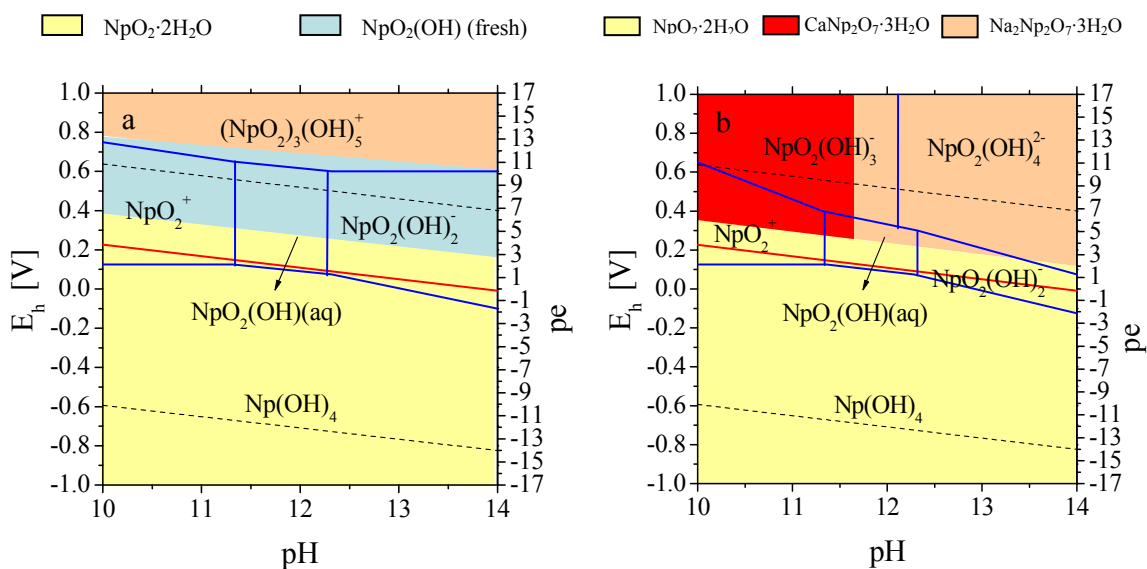
Figure 10: Neptunium predominance diagrams under alkaline conditions in the absence of CO_2 . [Ca]=10^{-2} M; [Na]=0.3 M. a. Calculations carried out using the existing chemical thermodynamic database (Hummel et al., 2002). b)Calculations assuming Np(VI) aqueous and solid speciation similar to U(VI); i.e. $NpO_2(OH)_3^-$, $NpO_2(OH)_4^{2-}$ stability constant and $CaNp_2O_7 \cdot 3H_2O$, $Na_2Np_2O_7 \cdot 3H_2O$ solubility products in analogy with U(VI . The red line is the redox neutral line (pe=13.8-pH (Neck et al., 2007)

To allow a proper interpretation of Np sorption data, it is necessary to have a knowledge of the precipitation behavior of Np under alkaline conditions. Therefore, prior to the sorption investigations, series of Np(V) and Np(IV) precipitation tests were carried out in alkaline solutions with different compositions and pH. Figure 11 shows the results of two precipitation tests with Np(V) in a 0.01 M $Ca(OH)_2$ solution at pH = 12.3 and in ACW at pH = 13.3.
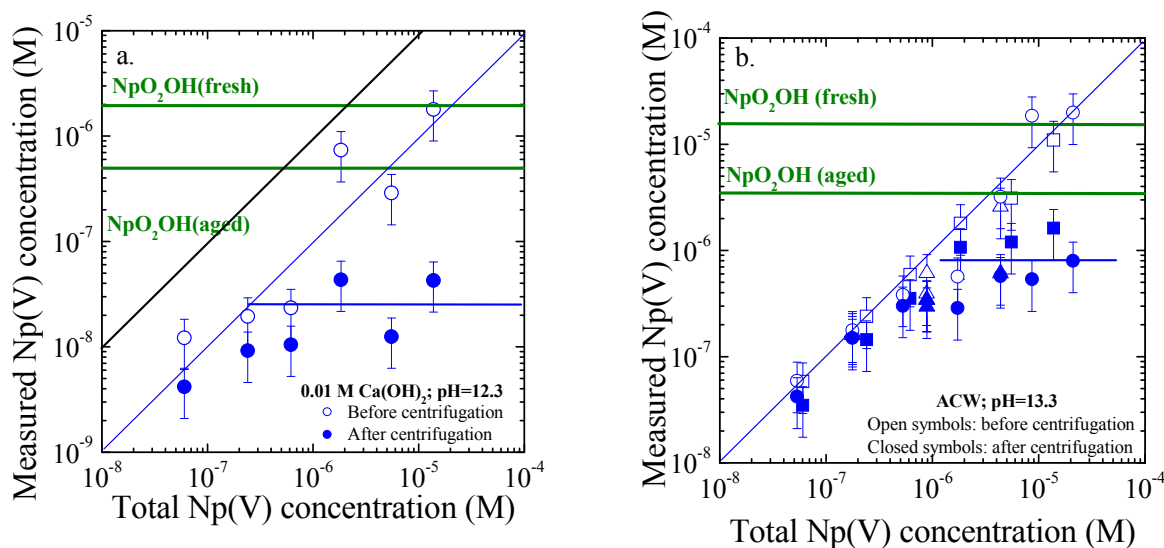
Figure 11: *Np(V) precipitation tests in alkaline solutions. Open symbols represent the Np(V) concentrations in solution before centrifugation. Closed symbols represent the Np(V) concentrations in solution after centrifugation. a. in 0.01 M Ca(OH)$_2$ at pH = 12.3. b) in ACW (0.112 M NaOH, 0.18 M KOH, 1.6·10^{-3} M Ca(OH)$_2$) at pH = 13.3.*

Overall the Np(V) solubilities found in both cementitious porewaters at pH 13.3 and 12.3, are significantly lower than the solubilities calculated assuming NpO$_2$OH(fresh) or NpO$_2$OH(aged) to be the solubility-controlling phase. The presence of mixed Ca-Np(V)-OH phases as observed by Altmaier et al. (2007) might explain the observed solubilities under highly alkaline conditions. The experimental Np(IV) solubilities measured in the presence of Na-dithionite (5±4·10^{-9} M) at pH = 12.3 and 13.3 fitted very well with calculated Np(IV) solubilities assuming NpO$_2$·2H$_2$O to be the solubility controlling phase (10^{-9} M). Np solubilites under hyperalkaline conditions will be investigated in more detail in collaboration with KIT/INE in the framework of an ACTINET-I3 project.

Np(V) sorption studies on C-S-H phases

Sorption studies were performed following the procedure described in the 1st Recosy Annual Workshop Proceedings (Tits, 2009). Most experiments were carried out without redox control, but in a few sorption tests, de E$_h$ value was fixed to +190 mV with the help of a potentiostat to ensure Np to remain in the fivevalent state. The sorption distribution ratios (R$_d$ values) measured for the Np(V) sorption onto C-S-H phases are surprisingly high (R$_d$=(6±4)·10^5 L kg^{-1}) (see Figure 12) compared to R$_d$ values for Th(IV) (R$_d$=(4±2)·10^5 L kg^{-1}) and U(VI) (10^3 L kg^{-1} < R$_d$ < 10^5 L kg^{-1}) measured in our laboratory on the same C-S-H phases in the same experimental conditions. Indeed, assuming that actinide sorption onto mineral oxide surfaces under the same chemical conditions is determined by their effective charge (E.C.) (Choppin, 2006), NpO$_2^+$ sorption (E.C. = +2.3) is expected to be weaker than AnO$_2^{2+}$ sorption (E.C. = +3.3) and An(IV) sorption (E.C. = +4) under similar chemical conditions.

Np(V) sorption kinetic tests showed that the sorption is a 2 step process; A fast step taking a couple of hours, is followed by a slower step continuing for approximately 1 week (Figure 12). During this slow sorption process, measured E_h values in the suspensions containing Np are ~0.15 V lower than E_h values in suspensions without Np. Furthermore the E_h values in the presence of Np appear to decrease gradually with the reaction from +0.1 V to ~0.0V. These observations and their consequences for the Np redox speciation are currently evaluated.
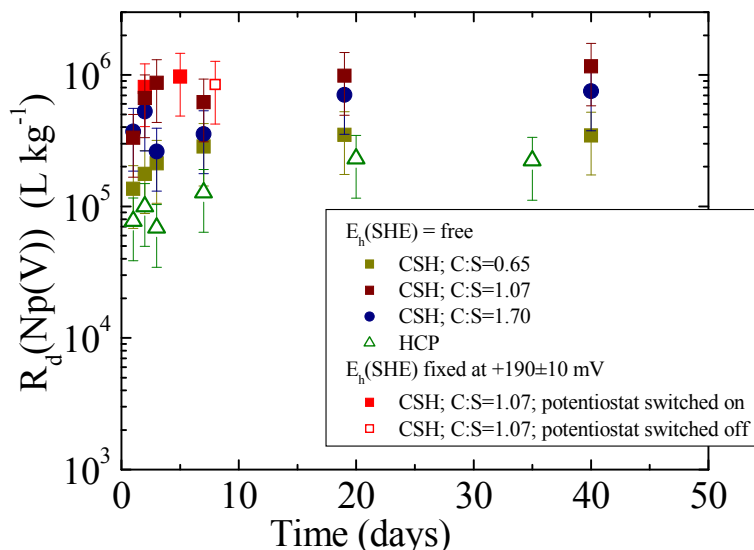
Figure 12: *Np(V) sorption on C-S-H phases with various C:S ratios as function of the reaction time.*

Np(IV) complexation with gluconate under alkaline conditions

In order to gain more confidence in the assumption that Th(IV) is a good chemical analogue of Np(IV) under hyperalkaline conditions, its complexation behaviour with gluconate (GLU) was studied and compared with the GLU complexation of Th(IV). The Np(IV) – GLU complexation was determined by measuring the effect of increasing aqueous GLU concentrations on the Np(IV) sorption on a Biorad 50W-X2 resin under hyperalkaline solutions having pH values between 11.0 and 13.3 and in the absence and presence of Ca. It was found that Np(IV) forms complexes with GLU having similar stiochiometry as Th(IV) - -GLU complexes (i.e., a 1:1 Np(IV)–GLU complex $(Np(OH)_4(GLU)^-)$ in the absence of Ca and a 1:1:2 Ca-Np(IV)–GLU complex $(CaNp(OH)_4(GLU)_2)$), but higher values for the respective complexation constants, as was predicted by linear free energy relationships (LFER).

References

Altmaier, M., Banik, N.L., Hauser, W., Klenze, R., Lindqvist-Reis, P., marquardt, Ch., Neck, V. Panak, P.J., Rabung, Th., Runke, J., Skerencak, A., Fanghänel, Th. 2007… Chemistry and thermodynamics of actinides in aqueous solution. In: Institute for Nuclear Waste Disposal, Annual Report 2007. H. Geckeis; R. Klenze (Eds.)

Wissenschaftliche Berichte FZKA 7444, Forschungszentrum Karlsruhe, Karlsruhe, Germany.

Choppin, G. R., 1983. Solution chemistry of actinides. Radiochim. Acta **32**, 43-53.

Choppin, G. R., 2006. Actinide speciation in aquatic systems. Marine Chemistry **99**, 83-92.

Fujiwara, K., Yamana, H., Fujii, T., Kawamoto, K., Sasaki, T., Moriyama, H., 2005. Solubility of uranium(IV) hydrous oxide in high pH solution under reducing conditions. Radiochim. Acta., 93, 347-350

Guillaumont, R., Fanghänel, J., Neck, V., Fuger, J., Palmer, D.A., Grenthe, I., Rand, M.H.. 2003. Chemical Thermodynamics 5. Update on the Chemical Thermodynamics of Uranium, Neptunium, Plutonium, Americium and Technetium. NEA OECD, Elsevier.

Hummel, W., Berner, U. R., Curti, E., Pearson Jr, F. J., and Thoenen, T., 2002. Nagra-PSI chemical thermodynamic database, version 01/01. Universal Publishers / Upubl.com, New York.

Lujanienė, G., Šapolaitė, J., Radžiūtė E. and Aninkevičius, V. 2009. Plutonium oxidation state distribution in natural clay and goethite, J Radioanal Nucl Chem. 282:793–797.

Wieland, E. and Van Loon, L. R., 2003. Cementitious Near-Field Sorption database for Performance Assessment of an ILW Repository in Opalinus Clay PSI Bericht 03-06. Paul Scherrer Institut, Villigen, Switzerland.

WP 4.2.

Chemical and redox behaviour of the investigated radionuclides in the different systems through microbial mediated processes

Evelyn Krawczyk-Bärsch[1], Dalis Baltrunas[2]

[1]Institute of Radiochemistry

Forschungszentrum Dresden-Rossendorf, Germany (FZD)

E.Krawczyk-Baersch@fzd.de

[2] Institute of Physics, Lithuania (IPL)

Introduction

Within WP 4.2 the participating institutes are focusing their work on the study of the microbial impact (IPL) and on the oxygen concentration and uranium redox state in-situ in biofilms with emphasis on biologically mediated redox processes (FZD). The studies are carried out on isolated microorganisms as well as on biofilms. Biofilms are composed of bacteria, fungi, algae, protozoa, exopolymeric substances (EPS), corrosion products and 50–95% water. They are ubiquitous and have to be considered as an important factor in natural biogeochemical processes influencing the redox state of radionuclides. They show a multiplicity of interactions with metals and contribute to metal mobility or immobilization.

Work performed by partners

The activities of **FZD (8)** during the second year of ReCosy were focused on biologically mediated redox processes of in-situ biofilms growing in a uranium mine in Saxony (Germany), which is currently in the process of being remediated. In the past the uranium production in this uranium mine was achieved by leaching the sandstone with sulphuric acid. As a consequence the geochemistry of the drainage waters of this mine site has changed resulting in acidic, sulfate-rich waters combined with a dramatic increase of heavy metals, especially uranium. Since 2001 the mine has been flooded for remediation processes. In the acid mine water biofilms have formed and occur as gelatinous filaments, so-called macroscopic streamers and as stalactite-like snottites, hanging from the ceiling of the galleries. The consistency of the biofilms is mostly mucilaginous due to the living microbiological community. Acidic mine water (pH = 2.61) with a uranium concentration of approximately $3x10^{-4}$ M is dropping from the ceiling and percolates the snottites (Arnold et al., 2010). Analysis of the amplified 16S

rRNA gene fragments were carried out on these snottite-biofilms for determination of the bacterial diversity. The results showed that the clone library from these biofilms is dominated by *Ferrovum myxofaciens*, acidophilic, autotrophic, iron oxidizing bacteria, which belongs to the *Betaproteobacteria*. A number of microsensor profiles of the redox potential were performed on these snottites. For this the microsensors of the Clark-type were immersed into the biofilms starting the microprofiling at the biofilm/air interface and becoming progressively immersed into deeper biofilm zones of the biofilm. A miniaturized platinum electrode from Unisense (Denmark) with a tip diameter of 10 μm was connected via a high-impedance millivoltmeter and fixed in a holder on a motor-driven micromanipulator stage, connected with a motor controller, for a precise small-scale positioning and for automated measurements in 20 μm steps. The reference electrode was a simple open-ended Ag/AgCl electrode with a gelstabilized electrolyte. The obtained values were corrected using a correction factor after Camman and Galster (1997), which is dependent on the temperature and the molar concentration of the electrolyte of the reference electrode. At the biofilm/air interface of the biofilm, where a thin water film covers the biofilm, a redox potential of 728 ± 9.5 mV was measured. Inside the biofilm the redox potential increased to 834 ± 10 mV in a depth of 1350 μm, where the highest values were observed. We assume that the increase of the redox potential results in the biological oxidation of Fe(II), which seems to be strongly catalyzed by the acidophilic, Fe-oxidizing bacteria *Ferrovum myxofaciens* following the equation:

$$Fe^{2+}_{(aq)} + 0.25\ O_{2\ (aq)} + H^{+}_{(aq)} = Fe^{3+}_{(aq)} + 0.5\ H_2O$$

As a result of the biologically catalysed rapid oxidation and subsequent hydrolysis of dissolved Fe meta-stable and poorly crystallized Fe mineral phases, e.g. schwertmannite are forming depending on the water pH. Precipitates of schwertmannite were determined by transmission electron microscopy (TEM) in combination with electron energy loss spectroscopy (EELS) in the extracellular polymeric substances (EPS) of the biofilms between the bacterial cells. However, analysis by TEM/EELS did not provide any microscopic and spectroscopic evidence for the presence of uranium immobilisation within the investigated snottite-biofilms. The analytical data of the bulk water was used for the calculation of the predominance fields of different uranium species in the pH-Eh diagram for the U-S-O-H-C system at 15°C by using the geochemical speciation code "Geochemist´s Workbench" Version 8.0.8 / ACT2 Version 8.0.8. The default data base used was the thermo.dat accompanying code, supplemented by the most recent NEA database for uranium (Guillaumont et al., 2003), and by solubility data for Uranophane from Nguyen et al. (1992). As shown in Fig. 1 the theoretical predominance fields of uranium species under the ambient condition found in the AMD are defined clearly in areas characterized by pH > 4.6 or by a redox potential < 280 mV. The mineral sequence is determined by the respective solubility constants, and follows for oxidizing conditions and increasing pH the order of Uranophane (Ca(UO$_2$)$_2$SiO$_3$(OH)$_2$•5(H$_2$O), Soddyite (UO$_2$)$_2$SiO$_4$•2H$_2$O, Bequerelite (Ca(UO$_2$)$_6$O$_4$(OH)$_6$•8H$_2$O) and CaU$_2$O$_7$•3H$_2$O.

The results of the redox potential measurements in the biofilm and in the bulk solution were plotted together with the achieved pH values of 2.58 in the biofilm and 2.61 in the bulk solution into the calculated pH-Eh diagram for the U-S-O-H-C system.

The plots appear in the area of aqueous solution, indicating that an aqueous uranium(VI) sulfate complexation exists under these conditions in the biofilm as well as in the bulk solution (see. Figure. 1).
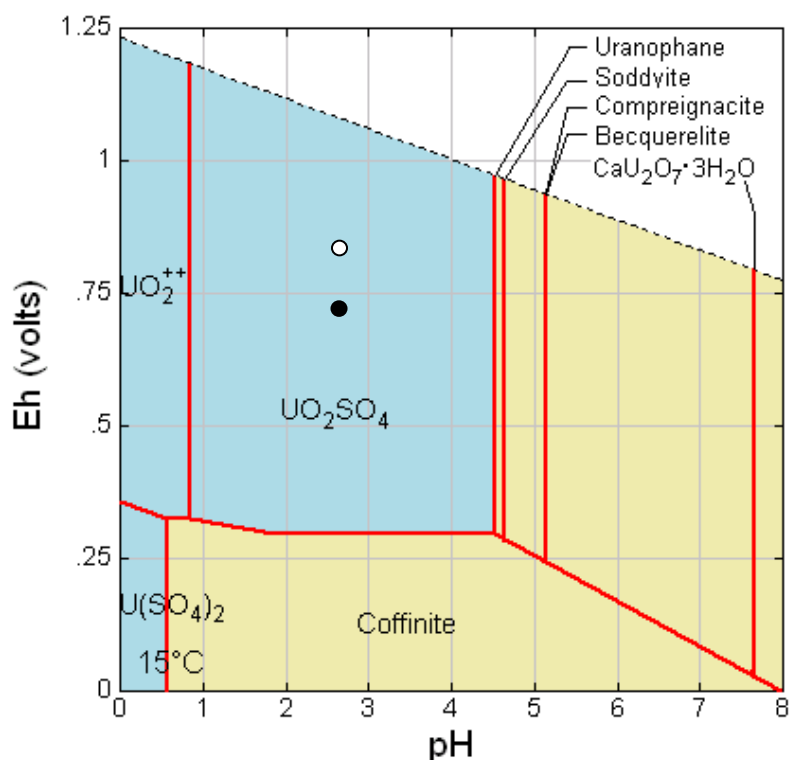
Figure. 1: *ph-Eh diagram for U-S-O-H –C system at 15 °C. The analytical data of the bulk water was used for the calculation of the predominance fields of different uranium species, using the database GWB. Eh and pH data correspond to the ambient condition measured in the AMD solution (●) and within the biofilm (⊗).*

In the case that the local conditions in the underground uranium mine will change (e.g. closure of the galleries, ingress of water) the situation described in the pH-Eh diagram will change rapidly. The microorganisms will adapt themselves to the new anaerobe conditions. Oxidizing conditions will change to reducing conditions accompanied by a decrease of the redox potential and an increase of the pH. Thus, the formation of solid uranium(IV) species could be expected.

The scientific activities of **IPL (21)** during the second year within ReCosy comprised the effect of microorganisms on plutonium oxidation states. First series of laboratory experiments of possible microbial activity mediated redox processes which can contribute to the change in plutonium mobility or immobilization and transport behavior were carried out. The tests were performed using microorganisms isolated from a dust on wooden (W) and cardboard (C) surfaces at a low-level waste repository site in the territory of the Ignalina NPP. Different species of cultivated microorganisms (bacteria *Bacillus mycoides, Rhodococcus lutesus,* and bacterium Gram$^-$; colony small, circular, raised, pale yellow, clear, bacilli) as well as fungi (*Paecillomyces lilacinus* and *Absidia* sp.) in 0.08 M brine were kept in contact with ^{239}Pu(IV) at low pH for 1 and 24

hours. The investigated plutonium samples with Pu(IV) concentration of $9.2 \cdot 10^{-12}$ M were prepared from Eckert & Ziegler Isotope Products stock solution. To evaluate the reaction progress, both, the solution and solid phase (microorganism biomass), were analyzed with respect to Pu oxidation states. The radiochemical trace analysis methods for determination of the oxidation states of aqueous Pu are generally effective at relatively low (10^{-8} – 10^{-12} M) concentration, therefore the anion exchange, electrodeposition and alpha spectrometry were applied in our investigations. At first, the coprecipitation of reduced plutonium on a rare earth fluoride enables the lower oxidation states of plutonium (III and IV) to be separated from the higher Pu (V and VI). The analytical procedure using the strong anion exchange resin BiO RaD AG 1x8 was applied for identification of the oxidation states of Pu (III and IV). After appropriate radioanalytical procedures were used, the electrodeposited Pu in separate oxidation states was measured alpha spectrometrically. According to the results, when $9.2\ 10^{-12}$ M ^{239}Pu in brine solution was in contact with different aerobic bacteria and fungi, bacteria *Bacillus mycoides* and Gram⁻; colony small, circular, raised, pale yellow, clear, bacilli displayed the highest effect on the plutonium oxidation states. They reduced Pu(IV) to Pu(III) in brine solution to 8-9 % during one hour, and with elapsed time of 24h of the interaction the amount of reduced plutonium came up to 15%. The tested fungi *Paecillomyces lilacinus* and *Absidia* sp. did not have an effect on the plutonium oxidation states under studied conditions.

Thus, results of our investigation suggest that some bacteria in far field waste repository environs with low-level radioactive pollution can participate in the redox processes and reductively solubilise Pu(IV) to Pu(III) in this way changing plutonium mobility.

References

Guillaumont R., Fanghänel T, Fuger J, Grenthe I, Neck V, Palmer DA, Rand MH (2003): Update on the chemical thermodynamics of uranium, neptunium, plutonium, americium and technetium. Chemical Thermodynamics Vol. 5 (OECD Nuclear Energy Agency, ed.), Elsevier, Amsterdam.

Nguyen AN, Silvac RJ, Weed HC, Andrews JW (1992) Standard Gibbs free energies of formation at the temperature 303.15 K of four uranyl silicates: soddyite, uranophane, sodium boltwoodite, and sodium weeksite. Journal of chemical thermodynamics, Vol. 24 (4), 359-376.

WORK PACKAGE 5:
REDOX PROCESSES IN RADIONUCLIDE MIGRATION

Juhani Suksi

University of Helsinki, Department of Chemistry, Laboratory of Radiochemistry, Finland

Introduction

WP5 studies the behavior of redox-active radionuclides Tc, Np, U, Pu, I and Se with an aim to determine the redox impact on their transport. Investigations are made in different redox-milieux that can be met around planned waste repositories. Radionuclide behaviour is studied in diffusion and sorption experiments and retrospectively using observations of radionuclide retardation in different natural conditions. An important question posed by WP5 is *"do the redox-reactions play a role in radionuclide retardation"*. The answer is searched for by studying the redox-state of retarded or immobilized radionuclides which is done with the help of modeling, by using various spectroscopic techniques and wet chemistry. In addition to the laboratory experiments investigations are made *in situ* at the planned repository site in Finland (Olkiluoto), in and around a phosphogypsum stack at the Vasilikos site in Cyprus and contaminated site in Mayak, Russia. The status of the investigations was presented by the partners in the 2nd ReCoSy AWS in Larnaca, Cyprus. The investigations by partners are high-lighted below.

Work performed by partners

Near natural laboratory experiments

KIT-INE continued batch-type experiments on the sorption/sorptive reduction kinetics of Tc(VII), Np(V) and Pu(IV) in the presence of fracture filling material. The Äspö granite and Grimsel granodiorite were used as sample material. Experiments were performed under equilibrium conditions to Grimsel ground water and mimicking glacial melt water intrusion. In a separate study column migration experiments were used to study the mobility of the same radionuclides as a function of ground water flow rate and in presence of FEBEX bentonite colloids. Batch experiments have been underway for one year and the kinetic data on U(VI), Np(V), Tc(VII) and Pu(IV) retardation (sorptive reduction?) are available. It was observed that the kinetics of radionuclide desorption from bentonite colloids and subsequent sorption onto fracture filling material can influence colloid-facilitated radionuclide migration. Post mortem analysis of the used

core will be made after the end of the planned experimental program. More information of the **KIT-INE**'s investigations can be found in the S+T contribution by Huber et al. in this Proceedings and in the presentation by Thorsten Schäfer presented in the 2nd AWS.

KIT-INE has collaborated with **MSU** (partner #27) in characterizing humic substances isolated from Mayak sediments and Lake Yrtyash humic colloids.

CEA continued investigations on the behaviour of U(VI) and long-lived redox active fission products Se(IV,VI) and I(-I,V) in contact with Callovo-Oxfordian (CO$_x$) argillite samples. The redox-activity of the sample material was deduced from the presence of FeS$_2$/FeOOH/FeCO$_3$ buffer. The redox impact of the buffer is being studied in diffusion experiments. Aqueous speciation of the elements is studied with HPLC, EC and TRLIF. Special effort was made to exclude experimental artefacts such as contamination by oxygen and dissolution or precipitation of carbonate phases. The experiments, from the sample preparation until the dismantling of the experiments were carried out in a N$_2$ glove box. The CO$_x$ diffusion properties for inert and anionic species were characterised using flow through experiments with HTO and ^{36}Cl. The experiments with Se (VI) and Se(IV) are under preparation. The Se, I and U species in the rock profiles will be studied using μ-LIBS and EXAFS. Through-diffusion experiment with U(VI) has been in progress for a year. The preliminary interpretation of the TRLFS spectra reveals the occurrence of CaUO$_2$(CO$_3$)$_3$$^{2-}$ or/and Ca$_2$UO$_2$(CO$_3$)$_3$^{0} as the main U(VI) species. The solutions are periodically sampled from upstream and downstream reservoirs. Quantitative analysis of U by ICP-MS is underway. Investigations are conducted by Sebastien Savoye who has replaced Michael Descostes.

Natural system studies

UH continued investigations on *in situ* behaviour of U. Investigations have been carried out in two parts: 1) by examining U series disequilibrium on fracture surfaces to identify U retardation or accumulation and 2) developing wet chemical method to study the redox-state of U accumulated on fracture surfaces. Fracture surface samples were from the groundwater infiltration area at the Olkiluoto study site. Over 40 samples were studied. Both U release from and deposition on fracture surfaces were observed. The observation of U deposition is important because relevant sample material for U redox-state investigations can be collected. Wet chemical method was further developed by studying the function of the 4M HCl extraction method to separate U oxidation states from arkose sandstone containing uraninite and brannerite as main U minerals. The minerals provide U in both U(IV) and U(VI) states, most of U occurring in U(IV), however. Extraction solution was spiked with ^{232}U(VI) to monitor U redox-state. The impact of the Fe^{2+}/Fe^{3+}-pair dissolved during the extraction was studied by masking Fe^{3+}. The status of the investigations and the results have been summarised in the S+T contribution submitted to the 2nd AWS Proceedings. Collaboration concerning development and application of the extraction method has been started with other partners.

II-HAS is investigating the reduction driven retention of I, Tc and U in a redox gradient in clay rock. Experimental design consists of a diffusion cell where a redox gradient is established by different redox conditions in the respective ends of the cell.

The cell is equilibrated with radionuclides keeping redox conditions constant along the clay sample. Then one end is subject to strongly reducing or oxidizing conditions. Depending on the radionuclide it will be enriched in the zone where the least mobile phase is formed. Post-mortem analysis, including Laser Ablation ICP-AES will be used to provide the information on the location of redox sensitive elements. Collaboration with KIT-INE and UH on the more advanced post-mortem analyses has been started.

UCYPRUS continued investigations to assess the impact of redox conditions on the stability of the phosphogypsum stack (e.g sulfate reduction) and U(VI). The redox conditions are correlated with the distribution and mobility of redox sensitive radionuclides. Samples have been collected directly from the phosphogypsum stack and from fluids from three different sub-areas of the phosphogypsum stack. The solid samples were investigated by TGA, XRF and XRD regarding their water content and composition. The stack fluids have been analyzed regarding pH, EC, Eh, the main constituents and uranium concentration in solution.

In situ measurements were carried out at the phosphogypsum stack. pH, E_H and solubility experiments were performed also in simulated laboratory systems. Generally, in the open phosphogypsum stack oxidizing conditions predominate stabilizing sulphur and uranium in their hexavalent oxidation state. After the application of a soil/vegetative cover and in the presence of natural organic matter, anoxic conditions prevail (E_H < -70 mV) probably resulting in S(VI) and U(VI) reduction to S(-II) and U(IV), respectively. UC and UH have started collaboration to study the redox-state of U in the samples.

MSU has investigated actinide speciation in samples collected at contaminated sites in Russia to verify the experimental data obtained under well-defined laboratory conditions. The methods included (1) redox speciation of actinides by spectroscopic methods (XPS, XAFS) and membrane extraction, (2) study of possibility of formation of An(IV) eigencolloids by alpha track analysis, TEM, STEM-HAADF, EELS and XAFS and their evolution upon redox transformations, dilution, changes of pH, Eh, ionic strength, interaction with NOM, (3) study of preferential binding of actinides to different colloids by nano-SIMS and their redox speciation by membrane extraction. MSU has collaborated with KIT-INE to characterize humic substances isolated from Mayak sediments and Lake Yrtyash humic colloids.

WORKPACKAGE 6:
REDOX PROCESSES AFFECTING THE SPENT FUEL SOURCE-TERM

Detlef H. Wegen[1][*], Paul Carbol[1], Alice Seibert[1], Thomas Gouder[1], Mats Jonsson[2], Martin Trummer[2], Andreas Loida[3], Bernhard Kienzler[3], Daqing Cui[4], Kastriot Spahiu[6], David Dobrev[5], Antonín Vokál[5], Petr Brůha[5], Radek Červinka[5]

[1] Institute for Transuranium Elements (ITU), (DE)

[2] KTH Chemical Science and Engineering, Nuclear Chemistry, Royal Institute of Technology, (SE)

[3] Institut für Nukleare Entsorgung (INE), KIT, (DE)

[4] Studsvik Nuclear AB, (SE)

[5] Nuclear Research Institute Řež plc (NRI), (CZ)

[6] Svensk Kärnbränslehantering AB (SKB), (SE)

* Corresponding author: Detlef.Wegen@ec.europa.eu

Introduction

The source term from spent fuel dissolution is subject to considerable uncertainties, both with respect to the presence and extent of oxidative dissolution processes of the spent fuel itself and the coupling with processes associated with the iron canister. Related problems to be examined in this work package are the representativeness and reliability of laboratory data with respect to the impact of unavoidable minor concentrations of oxygen also in inert-gas boxes used, the potential reactivity and its outcome of hydrogen from container corrosion in combination with high burn-up spent fuel, possible galvanic coupling of spent fuel and container material and the retention of redox sensitive radionuclides by relevant minerals, especially by steel container corrosion products.

A set of investigations has been conducted with the aim of getting better insight into redox processes determining spent fuel and iron canister corrosion. **ITU** reports on studies on spent fuel in presence of corroding Fe and on thin film model systems, on corrosion of spent fuel in presence of H_2 and on fuel corrosion studies on thin film model systems. Effects of Y_2O_3 doping on the redox reactivity of UO_2 have been studied at **KTH**. The reductive trapping of actinides in container corrosion products during spent fuel corrosion is investigated by **INE**. **Studsvik** reports on advances in the reductive immobilization of ^{237}Np on iron canister material under repository conditions

and on a problem connected with a temporally leave of a responsible scientist. As corrective action it is proposed to replace a part of the work programme with investigations on the hydrogen catalytic effect of SIMFUEL by D/H isotope exchange method. The effect of iron corrosion on redox potential was studied by **NRI**.

Advances within the work packages

Studies on spent fuel in presence of corroding Fe and on thin film model systems

ITU has prepared electrodes for galvanic coupling experiments from SIMFUEL and UO$_2$. Slices from SIMFUEL and UO$_2$ pellets were cut to act as electrodes. Stoichiometric UO$_2$ has a low electric conductivity at room temperature which results in a high ohmic resistance. A high ohmic resistance of electrodes in galvanic coupling experiments is a potential source for uncertainties.

The electrical resistivity of UO$_2$ decreases with increasing grain size and oxygen content. Therefore the UO$_2$ slices were slightly oxidised in two annealing steps. In a first annealing step in Ar/H$_2$ the O/U ratio was fixed at 2.00. Then in a second step the UO$_{2.00}$ was oxidised in a CO/CO$_2$ (1/100) gas mixture at 1300°C to UO$_{2.07}$. The stoichiometry was checked for both steps with thermal gravimetric analysis.

Measurements of the electrical resistivity by impedance spectrometry show (Figure 2) that the resistivity of the oxidised samples is reduced by a factor of two. A factor of 10 lower resistivities was found for the SIMFUEL samples simulating a burn-up of 3% - 8% which contain metallic particles.
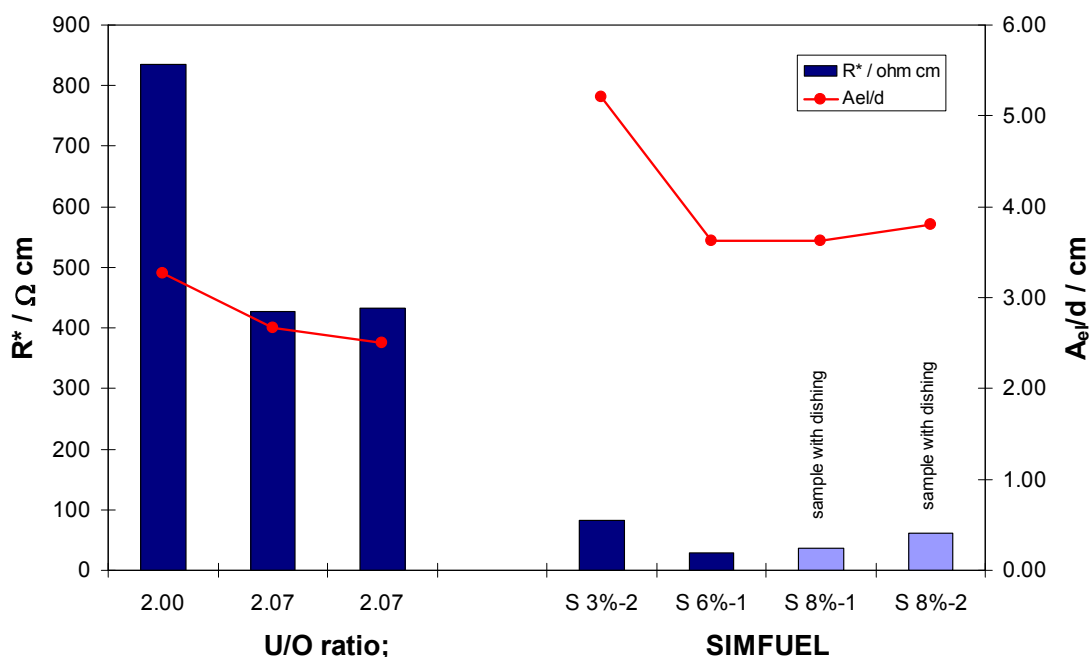
Figure 2: *Measured electrical resistivity of UO$_2$ and UO$_{2.07}$ (left) and SIMFUEL samples. The geometric surface (A$_{el}$) to thickness (d) ratio is also shown.*

The samples were then electrically conductive mounted in special electrode holders and after embedding in resin they were mechanically polished.

Due to a repair of the annealing device a delay of 6 months occurred. Therefore it was decided to start experiments with a new developed electrochemical cell for thin film applications. This cell is connected to the vacuum system of a XPS/UPS spectrometer. The construction allows a transfer of electrodes from the cell into the spectrometer without any exposure to air. A further advantage is the low resistance of thin UO$_2$ films. On the other hand is there a risk of O$_2$ inleakage because it is not installed inside a glove box.

Special manufactured carbon steel supports were fully or partially coated with UO$_2$ by reactive sputtering and then used as electrodes. The stoichiometry of the films was checked by XPS analysis before and after the experiments. It was found that the films contained a slight thorium contamination from the sputter source. After 2 minutes pre-cathodisation at -1.3 V open circuit potentials (OCP) were measured over 20 hours on uncoated, partially coated and fully coated carbon steel specimen in 10 mM NaCl solution under Ar-purging at 19°C-22°C. The measured Eh dropped in the first hours and increased then to a constant value after 10 hours between 440 and 490 mV$_{SHE}$. The pH was 4.5 to 5.
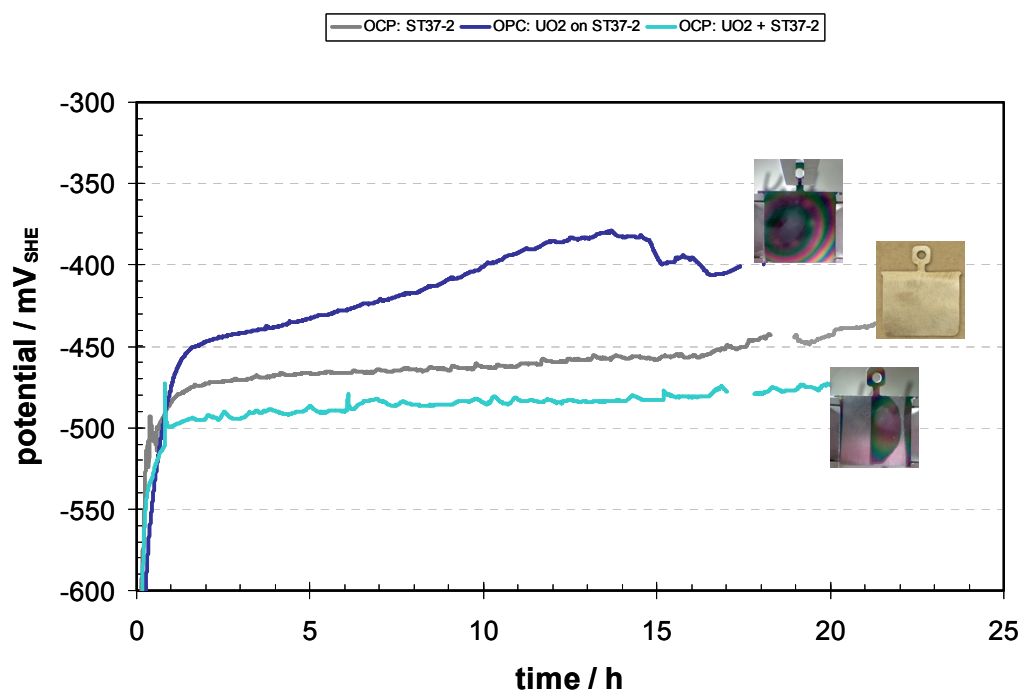
Figure 3: *Open circuit potentials (OCP) measured on carbon steel and on fully and partially UO$_2$ coated carbon steel in Ar-purged 10 mM NaCl solution at RT.*

The measured mean OCP are for carbon steel -450 mV$_{SHE}$ (Eh=+490 mV$_{SHE}$) and for the half with UO$_2$ covered carbon steel -480 mV$_{SHE}$ (Eh=+440 mV$_{SHE}$). Taking into account the slightly more oxidising condition in case of the steel the measured OCP are comparable. A still negative but clearly more anodic OCP of ~-400 mV$_{SHE}$ (Eh=+460 mV$_{SHE}$) was found for the fully UO$_2$ covered steel sample. Microscopic examination of the UO$_2$ film after the experiment show defects in the UO$_2$ film accompanied with a localised attack of the steel. The system shows a galvanic coupling, where the UO$_2$ is cathodically polarised by the corroding steel which predominates the measured OCP in all three cases. The potential at the UO$_2$ / solution interface is shifted

into the cathodic (reducing) regime, this protects the UO_2 surface to be oxidised. XPS surface analysis done immediately after exposure supports this. No oxidation of the UO_2 surface could be detected.

Corrosion of spent fuel in presence of H_2

The corrosion experiments of the high burn-up structure zone of commercial spent nuclear fuel in presence of 4.1 MPa hydrogen gas pressure, i.e., a dissolved H_2 concentration of 33 mM, has continued as planned at **ITU**. A detailed description of the fuel, the inventory and the initial corrosion results for the first 60 days is given in Buckau et al. (2009). Results obtained in the period 0 to 503 days are summarized in the following. Detailed information of the experiment can be found in Fors et al. (2009).

Sampling

Leachates were sampled 10 times throughout the corrosion experiment; during filling (5 hours after wetting the fuel), and after 1, 7, 62, 63, 138, 265, 313, 316, 319 and 329 days. The sampling sequence consisted of one rinse and two samples.

ICP-MS and γ-spectrometry analysis

Inductively coupled plasma mass spectrometry, ICP-MS (Thermo Element2, Thermo Electron Corporation, Germany), measurements were made on all samples to determine the concentration of the elements.

All samples were analysed in duplicates, one with and one without internal standard addition. The elements Sc, Co, In and Ho, and the isotope ^{236}U were used as internal standards. All samples were acidified to 1 M HNO_3. The limit of detection for actinides was approximately $1.0 \cdot 10^{-12}$ M whereas the transition elements and lanthanides had a limit of detection of $1.0 \cdot 10^{-11}$ M.

The concentration of the γ-emitters in the leachates were measured using γ-spectrometry. The limit of detection of the γ-spectrometry system depends on a number of parameters, but is in general in the range of 0.1 Bq.

Results of the corrosion experiment

The main concern of these results, in relevance to the ReCosy project, are the behaviour of redox sensitive actinides (U and Pu), fission product (^{137}Cs, fission Mo) and natural elements (Fe, Mn, and Mo) existing in the leachate in contact with the rim structure of the spent UO_2 fuel, during the period 0-313 days, the wash-out action (seven stepwise dilutions of the stagnant 140 cm^3 leachate, which always remains below the dip tube in the autoclave after emptying) during the days 313-314 and the sampling after this on day 329. The pH is in the range of 7.2-8.5 and the temperature 23±4 °C.

^{238}U and ^{137}Cs

In the initial 62 days of the experiment a fast instant release of ^{137}Cs from the fuel fragments is observed in the first leachate. The subsequent leachates contain lower Cs concentrations as a result of additional filling of the autoclave. The amount of dissolved ^{137}Cs remains constant at a level of $3.75 \cdot 10^{-7}$ mol during the time period 7-62 days. On the other hand, the concentration of ^{238}U in the leachate decreases by a factor of 40, from $6.3 \cdot 10^{-9}$ M to $1.5 \cdot 10^{-10}$ M, during the initial 62 days. The refilling of the autoclave with fresh solution leads to a sharp increase in the ^{238}U concentration and is a response to oxidation of the fuel surface. In the following the ^{238}U concentration is decreasing and the ^{137}Cs concentration is constant. During the following wash-out action the ^{238}U concentration was lowered to a concentration similar to the concentration before the refilling. The concentration of Cs was first lowered by three orders of magnitude during the wash-out action; and increases then towards a new stable concentration at $2.4 \cdot 10^{-9}$ M, an increase by a factor of 4 compared to the lowest value, but still 130 times lower than before the wash-out action.

^{239}Pu

Owing to the dissolution of the pre-oxidized surface layer, the ^{239}Pu concentration shows a correlated increase with the ^{238}U in the beginning of the experiment. The first sampling shows the expected Pu/U ratio of 0.015.

The almost parallel decrease in ^{239}Pu and ^{238}U concentrations, indicate that ^{239}Pu is very probably co-reduced with the ^{238}U. During this co-reduction part of the experiment, the ^{239}Pu concentration passes through a minimum and then starts to increase towards a steady state concentration level of $\sim 3 \cdot 10^{-11}$ M.

Fe, Mn and Mo

The stable redox sensitive elements such as Fe, Mn and Mo originating from the inner surfaces of the autoclave is of interest to study since they contribute to the understanding of the redox processes inside the autoclave.

The correlation between the elements Fe, Mn and ^{239}Pu is relatively strong. At the occasion of leachate refilling (day 63) the ^{239}Pu concentration increases due to dissolution of re-precipitated ^{239}Pu and fresh fuel while the concentration of Fe and Mn decreases, as expected due to dilution. No correlation was found between natural Mo and ^{239}Pu, the changes that occur are related to the dilution of the leachate during refill of the autoclave. The general conclusion is that the redox processes occurring in the autoclave affects all redox-sensitive elements.

Summarising the corrosion of high burn-up structure of a UO$_2$ fuel shows that the iron concentration is linked to the changes of Pu which in its turn is correlated to the ^{238}U concentration changes. It can also be concluded that both Fe and U varies within a concentration range of two orders of magnitude. On the other hand, the number of oxidised/reduced moles of Fe is much larger (two orders of magnitude) than the moles of U.

Conclusions

Steady state was reached for the U- and Pu-concentration of $1.5 \cdot 10^{-10}$ M and $3 \cdot 10^{-11}$ M, respectively. The release of Cs almost stopped which indicate an almost insignificant corrosion of the UO_2 matrix. The redox-sensitive natural elements; Fe, Mn, Mo behave more similarly to Pu than U. The fact that Fe behaves similarly to Pu makes it an important tool for redox determination.

Detailed information is can be found in the S&T contribution section of the 2nd Annual Workshop Proceedings 7th EC FP - ReCosy CP 2010 (P. Carbol et al., *"Corrosion of spent fuel in presence of H_2"*).

Fuel corrosion studies on thin film model systems

ITU has prepared thin films of uranium oxides with fission product (fp) inclusions by sputter deposition from uranium metal and palladium metal targets in the presence of O_2. These thin films can serve as model systems for spent nuclear fuel (Stumpf et al. 2009, 2010a).

The corrosion processes and the influence of the Pd inclusions (as model element for ε-particles) in these processes are investigated by gas adsorption experiments and electrochemical methods with the thin film samples.

First results on the influence of the Pd doping on reactions with H_2 are obtained from gas adsorption measurements (under vacuum conditions) with the pure and doped systems. Here we obtain no significant reaction in the system $UO_{2+x} + H_2$ while a significant reduction to stoichiometric UO_2 is observed in the system $Pd/UO_{2+x} + H_2$ (Stumpf et al. 2010b) already at very low dosages of about 5 minutes $\times$ $1.3 \cdot 10^{-5}$ mbar H_2. Obviously, the Pd is involved in the activation of H_2 on the surface. Additional experiments show that a similar reduction of pure UO_{2+x} can be obtained when activated species H_{atom} (produced in an atom source) are used instead of the H_2 molecular species. The mechanism of the H_2 activation can be deduced from these results. H_2 does not readily chemisorb and dissociate on pure $UO_{2(+x)}$, at least in the low pressure and temperature (room temperature) ranges investigated. On Pd, which is since long known as a hydrogenation catalyst, this chemisorption and dissociation reactions take place effectively and the hydrogen atoms may leave the Pd and diffuse onto the UO_2 phase. Recent studies have shown that such spill-over of adsorbed species (hydrogen, oxygen) is a fast phenomenon which can compete with the rate of catalytic reactions (Teichner (1990). Beside the inhibition mechanisms for UO_2 oxidation considered in literature (reduction of radiolytically produced oxidants by hydrogen catalysed by Pd particles, and galvanic coupling to the UO_2) a third mechanism is implied by our findings: the solid-state reaction between lattice oxygen of UO_{2+x} and surface hydrogen, reaching the UO_{2+x} phase by spill-over. The robustness of this process under repository conditions, e.g. the interaction of the ε-phase with secondary phases, sulphides (a catalyst poison), etc. has to be investigated now.

For the electrochemical investigations an electrochemical quartz crystal microbalance system (EQCM) is used. This technique allows the in-situ measurement of current response and mass changes of the electrode and therefore facilitates the interpretation of the electrochemical data and allows drawing conclusions on the underlying mechanisms more reliably. Cyclovoltammetric (CV) results for pure UO_2

thin film electrodes up to now only under oxic conditions (aerated 0.01 M NaCl solutions) at pH values varying from 5 to 10 with this advanced system are comparable with former results for bulk UO_2 electrodes (Shoesmith et al., 1994, Miserque et al., 2001, Seibert et al., 2010). For the Pd-doped UO_2 systems first results also under oxic conditions show significant differences to this behaviour: features (seen in current and mass results) in the oxidative region (> 0 V_{SHE}) are strongly suppressed for early scans, but increase with successive scans significantly. Concentration effects due to the increased Pd content of the surface can be ruled out since the comparative study with a UO_2-Au film does not show a correlation between current decrease and increase of metal concentration. Therefore, this inhibition of the oxidative UO_2 dissolution can be directly linked to the presence of Pd. Also in the reductive scan the typical feature obtained on pure UO_2 electrodes are observed with suppressed current and mass recovery at ~ -0.2 V_{SHE} in the early scans, but is found increasing in the successive scans. Additionally a feature showing a much more significant reduction current than obtained for the pure system is observed in the region ~ 0.55 V_{SHE} together with a slight mass increase. This feature distinctly increases with the Pd content but at the moment its interpretation is not accurately defined. In summary one could say that with increasing Pd doping (2 to 50 %) a stronger deviation from UO_2 behaviour is observed which also does not resemble the pure Pd system. On the other hand with increasing scans the doped electrodes converge to a behaviour resembling more and more the UO_2 electrode behaviour. The electrochemical data give rise to the assumption that Pd has an inhibiting influence on the oxidative dissolution of UO_2. Such influence can be suppressed when reductive conditions lead to the formation of secondary phases at the surface. Then the over all electrochemical behaviour is determined by the formed precipitates that overlay the Pd inclusions. Ongoing investigations deal with the post reaction characterisation of the electrodes and the influence of H_2 on the processes in solution.

Detailed information is reported in the S&T contribution section of the 2nd Annual Workshop Proceedings 7th EC FP - ReCosy CP 2010 (S. Stumpf et al., "*UO₂ Fuel Corrosion – Reactions at a UO₂-Palladium Spent Fuel Model Surface*").

Effects of Y₂O₃ doping on the redox reactivity of UO₂.

Reactivity of H₂O₂ towards Y₂O₃ and Y₂O₃/UO₂ in powder suspensions

Preliminary studies at **KTH** have shown that Y_2O_3 doped UO_2 pellets are significantly less reactive towards H_2O_2 than pure UO_2 pellets. To elucidate the effect of Y_2O_3, we have studied the stability of H_2O_2 in aqueous Y_2O_3 suspensions. The experiments clearly show that H_2O_2 reacts with Y_2O_3. The mode of reaction is most likely oxide catalyzed decomposition of H_2O_2 to H_2O and O_2. The rate constant for this reaction was determined to 10^{-8} m s^{-1}. Experiments were also performed on UO_2 powder suspensions containing 1% Y_2O_3 powder. In this case, the rate of H_2O_2 consumption and the rate of U(VI) dissolution are not significantly affected by the presence of Y_2O_3 which is also what would be expected from a strict competition kinetics point of view.

H2O2 induced oxidative dissolution of UO2 pellets doped with Y2O3, Pd and Y2O3/Pd

Experiments using pellets doped with 0.3 % Y_2O_3 and 0.1 and 1 % Pd have been performed. The main results are illustrated in Figure 4 (1 % Pd).
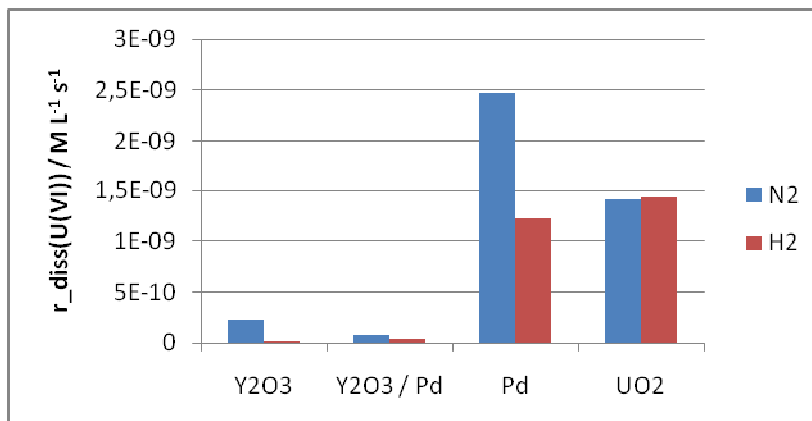
Figure 4: *Uranyl dissolution under N_2 and 1 bar H_2 atmosphere with Y_2O_3 and Pd as additives.*

As can be seen, the rate of oxidative dissolution is significantly lower for the Y_2O_3 doped material. This difference cannot be attributed to competition kinetics. Furthermore, it is clear that the oxidative dissolution yield (ratio between dissolved uranium and consumed H_2O_2) is significantly lower for the Y_2O_3 doped pellets. This implies that Y_2O_3 doping increases the activation energy for oxidative dissolution. In general, the reactivity of the pellets towards H_2O_2 is also reduced upon Y_2O_3 doping. Interestingly, this effect is enhanced in the presence of Pd.

The effect of H_2 (1 bar) was also studied. As previously shown, H_2 inhibits oxidative dissolution of Pd doped pellets. The relative impact of this effect is unaffected by the presence of Y_2O_3 (Trummer et al. 2010).

Radiation induced dissolution of UO2 pellets doped with Y2O3, Pd and Y2O3/Pd

The pellets above were also used in experiments on radiation induced dissolution of UO_2. These experiments revealed the same trends as observed in the H_2O_2 experiments.

Electrochemical studies of UO2 pellets doped with Y2O3, Pd and Y2O3/Pd

(Collaboration with Prof. David Shoesmith, University of Western Ontario, London, Ontario, Canada)

The electrochemical characteristics of pellets described above were studied. Martin Trummer spent three weeks in Canada in December 2009. So far, the preliminary results have not been fully analyzed. Cyclic voltammetry reveals significant differences between pellets containing Pd and pellets not containing Pd. Pellets doped

with Y_2O_3 did not differ significantly from pure UO_2 pellets. The electrochemical studies will be continued.

Reductive Trapping of Actinides in Container Corrosion Products during Spent Fuel Corrosion

The source term from spent nuclear fuel (SNF) dissolution is highly dependent on oxidative dissolution of the fuel matrix. Various experimental data on the dissolution behaviour of the spent fuel matrix itself and in some cases in presence of container material (initial metallic Fe powder) as well, and the associated releases of radioelements were already obtained by extensive laboratory test programs and reported e.g. in Shoesmith (2000), Ferry et al. (2005), Loida et al. (1996). The capacity of corroded canister iron phases to incorporate radionuclides is under investigation within the European collaborative project "ReCosy". The stable corrosion product of steel canister material under reducing disposal conditions is magnetite. In the present study, it was intended to investigate the reductive trapping of actinides in metallic corrosion products which may provide for a driving force for SNF dissolution. About 10 years ago, an experiment ("denoted as K14Mt") was designed at **INE** investigating the effect of magnetite on the overall corrosion behaviour of SNF in NaCl solution. This experiment was terminated and the investigations of gas atmosphere, solution composition and solid material were started.

Experimental

The corrosion experiment was performed by using a pellet sized segment of high burnup SNF (50 MWd/kg U, linear power 260 W/m), 6.6 g fuel, and 10 mm in length together with commercial available magnetite (ALFA 012962, grain size ~ 5 μm). SNF sample and magnetite were immersed simultaneously in 5 mol/L NaCl solution (initial volume 200 ml, under Ar-atmosphere), using a glass vessel. During the initial phase of the experiment, the leachant was replaced entirely by fresh solution for four times until total 65 days. This procedure reduced effectively the "initial release fraction (IRF)", such as Cs and fission gases in the gap and on grain boundaries. Afterwards the experiment was continued without replacing the solution (static), lasting over 3562 days. The gas phase and solution were sampled at 78, 215, 349, 771, 1895 and 3562 days after start of the static phase. The analytic procedures are described by Grambow et al. 1996. A detailed description of the entire experimental procedure is given by Loida et al. 2003. After termination of the experiment, fractions of the magnetite were removed and analyzed. Various methods have been applied: SEM/EDX, XRD, Raman spectroscopy, XPS, digestion in HNO_3 and consecutive radiochemical analyses. The analyses are not yet completed.

Results

Results concerning the reductive trapping of actinides in corrosion products as a driving force for spent fuel dissolution depend on the conditions kept during the 10 years of the experiment:

- Gases: In the observation period, only a slight release of Xe of < 0.01 vol.% was found. Until 10 years, the H_2 concentration in the leaching vessel

amounted to 18.5 vol.% and O_2 to 5.4 vol.%. After the first year, the CO_2 concentration raised from 0.1 to 0.8 vol.%, a value which cannot be explained by contact with air. The reason is still under investigation.

- Solution concentrations: The temporal evolution of the concentrations of released radionuclides reveals considerable differences. Between 215 and 3562 days, the Sr concentration increases from $6 \cdot 10^{-7}$ to $2 \cdot 10^{-6}$ mol/L. Release of Cs is slightly faster, whereas the mobilization of U is at the highest rate. The final U concentration was measured up to $1 \cdot 10^{-4}$ mol/L. The other radionuclides (Tc, Np, Pu and Am) are released at an intermediate rate. In total, fission gas release was >16%, Cs ~ 0.7%, Sr ~ 0.3%, and the actinides <0.1% of the inventory. After one year, the measured pH increased to 7.6 and dropped after 10 years to ~ 6.

  Model calculations for 5 mol/L NaCl solution in contact with the measured $p(CO_2)$ revealed a decrease of the pH and the presence of dissolved carbonate. Under these conditions, initially generated solid $Na_2U_2O_7$ is dissolved forming U carbonato complexes in the range of the observed concentration of $1 \cdot 10^{-4}$ mol/L. Vice versa, at pH_{exp} ~ 7.6 in combination with the measured CO_2 partial pressure, the calculated Sr concentration is in equilibrium with solid $SrCO_3$ (strontianite). The evaluation of the radionuclide release rates in relation to the actual CO_2 partial pressures is not yet completed.

- Solids: Grain agglomerations of the magnetite were recovered and investigated. Measurable amounts of U were found upon the surfaces by SEM/EDS and XPS.

  Raman spectroscopy was applied to investigate (a) if magnetite has undergone any transformation during the 10 years experiment, and (b) the redox state of U on the magnetite surfaces. The magnetite spectra of the exposed magnetite and fresh material were identical. XPS measurements show that U was present in the hexavalent state exclusively.

Conclusions

In the glass vessel used for SNF corrosion experiments over almost 10 years the atmospheric conditions were not sustained. In particular, the origin of the high $p(CO_2)$ is not yet resolved. The presence of CO_2 and O_2 explained the observed U and Sr concentrations. Under these conditions, Sr cannot be used as indicator for SNF matrix dissolution. The effect of CO_2 on the SNF dissolution rate is not yet clear.

Certain amounts of radionuclides are retained by the magnetite. Quantification is still pending. Due to the relatively high $p(O_2)$ the expectations with respect to the reductive trapping of actinides in corrosion products may not be achievable.

Future work is focused to complete the studies on radionuclide retention upon the solid phases in the system.

More detailed information is reported in the S&T contribution section of the 2nd Annual Workshop Proceedings 7th EC FP - ReCosy CP 2010 (A. Loida et al., "*Trapping of Radionuclides/Actinides in Canister Corrosion Products*").

The reductive immobilization of ^{237}Np on iron canister material under repository conditions

Interaction between iron canister material and redox sensitive radionuclides $UO_2(CO_3)_2^{2-}$, Se(IV), Se(VI) under simulated deep groundwater conditions have been investigated by **Studsvik** and it has been concluded that $UO_2(CO_3)_2^{2-}$, Se(VI)/Se(IV) can be effectively reduced and precipitated as $UO_2(s)$ or $FeSe_2$ respectively on corroded iron surface. Due to the limitation of beam line at SLS, PSI the oxidation state of reduced Tc has not been identified. A part of experimental work on the redox reactions between Np(V) and Pu(VI) and iron canister material has been conducted since 2006-2007 at Institute for Transuranium Elements, Joint Research Centre, European Commission by D. Cui during his stay as a visiting scientist, Under support and coordination of European 7th frame work, RECOSY project and **SKB**, during the first year 2008.04.01-2009-03-31, the solution samples were taken and analysed by ICP-MS. The polished and pre-corroded iron coupons with immobilized Np were prepared and analysed by SEM-EDS, and micro XRF and XANES. The detail information was reported in the FP7th EU ReCosy report proceeding (2009)

More data and results obtained in 2009 were analyzed and re-evaluated.

Np(V) immobilization on iron surfaces

Assuming the interaction between Np(V) and iron surfaces in the first 12 days at the given conditions (S/V= 0.3 cm^2/30cm^3 = 0.01 cm^{-1}) was dominated by first order reaction, the reaction rate constants for polished and pre-corroded (Fe_3O_4 coated) iron surfaces are 0.015 day^{-1} and 0.16 day^{-1}, respectively. The initial faster Np(V) immobilization on pre-corroded iron coupon than that on polished iron coupon may be explained by the availability of more surface sites on Fe_3O_4 coated iron coupons which can immobilize Np(V) by forming surface complexation.

Micro-XRF
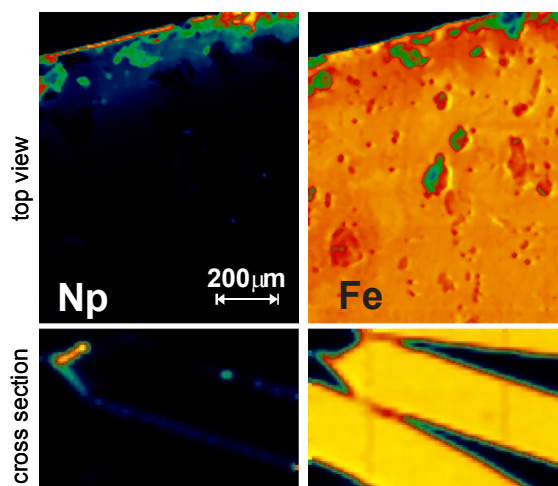
Figure 5: Results of μ-XRF analysis.

Figure 5 shows elemental spatial distributions of Fe (right) and Np (left) on a top surface (top images) as well as on a cross section (bottom images) of a representative polished iron sample determined by μ-XRF. In the bottom right- image, 3 iron samples are shown: only the arrow marked middle piece is the polished iron sample that reacted in Np(V) solution, whereas the other two are blank iron samples are given as references. Immobilized Np was found to be concentrated at the sharp rough edge of the iron sample on the left side. This edge had been cut, but not polished (bottom left image).

XANES analysis
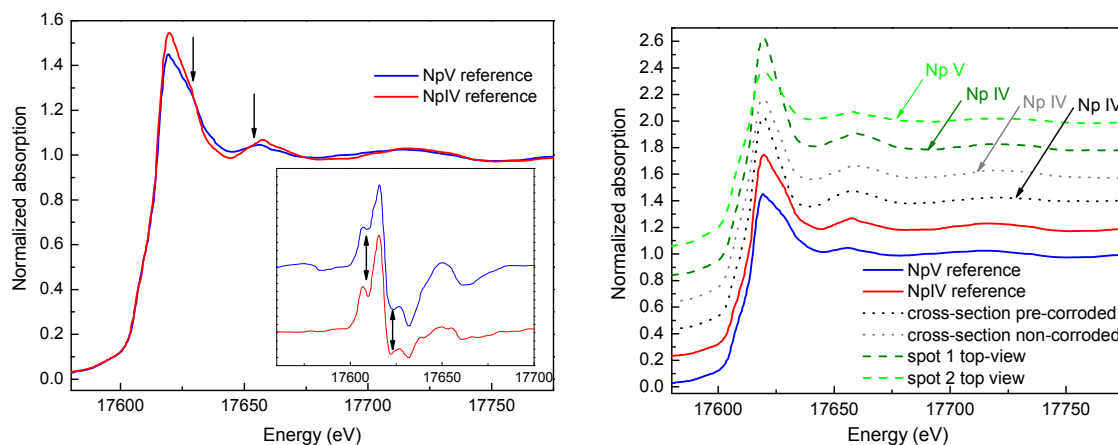
Figure 6: *Results of XANES analysis.*

Results of XANES analysis are shown in Figure 6.

The comparison of the Np L3 edge XANES spectra for Np(IV) (red) and Np(V) (blue) references can be seen on the left diagramme. The inset shows the first derivative curves. The arrows indicate differentiating features which can be used to distinguish Np(IV) from Np(V).

The plot on the right shows Np L3 edge XANES acquired for the Np(IV) (red) and Np(V) (blue) references as well as in different locations on the top-view and on the cross-section of the exposed sample on several spots on the iron sample surface, close to the edge, as well as on pre-corroded (Fe_3O_4 coated) and fresh (polished) cross-sections. Note the substantial decrease in white line intensity for the top-spectrum (taken on the top-view), indicating the presence of Np(V). Micro-XANES spectra were acquired. An article on Se(IV)/Se(IV) immobilization on iron was published (Cui et al. 2009) and a manuscript was submitted to ES&T for publication.

New experiment for Pu(VI) - Fe interactions

In the previous experiment with Pu(VI) and iron coupons, only some information about immobilization ppb level Pu(VI) was obtained. In this experimental work a new experiment with 20 ppm level Pu(VI) will be conducted in cooperation with and at **ITU**. Daqing Cui visited **ITU** in Nov 2009 to arrange and install an experimental setup in a glove box. A $PuO_2(CO_3)_2^{2-}$ species dominated Pu(IV) solution with 10mM NaCl + 2mM $NaHCO_3$ solution (pH 8) is in preparation.

Investigation on the hydrogen catalytic effect of SIMFUEL by D/H isotope exchange method

Due to the temporary leave of a co-worker at **Studsvik**, it was discussed on the 2nd annual ReCosy workshop to replace her initially foreseen activities in WP6 by the following proposed work. Beside ReCosy, **SKB** will support and coordinate this work.

In several previous experiments using normal spent fuel and ^{233}U or ^{239}Pu doped UO_2, it was observed that in the deoxygenated and hydrogen saturated water solution (simulating deep groundwater), the corrosion/leaching of either SNF (containing 4d-transition metal fission product alloy particles) or α-doped UO_2 were found to be completely blocked. These observations were explained by the following hypotheses:

1) O_2, H_2O_2 and other oxidative species generated from water radiolysis can be reduced by hydrogen only with presence of catalytic surfaces. UO_2 and fission product alloy particles may have some catalytic effect.

2) The reducing effect of hydrogen may be enhanced by radiation (in cases of SNF, alpha emitter doped UO_2. If there is α–, β–, and/or γ-radiation, H_2O_2 and OH-radicals will be generated from water radiolysis. Dissolved hydrogen (H_2 or D_2) will react with OH• and produce H_2O (HDO, D_2O) and H• (D•) radicals.

4d-transition element fission product alloy particles exist in SNF and SIMFUEL have been considered to be excellent hydrogen catalysts. However, there is a lack of direct evidence to prove its catalytic effect.

The basic assumption of the proposed experiments is that without catalysts, both hydrogen-oxygen interaction and isotope exchange between H_2 and H_2O at room temperature are extremely slow (Criss 1999, O'Neil 1986, Cole and Ohmoto 1986, Lecluse and Robert, 1994).

If the above mentioned $D_2 + O_2$ redox reaction and $D_2 – H_2O$ isotope exchange reaction in the blank experiment in a certain period (e.g., one/some week/s) can be proved to be insignificant, the observation of HDO and D_2O formed in solution with the presence of solid surfaces and/or radiation can be used as evidences for the hydrogen catalytic effects of the existing surfaces.

As a first step the hydrogen catalytic effect of SIMFUEL (containing 4d-alloy particles) will be investigated in the frame of ReCosy.

Experimental planning

D_2 with 0.003% CO_2 has been ordered. Concentration of dissolved D_2 at 10 bars will be around 15 ppm. D_2 can be purged out by Ar but all D_2O formed in solution should be stable. In experiments involving spent fuel fragments or radioactive alloy particles, the solution will be evaporated and condensed to get rid of radionuclides. If D_2O and/or HDO are detected in solution in contact with any added solid surfaces, but not in the blank experiments, the added solid should have some hydrogen catalytic effect. The 0.2% O_2 will be added stepwise by gas sampler (mL). O_2 content and N_2/O_2 ratio in the gas phase will be monitored by gas samples.

In case that the O_2 concentration will drop, 10 bar pressure will be released and 2.5 mL air will be added stepwise up to 0.2% O_2. The schedule of different batch experiments is listed below.

Exp	Gas 200mL 10bar	Solid	Location and start time
1	D_2 + 0.003%CO_2+ total 0.2%O_2	0, blank	Studsvik, 2010-03
2	D_2+ 0.003%CO_2 + total 0.2%O_2	SIMFUEL	Studsvik, 2010-05

The effect of iron corrosion on redox potential

Measuring of the redox potential evolution and modelling of the redox potential in geochemical program PHREEQC in a corrosion system under anaerobic conditions was carried out last year at **NRI**. Corrosion is affected by the redox potential, which in turn is affected by the corrosion products. Therefore the detailed knowledge of iron corrosion is crucial for the determination of the redox potential of the repository environment.

The corrosion systems consisted of 10 carbon steel plates (total surface area 997 cm^2) and 2 litres of synthetic bentonite pore water. Before the experiments carbon steel plates was polished by a sandpaper of grid 600 and washed by ethanol. Synthetic bentonite water was prepared on the same basis as that used in the NF-PRO project (Baeyens, 2005). It corresponded to the composition of sodium bentonite Volclay KWK 20-80 of a density of 1600 kg.m^{-3}. The corrosion system was placed inside the anaerobic glove box with concentration of oxygen of less than 0.1 ppm. The synthetic bentonite water was put into anaerobic box 14 days before the experiment begun.

The experiments were performed at temperatures from 40°C – 70°C for 30 days. The redox potential was measured continuously by platinum and gold electrodes and discontinuously using a platinum electrode. Also pH and hydrogen evolution rate, caused by corrosion, were measured during the experiments. After the experiment the weight loss of the carbon steel plates and concentration of Fe^{3+}, Fe^{2+} ions in the solution by UV/VIS and AAS spectroscopy was measured.

The redox potential, measured discontinuously by platinum electrode, slowly increased in all experiments except in the experiment carried out at 40 °C. In this experiment the redox potential was practically unchanged (Figure 7). It was found that the surface of gold and platinum electrodes became covered with corrosion products (oxides and hydroxides of iron). They needed to be cleaned of the corrosion products during the experiments to get reliable results. Eh values measured after cleaning electrodes were similar to values from discontinuous measuring. Contrary to Eh, the pH slowly decreases in all the experiments. The concentrations of Fe^{3+} ions in the solution after the experiments were negligible compared with concentration of Fe^{2+} ions. Corrosion rates determined by weight loss measurements were: r(70°C) = (3.5 ± 0.1) μm/year, r(60°C) = (4.01 ± 0.08) μm/year, r(50°C) = (4.3 ± 0.4) μm/year and r(40°C) = (3.1 ± 0.1) μm/year.
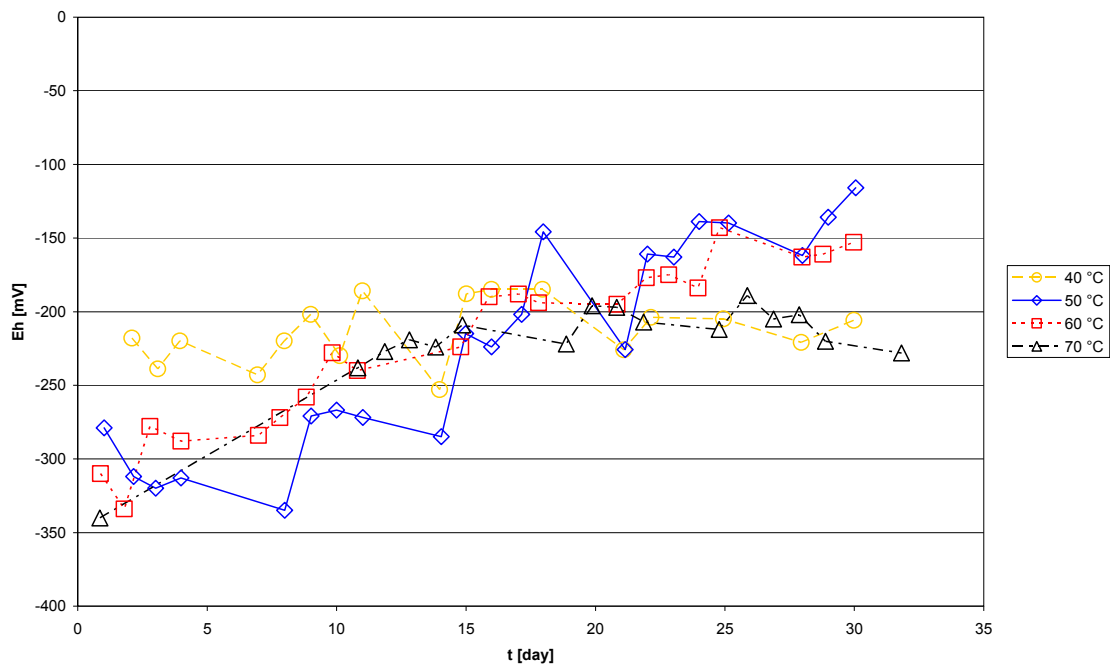
Figure 7: *Changes of Eh potentials due to corrosion of carbon steel plates.*

A simplified two stage approach was chosen for simulation of Eh evolution during the corrosion process. First, Fe was kinetically added into the bentonite porewater solution according to measured corrosion rate and on the basis of speciation in solution and Fe(II)/Fe(III) activities the Eh was calculated. In a second stage the solution was equilibrated with Fe-bearing minerals (magnetite, Fe(OH)$_2$) and Eh was calculated again. All calculations have been carried out using geochemical programme PHREEQC version 2.15.07 (Parkhurst and Appelo (1999)) with OECD NEA database (TDB NEA 17, 2005).

The input data to the model are summarised below:

- Volclay KWK 20-80 porewater was used (Baeyens, 2005).

- The pH of initial solution was 8 and Eh was –225 mV.

- Temperatures were 40, 50, 60, 70 °C and the stability constants (log K) were recalculated to this temperature on the basis of reaction enthalpy (ΔH_r^0) and Van't Hoff equation by PHREEQC itself. We supposed that the reaction enthalpy is a constant until this temperature for constant pressure for involved species and phases.

- Additions of Fe (as Fe^{2+}) into solution were simulated kinetically according to the experimental corrosion rate.

- Reduction reactions of carbonate to methane and sulphate to sulphide were not allowed in the model calculations, because of kinetic constraints. It is noticed that these reactions are of course thermodynamically possible and very often enhanced by microbes.

- Evolution of Eh reflected the redox couple Fe(II)/Fe(III).

Figure 8 shows the modelled Eh evolution during the corrosion process in strictly anaerobic conditions at four different temperatures considering precipitation of Fe-bearing minerals as only magnetite and solid $Fe(OH)_2$. Generally Eh values gradually decrease following the concentration difference in redox couple Fe(II)/Fe(III). This is contrary to experimental results (Figure 7). The differences between experimental and modelled results are probably caused by; precipitation of corrosion products, which are not at equilibrium with solution, adsorption of Fe on corrosion cell, influence of O_2 traces (value in anaerobic glove box < 0.1 ppm of O_2). The further work will be more focused on these issues and on the model completion.
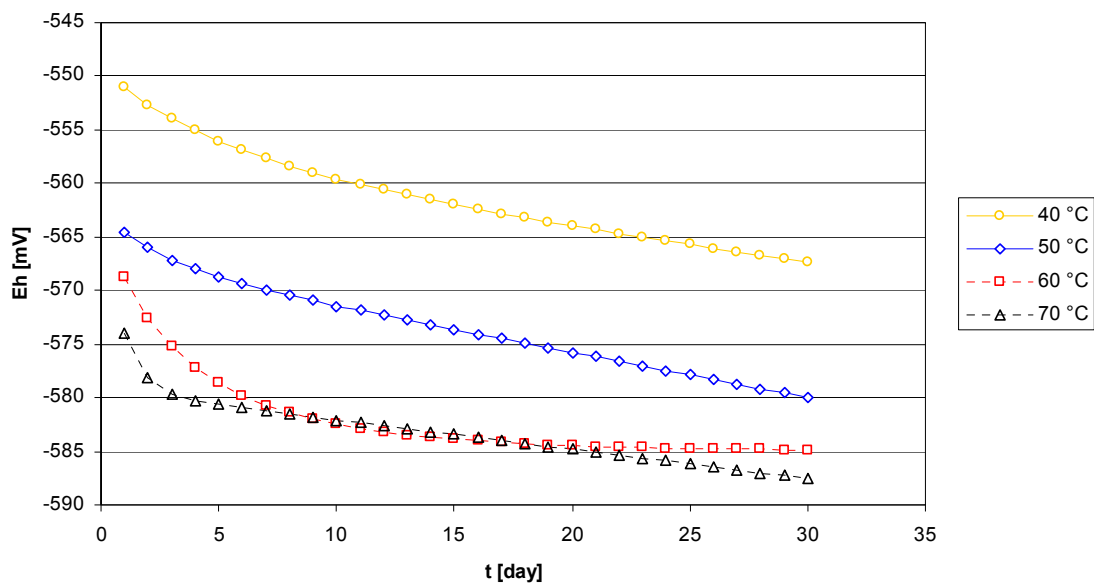
Figure 8: *The evolution of Eh vs. time at several corrosion experiments with different temperatures. Precipitation of magnetite (70°C) and ferrous hydroxide (40, 50, 60°C) was considered.*

References

Baeyens B. (2005): Information from WP 2.5 of 6th EC integrated project NF-PRO

Buckau G., Kienzler B., Duro L., Grivé M., Montoya V. (2009): Collaborative Project "Redox Phenomena Controlling Systems" - 1st Annual Workshop Proceedings, Forschungszentrum Karlsruhe, Wissenschaftliche Berichte, FZKA 7466, Karlsruhe, pp.52.

Cole D.R., Ohmoto H. (1986): Kinetics of isotopic exchange at elevated temperatures and pressures, Rev. in Min., 16, 41-90

Criss R.E. (1999): Principles of stable isotope distribution, Chart 4

Cui D., Puranen A., Scheidegger A., Leupin O., Gens R., Spahiu K. (2009): On the speciation of [79]Se immobilized on iron canister material under simulated deep repository environment, J. Radioanalytical and Nuclear Chemistry, 282, 349-354.

Ferry C., Poinssot C., Broudique V., Cappelaere C., Desgranges L., Garcia P., Jegou C., Lovera P., Marimbeau P., Piron J.P., Poulesquen A., Roudil D., Gras J.-M., Bouffioux P. (2005): Synthesis of the Spent Fuel Long-Term Evolution, Rapport CEA-R-6084

Fors P., Carbol P., Van Winckel S., Spahiu K. (2009): Corrosion of high burn-up structured UO_2 fuel in presence of dissolved H_2. J. Nucl. Mater. 394, 1-8.

Grambow B., Loida A., Dressler P., Geckeis H., Gago J., Casas I., de Pablo J., Gimenez J., Torrero M.E. (1996): Long-Term Safety of Radioactive Waste Disposal: Chemical Reaction of Fabricated and High Burnup Spent UO_2 Fuel with Saline Brines, Wissenschaftliche Berichte FZKA 5702, März

Lecluse C., Robert F. (1994): Hydrogen isotope exchange reaction rates origin of water in the inner solar system. Geochimica et Cosmochimica Acta, 58, 2927-2939

Loida A., Grambow B., Geckeis H. (1996): Anoxic corrosion of various high burnup spent fuel samples. J. Nucl. Mater. 238, 11-22.

Loida A., Kienzler B., Geckeis H. (2003): Mobilization/Retention of Radionuclides during Corrosion of High Burnup Spent Fuel and Backfill Materials in Salt Brines, Mat. Res. Soc. Symp. Proc., 757, 433-439

Miserque F., Gouder T., Wegen D. H., Bottomley P. D. W. (2001): Use of UO_2 films for electrochemical studies, J. Nucl. Mater. 298, 280.

O'Neil J.R. (1986): Theoretical and experimental aspects of isotopic fractionation, Rev. in Min., 16, 1-40 and references

Parkhurst D.L., Appelo C.A.J. (1999): User's guide to PHREEQC (version 2). A computer program for speciation, batch-reaction, one-dimensional transport and inverse geochemical calculations. USGS, Water resources investigations report, 99-4259.

Seibert A., Wegen D.H., Gouder T., Wiss T., Denecke M.A. (2010): The use of the electrochemical quartz crystal microbalance in corrosion studies of UO_2 thin film models, to be submitted to J. Nucl. Mater.

Shoesmith D.W. (2000): Fuel corrosion processes under waste disposal conditions, J. Nucl. Mater. 282, 1-31.

Shoesmith D.W., Sunder S., Hocking W.H. (1994): Electrochemistry of novel Materials, Chapter 6, p. 297, Eds. J. Lipkowski, P.N. Ross, VCH Verlagsgesellschaft, New York, Weinheim, Cambridge

Stumpf S., Seibert A., Gouder T., Huber F., Petersmann T., Denecke M.A., Fanghänel Th. (2010b): The inhibiting effect of H_2 on the UO_2 spent fuel corrosion, submitted to Nature Mater.

Stumpf S., Seibert A., Gouder T., Huber F., Wiss T., Römer J. (2009): Development of fuel-model interfaces: Investigations by XPS, TEM, SEM and AFM. J. Nucl. Mater. 385, 208.

Stumpf S., Seibert A., Gouder T., Huber F., Wiss T., Römer J., Denecke M.A.. (2010a): Development of fuel-model interfaces: Characterization of Pd containing UO_2 thin films. J. Nucl. Mater. 397, 19.

TDB NEA 17 (2005): HATCHES, the Harwell/Nirex Thermodynamic Database for Chemical Equilibrium Studies, Version NEA 17 at 25° C.

Teichner S.J. (1990): Recent studies in hydrogen and oxygen spillover and their impact on catalysis. Appl. Catalysis 62, 1.

Trummer M., Dahlgren B., Jonsson M. (2010): On the dynamics of oxidative dissolution of Y_2O_3 doped UO_2. Submitted to J. Nucl. Mater.

S + T CONTRIBUTIONS

S + T CONTRIBUTIONS

List of contributions

REDOX PROPERTIES OF HUMIC SUBSTANCES: IDENTIFICATION OF REDOX FUNCTIONAL GROUPS BY TRLFS.

Shcherbina N.S.[a*], Perminova I.V.[b], Novikov A.P.[c], Kalmykov S.N.[b], Marquardt C.M.[d], Walther C.[d], Buckau G.[d], Kumke M.[e], Eidner S.[e]

[a] Isotope and Elemental Analysis, Department Nuclear Energy and Safety, PSI, Switzerland

[b] Department of Chemistry, Lomonosov Moscow State University, 119991, Moscow, Russia

[c] Vernadsky Institute of Geochemistry and Analytical Chemistry, RAS, 119991, Moscow, Russia

[d] Institut für Nukleare Entsorgung, KIT, Campus Nord, 76344, Eggenstein-Leopoldshafen, Germany

[e] Professur für Physikalische Chemie, University of Potsdam, 14476 Golm, Germany

*Corresponding author: natalia.shcherbina@psi.ch

Abstract

Humic substances (HS) are redox active. The redox functionality of HS is not yet fully understood. There are open questions with respect to the redox buffer inventory, the pKa distribution and the responsible functional groups. The inventory of redox buffering groups is expected to be in the range between about 0.5 and 2 mmol/g [Aeschbacher et al. (2010)]. This corresponds to about one redox active group in four humic or fulvic acid molecules, and one redox active group per molecule, respectively [Buckau (2010)]. Quinonoid-type groups are proposed to be responsible for the redox function [Mathiessen (1995), Struyk and Sposito (2001), Bauer et al. (2007), Aeschbacher et al. (2010)]. Amongst others, sulphur-containing groups have also been suggested [Bruechert (1998)]. Phenolic groups in combination with quinones are also proposed [Schmeide and Bernhard (2009)].

The present paper presents initial results on the combination of time-resolved laser fluorescence spectroscopy (TRLFS) with change in the humic acid redox state by titration with reducing and oxidizing agents. Hydroquinone-enriched humic acids were also studied for comparison of the findings with natural ones. The studies are conducted under inert gas (Ar).

The work was conducted within a training mobility measure of the EURATOM FP7 Collaborative Project "Redox Phenomena Controlling Systems", April to July 2009, where the main author from MSU visited KIT-INE, University of Potsdam and Brookhaven National Lab.

The overall conclusion is that the findings agree with quinonoid groups responsible for the humic acid redox function. The impact also of other groups, however, cannot be excluded. The determination of the redox buffer inventory by electrochemical oxidation or reduction was not exhaustive and was found to be very slow [Aeschbacher et al. (2010)]. Changing the redox state with reducing and oxidizing agents ($Na_2S_2O_4$ and CeO_2, respectively), introduces residues that can change the properties. This is especially true for complexation with the resulting Ce(III) [Zhang, 2008]. Improved electrochemical reduction and oxidation (see for example [Aeschbacher et al. (2010)]), refined spectroscopic analysis and identification of different redox buffer inventory contributors are recommended.

Natural HS and Reference Materials

Table 1. Names and descriptions of HS tested

Natural HS	Comments on HS Origin	Reference material	Comments on synthesis
Gohy-573(HA) Gohy-573(FA)	Natural HA and FA, extracted from Gorleben groundwater at 140 m depth.	HQ100(HS)	Hydroquinone-enriched leonardite HA: hydroquinone/CHP = 0.1 g/g ; quinone function reference
Mayhak(HA)	Natural HA, extracted from Mayhak bottom sediments.	HQ250(HS)	Hydroqquinone-enriched leonardite HA: hadroquinone/CHP = 0.25 g/g; quinone function reference
Enisey(HA)	Natural HA, extracted from Yenisey river sediments.	HQ500(HS)	Hydroqquinone-enriched leonardite HA: hydroquinone/CHP = 0.5 g/g; quinone function reference
Leonardite(HA)	Leonardite HA (CHP) isolated from Humintech Humate*.	HQm	Hydroquinone homopolymer quinone function reference

*: www.humintech.com

Four natural humic acids (HA) and one fulvic acid (FA) were investigated. Isolation and characterization of Gorleben HS (Germany) is described in [Kim et al. (1990)]. Isolation of two other HA (Mayhak and Yenisei, Russia) was performed according to the standard technique used in [Kim et al. (1990)]. For reference to quinone and phenolic functions, three hydroquinone-enriched humic derivatives (HQ100, HQ250 and HQ500) and hydroquinonde homopolymer (HQm) were also used. Leonardite HA (CHP) was

used as a parent material to obtain hydroquinone-enriched humic derivatives. In addition, hydroquinone homopolymer (HQm) was used as a reference material consisted of only quinonoid moiety. Hydroquinone homopolymer (HQm) was obtained using formaldehyde polycondensation of hydroquinone monomers according to the method described in [Lee et al., 2003]. The same procedure of copolycondensation between CHP and hydroquinone was used for synthesis of hydroquinone-enriched HS. Details of the synthesis and derivatives characterization are described in [Perminova et al. (2005)]. The natural HA and FA, and reference materials studied are listed in Table 1.

Experimental

All experiments were performed under Ar atmosphere in a glove box. Solutions of HA and FA of constant concentrations 12.5 mg C/L at pH 7.6 were prepared in 1 mmol/L piperazine-N,N'-bis(2-ethanesulfonic acid) buffer (PIPES buffer) in 0.1 M $NaClO_4$. Chemical reduction of the samples was done by addition of $Na_2S_2O_4$ (Merk). All reagents were of analytical grade.

HA or FA were reduced by mixing with different aliquots of $Na_2S_2O_4$ at pH~10 to create appropriate Eh conditions. After the certain incubation time (>24 hours) mixture was diluted by background electrolyte up to 10 ml. Final HS concentration was constant (12.5 mgC/L), while sodium dithionite concentration was varied between 0 and $2 \cdot 10^{-3}$ M. After pH and Eh measurements fluorescence spectra were recorded.

Eh in FA and HA solutions before and after treatment was measured up to 1 h until the value shift was < 0.5 mV/min using a Ag/AgCl reference electrode (Metrohm, USA) and normalized versus SHE.

Stationary fluorescence spectra were recorded at room temperature using pulsed Excimer pumped dye laser and Optical Parametric Oscillator (OPO) system, respectively. Excitation was done at $\lambda_{ex} = 375$ nm (dye laser) and $\lambda_{ex} = 325$, 290 and 265 nm (OPO). The emission spectra were recorded between 350 nm and 650 nm. In time-resolved measurements, the dye laser was employed with a repetition rate of 20 Hz operating at 375 nm. The fluorescence intensity after a certain delay period was recorded for a gate of 111 μs, which was shifted in steps of 2.5 ns. To prevent HS oxidation during spectra collection, samples were measured in sealed cuvettes. Between the measurements samples were stored in a glove box.

Results and Discussion

The results are presented along with fluorescence intensity, emission peak position and fluorescence decay life-time as a function of redox condition for HA and FA, as well as quinone reference substances. Results presented for humic material focus on HA and FA from the Gorleben groundwater "Gohy-573". The properties of reference substances are also discussed for identification of key type of processes. Full presentation of data, including all the other humic substances, will be given in the full paper in preparation.

Fluorescence intensity

The fluorescence intensity of Gohy-573(HA) is measured as a function of the redox state (Fig. 1). The fluorescence intensities of completely reduced (Eh -420mV) and non-treated (Eh +356 mV) forms are comparably low, while in between, the fluorescence intensity shows much higher values. This behaviour points to the possibility that the redox sensitive groups in HS are of benzoquinone type according to the fig. 2: UV molar absorption coefficients for hydroquinone (reduced form), semiquinone (radical intermediate form) and quinone (oxidized form) follows the same trend. The values of molar absorption at 420 nm (L/mol·cm) are reported as negligible, 7200 and 500-600, for the quinone species in three different forms in that sequence [Ayako and Gauska 1979].
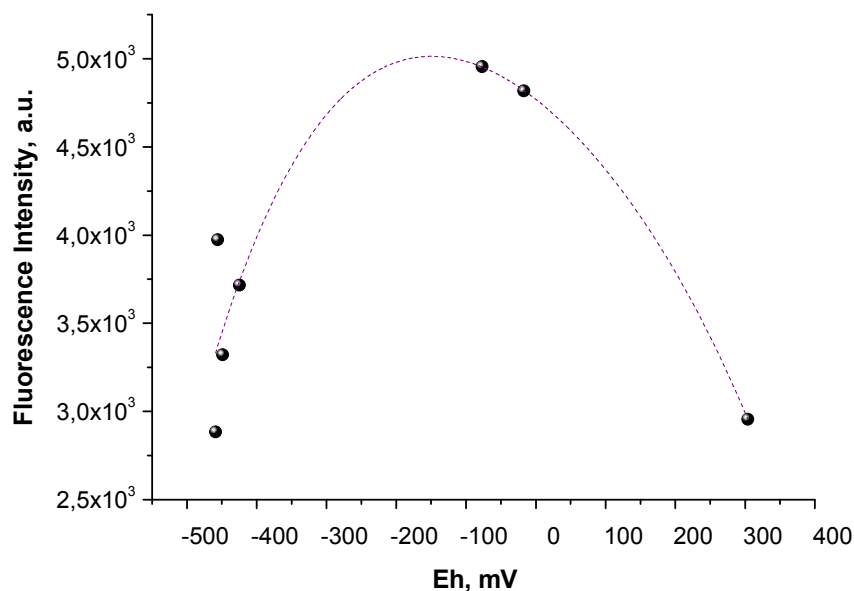
Figure. 1: *Fluorescence intensity of the humic acid Gohy-573(HA) as a function of the redox state.Fluorescence intensity is traced at 515 nm.*
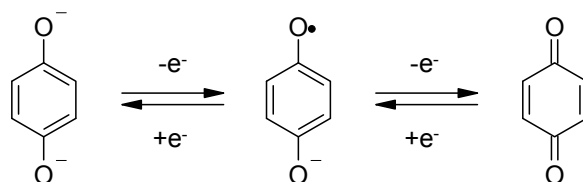
Figure. 2: *Quinone-hydroquinone redox equilibrium.*

This is an indication that the inventory of groups resulting in the redox properties of humic matter may be based on the quinone system. Another indicator could be the emission peak position.

Emission peak position

The peak positions of the non-treated and reduced forms of hydroquinone homolopymer (HQ_m) are shown in fig. 3. This reference or model system consisted of only hydroquinone moiety shows a clear blueshift when transferring from the parent to the reduced form. In Fig. 4 the emission spectra of CHP and hydroquinone-enriched humic derivatives in their reduced form are shown. These substances in their reduced form show strong emission bands in the blue-shifted range of the reduced quinone reference compound (Fig. 3). This is another indicator supporting the possibility that the redox determining inventory of functional groups in humic acids are based on the quinone – hydroquinone system.
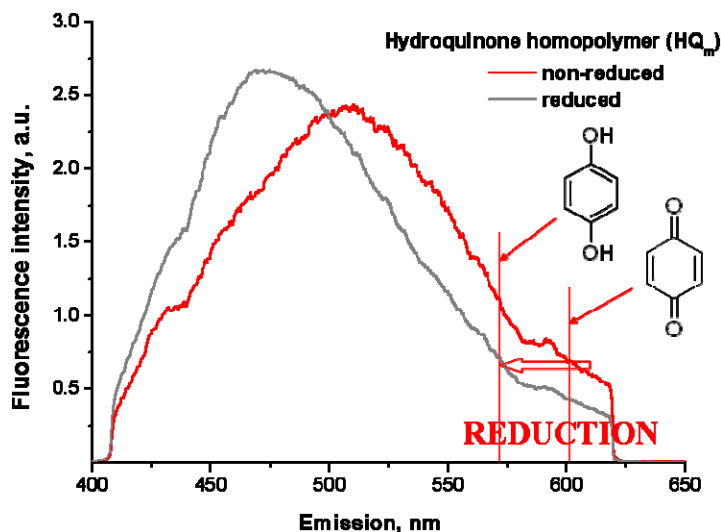
Figure. 3 *Fluorescence peak positions for the oxidized and reduced forms of the hydroquinone homopolymer (emission excited at 375 nm).*

Effect of radical content on HS emission intensity is shown in Figure. 4, representing radical content of leonardite HA and hydroquinone-enriched HS determined using EPR in [Perminova et al. (2005)]. Since it was mentioned, the condenced quinonoid moiety may be responsible for emission intensity and at the same time can stabilize radicals, content of free radicals in Fig. 4 is given as normalized by ArOH (phenolic hydroxyl groups) inventory of each sample (values can be found in [Perminova et al. (2005)]) . This example demonstrates that emission intensity decreases along with the radical content in the following order: CHP > HQ500 > HQ100 ≈ HQ250.
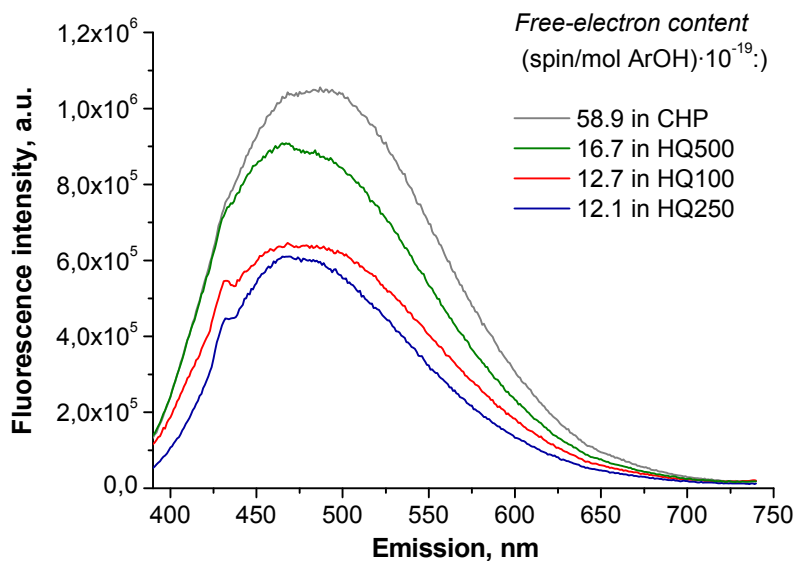
Figure. 4: *Fluorescence spectra of Leonardite (CHP) and hydroquinone-enriched HA (HQ100, HQ250, HQ500; in reduced form) excited at 375nm: pronounced fluorescence emission band intensity in the range of the reduced quinone/hydroquinone couple (reference peak positions, see Fig. 2). Spin/mol ArOH means a normalization of the measured free-electron content with the content of phenolic hydroxyl groups (ArOH) of the corresponding HA.*

Fluorescence life-time

The fluorescence life-time monitored by the present set-up, i.e. falling within the time window of excitation and fluorescence emission detection as given by the experimental and analytical system, is shown in Fig's 5 and 6. As it is seen, emission short-lived components (~0.1 μs) are invariant within the whole Eh range, while long-lived components (<0.1 μs) varies significantly.

Both in the case of the reduced form of Gohy-573(HA) (Fig. 5) and Gohy-573(FA) (Fig. 6), the emission intensity function on time obeys a bi-exponential decay:

$$I = A_1 \exp[-t / \tau_1] + A_2 \exp[-t / \tau_2]$$

The results from the evaluation of the different emission life-time components are illustrated in Fig's 7 and 8, for the Gohy-573 HA and FA, respectively, where τ_1 and τ_2, traced at 462 and 515 nm, are plotted against the redox conditions. The fast component (τ_1) in this bi-exponential decay remains rather constant. Contrary to this, the second, more long-lived component (τ_2) varies significantly. Thereby, there is not a linear change with the redox state, but rather τ_2 reaches a maximum close to Eh=-300mV (vs. SHE). Consequently, the relative contribution of the second component to the total fluorescence is lower at the end-points and higher at intermediate redox potentials.
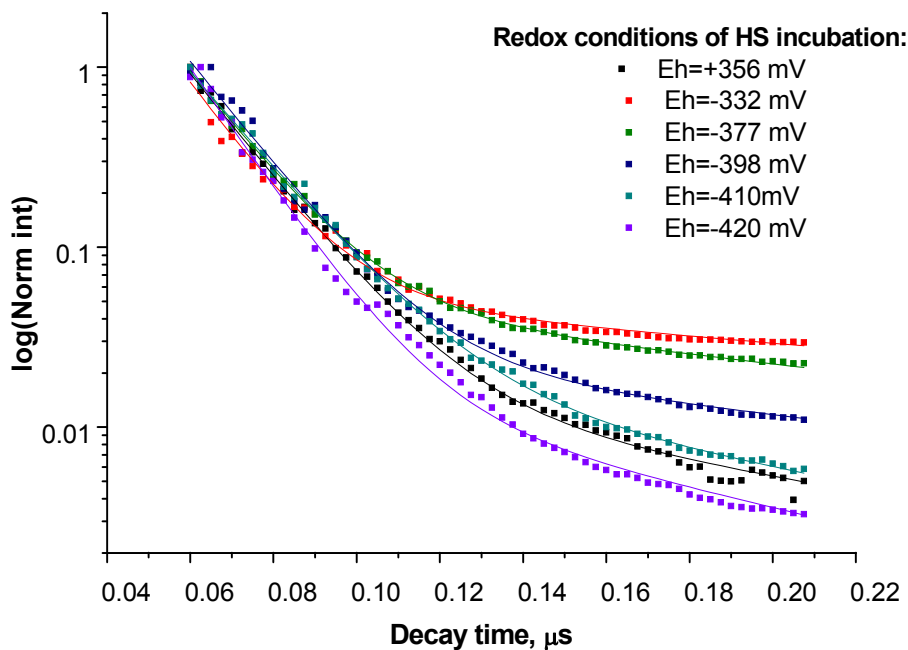
Figure. 5: *Fluorescence decay for Gohy-573(HA) under different redox conditions. Emission was excited at 375 nm, life-time was trased at 515 nm.*
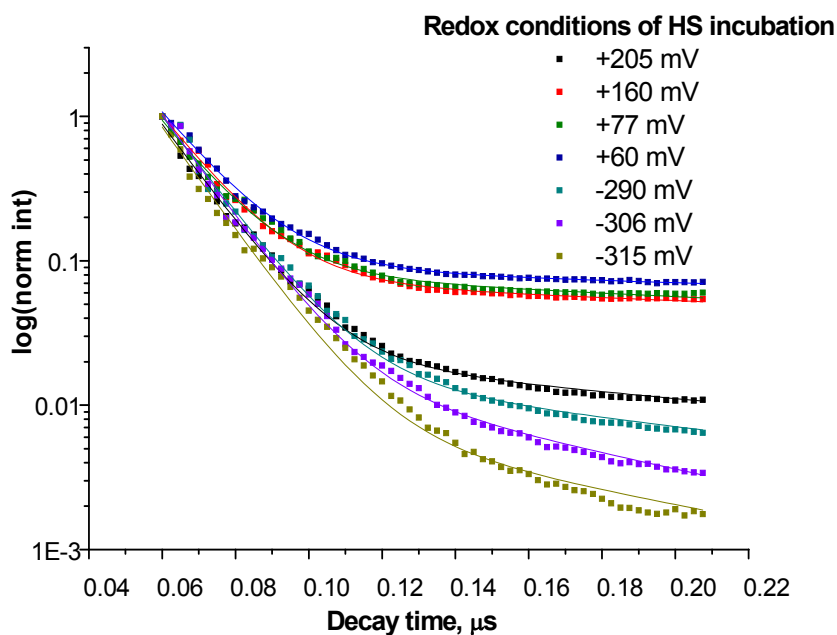
Figure. 6: *Fluorescence decay for Gohy-573(FA) under different redox conditions. Emission was excited at 375 nm, life-time was trased at 515 nm.*
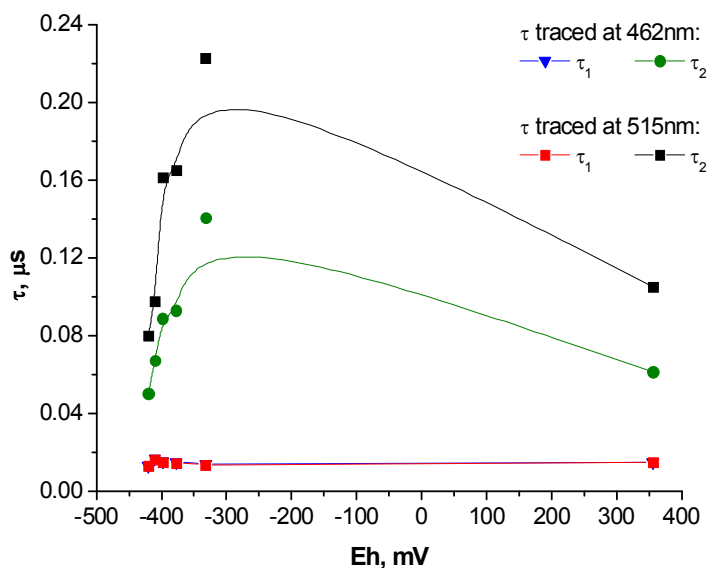
Figure. 7: *Fluorescence life-time components for Gohy-573(HA) under different redox conditions.*

In case of FA the same behaviour of life-time components is observed: almost constant values of τ_1 along the whole Eh range and significantly different values of τ_2. However contributions of long-lived components to the total fluorescence intensity of FA is absolutely different from HA: τ_2 reaches maximum at about Eh=+100mV (vs. SHE).
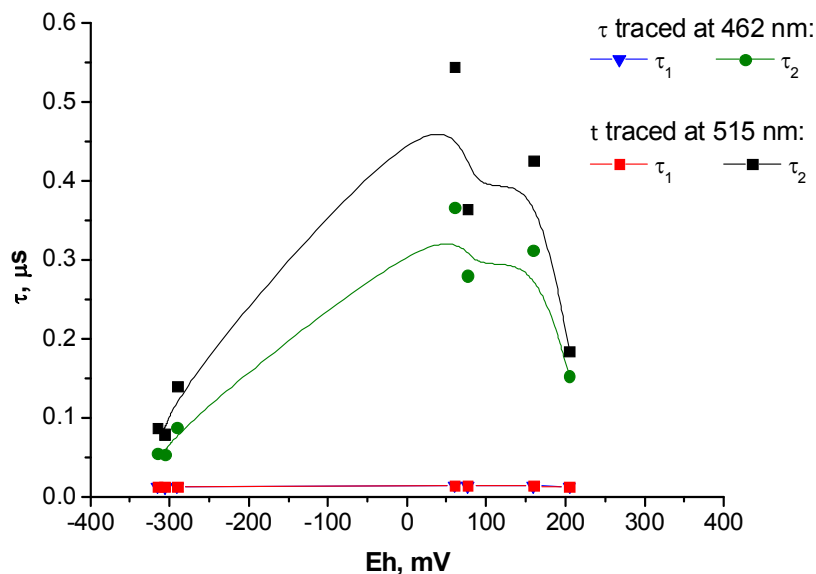
Figure. 8: *Fluorescence life-time components for Gohy-573(FA) under different redox conditions.*

The general trends of life-time functions of redox state are the same for HA and FA, namely the life-time of this second longer component reaches a maximum in the intermediate redox range, whereas the life-time of this component decreases both towards more non-treated and reduced forms. As in the case with the above-discussed overall fluorescence intensities and the emission peak positions, also this latter evaluation is in agreement with the redox state being reflected by a quinone-hydroquinone system transition (Fig. 2).

Conclusions

Quinoid systems are likely to be key contributors to the redox behaviour of humic substances.

Acknowledgements

References

Aeschbacher M., Sander M., Schwarzenbach R.P. (2010) "Novel Electrochemical Approach to Assess the Redox Properties of Humic Substances", Environ. Sci. Technol., 44/87-93.

Ayako Futami, Günter Gauska (1979) "Vectorial redox reactions of physiological quinones. II. A study of transient semiquinone formation", Biochimica et Biophysica Acta, 547(3)/597-608.

Bauer M., Haitnamm T., Macalady D.L., Blodau Ch. (2007) "Electron Transfer Capacities and Reaction Kinetics of Peat Dissolved Organic Matter", Environ. Sci. Technol., 41/139-45.

Bruechert V. (1998) "Early diagenesis of sulphur in estuarine sediments: The role of sedimentary humic and fulvic acids", Geochim. Cosmochim. Acta, 62(9)/1567-86.

Buckau G. (ed.) (2010) "Expert views on the state-of-the-art on humate complexation processes with recommendations for future studies", Report FZKA 7465, (in preparation).

Kim J.I., Buckau G., Li G.H., Duschner H., Psarros N. (1990) "Characterization of Humic and Fulvic Acids from Gorleben Groundwater", Fresenius J. Anal. Chem., 338/245-52.

Lee Y.-K., Kim D.-J., Kim H.-J., Hwang T.-S., Rafailovich M., Sokolov J. (2003) "Activation energy and curing behavior of resol- and novolac-type phenolic resins by differential scanning calorimetry and thermogravimetric analysis", J. Appl. Polym. Sci. 89/2589-96.

Matthiessen A. (1995) "Determining the redox capacity of humic substances as a function of pH", Vom Wasser, 84/229-35.

Perminova I.V., Kovalenko A.N., Schmitt-Kopplin P., Hatfield K., Hertkorn N., Belyaeva E.Y., Petrosyan V.S. (2005), Design of quinonoid-enriched humic materials with enhanced redox properties, Environ. Sci. Technol. 39(21)/8518-24.

Schmeide K., Bernhard G. (2009) "Redox stability of neptunium(V) and neptunium(IV) in the presence of humic substances of varying functionality", Radiochim. Acta, 97/603–611.

Struyk Z., Sposito G. (2001) "Redox properties of standard humic acids", Geoderma, 102/329-46.

Zhang T., Junfeng L., Jun M., Zhimin Q. (2008) "Fluorescence spectroscopic characterization of DOM fractions isolated from a filtered river water after ozonation and catalytic ozonation" Chemosphere, 71/911-921.

SORPTION/SORPTIVE REDUCTION STUDIES ON THE INTERACTION OF RADIONUCLIDES WITH FEBEX BENTONITE COLLOIDS/NANOPARTICLES UNDER GRIMSEL GROUNDWATER CONDITIONS IN THE PRESENCE OF FRACTURE FILLING MATERIAL

Florian Huber [1*], Peter Kunze [1], Horst Geckeis [1], Thorsten Schäfer [1]

[1] Karlsruhe Institute of Technology, Institute for Nuclear Waste Disposal (INE); (DE)

* Corresponding author: florian.huber@kit.edu

Abstract

The kinetics of radionuclide desorption from bentonite colloids and subsequent sorption onto fracture filling material (FFM) can influence colloid-facilitated radionuclide (RN) migration in groundwater. To shed light on the significance of these issues batch-type experiments using a cocktail of strong and weak sorbing radionuclides containing FEBEX bentonite colloids in the presence of fracture filling material from Grimsel under Grimsel groundwater conditions have been conducted. Results show that tri- and tetravalent radionuclides, ^{232}Th(IV), ^{242}Pu(IV) and ^{243}Am(III) are clearly colloidal associated in contrast to ^{233}U(VI), ^{237}Np(V) and ^{99}Tc(VII). Concentrations of colloid-borne ^{232}Th(IV), ^{242}Pu(IV) and ^{243}Am(III) decrease after ~ 100h showing desorption from bentonite colloids while ^{233}U(VI) and ^{99}Tc(VII) concentrations remain constant over the experimental time thus showing no interaction neither to colloids nor to the fracture filling material. ^{232}Th(IV) results indicate a slower dissociation from colloids compared to ^{242}Pu(IV) and ^{243}Am(III) indicating stronger RN-colloid interaction. In the case of ^{237}Np(V), a decrease in concentration after ~300h is observed which can be explained either by slow reduction to Np(IV) and subsequent sorption to mineral surfaces in accordance with the evolution of experimental pe/pH conditions and/or by a slow sorption kinetic on the fracture filling material. The driving force of the observed metal ion desorption from colloids is binding to FF material surfaces being in excess of the available colloid surface area (44:1).

Introduction

Much effort has been spent in the past and is still ongoing today to shed light on the various complex geochemical processes and their impact on the migration behaviour, among them, the sorption/sorptive reduction of radionuclides on colloids/nanoparticles. Colloids/nanoparticles are ubiquitous in natural surface and subsurface waters and their mineralogy often is closely related to the host rock formation. Some radionuclides, especially the tri- and tetravalent actinides (Th, Pu, Am) show strong hydrolysis and can therefore form so called "eigen-colloids". The importance of colloids for migration of contaminants has been proven by various laboratory and field studies carried out in the past, among them the colloid and radionuclide retardation (CRR) experiments conducted at the Grimsel Test Site (Geckeis et al., 2004). These experiments revealed under the given hydrogeochemical conditions that especially the transport of tri- and tetravalent radionuclides, Am(III) and Pu(IV), is facilitated in presence of colloidal phases leading to an un-retarded breakthrough whereas not colloidal-associated radionuclides like U(VI) or Np(V) exhibit strong retardation due to fracture surface interaction. Variation of the ground water residence time in laboratory column migration experiments revealed an attachment/filtration of colloids/nanoparticles onto the rock matrix under geochemical/electrostatic conditions favouring the stability of colloids in the bulk solution (Missana et al., 2008; Schäfer et al., 2004). Reasons for the latter findings were attributed to chemical and physical heterogeneity of the fracture surface or flow path geometry. Another key aspect regarding the potential influence of colloids/nanoparticles on contaminant mobility is sorption reversibility/sorptive reduction and kinetics involved. The aim of this study is to investigate the sorption and desorption process of ^{99}Tc(VII), ^{232}Th(IV), ^{233}U(VI), ^{237}Np(V), ^{242}Pu(IV) and ^{243}Am(III), onto FEBEX bentonite colloids under Grimsel groundwater conditions in the presence of Fracture Filling Material (FFM) from the Grimsel Test Site (GTS) for long (weeks-months) equilibrium time. Therefore batch-type studies were conducted regarding the following aspects: Impact of (i) ^{237}Np(V), ^{242}Pu(IV) and ^{243}Am(III) concentration and (ii) equilibrium time on RN sorption and reversibility processes.

Materials & Methods

Fracture Filling Material. Fracture filling material originates from the Grimsel Test Site (GTS), Switzerland. The host rock in GTS is the so called Grimsel granodiorite consisting mainly of plagioclase (29–33 vol.%), quartz (27–28 vol.%), K-feldspar (12–24 vol.%) and biotite (7–11 vol.%). For the batch type sorption studies fracture filling material (FFM) was crushed, sieved and freeze dried under atmospheric conditions. One size fraction (1-2 mm) of the Grimsel FFM has been separated. Specific surface area measurements by BET N$_2$-adsorption of the Grimsel FFM yielded a value of 0.153-0.166 m^2 g^{-1} (1-2 mm size fraction). Major elemental composition determined by X-ray fluorescence (XRF) is dominated by SiO$_2$, Al$_2$O$_3$, Na$_2$O and K$_2$O representing the main mineral elements quartz and k-feldspar/albite which is in accordance to the EDX analysis. Interestingly the total iron content (2.96 wt% Fe$_2$O$_{3(t)}$ is mainly composed of ferrous iron with 1.87 wt% FeO).

FEBEX bentonite colloid characterisation. For the experiments FEBEX (full-scale engineered barrier experiment) bentonite from the deposit of Cabo de Gata, Almería (Spain) is used. The bentonite was sieved to obtain the <63 μm size fraction and equilibrated with 1 mol·L^{-1} NaCl to transfer the bentonite to its mono-ionic Na-form. The Na exchanged bentonite is washed with de-ionized (Milli-Q) water to remove excess salt after one week equilibration time. Further preparation steps to obtain the colloid suspension is described in detail in Nagra (2006). The extracted colloidal fraction consists quantitatively of montmorillonite. Specific surface area of the FEBEX bentonite colloids have been measured by Missana et al. (2008) yielding a value of 33 m^2 g^{-1}.

Radionuclide cocktail characterization. The radionuclide cocktail was prepared in a glove box under Ar atmosphere by spiking radionuclides to Grimsel groundwater (GGW) containing prior added bentonite colloids (25.56 mg·L^{-1}). After spiking of the radionuclides only a slight pH decrease to a lower value of 9.1 was measured, likely due to buffering capabilities of the bentonite colloids. Subsequently pH was readjusted using CO$_2$-free NaOH. The prepared cocktail was equilibrated for 24 hours before aliquots of the radionuclide cocktail were spiked to the sample batches containing fracture filling material. The following radiotracers and oxidation states have been used: ^{99}Tc(VII), ^{232}Th(IV), ^{233}U(VI), ^{237}Np(V), ^{242}Pu(IV), and ^{243}Am(III). ^{242}Pu was added as ^{242}Pu(III) after electrochemical reduction and quantitatively transferred to ^{242}Pu(IV) through pH adjustment of the cocktail. An aliquot of every sample was ultra-centrifuged to remove colloid associated radionuclides. Aliquots for ultra-centrifugation were pipetted in ultra-centrifugation vials, sealed by welding and subsequently centrifuged for 1h at 90,000 rpm. Afterwards aliquots of the ultra-centrifuged supernatant were taken and analyzed by ICP-MS. ^{232}Th(IV) and ^{243}Am(III) are almost quantitatively bond to the bentonite colloids and for ^{242}Pu(IV) ~15% are not colloid associated in contrast to the ^{233}U(VI), ^{99}Tc(VII) and ^{237}Np(V) colloid bond fraction yielding values below 2% of the initial concentration C$_0$.

Experimental conditions and procedure. All experiments were conducted in a glove box under Ar atmosphere (< 1 ppm O$_2$). All pH measurements were undertaken using a Ross electrode and an Orion pH meter. The FFM material was equilibrated prior to the batch-type experiments with fresh Grimsel groundwater in Zinsser vials (20 mL HDPE) over a period of six weeks, exchanging the solution at least 5 times within this period. The solid to liquid ratio is 1:4 (g·mL^{-1}) for all experiments. After this equilibration phase the supernatant was exchanged with the radionuclide cocktail. Triplicates of every sample were prepared. An aliquot of every sample was ultra-centrifuged (90,000 rpm; 1h) to remove colloid associated radionuclides and analyzed by ICP-MS.

Results & Discussion

From a comparison of ultra-centrifuged (UC) with non ultra centrifuged samples it is obvious that ^{99}Tc(VII), ^{233}U(VI) and ^{237}Np(V) are not colloidal associated in contrast to the tri- and tetravalent radionuclides ^{232}Th(IV), ^{242}Pu(IV) and ^{243}Am(III) which are clearly colloid bound (see Table 1). The differences in radionuclide concentration are 1-2 orders of magnitude for the colloid-bond radionuclides which also reflect the effective separation of the colloids through the experimental procedure. This is furthermore documented in the Al ICP-MS signal, which gives information on the structural alumina

of the FEBEX bentonite colloids. It can be stated that no colloid sorption to the fracture filling material is detectable, which would obscure the results for the colloid bound RNs. The Al concentration after ultra-centrifugation is reduced by around one orders of magnitude. Al concentrations after ultra-centrifugation are in the range of the natural Al content (~ 20ppb) in Grimsel groundwater. Since the radionuclide cocktail included several redox sensitive radionuclides, i.e. ^{99}Tc(VII), ^{233}U(VI), ^{237}Np(V) and ^{242}Pu(IV) and it was mandatory to monitor the contact time dependent evolution of pH and Eh$_{(SHE)}$ values. The response time for the pH electrode was rather uncritical, whereas for the Eh measurement the criterion to accept the measured value is not well documented and established in the literature (see i. a. Grenthe et al., 1992). In this study we monitored the time dependent change in the redox value although the automatic slope analysis of the Orion instrument already indicated a constant value after < 1h. The Eh$_{(SHE)}$ drifted over several hours and we took the value when a plateau was reached. In Figure 1a a typical redox measurement is shown. The measured plateau values for pH dropped from pH 9.6 originally found in the Grimsel groundwater to 9.0 after 7500h as depicted in Figure 1b. Meanwhile, the Eh$_{(SHE)}$ values dropped from ~50 mV to ~0 mV within the first two days and remained between ~ 0 mV and ~ 20 mV until 624h. Afterwards the redox potential started to decrease again to values of ~ -15 mV in the Grimsel FFM system after 7500h (Figure 1b).

Table 1: *Characterization of the radionuclide cocktail including concentration, initial association to bentonite colloids determined by ultra-centrifugation and the analytical method used in this study.*

	Initial concentration C_0 (mol·L^{-1})	Colloid bound concentration (%)	Analytical method
[^{99}Tc(VII)]	$1 \cdot 10^{-8}$	0.9	ICP-MS
[^{232}Th(IV)]	$7.3 \cdot 10^{-9}$	99.7	ICP-MS
[^{233}U(VI)]	$4 \cdot 10^{-7}$	1.6	ICP-MS
[^{237}Np(V)]	$1.8 \cdot 10^{-6}$	0.1	ICP-MS
[^{242}Pu(IV)]	$1.3 \cdot 10^{-8}$	84.1	ICP-MS
[^{243}Am(III)]	$8 \cdot 10^{-9}$	94.8	ICP-MS
[Colloid]	25.56 mg·L^{-1}		ICP-MS/ LIBD
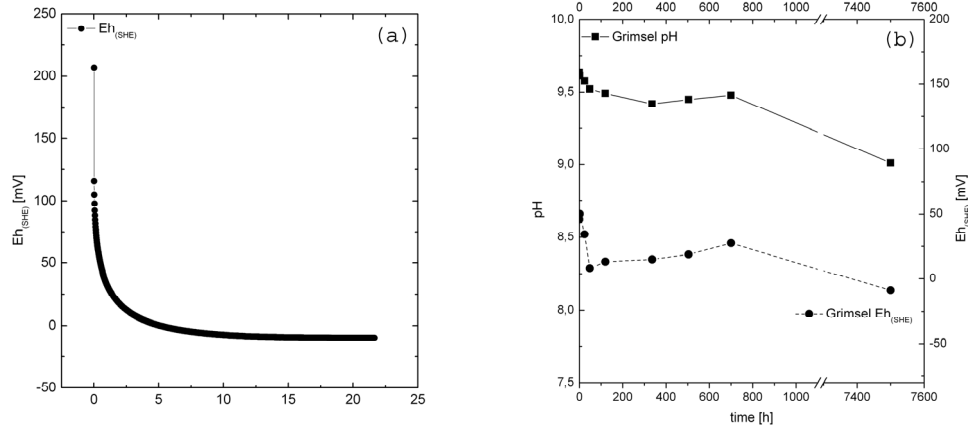
Figure 1: *(a) Eh$_{(SHE)}$ measurement for a single point plotted in the right figure showing the response time of the redox electrode reaching asymptotically a constant plateau value after several hours (x-axis in hours). (b) Measured final pH and Eh$_{(SHE)}$ values in the batch-type studies after various contact times.*

Np, Pu and Am sorption/reversibility

To study the influence of RN concentration on sorption and reversibility two series with the 1-2 mm FFM fraction have been prepared applying two different ^{237}Np(V), ^{242}Pu(IV) and ^{243}Am(III) concentrations. For all sample sets with higher concentration two samples for long term measurements after 7500h have been prepared to examine if sorption and/or reversibility equilibrium conditions have been established. In Figure 2 results for ^{237}Np(V), ^{242}Pu(IV) and ^{243}Am(III) are depicted.

Additionally inserted in Figure 2 are calculated data points of the ternary system taking batch sorption data derived partitioning coefficients of the binary systems "bentonite colloids – radionuclide" ($R_{d,coll}$) and "FFM – radionuclide" ($R_{d,FFM}$) published in Nagra (2006). The stable Al concentration measured throughout the experimental period infers that the interaction of colloids with the fracture filling material can be neglected ($R_{d,coll-FFM}$=0) and therefore the following equation can be applied:

$$R_{d,tot} = \frac{R_{d,FFM}}{1 + C_C \cdot R_{d,coll}}$$ (Eq. 1)

whereas C$_c$ is the bentonite colloid concentration in solution. From the calculated distribution coefficient R$_{d, tot}$ the solution concentration in the ternary system C$_f$ is derived by:

$$C_f = \frac{C_0}{(m/_V \cdot R_{d,tot} + 1)}$$ (Eq. 2)

The time dependent ^{243}Am(III) and ^{242}Pu(IV) concentration variation of the ternary system (black symbols) in Fig. 2 is within the first approx. ~500h above the calculated equilibrium solution concentration (red symbols) expected based on the binary system data. This observation can be interpreted as an effect of slow radionuclide bentonite colloid dissociation kinetics. However, after approx. 500h contact time the estimated

solution concentration expected from the binary systems is comparable to the established radionuclide solution concentrations after 7500h in the ternary system. Taking into account the given uncertainties of the data, near- equilibrium conditions can be assumed. Results for ^{232}Th(IV) do not significantly differ from the ^{242}Pu(IV) data in terms of the reversibility kinetics. The ^{232}Th(IV) solution concentration after 7500h is within the range expected from the binary system data.
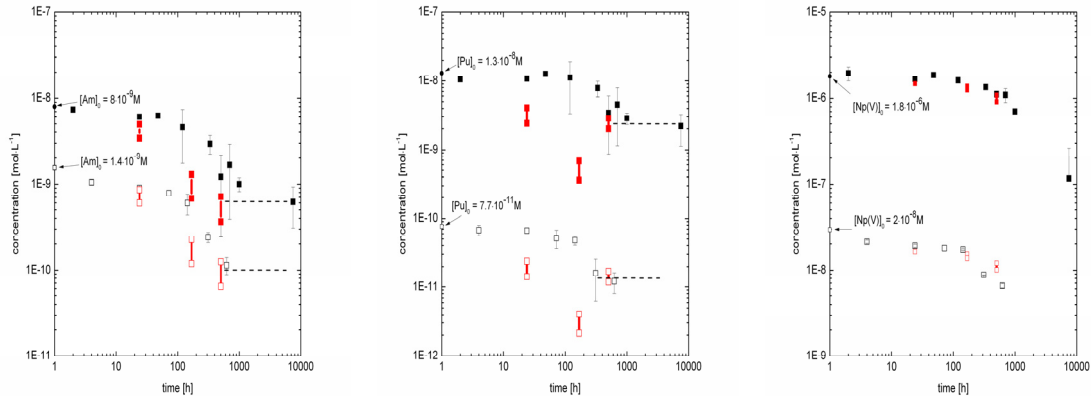
Figure 2: *Time dependent evolution of radionuclide concentration in the experiments using 1-2mm FFM for different RN concentrations. (left) ^{243}Am(III) (middle) ^{242}Pu(IV) (right) ^{237}Np(V). Values are given for non ultra centrifuged samples. The red symbols give the margins of expected ternary solution concentrations calculated via eq. 2 based on the binary systems distribution coefficients $R_{d,coll}$ and $R_{d,FFM}$.*

Regarding ^{237}Np(V), samples with $2 \cdot 10^{-8}$ mol·L^{-1} and $1.8 \cdot 10^{-6}$ mol·L^{-1} ^{237}Np(V) concentration have been prepared. As shown in Figure 2 a decrease in solution concentration can be observed starting at ~300h for both concentrations. The observed ^{237}Np(V) concentration decrease can either be explained by a slow reduction kinetic to Np(IV) in accordance with the experimental pe/pH conditions reached and/or with a slow sorption kinetic on the fracture filling material. Approximately 95% of the initial ^{237}Np(V) concentration is removed from solution after 7500h. The borderline of ^{237}Np(V) reduction is at Eh$_{(SHE)}$ around -60 mV (50% reduced Np), which is slightly lower than our measured Eh$_{(SHE)}$ values of -15 mV in the Grimsel system. Due to serious uncertainties in redox measurements, especially in natural groundwater with low concentrations of redox sensitive species like e.g. (Fe^{2+}/Fe^{3+}) (Grenthe et al., 1992), these values are likely in the range of the borderline for reduction. The experimental data obtained so far show that the time frame is insufficient to reach equilibrium conditions. A partial reduction at shorter contact times might occur, but cannot be resolved within the analytical uncertainties. Calculations based on equation 3 (Neck et al., 2009) can be used to estimate the amount of reduced ^{237}Np.

$$pe = \log K_{V-IVcoll} + \log[Np]_{tot} - \log(2) + \log \gamma NpO^{2+} - \left\{1 + \sum \beta'n, L[Lz-]n\right\} \qquad (Eq.3)$$

Under the experimental conditions of pH 5-10 and I ≤ 0.1 mol·L^{-1} background electrolytes and Ar atmosphere the following simplifications of eq. 3 can be made: (i) Formation of hydrolysis species and other complexes can be neglected and the term {1 + Σ β'n,L [Lz-]n } can be omitted. (ii) Concerning the ^{237}Np(V) total concentration ([Np]$_{tot}$ = [Np$^{(V)}$]° = (1.8 ± 0.2)·10^{-6} mol·L^{-1}) the SIT calculated activity coefficient for NpO$_2^+$ in 0.1 mol·L^{-1} NaCl (log γNpO$_2^+$ = - 0.10) is constant. With pe = 0.15 ± 0.35 the following equilibrium constant for I = 0 can be obtained: log K°$_{V-IVcoll}$ = 5.0 ± 0.4. Calculating the pe based on the values given above results in the borderline for 50% Np(V) reduction at pe = ~ -1 as given in Figure 3. This calculated pe is not far away from the measured pe values in the batch experiments, therefore a partial reduction of Np(V) on the FFM surface is plausible.
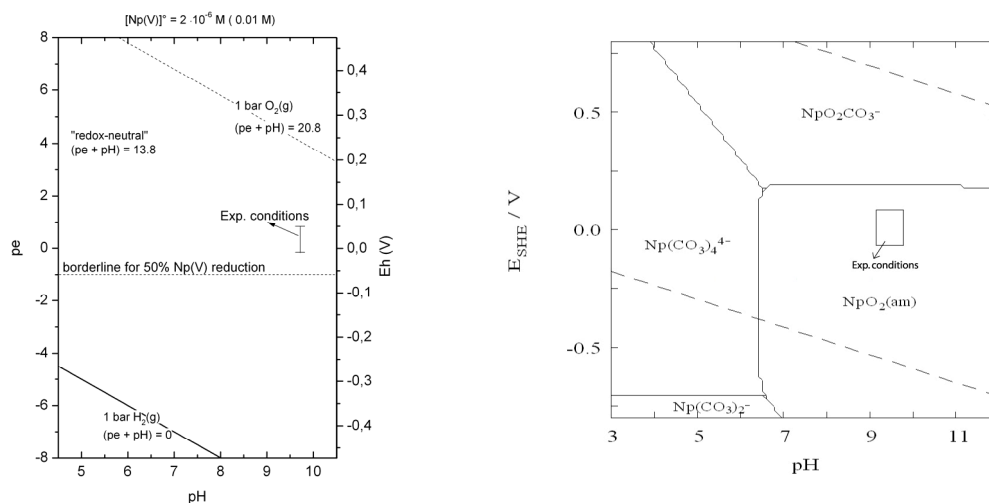
Figure 3: *(left) pe/pH diagram showing the experimental pe/pH range and the pe borderline for 50% Np reduction.(right) Predominance fields for Np species as a function of E$_H$/ pH range.*

The case of ^{99}Tc(VII) and ^{233}U(VI)

The concentrations of ^{99}Tc(VII) and ^{233}U(VI) remain constant over the experimental period with 1.3·10^{-8} ± 1.4·10^{-9} mol·L^{-1} and 5·10^{-7} ± 3·10^{-8} mol·L^{-1}, respectively indicating an absence of sorption to fracture filling material or reduction within the analytical uncertainty in both investigated systems. Besides, both elements show no interaction with the FEBEX colloids which is depicted by the comparison between UC and not-UC samples an absence of sorption/reduction to the FFM could be corroborated by means of geochemical calculations using Hydra/Medusa code and its internal thermodynamic database yielding negatively charged uranyl-carbonato complexes and pertechnetate as predominant solution species. Furthermore, a reduction to sparingly soluble phases like UO$_2$ and TcO$_2$ is thermodynamic not feasible under the prevailing geochemical conditions of the experiments. A Kd value of ~0.87 for ^{99}Tc(VII) and ~1.74 for ^{233}U(VI) could be determined. These Kd values are comparable to data of Kd ^{99}Tc(VII) = 0.38±0.10 and Kd ^{233}U(VI) = 1.81±0.19 obtained after one week contact time for fracture filling material fraction <1160 μm published in Nagra (2006), but significantly lower than Kd ^{99}Tc(VII) = 2.5±0.10 and Kd ^{233}U(VI) = 10.4±0.10 obtained

after five weeks contact time. Interestingly, the uranium in-situ Kd simply calculated based on the given FFM uranium concentration and the groundwater uranium concentration is orders of magnitude higher with Kd = ~3800 which clearly indicates that a large part of the natural uranium pool present in the FFM does not interact with the groundwater or is present in the tetravalent oxidation state.

Summary and Conclusions

Batch type experiments studying the RN bentonite reversibility in presence of Grimsel FFM with a grain size fraction of 1-2 mm have been conducted in natural Grimsel groundwater. ^{99}Tc(VII), ^{233}U(VI) and ^{237}Np(V) are not colloidal associated. Concentrations of ^{99}Tc(VII) and ^{233}U(VI) remain constant over the whole experimental duration (7500h) showing both no interaction with the FFM and no reduction to sparingly soluble phases. In contrast, the tri- and tetravalent radionuclides ^{232}Th(IV), ^{242}Pu(IV) and ^{243}Am(III) are almost quantitatively associated to bentonite colloids. The three colloid associated RNs show bentonite sorption reversibility kinetics which starts after ~100h contact time with the FFM and lasts at least to 7500h. The reason for the observed desorption of ^{232}Th(IV), ^{242}Pu(IV) and ^{243}Am(III) in the presence of FFM could be attributed to the higher surface area available for radionuclide sorption by the FFM compared to the bentonite surface area under the given experimental conditions. Results for ^{232}Th(IV) slightly differ from ^{242}Pu(IV) and ^{243}Am(III) in terms of the slower reversibility kinetics. Equilibrium conditions for sorption reversibility are indicated in the case of ^{242}Pu(IV) and ^{243}Am(III). In the case of ^{237}Np(V) a decrease in concentration could be explained by both sorption to fracture filling material and, more likely, by reduction to ^{237}Np(IV). The latter assumption is corroborated by means of geochemical modelling yielding furthermore no reduced species of ^{233}U(VI) and ^{99}Tc(VII) under the prevailing geochemical conditions of the experiments.

Taking into account the available surface area of porous fracture filling material in natural fractures in conjunction with natural residence times (low flow velocities) prevailing in deep ground waters (~ 1-10 m/a) sorption reversibility should likely occur in natural systems. Thus, the results strongly indicate the significance of RN sorption reversibility on RN migration which has to be considered and incorporated in modeling codes for colloid facilitated radionuclide transport to further increase the reliability in the simulated results.

References

Geckeis, H., T. Schäfer, W. Hauser, T. Rabung, T. Missana, C. Degueldre, A. Möri, J. Eikenberg, T. Fierz, W.R. Alexander, (2004) Results of the Colloid and Radionuclide Retention experiment (CRR) at the Grimsel Test Site (GTS) -Impact of reaction kinetics and speciation on radionuclide migration-. Radiochimica Acta, 92, 765-774.

Grenthe, I., W. Stumm, M. Laaksuharju, A.C. Nilsson, P. Wikberg (1992) Redox potentials and redox reactions in deep groundwater systems. Chemical Geology, 98, 131-150.

Missana, T., U. Alonso, M. Garcia-Gutierrez, and M. Mingarro (2008) Role of bentonite colloids on europium and plutonium migration in a granite fracture. Applied Geochemistry, 23(6), 1484-1497.

Nagra NTB 03-02 (2006) GTS Phase V (CRR Experiment): Supporting laboratory experiments with radionuclides and bentonite colloids. Nagra Technical Report NTB 03-02, Nagra, Wettingen, Switzerland.

Neck, V., M. Altmaier, D. Fellhauer, J. Runke, and T. Fanghänel (2009) Quantification of the redox potential for the reduction of Np(V) in non-complexing aqueous solutions at pH 5-10. in 1st Annual Workshop Proceedings 7th EC FP – Recosy CP, Barcelona 10-12th February 2009,122-129.

Schäfer, T., H. Geckeis, M. Bouby, T. Fanghänel (2004) U, Th, Eu and colloid mobility in a granite fracture under near-natural flow conditions. Radiochim. Acta, 92, 731-737.

THE REDOX POTENTIAL OF PU CONTAINING ACIDIC SOLUTIONS AND THE FATE OF "PU(IV)-COLLOIDS": DIRECT MEASUREMENT VERSUS OPTICAL ABSORPTION SPECTROSCOPY

Mirek Icker, C. Walther*, H. Geckeis

Institute for Nuclear Waste Disposal, Karlsruhe Institute of Technology, PO 3640,

D 76021 Karlsruhe, (D)

* Corresponding author: Clemens.walther@kit.edu

Abstract

Redox potentials were measured in acidic aqueous solutions ($-\log_{10}[H^+]=0.7$) containing different fractions of tri- and tetravalent plutonium. Eh values measured directly by a Pt electrode vs Ag/AgCl reference electrode agree very well with the redox potential calculated from the oxidation state distribution Pu(III)/Pu(IV). By monitoring the solutions over 120 days the kinetics of redox state distribution and dissolution of initially present Pu(IV)-colloids were studied. In solutions of Eh>950mV colloids dissolve and form Pu(VI), whereas at lower Eh the dissolution of colloids leads to formation of Pu(III). These findings corroborate the assumption that colloids are an integral part of the aqueous Pu redox chemistry and that formation and dissolution can be fully understood by means of Eh / pH stability calculations.

Introduction

Hydrolysis-, polymerization-, and redox reactions of tetravalent Pu in acidic aqueous solution take place simultaneously and it is often difficult to investigate one reaction without interference of the others. In solutions containing only one oxidation state of Pu, over time equilibrium of two or more oxidation states may form. In this case, Pu is oxidizing and reducing agent at the same time - so called disproportionation *Connick(1949)*. The prediction of the equilibrium oxidation state distribution in plutonium solutions was facilitated by use of more than ten disproportionation equations and corresponding equilibrium constants *Clark et al.(2006), Katz(1986), Newton(2002)*. The kinetics of Pu redox reactions depends strongly on the initial

oxidation state distribution and the acidity of the sample. In particular, those reactions involving formation or breaking of Pu-O bonds proceed quite slowly and it may take weeks or even months to reach a steady state. A considerable number of studies on this topic were performed since the 1950s (reviews in *Clark et al.(2006), Newton(2002)*) and Pu reaction kinetics are still an active area of research (e.g. *Haschke(2007))*.

In the present work we show that redox reactions of Pu are fully determined by knowing pH and redox potential of the solution. Redox potentials are measured by Pt-electrodes combined with a Ag/AgCl reference electrode and agree very well with those obtained from the distribution of oxidation states. As one of the main results we find that Pu(IV) colloids can dissolve and form Pu(III) or Pu(VI) respectively, depending on whether the solution is in the stability field of Pu(III) or Pu(VI).

Hydrolysis and redox reactions

The terminology used in the present work is adapted from *Walther et al.(2007)*: The oxidation state of aquatic species is designated Roman numerals, e.g. Pu(III). In the case of simultaneous presence of aquatic species and solid the subscript "aq" refers to the aquo ions, *e.g.* $Pu(IV)_{aq}$, whereas tetravalent colloidal Pu particles are designated $Pu(IV)_{coll}$. The exact ion is written with Arabic numbers and charges (*e.g.* Pu^{4+} or $Pu(OH)_y^{4-y}$). Due to the strong hydrolysis reactions of (mononuclear) Pu^{4+} ions starting already at ~pH 0.3 the total Pu(IV) equilibrium concentration is expressed by

$$[Pu(IV)]_{aq} = [Pu^{4+}] + \sum_{y=1}^{4}[Pu(OH)_y^{4-y}] = (K'_{sp}[OH^-]^{-4})(1 + \sum_{y=1}^{4}\beta'_{1y}[OH^-]^y) \qquad (1)$$

with the conditional solubility constant of amorphous $Pu(OH)_4$, $K'_{sp} = K^\circ_{sp}(\gamma_{Pu})^{-1}(\gamma_{OH})^{-4}$.

β'_{1y} are the conditional formation constants of $Pu(OH)_y^{4-y}$ complexes (see Table 2).

$$\beta'_{1y} = \frac{[Pu(OH)_y^{4-y}]}{[Pu^{4+}][OH^-]^y} = \frac{\beta^\circ_{1y}(\gamma_{Pu^{4+}})(\gamma_{OH^-})^y}{(\gamma_{Pu(OH)_y^{4+y}})} . \qquad (2)$$

[i] denotes the concentration of species i, γ_i its activity coefficient taking into account (log K'$_w$ = -13.885 at I=0.25 M *Rand et al. (2008)*). β°_{1y} are the formation constants at zero ionic strength, γ_i are calculated using the SIT formalism *Ciavatta(1980), Grenthe et al.(1992)*

$$\log_{10}\gamma_i = -z_i^2 D + \sum_j \varepsilon_{ij} m_j \qquad (3)$$

z_i is the charge of ion i, ε_{ij} is the interaction parameter for ion i and an oppositely charged ion j, and m_j (mol/kg~H_2O) is the molal concentration of ion j. D is the Debye-Hückel term at 25°C: $D = 0.509\sqrt{I}/(1 + 1.5\sqrt{I})$ with I the molal ionic strength)

The equilibria between Pu^{3+} and Pu^{4+} and between PuO_2^+ and PuO_2^{2+} are fast because the electron transfer between two species of the same structure is rapid and reversible:

$$Pu^{4+} + e^- \leftrightarrows Pu^{3+} \qquad , \log_{10}K°_{III/IV} = -17.69 \pm 0.04 \quad \textit{Lemire et al.(2001)} \qquad (4)$$

$$PuO_2^{2+} + e^- \leftrightarrows PuO_2^+ \quad , \log_{10}K°_{V/VI} = -15.82 \pm 0.09 \quad \textit{Lemire et al.(2001)} \qquad (5)$$
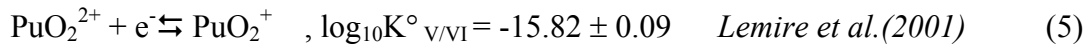
In contrast, the conversion of the lower oxidation states (Pu(III) or Pu(IV)) to the higher ones (Pu(V) or Pu(VI)) and vice versa are slow since formation or rupture of Pu-O bonds is involved *Katz(1986)*: $Pu^{4+} + 2\ H_2O \leftrightarrows PuO_2^+ + 4\ H^+ + e^-$ ($\log_{10}K°_{IV/V} = -17.45 \pm 0.17$ *Lemire et al.(2001)*). Note the fourth power dependence on hydrogen ion concentration which explains the increasing stability of the Pu(V) state with decreasing H^+ concentration *Fuger and Oetting(1976)*. Finally, if Pu(IV) oxyhydroxide colloids or precipitate are present, then solid Pu(IV) is in equilibrium with Pu(V)$_{(aq)}$ according to $Pu(OH)_4$ (am) $\leftrightarrows PuO_2^+ + 2\ H_2O + e^-$ ($\log_{10}K° = -19.8 \pm 0.9$ *Guillaumont et al.(2003)*).

Besides measuring the redox potential by means of ion sensitive electrodes, it can be determined from the activities of oxidized (a_{Ox}) and reduced (a_{Red}) species in solution. If complexation of one of the redox partners takes place, e.g. by hydrolysis of Pu(IV)$_{aq}$, the amount of Pu^{4+} must be calculated from the spectroscopic information on the amount of Pu(IV)$_{aq}$ via equation (1). We used equilibrium constants from *Yun et al.(2007)*) and performed ionic strength correction according to eq. (3) (I=0.25m). The redox potential E is obtained from the standard potential $E°$ and the activities of Pu^{3+} and Pu^{4+}, using Nernst's equation.

$$E = E° + \frac{RT}{z_e F} \ln \frac{a_{Ox}}{a_{Red}} \qquad (6)$$

R=8.31447 J/mol K, T is the temperature, z_e is the number of electrons involved in the redox reaction and F =96485 C/mol . Using the definition

$$pe = -\log_{10} a_{e^-} = 16.9\ E \qquad (7)$$

pe is related to the Pu concentrations via

$$pe = \log_{10} \frac{[Pu^{4+}]}{[Pu^{3+}]} - \log_{10} K'_{III/IV} \qquad (8)$$

$K'_{III/IV}$ is the conditional equilibrium constant, related to $K°_{III/IV}$ by

$$\log_{10} K'_{III/IV} = \log_{10} K^o_{III/IV} - \log_{10} \gamma_{Pu^{4+}} + \log_{10} \gamma_{Pu^{3+}} \qquad (9)$$

Analogously, the redox couple Pu(V) / Pu(VI) is related to pe via

$$pe = \log_{10} \frac{[PuO_2^{2+}]}{[PuO_2^+]} - \log_{10} K'_{V/VI} \qquad (10)$$

Sample preparation

A ^{242}Pu stock solution in 0.5M HCl was electrolyticaly oxidized to Pu(VI) and subsequently reduced to Pu(III) (stock solution **SIII**: [Pu$_{tot}$]= 8.24×10^{-3} M: [Pu(III)] =8.05×10^{-3} M and [Pu(IV)$_{aq}$] =0.191×10^{-3} M). A part of the stock solution was oxidized to Pu(IV) (**SIV**: [Pu$_{tot}$]= 6.22×10^{-3} M: [Pu(IV)$_{aq}$] =5.64×10^{-3} M and [Pu(III)] =8.95×10^{-5} M). From these stock solutions, five samples were prepared in 0.25M HCl (Table 1).

pH$_C$ (i.e. $-\log_{10}[H^+]$) of the samples were measured by a micro glass combination electrode (ROSS type) from Thermo Scientific calibrated against ten different HCl solutions between $[H^+]=1M$ and $[H^+]=0.1M$. The concentration $[Pu_{tot}]$ was measured by ICP-MS. Over a time period of six months the redox potentials of the samples were measured (Pt wire against a Ag/AgCl, Kurt Schwabe, Meinsberg). The measured potential was corrected by $\Delta V=207mV$ to obtain Eh (SHE). The oxidation state distribution and the fraction of Pu(IV) colloids was observed by absorption spectroscopy (Cary 5R) and was evaluated as described in *Walther et al.(2007)*. $[Pu(IV)_{coll}]$ was obtained from the optical absorption at 630nm. Errors are about 3% for Pu(III), Pu(IV) and Pu(VI), and some 10% for the Pu(IV)$_{coll}$ fraction, since the absorption cross section depends on age and composition of the colloids *Lloyd and Haire (1978)*.

Table 1. *Concentrations, pH$_C$ and relative abundance of Pu(III) and Pu(IV) in the freshly prepared samples (1) through (5)*

Sample	1	2	3	4
[Pu(III)] / %	8.00	9.10	50.00	80.00
[Pu(IV)] / %	92.00	90.9	50.00	20.00
pH$_C$	0.63	0.62	0.64	0.64
[Pu$_{tot}$] / M	3.25×10^{-4}	3.28×10^{-4}	3.43×10^{-4}	3.46×10^{-4}
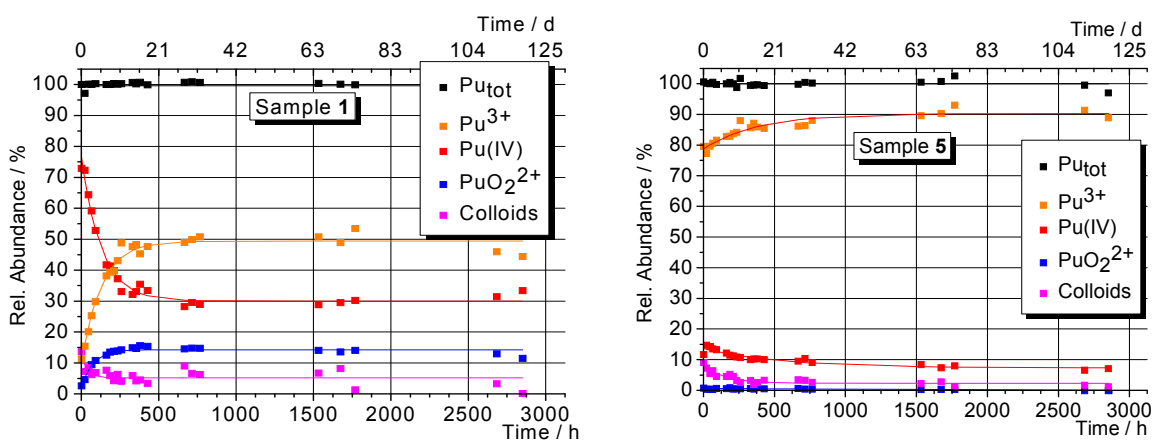
Figure 1. *Redox state distributions of (1) and (5) measured by absorption spectroscopy.*

Results

The Pu oxidation state distribution in all five samples was measured over a time period of 120 days (Fig. 1). In all cases the fraction of Pu(IV)$_{aq}$ (Pu^{IV}(OH)$_n^{z+}$, n=0-3) decreases while Pu(III) increases. A steady state is reached after some 30 days in samples (1) - (3), kinetics is more slowly in case of samples (4) and (5). Simple exponential decay functions (f_D), or growth functions (f_I), respectively,

o

$$f_D(t) = c_0 + \left(\Delta c \; e^{-t/\tau} \right) \qquad ; \qquad f_I(t) = c_0 + \Delta c \; \left(1 - e^{-t/\tau} \right) \qquad (11)$$

fitted to the spectroscopically obtained oxidation state distributions of Fig. 1 yield time constants of τ=128 h, 128 h, 139 h, 351 h and 555 h, for the decrease of Pu(IV)$_{aq}$ in samples **(1)** through **(5),** respectively. The increase of Pu(III) proceeds on similar time scales. The observed formation of Pu(VI), however, proceeds significantly faster in all cases. In samples **(1)** and **(2)** (hexavalent) PuO$_2^{2+}$ increases up to a relative abundance of some 10%, whereas in samples **(3)** to **(5)** PuO$_2^{2+}$ contributes less than 5%. Pu(V) cannot be measured at concentrations below 10^{-5}M. Upper limit estimations show that Pu(V) contributions are negligible in all samples. At time zero all samples contain, presumably amorphous, Pu^{IV}-oxo-hydroxide colloids at some [Pu$_{coll}$] = 4×10^{-5}M (*Walther et al.(2009)*). Over time the largest fraction of these colloids dissolve.

Discussion

The concentration of Pu^{4+} is obtained from the spectroscopically measured [Pu(IV)]$_{aq}$ according to eq. (1) using the parameters of Table 2. Subsequently, the redox potentials calculated from the Pu(III)/Pu(IV) abundances according to eq. (8) (denominated "spectroscopic", solid symbols) are compared to the redox potentials measured by the Ag/AgCl electrode (denominated Eh-Electrode, open symbols) in Figure 2. Samples **(1)** through **(3)** show very good agreement, indicating that at all times the redox couple Pu^{3+}/Pu^{4+} reflects exactly the redox state of the sample. However, the sample does not reach a steady state until t~30 d. Hence we do not denominate the agreement of measured Eh and spectroscopically obtained Eh an equilibrium, at least not for fresh solutions. For samples **(4)** and **(5)** slight deviations within the limits of analytical uncertainties are observed. The systematically lower spectroscopically obtained values might originate from the small concentrations of [Pu(IV)$_{aq}$]< 3×10^{-5} M close to the detection limit of our absorption spectrometer.

SIT parameters

i	j	ε_{ij} (kg mol^{-1})
H$^+$	Cl$^-$	0.12
OH$^-$	Na$^+$	0.04
PuO$_2^+$	Cl$^-$	0.09
PuO$_2^{2+}$	Cl$^-$	0.21
Pu^{3+}	Cl$^-$	0.23
Pu^{4+}	Cl$^-$	0.4
Pu(OH)$^{3+}$	Cl$^-$	0.2
Pu(OH)$_2^{2+}$	Cl$^-$	0.1

Conditional constants	Zero ionic strength
$\log_{10}\beta_{11}$' = 13.03 (Pu(OH)$_1^{3+}$)	$\log_{10}\beta_{11}°$ = 14.0 [a]
$\log_{10}\beta_{12}$' = 25.10 (Pu(OH)$_2^{2+}$)	$\log_{10}\beta_{12}°$ = 26.8 [a]
$\log_{10}$ K'$_{III/IV}$ = -16.72	$\log_{10}$K°$_{III/IV}$ = -17.69[b]
$\log_{10}$ K'$_{V/VI}$ = -15.32	$\log_{10}$ K°$_{V/VI}$ = -15.82 [b]

[a] from *Yun et al.(2007)*
[b] from Lemire et al.(2001)

Table 2. *SIT parameters and equilibrium constants used in the present work (I=0.25 m)*

Assuming simultaneous (fast) equilibration of the Pu(III)/Pu(IV) and the PuO$_2^+$/PuO$_2^{2+}$ couples, the concentration of PuO$_2^+$ (*i.e.* [Pu(V)]) can be calculated using eqs.(7), (10) and K'$_{V/VI}$ = -15.32 (from Tab. 2). This approach was validated *e.g.* in *Yun et al.(2007)*. The maximum relative abundances of Pu(V) range from 0.25 to 2% of [Pu$_{tot}$] corresponding to [Pu(V)] = 5×10^{-7} M to 6×10^{-6} M, which is below the optical detection limit. It is justified to neglect Pu(V) in the total balance of Pu obtained from

spectroscopic data, but its presence is nevertheless important for explaining the redox chemistry and the kinetics of the present experiments.

It was shown before by *Cho et al.(2005), Yun et al.(2007)* that the formation of trans-dioxo species from Pu(IV)$_{aq}$ cannot be explained by disproportionation according to $3Pu4^+ + 2\ H_2O \Leftrightarrow 2\ Pu^{3+} + PuO_2^{2+} + 4\ H^+$ since one would expect equal time constants for consumption of Pu(IV)$_{aq}$ and formation of Pu(III) and Pu(VI). The central result of the present work, however, is the role of the colloidal plutonium: The required ratios of consumption of three parts Pu(IV)$_{aq}$ for two parts of Pu(III) and one part Pu(VI) formed are not fulfilled. As reported in *Cho et al.(2005)* decrease of Pu(IV)$_{aq}$ and increase of Pu(III) are approximately equal under the conditions of samples **(1)** through **(3)**. Samples **(4)** and **(5)** behave differently. The increase of Pu(III) exceeds the decrease of Pu(IV)$_{aq}$, ruling out an exclusive formation of Pu(III) from Pu(IV)$_{aq}$. However, in both cases a large number of colloids were present in the freshly prepared solutions that dissolve over time. In recent publications Pu(IV)-oxy-hydroxide colloids were treated as part of the aqueous Pu redox system in so far as they are in equilibrium with (a) Pu(IV)$_{aq}$ as well as (b) with Pu(V) *Neck et al.(2007)*. The reaction Pu(IV)$_{coll}$ $\Leftrightarrow$ Pu(IV)$_{aq}$ is directly plausible. The equilibrium with Pu(V) may be understood through the existence of hyperstoichiometric PuO$_{2+x}$ reported in *Conradson et al.(2005)* and further supported by the observation of small mixed valence Pu(IV)/Pu(V) polymers described in *Walther et al.(2009)*. Whether Pu(III) or Pu(VI) is formed at the expense of the colloidal fraction is determined by the redox potential in the solution: Fig. 3 displays the samples in the Pourbaix diagram for [Pu$_{tot}$]=2×10^{-4}M. Samples **(1)** and **(2)** are in the stability field of Pu(VI) in agreement with the formation of Pu(VI) after dissolution of colloids. Samples **(3)-(5)**, at lower Eh, are in the stabiliy field of Pu(III) and consequently dissolution of colloids leads to the formation of Pu(III).
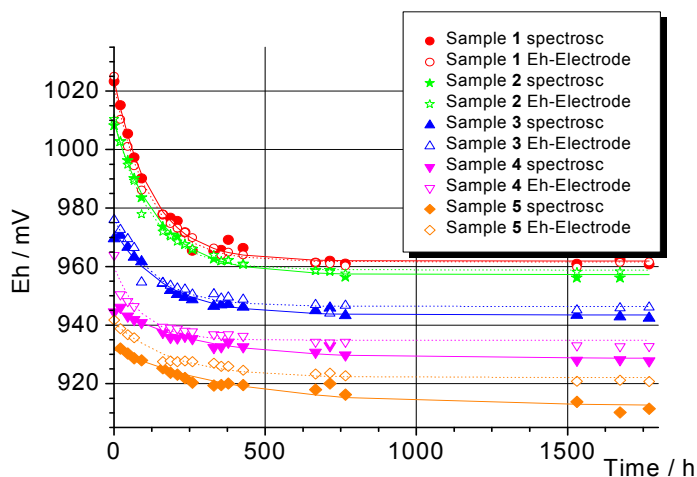
Figure 2. *Redox potentials of samples (1) – (5) measured with a Ag/AgCl electrode (open symbols) and by evaluation of the redox state distribution (solid symbols*

Summary and Conclusions

 The present results fit into the picture drawn by various authors over the last 50 years: *Connick and McVey(1949)* reported that in solutions with approximately 5% polymeric

plutonium, disproportionation was violated. *Costanzo et al.(1973)* observed excess reduction of Pu(V) in rather concentrated solutions which were oversaturated with respect to formation of Pu(IV) hydrous oxide and most likely contained Pu(IV) polymers or colloids. Strong deviations of steady state distributions from the expected equilibria were reported by *Romanovski et al.(2000)* and *Nitsche et al.(1994)* over a wide range of acidity and Pu concentration. On the other hand, acceleration of redox reactions by Pu(IV) polymers was suggested by *Madic et al.(1984)* and *Newton and Rundberg(1983)*. *Newton et al.(1986)* assumed that Pu(V) disproportionation cannot proceed at all in the absence of Pu(IV) polymers. The effects of polymers become even more pronounced as the colloidal fraction increases for strongly oversaturated solutions. *Yun et al.(2007)* observed decrease of Pu(IV)$_{aq}$ and dissolution of colloids at [Pu$_{tot}$]= 1×10^{-5}M, pH$_C$ 2, pe 14.0. However, Pu(V) was building up faster than Pu(IV)$_{aq}$ decreased and the formation of Pu(V) correlated well with the decrease of the colloidal fraction $-\Delta$[Pu(IV)$_{coll}$]=Δ[Pu(V)]. Introducing this additional data point in Figure 3 (open green square) it is easily seen that the sample discussed by Yun is situated in the (meta)stability field of Pu(V) (dashed green lines).
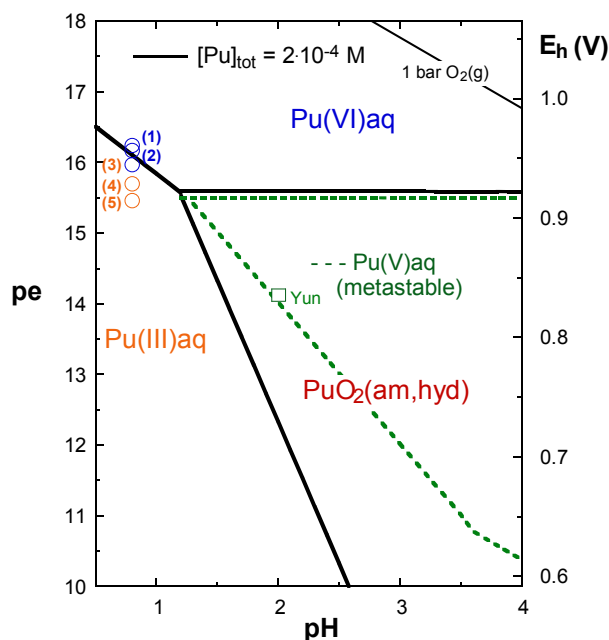
Figure 3. *Pourbaix diagram of [Pu$_{tot}$]=2×10^{-4}M, I=0.1 M (stability constants of Guillaumont et al.(2003) and β_{1n} for n=1–3 from Yun et al.(2007)). Open circles represent samples (1)-(5), the open square data from Yun et al.(2007). The dashed lines (metastable field of Pu(V)) refer to the reducton of PuO$_2^+$ to Pu^{3+} or Pu(IV). In this field PuO$_2$(am,hyd) is thermodynamically stable but the reduction of PuO$_2^+$ to PuO$_2$(am,hyd) is kinetically hindered, because PuO$_2$(am,hyd) cannot be formed directly; the first step requires the reduction of PuO$_2^+$ to aqueous Pu(IV) species*

We conclude that colloids are in equilibrium with both, Pu(IV) and Pu(V) and act as an intermediate for formation and breaking of the Pu-O bond. The present observations provide further evidence for the hypothesis made in *Cho et al.(2005)* that the redox

reactions of Pu(IV) proceed by a two step meachanism, namely the formation of PuO_2^+ followed by simultaneous equilibration of the redox couples Pu(V)/Pu(VI) and Pu(III)/Pu(IV). Whether the colloids dissolve and form Pu(III)/Pu(IV) or Pu(V)/Pu(VI) depends on the position within the pH-Eh stability fields. Non-equilibrium samples experience a driving force towards their respective stability fields which determines not only the end point but also the kinetics of the reaction. Hence, reactions might be kinetically hindered due to a low driving force and Pu species can be metastable on rather long time scales.

Acknowledgements

References

Cho, H.R.,Marquardt, C.M.,Neck, V.,Seibert, A.,Walther, C.,Yun, J.I.,Fanghänel, T. Redox behavior of plutonium(IV) in acidic solutions. in Recent Advances in Actinide Science. 2005. Manchester: RCS Publishing, Cambridge, UK.

Ciavatta, L. (1980): The specific interaction theory in evaluationg ionic equilibria. Ann. Chim. (Rome), 70, 551

Clark, D.L.,Hecker, S.S.,Jarvinen, G.D.,Neu, M.P., Chapter 7 in The chemistry of actinide and transactinide elements, L.R. Morss, et al., Editors. 2006, Springer. p. 813.

Connick, R.E. (1949): Mechanism of the disproportionation of plutonium(V). J. Am. Chem. Soc., 71, 1528

Connick, R.E.,McVey, W.H. (1949): The peroxy complexes of plutonium(IV). J. Am. Chem. Soc., 71, 1534

Conradson, S.D.,Begg, B.D.,Clark, D.L.,den Auwer, C.,Ding, M.,Dorhout, P.K.,Espinosa-Faller, F.J.,Gordon, P.L.,Haire, R.G.,Hess, N.J.,Hess, R.F.,Keogh, D.W.,Lander, G.H.,Manara, D.,Morales, L.A.,Neu, M.P.,Paviet-Hartmann, P.,Rebizant, J.,Rondinella, V.V.,Runde, W.,Tait, C.D.,Veirs, D.K.,Villella, P.M.,Wastin, F. (2005): Charge distribution and local structure and speciation in the UO_{2+x} and PuO_{2+x} binary oxides for x <= 0.25. J. Solid State Chem., 178, 521

Costanzo, D.A.,Biggers, R.E.,Bell, J.T. (1973): Plutonium polymerization. I. A spectrophotometric study of the polymerization of plutonium(IV). J. Inorg. Nucl. Chem., 35, 609

Fuger, J.,Oetting, F.L., The chemistry thermodynamics of actinide elements and compounds part 2: The actinide aqueous ions. 1976, Vienna: IAEA.

Grenthe, I.,Fuger, J.,Konings, R.J.M.,Lemire, R.J.,Muller, A.B.,Nguyen-Trung, C.,Wanner, H., Chemical Thermodynamics of Uranium. Chemical Thermodynamics. Vol. 1. 1992, Amsterdam: Elsevier.

Guillaumont, R.,Fanghänel, T.,Fuger, J.,Grenthe, I.,Neck, V.,Palmer, D.A.,Rand, M.H., Update on the chemical thermodynamics of uranium, neptunium, plutonium, americium and technecium. Chemical Thermodynamics, ed. D.B. OECD Nuclear Energy Agency. 2003, Amsterdam: Elsevier, North-Holland.

Haschke, J.M. (2007): Disproportionation of Pu(IV): A reassessment of kinetic and equilibrium properties. J. Nucl. Mat., 362, 60

Katz, J.J., Chemistry of the actinide elements. 1986, London: Chapman and Hall.

Lemire, R.J.,Fuger, J.,Nitsche, H.,Potter, P.,Rand, M.H.,Rydberg, J.,Spahiu, K.,Sullivan, J.C.,Ullman, W.J.,Vitorge, P.,Wanner, H., Chemical thermodynamics of neptunium and plutonium. Chemical Thermodynamics, ed. D.B. OECD Nuclear Energy Agency. Vol. 4. 2001, Amsterdam: Elsevier, North-Holland.

Madic, C.,Begun, G.M.,Hobart, D.E.,Hahn, R.L. (1984): Raman spectroscopy of neptunyl and plutonyl ions in aqueous solution: Hydrolysis of Np(IV) and Pu(VI) and disproportionation of Pu(V). Inorg. Chem., 23, 1914

Neck, V.,Altmaier, M.,Seibert, A.,Yun, J.I.,Marquardt, C.M.,Fanghänel, T. (2007): Solubility and redox reactions of Pu(IV) hydrous oxide: Evidence for the formation of PuO_{2+x}(s,hyd). Radiochim. Acta, 95, 193

Newton, T.W.,Rundberg, V.L. Disproportionation and polymerization of plutonium (IV) in dilute aqueous solutions in Materials Research Society annual meeting. 1983. Boston, MA: MRS, Pittsburgh.

Newton, T.W.,Hobart, D.E.,Palmer, P.D. (1986): The formation of Pu(IV)-colloid by the alpha-reduction of Pu(V) or Pu(VI) in aqueous solutions. Radiochim. Acta, 39, 139

Newton, T.W., Redox Reactions of Plutonium Ions in Aqueous Solutions, in Advances in Plutonium Chemistry, 1967-2000, D.C. Hoffman, Editor. 2002, American Nuclear Society: La Grange park, Illinois. p. 24.

Nitsche, H.,Roberts, K.,Xi, R.H.,Prussin, T.,Becraft, K.,Almahamid, I.,Silber, H.B.,Carpenter, S.A.,Gatti, R.C.,Novak, C.F. (1994): Long-term plutonium solubility and speciation studies in a synthetic brine. Radiochim. Acta, 66-67, 3

Rand, M.H.,Fuger, J.,Grenthe, I.,Neck, V.,Rai, D., Chemical thermodynamics of thorium. Chemical Thermodynamics, ed. M.I. F. Mompean, J. Perrone, OECD Nuclear Energy Agency, Data Bank. Vol. 11 (in print). 2008 Amsterdam: Elsevier, North-Holland.

Romanovski, V.V.,Brachmann, A.,Palmer, C.E.,Shaw, H.F.,Bourcier, W.L.,Jardine, L.J. (2000): Characterization of Pu colloidal and aqueous speciation in Yucca mountain groundwater surrogate. Abstr. Pap.Am. Chem. Soc., 219, U80

Walther, C.,Cho, H.R.,Marquardt, C.M.,Neck, V.,Seibert, A.,Yun, J.I.,Fanghänel, T. (2007): Hydrolysis of plutonium(IV) in acidic solutions: No effect of hydrolysis on absorption-spectra of mononuclear hydroxide complexes. Radiochim. Acta, 95, 7

Walther, C.,Rothe, J.,Brendebach, B.,Fuss, M.,Altmaier, M.,Marquardt, C.M.,Büchner, S.,Cho, H.-R.,Yun, J.-I. (2009): New insights in the formation processes of Pu(IV) colloids. Radiochim. Acta, 97, 199

Yun, J.I.,Cho, H.R.,Neck, V.,Altmaier, M.,Seibert, A.,Marquardt, C.M.,Walther, C.,Fanghänel, T. (2007): Investigation of the hydrolysis of plutonium(IV) by a

combination of spectroscopy and redox potential measurements. Radiochim. Acta, 95, 89

RELEASE AND RETENTION OF RADIONUCLIDES DURING 10 YEARS CORROSION OF SPENT NUCLEAR FUEL (SNF) IN PRESENCE OF MAGNETITE

Andreas Loida[*], Elke Bohnert, Bernhard Kienzler, Nikolaus Müller,
Markus Plaschke, Dieter Schild, Eva Soballa

Karlsruhe Institute of Technology, Institut für Nukleare Entsorgung (KIT-INE), DE

*Corresponding author: Andreas.Loida@kit.edu

Abstract

Relevant reactions affecting the observed radionuclide concentrations released from spent nuclear fuel may be determined by redox phenomena. In order to investigate these reactions, the reductive trapping of radionuclides/actinides onto canister corrosion products was investigated. The system under investigation consists of magnetite that has been in contact with spent fuel for ten years immersed in concentrated NaCl solution. The experiment was terminated and the gas phase and the solution composition were analyzed. Magnetite was recovered from the experimental vessel. The surface specific analyses show first results with respect to SEM/EDS and XPS of uranium. Unfortunately, a relatively high $p(O_2)$ due to radiolysis and $p(CO_2)$ was found in the gas phase. For this reason, the reductive trapping of actinides onto the corrosion products may interfere with other sorption processes. Future work is focused on the completion of the studies to characterize the nature of radionuclide retention upon the solid phases in the system. SEM/EDS, XRD, XPS and in situ Raman measurements on the corroded SNF sample will be applied.

Introduction

The source term from spent nuclear fuel (SNF) dissolution is highly dependent on oxidative dissolution of the fuel matrix. Various experimental data on the dissolution behaviour of the spent fuel matrix itself and in some cases in presence of container material (initial metallic Fe powder) as well, and the associated releases of radioelements were already obtained by extensive laboratory test programs. Overviews are given among others by Shoesmith (2000) and Ferry et al. (2005). The capacity of

corroded canister iron phases to incorporate radionuclides is under investigation within the European collaborative project "ReCosy". The stable corrosion product of steel canister material under reducing disposal conditions is magnetite. In the present study, it was intended to investigate the reductive trapping of actinides in metallic corrosion products which may provide for a driving force for SNF dissolution. About 10 years ago, an experiment ("denoted as K14Mt") was designed investigating the effect of magnetite on the overall corrosion behaviour of SNF in NaCl solution. This experiment was terminated and the investigations of gas atmosphere, solution composition and solid material contained in the system were started.

Experimental

The corrosion experiment was performed by using a pellet sized segment of high burnup SNF (50 MWd/kg U, linear power 260 W/m), 6.6 g fuel, and 10 mm in length together with commercial available magnetite (ALFA 012962, grain size ~ 5 μm). SNF sample and magnetite were immersed simultaneously in 5 mol/L NaCl solution (initial volume 200 ml, under Ar-atmosphere), using a glass vessel. During the initial phase of the experiment, the leachant was replaced entirely by fresh solution for four times until total 65 days. This procedure removed the "initial release fraction (IRF)", such as Cs and fission gases in the gap and on grain boundaries. Afterwards the experiment was continued without replacing the solution (static), lasting over 3562 days. Both, the gas phase and the solution were sampled at 78, 215, 349, 771, 1895 and 3562 days after start of the static phase. The analytical procedures are described by Grambow et al. (1996). A detailed description of the entire experimental procedure is given by Loida et al. (2003). After termination of the experiment, fractions of the magnetite were removed and analyzed. Various methods have been applied: SEM/EDX, XRD, Raman spectroscopy, XPS, digestion in HNO_3 and consecutive radiochemical analyses. The analyses are not yet completed.

Results and discussion

Results concerning the radionuclide release depend on the conditions kept during the 10 years of the experiment:

Gases: In the observation period, only a slight release of Xe of < 0.01 vol.% was found. Until 10 years, the H_2 concentration in the leaching vessel amounted to 18.5 vol.% and O_2 to 5.4 vol.%. After the first year, the CO_2 concentration raised from 0.1 to 0.8 vol.%, a value which cannot be explained by contact with air. The reason is still under investigation.

Solution concentrations: Fig. 1 shows the measured concentrations of the fission products Sr, Tc, Cs and the actinides U, Np, Pu, Am during the "static phase". Additionally, measured pH is also shown (right axis).

Fig. 1 shows considerable differences in the temporal evolution of the released radionuclides. Between 215 and 3562 days, the Sr concentration increases from $6 \cdot 10^{-7}$ to $2 \cdot 10^{-6}$ mol/L. Release of Cs is slightly faster, whereas the mobilization of U is at the highest rate. The final U concentration was measured up to $1 \cdot 10^{-4}$ mol/L. The other

radionuclides (Tc, Np, Pu and Am) are released at an intermediate rate. In total, fission gas release was >16%, Cs ~ 0.7%, Sr ~ 0.3%, and the actinides <0.1% of the inventory. After one year, the measured pH increased to 7.6 and dropped after 10 years to ~ 6.

Model calculations for 5 mol/L NaCl solution in contact with the measured $p(CO_2)$ revealed a decrease of the pH and the presence of dissolved carbonate. Under these conditions, initially generated solid $Na_2U_2O_7$ is dissolved forming U carbonato complexes in the range of the observed concentration of $1 \cdot 10^{-4}$ mol/l. Vice versa, at $pH_{exp} \sim 7.6$ in combination with the measured CO_2 partial pressure, the calculated Sr concentration is in equilibrium with solid $SrCO_3$ (strontianite). The evaluation of the radionuclide release rates in relation to the actual CO_2 partial pressures is not yet completed.

Figure 1: *Dissolved element concentrations of the experiment K14Mt. Solid line: measured pH.*

Solids: Figure 2 shows light optical micrographs of one of the cut surfaces of SNF pellet K14, covered by a layer, consisting predominantly of magnetite. Grain agglomerations of the magnetite were recovered and investigated outside the hot cell. In this case, their γ-dose rate was < 10 µSv/h.
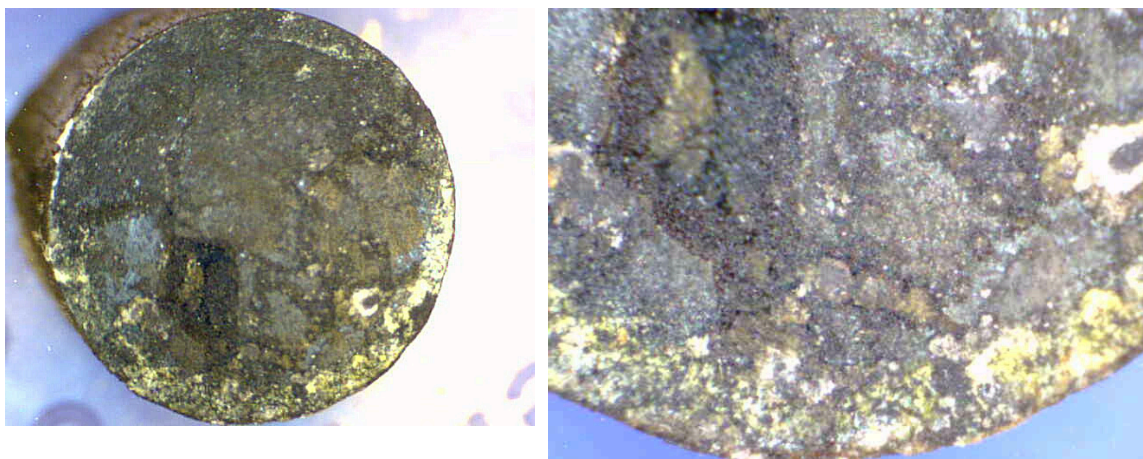
Figure 2:*Light optical micrographs of one of the cut surfaces of SNF pellet K14 (Ø: 10 mm) after termination of the experiment, covered by a layer consisting predominantly of magnetite.*

Figure 3 shows SEM micrographs of magnetite agglomerations at different magnifications. In both agglomerations the U content was measured to be around 0.05 at% (0.45 wt%) by means of EDS analysis. XPS investigations upon magnetite agglomerations have shown U contents of up to 0.9 at%.
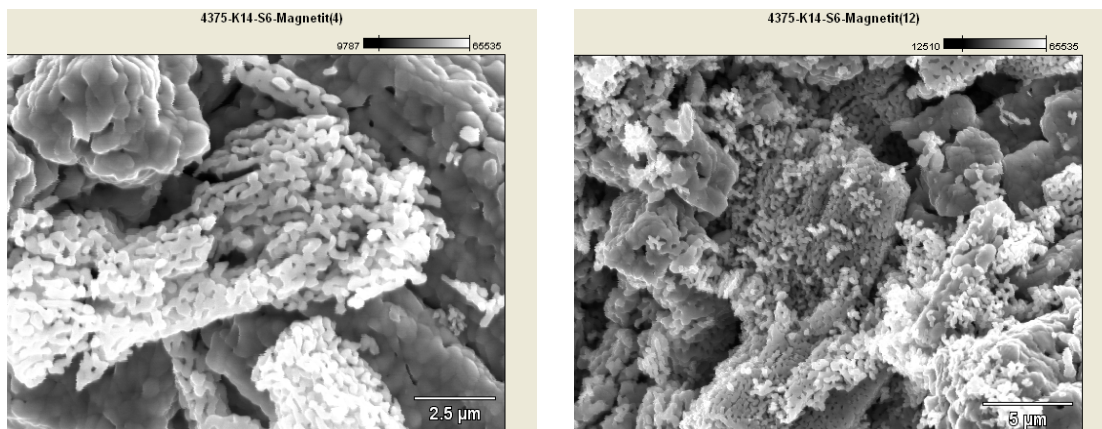
Figure 3: *SEM micrographs of magnetite agglomerations recovered after termination of the experiment with U contents around 0.5 at%.*

The magnetite spectra of the exposed magnetite and fresh material were identical. Figure 4 shows a narrow scan of the U 4f7/2 XPS spectrum and the resulting curve fit (red curve: sum curve of fitted functions). The diameter of the analysis area was roughly 400 µm. This spectrum demonstrates that U was present in the hexavalent state exclusively.
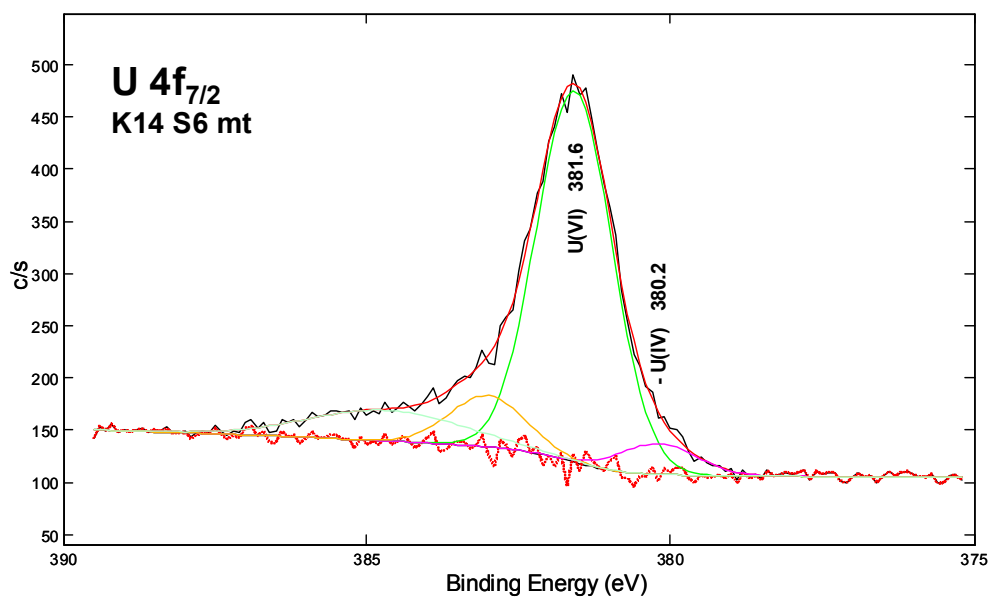
Figure 4: *XPS spectroscopy of U onto magnetite: Narrow scan of the U 4f7/2 spectrum and result of a curve fit (red curve: sum curve of fitted functions). Analysis area: Ø 400 μm.*

Conclusions

In the glass vessel used for SNF corrosion experiments over almost 10 years the atmospheric conditions were not sustained. In particular, the origin of the high $p(CO_2)$ is not yet resolved. The presence of CO_2 and O_2 explained the observed U and Sr concentrations. Under these conditions, Sr cannot be used as indicator for SNF matrix dissolution. Due to the relatively high $p(O_2)$ the expectations with respect to the reductive trapping of actinides in corrosion products may not be achievable.

Certain amounts of radionuclides are retained upon the magnetite. To quantify and to study the nature of their retention, "sequential extraction method" will be applied. Additionally, solid phase characterization work will be performed, with special attention on the cut surfaces of the SNF pellet, applying XRD, SEM/EDS, XPS and in-situ Raman spectroscopy.

References

Ferry,C., Poinssot,C., Broudique,V., Cappelaire, C, Desgranges,L., Garcia,P., Jegou, C., Lovera, P., Marimbeau, P., Piron, J.P., Poulesquen, A., Roudil, D., Gras, J.-M., Bouffioux, P. (2005), Synthesis of the Spent Fuel Long-Term Evolution, Rapport CEA-R-6084

Grambow, B., Loida, A., Dressler,P., Geckeis, H., Gago, J., Casas,I., de Pablo, J., Gimenez, J., Torrero, M.E. (1996) Long-Term Safety of Radioactive Waste Disposal: Chemical Reaction of Fabricated and High Burnup Spent UO2 Fuel with Saline Brines, Wissenschaftliche Berichte, FZKA 5702

Loida, A., Kienzler, B., Geckeis, H. (2003), Mobilization/Retention of Radionuclides during Co-dissolution of high burnup spent fuel and near field materials in salt brines. Mat. Res. Soc. Symp. Proc. Vol.757, pp. 433-439

Shoesmith, D.W. (2000) Fuel corrosion processes under waste disposal conditions, Journal of Nuclear Materials, 282, pp.1-31

MODELLING THE DIOCTAHEDRAL SMECTITES CEC. VARIATION VERSUS STRUCTURAL IRON LEVEL

J. Hadi[1], C. Tournassat[1], S. Betelu[1], L. Charlet[2] and I. Ignatiadis[1]

[1] BRGM, Environment and Process Division, 3, avenue Claude Guillemin, BP 36009, 45060 Orléans, Cedex 2, France

[2] LGIT, Geochemistry group, BP 53, 38041 Grenoble, Cedex 9, France

* Corresponding author: i.ignatiadis@brgm.fr

Abstract

A model to compensate the 2:1 layer excess negative charge induced by the Fe(III) to Fe(II) reduction by sodium dithionite buffered with citrate-bicarbonate in nontronite, beidellite, and montmorillonite is proposed. This model is based on reassessing published experimental data for iron-containing smectites and on the structural model published by Drits and Manceau (2000). According to these authors, Fe(II) coordination remains octahedral upon reduction. The increase in negative charge in the 2:1 layer due to the Fe(III) to Fe(II) reduction is thus compensated by the sorption of Na^+ and H^+ from solution. Some of the incorporated protons react with structural OH groups, leading to a dehydroxylation of the structure. Also, some protons bond with undersaturated oxygen atoms of the octahedral sheet. We developed an extended version of the model from Drits and Manceau (2000) giving the relative amounts of Na^+ (p) and H^+ (n_i) cations incorporated in the structure as a function of the amount of reduced Fe. Two equations enable to describe the investigated systems: $p=m/(1 + K_r.\omega.m_{rel})$ and $n_i=K_r.\omega.m.m_{rel}(1 + K_r.\omega.m_{rel})$; where K_r is a function of the total Fe content in the smectite, m, the Fe(II) content, m_{rel}, the reduction level (m/m_{tot}), CEC, the cation-exchange capacity (ω), and K_r, a constant specific to the smectite. Empirical relationships are given for K_r values as a function of clay types: montmorillonites, beidellites and nontronite. Additional data are necessary to confirm the model parameters.

Introduction

Iron is one of the most common redox species in soils and sedimentary rocks. Oxidation and reduction reactions involving Fe(II)/Fe(III) redox couple are usually kinetically fast. Among the different Fe(II)/Fe(III) couples present in soils and sediments, thermodynamic properties of structural Fe(II)/Fe(III) in clay lattice are not well known, although they could give valuable information on the redox environment of a system when coupled to a detailed mineralogical analysis (Favre *et al.,* 2006). The understanding of redox properties of the structural iron relies partly on a clear understanding of the mechanisms for Fe(III) to Fe(II) reduction. The present study aims at quantitatively modelling the above mentioned phenomena. The clays concerned by this study are mainly dioctahedral smectites.

Previous authors have demonstrated that reduction of Fe(III) in dioctahedral smectites is followed by an increase of the Cation Exchange Capacity (CEC) due to the increase of charge deficit. However, this increase of CEC is not directly proportional to the amount of Fe(III) that is reduced (Stucki *et al.* 1984). This phenomenon is also an evidence of a link between the CEC, the iron content and the redox potential and reactivity of the clay.

The goal of the preliminary model presented in this study is to predict the variation of the CEC (noted ω) as a function of the reduction level of the structural iron in dioctahedral smectites. The equations are based on previous published models, especially the one which was established by Drits and Manceau (2000) that we discuss here and try to improve. The other contributions that lead to our models are also briefly summarized.

Theoretical background: existing models

Experiments have shown that the mechanism of Fe(III) to Fe(II) conversion in iron containing dioctahedral smectites depends partly on the reducing agent, and on the physical and chemical parameters of the solution where the redox reaction takes place (Stucki, 1988). For this reason, the description of the mechanistic models presented in this study is restricted to those involving sodium dithionite ($Na_2S_2O_4$) as reducing agent, buffered with citrate bicarbonate solution (CBD).

Several models have been developed during the last three decades. As shown on figure 1, the first models (ω as a function of the reduction level of the structural iron) that were established (Roth and Tullock, 1973; Stucki and Roth, 1977; Gast, 1977) were linear functions and failed to reproduce the curvilinear profile of the experimental measurements (Stucki *et al.* 1984; Lear and Stucki, 1985). Another model was developed by Gan *et al.* (1992), but it was not taking into account of the variation of the CEC.

The later model (Drits and Manceau, 2000) appears to be more appropriate for modelling the variation of the CEC as a function of the amount of structural Fe(II). Drits and Manceau, (2000) developed their mechanism by adapting the previous mechanistic descriptions, considering this ideal nontronite structure:

$$Na_1(Si_7Al_1)Fe^{3+}_4O_{20}(OH)_4 \qquad\qquad (1)$$

In this model, the increase of the negative layer charge resulting from the reduction of Fe(III) is compensated by two mechanisms:

- an increase of the amount of interlayer positive charge by the adsorption of sodium cations from solution (Stucki *et al.*, 1984);
- a decrease of the total negative charge of the anionic structure of the 2:1 layers across the loss of structural hydroxyl groups (Roth and Tullock, 1973);
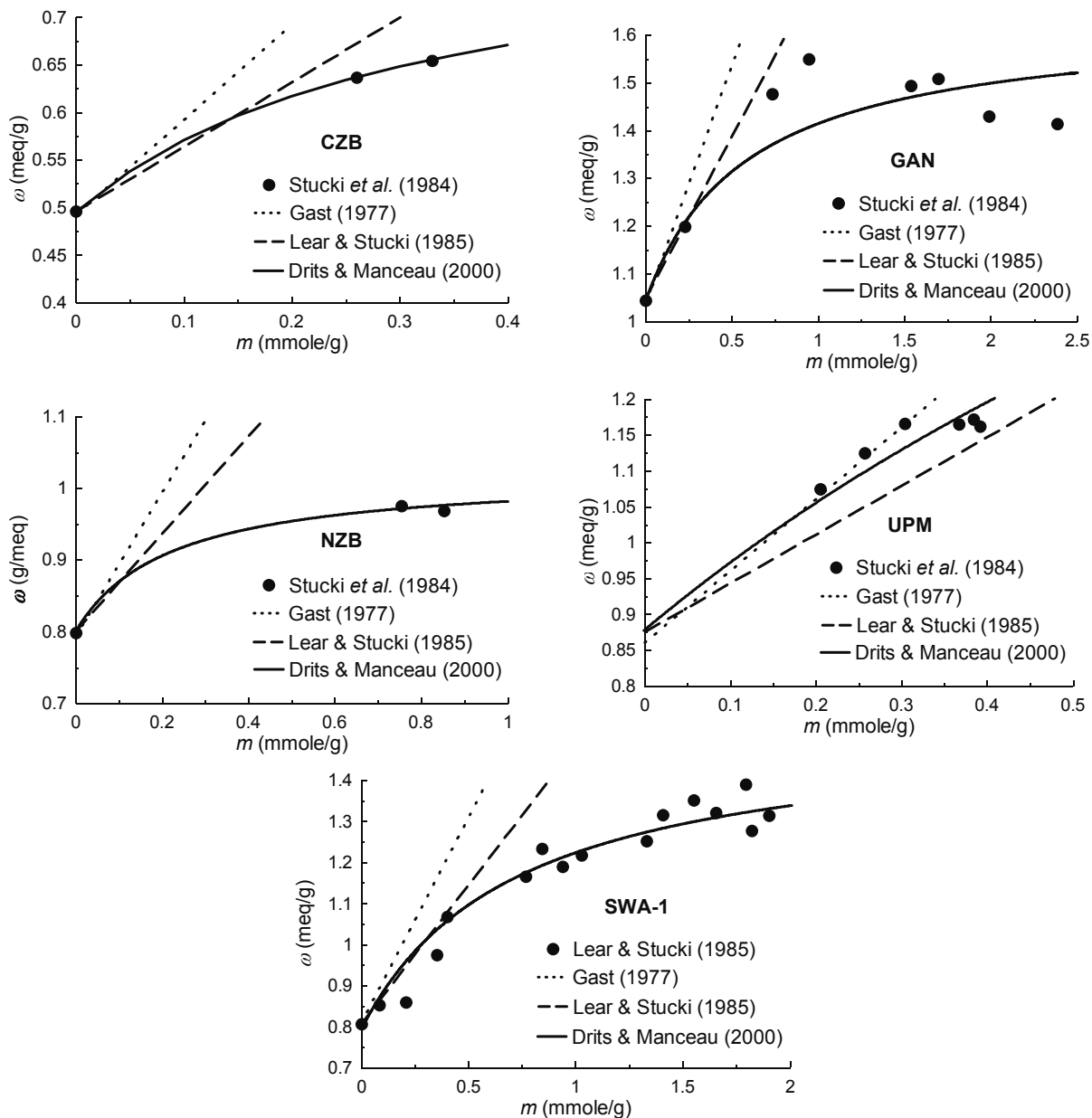
Figure 1: *Variation of CEC, ω, as a function of m, (the amount of structural Fe(II) in mmol per gram of clay). Experimental data were obtained by Stucki et al. (1984) on beidellites from Czechia (CZB) and New Zealand (NZB), on a montmorillonite from Upton, Wyoming (UPM), on a nontronite from Garfield, Washington (GAN) ; and by Lear and Stucki (1985) on a nontronite from Grant County, Washington (SWA-1).*

These two phenomena occur simultaneously. According to their observations, the reduction of Fe(III) occurs in the following mechanism:

$$m\mathrm{Fe}^{3+}_c + m\mathrm{e}^-_s \rightarrow m\mathrm{Fe}^{2+}_c \tag{2a}$$

$$\omega_0 \mathrm{Na}_c + p\mathrm{Na}_s \rightarrow \omega\mathrm{Na}_c \tag{2b}$$

$$n_i(\mathrm{OH})^-_c + n_i\mathrm{H}^+_s \rightarrow n_i(\mathrm{H}_2O)_s \tag{2c}$$

$$m = p + n_i \tag{2d}$$

$$m\mathrm{Fe}^{3+}_c + m\mathrm{e}^-_s + \omega_0\mathrm{Na}_c + p\mathrm{Na}_s + n_i(\mathrm{OH})^-_c + n_i\mathrm{H}^+_s \rightarrow m\mathrm{Fe}^{2+}_c + \omega\mathrm{Na}_c + n_i(\mathrm{H}_2O)_s \tag{2}$$
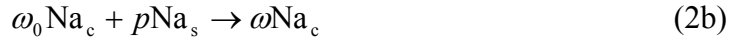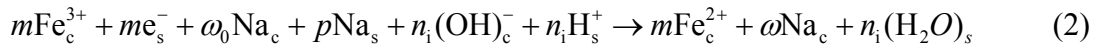
where m represents the amount of structural Fe(II) produced (expressed in mmol of structural Fe(II) per gram of clay), ω_0 and ω represent the layer charge respectively before and after reduction (expressed in mmol of interlayer Na^+ per gram of clay), thus p represents the quantity of Na^+ coming to the interlayer, n_i the quantity of adsorbed H^+. Subscripts c and s refer respectively to species coming from the structure or the solution. Note that, in the following works, ω_0 refers to cation exchange capacity of the clay in its fully oxidised state.

Equation (2a) corresponds to the reduction step driven by the electron produced by free radicals present in $\mathrm{Na}_2\mathrm{S}_2\mathrm{O}_4$ solution. Equations (2b) and (2c) represent the change in composition respectively in the interlayer and in the anionic structure. The compensation by Na^+ and H^+ sorption of the positive charge deficit created by Fe(III) reduction is given y equation (2d).

Equation (2) is based on the structural model proposed by Manceau *et al.* (2000) for the reduced nontronite. In this model, the coefficient n_i refers to the quantity of adsorbed H^+ and the loss of OH⁻ groups from the anionic structure after protonation. Problems come from the fact that the amount of structural OH groups in a reduced smectites is unknown and could not be easily derived. Thus, all of the H^+ initially incorporated is supposed to be consumed in the dehydroxylation step of the 2:1 layer (2c). Based on this statement, the structure (1) can be expressed as a function of the reduction level:

$$\mathrm{Na}_{1+p}(\mathrm{Si}_7\mathrm{Al}_1)(\mathrm{Fe}^{3+}_{4-m}\mathrm{Fe}^{2+}_{m})\mathrm{O}_{20}(\mathrm{OH})_{4-ni} \tag{3}$$
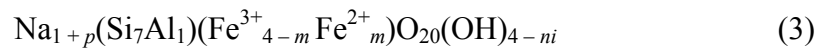
In order to evaluate if this model can fit the experimentally observed variation of the layer charge, an additional relationship between m, n_i and p. is required. The relative values of n_i and p are supposed to vary with the reduction level. When the amount of structural Fe(II) is relatively low, the layer charge variation is mainly compensated by sorption of Na^+. In this case, $p > n_i$. When the reduction level increases, the proportion of Na^+ sorbed from solution will decrease progressively, and the crystal-lattice energy will stabilize by the hydration of structural OH groups. Thus, at a certain stage of the reduction process, $n_i > p$. The compensation of the layer charge as a function of the reduction level can thus be written:

$$\frac{n_i}{p} = K_0 \frac{m}{m_{tot}} = K_0 m_{rel} \qquad (4)$$

Where, m represents the amount of reduced iron, m_{tot} represents the amount of total iron, thus m_{rel} is the reduction level ($m_{rel} \leq 1$), K_0 is a constant characteristic of a sample ($K_0 > 0$). The equation shows that when $K_0 m_{rel} \leq 1$) then $p > n_i$, and *vice versa*. Combining equation (2d) and (4) leads to:

$$p = \frac{m}{1 + K_0 m_{rel}} \qquad (5a)$$

$$n_i = \frac{m K_0 m_{rel}}{1 + K_0 m_{rel}} \qquad (5b)$$

Because, p and n_i only depends on m and m_{tot} (when expressed this way), equations (5a) and (5b) can be applied to any kind of iron bearing dioctahedral smectites. Thus, the structural formulae of a partially reduced dioctahedral smectite can be expressed as:

$$Na_{x+z+p}(Si_{8-x}Al_x)(Al_{4-mtot-z}Fe^{3+}_{mtot-m}Fe^{2+}_{m}Mg_z)O20(OH)_{4-ni} \quad (6)$$
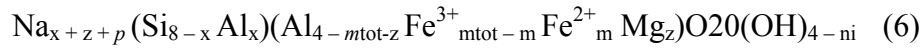
Combining equations (2b) and (5a), the layer charge ω can be expressed as a function of the amount m of Fe(II) produced:

$$\omega = \omega_0 + \frac{m}{1 + K_0 \dfrac{m}{m_{tot}}} \qquad (7)$$

Thus, p, n_i and so ω can be calculated as a function of m and m_{tot}, if K_0 is known. For each sample (GAN, CZM, NZM, UPM and SWA-1), Drits and Manceau (2000) have calculated the variation of the layer charge by varying K_0 (table 1) in order to fit the experimental data (figure 1).

Table 1: *CEC (ω_0), total iron content, K_0 and K_r values for the smectite samples studied by [a]Stucki et al. (1984) and by [b]Lear and Stucki (1985).*

Clay	w0 (meq/g)	Total Fe (mmol/g)	K₀	K_r (g/meq)
GAN[a]	1.046	4.201	5.5	5.26
SWA-1[b]	0.806	3.545	4.73	5.83
NZB[a]	0.799	1.502	6.25	7.81
CZB[a]	0.496	1.257	3.93	8
UPM[a]	0.876	0.539	0.32	0.37

Because there is no correlation between the values of K_0 and the total Fe content, Drits and Manceau (2000) introduced another parameter by normalizing the K_0 value by the CEC of the fully oxidized sample:

$$K_r = \frac{K_0}{\omega_0}$$ (8)

The calculated K_r values allowed them to establish a linear relationship between m_{tot} and K_r, but only for beidellites and nontronites (figure 2):

$$K_r = 9.32 - 1.06 m_{tot} + 0.02 m_{tot}^{\ 2}$$ (9)

This relationship is however questionable as it is shown in the next section.

Modified model

Drits and Manceau's model is subject to debate because:

- only few (5) samples have been studied

- the fitting was made on only 3 points in the beideillite cases

- two other samples have only few data points, therefore only SWA-1 has enough data

- the fitted parameters are not necessarily optimal (in a least square fitting sense) with regards to experimental data, as shown in table 2 (compare column 5 and 7) and figure 2

- the rationale behind equation (8) remains unclear.

Table 2: CEC (ω_0), total iron content, K_0 and K_r values for the smectites sample studied by [a]Stucki et al. (1984) and by [b]Lear and Stucki (1985).

Clay	ω_0 (meq/g)	Total Fe (mmol/g)	K_0^1	K_r (g/meq)[1]	K_r (g/meq)[2]	K_r (g/meq)[3]	K_0^3
GAN[a]	1.046	4.201	5.5	5.26	5.26	6.80	7.11
SWA-1[b]	0.806	3.545	4.73	5.83	5.87	5.99	4.83
NZB[a]	0.799	1.502	6.25	7.81	7.82	8.53	6.82
CZB[a]	0.496	1.257	3.93	8	7.92	8.29	4.11
UPM[a]	0.876	0.539	0.32	0.37	0.37	0.40	0.35

1. Values calculated by Drits and Manceau (2000)
2. Values calculated by equation (8)
3. Values obtained by linear least square method

In their model, calculation of the layer charge, ω, based on Fe(II) content, m, is made with a K_0 value constant over the entire reduction domain (equation 7). This constant K_0 is linked to the CEC of the fully oxidized sample by the equation (8). Thus K_r is set as a

constant, specific of the considered clay, and is a function of the total iron content m_{tot}. However, CEC also depends on the iron reduction level. Therefore, K_0 value should vary as a function of Fe reduction. K_r can still be a constant characteristic of a given clay, but its value should be obtained by normalizing the value of K_0 by the CEC at a given reduction level.
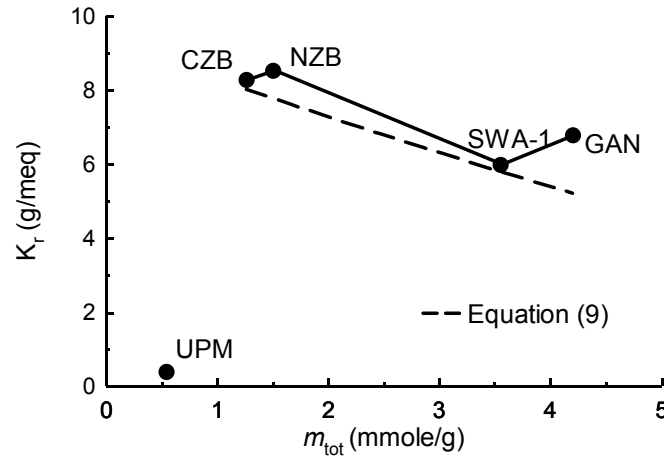
Figure 2: *Values of K_r for the different samples of smectites versus their total iron content m_{tot} (best-fitting curve for K_r parameter obtained by the method of least squares).*

Thus we propose to adapt their model by modifying the equations (7) and (8) in the following way:

$$K_0 = K_r \cdot \omega \tag{10}$$

$$\omega = \omega_0 + \cfrac{m}{1 + Kr \cdot \omega \cdot \cfrac{m}{m_{tot}}} \tag{11}$$

This equation can then be rewritten as a polynomial function:

$$a\omega^2 + b\omega + c = 0 \tag{12}$$

$$a = K_r \cdot \frac{m}{m_{tot}} \tag{12a}$$

$$b = 1 - a\omega_0 \tag{12b}$$

$$c = -(m + \omega_0) \tag{12c}$$

For a given amount m of Fe(II) produced ($m \neq 0$), the value of the corresponding CEC is given by the main root of the polynomial function (12):

$$\omega = \frac{\omega_0}{2} - \frac{1}{2a} + \frac{1}{2a}\sqrt{1 - a(2\omega_0 - a\omega_0^2 + 4c)} \qquad (13)$$

Results

This model has been applied to the experimental data given by Stucki *et al.,* (1984) and Lear and Stucki, (1985). Data were fitted by varying K_r value (table 3). The method of linear least squares was used to obtain the best-fitting values for K_r parameter. Results are shown in figure 3.
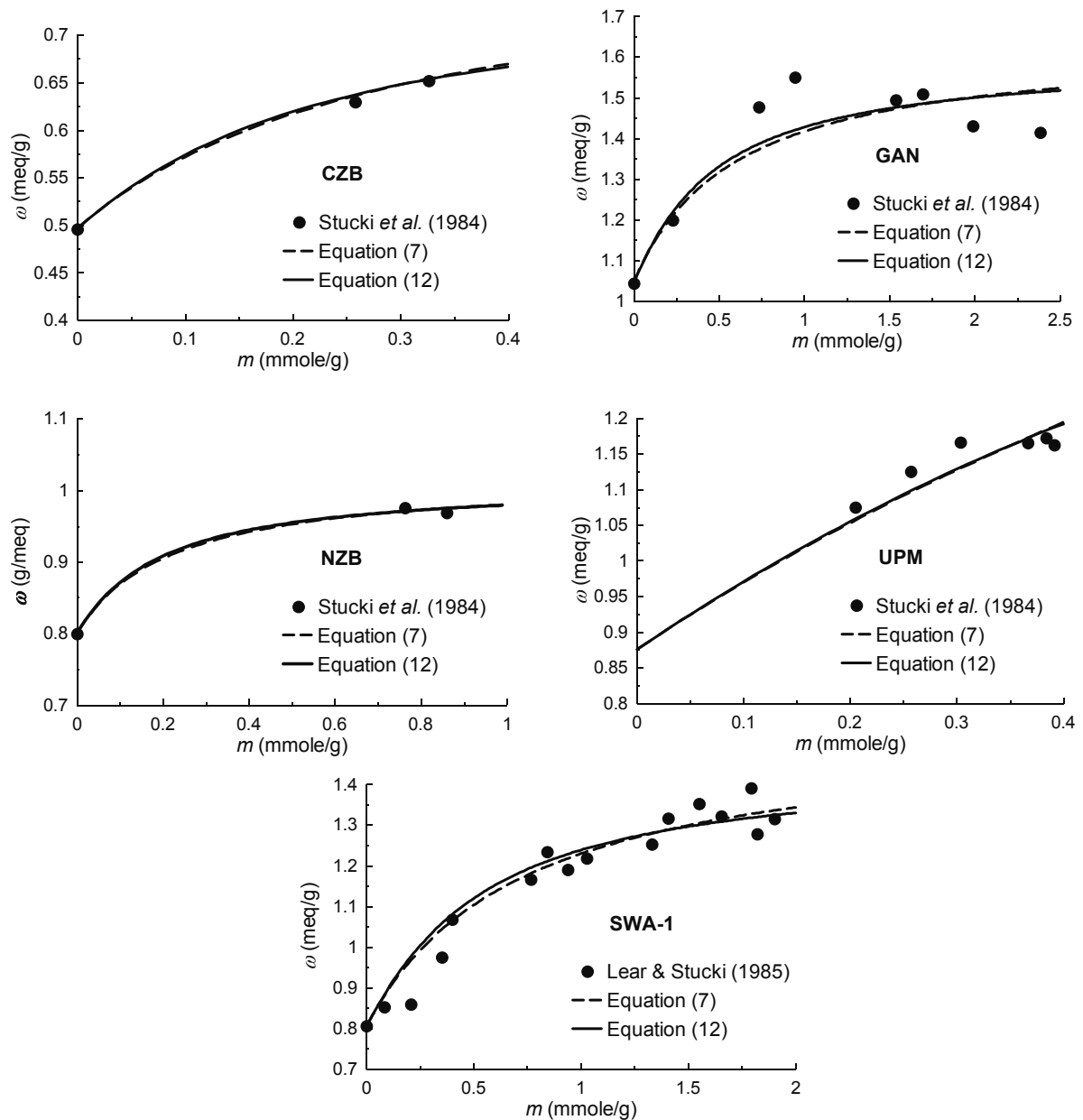
Figure 3: *Application of our model to the data obtained by Stucki et al. (1984) and Lear and Stucki (1985) and comparison with Drits and Manceau's model (2000)*

Table 3: *CEC (ω_0), total iron content, K_0 and K_r values for the smectites sample studied by [a]Stucki et al. (1984) and by [b]Lear and Stucki (1985).*

Clay	ω_0 (meq/g)	Total Fe (mmol/g)	K_r (g/meq)[1]	K_r (g/meq)[2]
GAN[a]	1.046	4.201	4.76	6.80
SWA-1[b]	0.806	3.545	3.76	5.99
NZB[a]	0.799	1.502	7.01	8.53
CZB[a]	0.496	1.257	6.35	8.29
UPM[a]	0.876	0.539	0.30	0.40

1. Optimal values for equation (12)

2. Optimal values for equation (7)

Discussion

As shown by figure 3, our model curve (equation 12) shape is identical to the one developed by Drits and Manceau (equation 7). The main difference lies: (i) in the way the CEC is calculated and (ii) in a major change in K_r values. The newly obtained values show an interesting trend (figure 4).
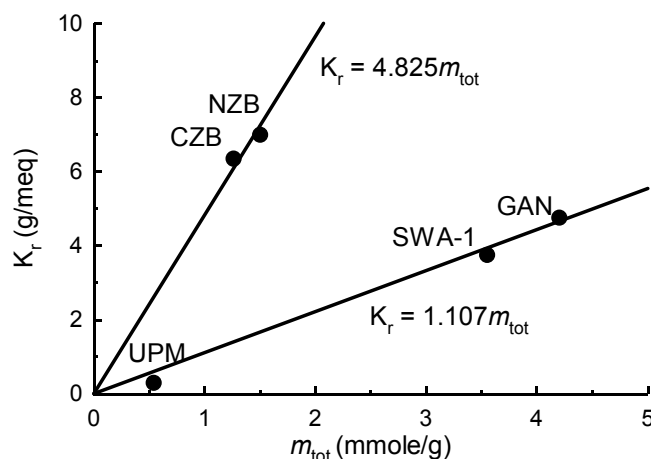
Figure 4: *K_r values for the different samples of smectite (CZB, NZB, GAN, SWA-1, UPM) versus their total iron content m_{tot} (best-fitting value for K_r parameter obtained by the method of linear least squares..*

K_r values appear to be a linear function of the total iron content, and the slope of this function appear to depend on the considered sub-group of dioctahedral smectites (i.e. beidellite, nontronite or montmorillonite). Only one point has been calculated for

montmorillonite (UPM), so we cannot say if the K_r value point belongs to the beideillite line or to another curve related to the montmorillonite group.

K_r can be considered as a buffer coefficient. The larger it is, the lower is the dependence of CEC to the amount of Fe(II) produced. This can be explained in the following way.

- On one hand, for electrostatic reasons, the higher the initial clay CEC (before reduction), the lower is the relative CEC increase for a given amount of Fe(III) reduced, as the interlayer is initially relatively more occupied by cations;
- on the other hand, the higher the total iron content, the larger is the amount of reducible iron. The increase in negative structural charge resulting from iron reduction is therefore larger and leads to increased H^+ incorporation and subsequent dehydroxylation. Thus, the increase in CEC is lowered for the same electrostatic reason as explained above (adsorption of cations is more and more limited).

Conclusion and perspectives

For each clay family, the K_r value seems to be a linear function of the total structural iron-content. Nonetheless, this new relationship has been calculated on an extremely limited number of data points. New measurements of CEC as a function of Fe-reduction level on other clay samples (characterized by different total iron-content and CEC values) are required to confirm the accuracy and relevance of the observed trend.

Acknowledgements

References

Drits, V. A. and Manceau, A., 2000. A model for the mechanism of Fe^{3+} to Fe^{2+} reduction in dioctahedral smectites. *Clay. Clay. Miner.* 48, 185-195.

Favre, F., Stucki J.W. and Boivin. P. 2006. Redox properties of structural Fe in ferruginous smectite. A discussion of the standard potential and its environmental implications. *Clay.Clay. Miner.* 54, 466-472.

Gan, H., Stucki, J. W., and Bailey, G.W., 1992. Reduction of structural iron in ferruginous smectites by free radicals. *Clay. Clay. Miner.* 40, 659-665.

Gast, R.G., 1977. Surface and colloid chemistry: in *Mineral in Soil Environments*, J.B. Dixon and S.B. Weed, eds., Soil Sci. Soc. Amer., Madisson, Wisconsin, 61-62.

Lear, P.R. and Stucki, J. W., 1985. Role of structural hydrogen in the reduction and reoxidation of iron in nontronite. *Clay. Clay. Miner.* 33, 539-545.

Manceau, A., Drits, V.A., Lanson, B., Chateigner, D., Wu, J., Huo, D.F., Gates, W.P., and Stucki, J.W., 2000. Oxidation-reduction mechanism of iron in dioctahedral smectites. 2. Structural chemistry of reduced Garfield nontronite. *American Mineralogist*, 85, 153-172.

Roth, C.B., and Tullock, R.J., 1973. Deprotonation of nontronite resulting from chemical reduction of structural ferric iron. In *Proceeding of the International Clay Conference*, J.M. Serratosa, ed., Division Ciencas C.S.I.C., Madrid, 107-114.

Stucki, J. W. and Roth, C.B., 1977. Oxidation-reduction mechanism for structural iron in nontronite. *Soil Science Society of Amercica Journal*, 41, 808-814.

Stucki, J. W., Golden, D.C. and Roth, C.B., 1984. Effects of reduction and reoxidation of structural iron on the surface charge and dissolution of dioctahedral smectites. *Clay. Clay. Miner.* 32, 350-356.

Stucki, J. W., 1988. Structural iron in smectites. *Soils and Clay Minerals*, J.W. Stucki, B.A. Goodman, and U. Schwertmann, eds., Riedel Publishing Company, Dordrecht. 217: 625-676.

Stucki, J. W., Bailey, G.W., and Gan, H., 1996. Oxidation-reduction mechanisms in iron bearing phyllosilicates. Applied Clay Science. *Clay. Clay. Miner.* 10, 417-430.

KINETICS OF PYRRHOTITE OXIDATION

David Arcos [1*], Lara Duro [1], Laurent Richard [1], Isabel Rojo [2], Frederic Clarens [2], Joan de Pablo [2]

[1] Amphos 21 (ES)
[2] CTM (ES)

* Corresponding author: david.arcos@amphos21.com

Abstract

Experiments on the dissolution kinetics of natural pyrrhotite (FeS_{1-x}) under variable and imposed redox conditions have been carried out at 25ºC and 1 bar. The dissolution of pyrrhotite appears to be incongruent, with the early formation of secondary ferrihydrite ($Fe(OH)_3$). Saturation index calculations indicate that ferrihydrite formed during the experiments from initially supersaturated solutions. If the redox conditions are not imposed, the system is shown to evolve towards an equilibrium state which involves pyrrhotite, ferrihydrite, and the aqueous solution. The results of kinetic experiments carried out far from equilibrium are currently being used analyses to derive a dissolution rate law for pyrrhotite.

Introduction

Under the reducing conditions prevailing in the deep water-rock systems considered for nuclear waste disposal, uranium is essentially present under its tetravalent state [U(IV)], which is relatively insoluble. Infiltration of oxidizing groundwaters into these systems may perturb their redox state, leading to a mobilization of uranium under its hexavalent form [U(VI)]. In order to evaluate the extent to which this may affect nuclear waste repositories, the redox buffer capacities of host-rocks must be known. In that respect, iron-bearing mineral phases such as iron sulphides or iron silicates are of primary importance. Although the oxidative dissolution of pyrite has received considerable attention from geochemists, pyrrhotite (which could be present as accessory mineral in igneous rocks) has been comparatively much less studied. Experiments have consequently been undertaken to characterize the oxidative dissolution kinetics of pyrrhotite.

Material and methods

Pyrrhotite

The pyrrhotite considered for the experiments is a natural sample from the skarn sulfide deposit of Gualba (NE Spain). A characterization of the sample by X-ray diffraction (XRD) has indicated the presence of subordinate amounts of quartz, pyrite, calcite, kaolinite, chlorite, and muscovite.

Experimental setup

Figure 1: *Batch reactor used for the pyrrhotite dissolution experiments.*

Experiments were carried out in a batch reactor (Figure 1) by adding between 1 and 4 g of pyrrhotite to 300-350 mL of a 0.01 M $NaClO_4$ solution. Stirring was provided by orbital shaker (not shown in Figure 1) at 80 rpm in order to keep the solution as homogenous as possible while minimising the risk of grinding pyrrhotite. Two kinds of experiments have been performed. In a first series of experiments carried out under N_2 atmosphere, the response of the system to a perturbation (injection of oxygen) has been investigated. These experiments will be referred as thermodynamic experiments and designated by ET. In a second set of experiments, the consumption of oxygen by pyrrhotite as a function of time has been evaluated for different initial dissolved oxygen concentrations. These experiments were performed in the absence of a free gas phase, reducing the volume of the reactor during sampling. These latter experiments are referred to as kinetic experiments, and designated by EC. Continuous monitoring of pH, Eh (Pt and Au electrodes) and dissolved oxygen (DO) was carried out with commercial electrodes. Calibration of pH and Au and Pt Eh electrodes (Crison, models 5221, 5262 & 5269 respectively) was performed against commercial standard buffers before and

after each experiment. Additionally, Eh electrodes were mechanically cleaned before each experiment. DO concentrations were measured only in EC experiments by means of an optical sensor (Ocean Optics, FoxyOR125GT) using two calibration points: 0 % measured in O_2 scavenging solution with 20 % Na_2SO_3 and 20.9% in open air. Aliquots were taken at elapsed times to follow the aqueous concentrations of iron (Fe(II) and Fe(total)) and total sulphur, by ICP-MS (Agilent 7500cx) and UV-Ferrozine method for iron speciation. Samples were filtered through 0.45 μm pore size filters before analysis. Experiments were performed inside a thermostatised chamber in order to keep the temperature constant at 25±0.2 ºC.

Results and discussion

Evolution of the system towards equilibrium

The evolution of pH and pe as a function of time during one of the thermodynamic experiments (ET001) is shown in Figure 2. The evolution path followed in this experiment is also depicted graphically in Figure 3. It can be deduced from these figures that the system evolves from initial values of pH = 6.0 and pe = 6.0 to values of pH = 9.5 and pe = - 8.0 which appear to remain essentially constant after approximately fifty days, consistent with an approach to an equilibrium state among pyrrhotite, ferrihydrite and the aqueous solution. It also appears from *Figure 3* that the solutions are initially supersaturated with respect to ferrihydrite, and subsequently evolve towards equilibrium with respect to this phase by precipitating it. The precipitation of ferrihydrite is further discussed in the following section.
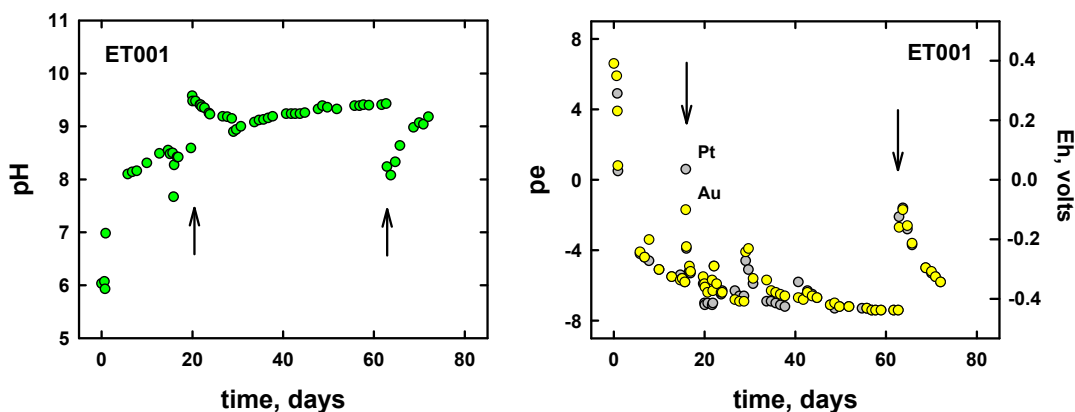
Figure 2: Evolution of pH and pe (measured with Pt and Au electrodes) as a function of time during a thermodynamic experiment. The arrows indicate perturbations of the system by adding 0.4 ml of NaOH 0.1 M after 20 days of experimental time and the intrusion of oxygen during sampling after 20 and 62 days of experimental time.

Ferrihydrite precipitation

Saturation index (Ω = log Q/K) values calculated for amorphous and crystalline ferrihydrite using the PHREEQC computer program (Parkhurst and Appelo, 1999) and the ThermoChimie database (Duro et al., this volume) are shown in Figure 4. These values have been calculated using the pH, pe and total iron concentrations measured as a function of time during one of the kinetic experiments (EC070). After approximately

200 hours of reaction, the solution appears to be in equilibrium with a phase having a solubility which is similar to that of crystalline ferrihydrite.

The reaction path followed by the solution during experiment EC008 is also depicted in the activity diagram shown in Figure 5. It can be seen in this diagram that the composition of the solution initially plots into the stability field of ferrihydrite and then evolves towards the saturation of amorphous and crystalline ferrihydrite, as well as to equilibrium with pyrrhotite (not shown in the diagram).

The precipitation of ferrihydrite is even more pronounced in the experiment EC137, where after the initial oxygen consumption, more oxygen has been added to the system and repeating the operation until 3 cycles of oxidation and oxygen consumption have been fulfilled. These 3 cycles of oxidation resulted in the precipitation of three distinctive layers of ferrihydrite on the pyrrhotite surface (Figure 4), clearly indicating that the precipitation of this phase is the responsible for the incongruent dissolution of pyrrhotite (scavenging part of the iron).
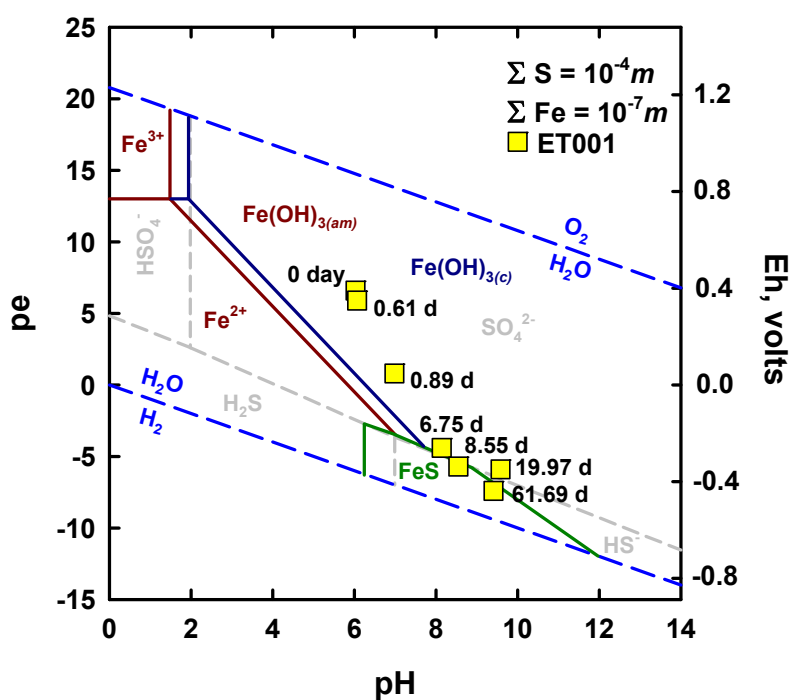
Figure 3: *pe-pH diagram for part of the Fe-S-O-H system. The diagram has been constructed for the concentrations of iron and sulphur measured at the end of experiment ET001. The symbols correspond to values of pH and pe measured at the indicated time during this experiment. Dark blue and red lines represent calculations considering crystalline or amorphous ferrihydrite respectively.*
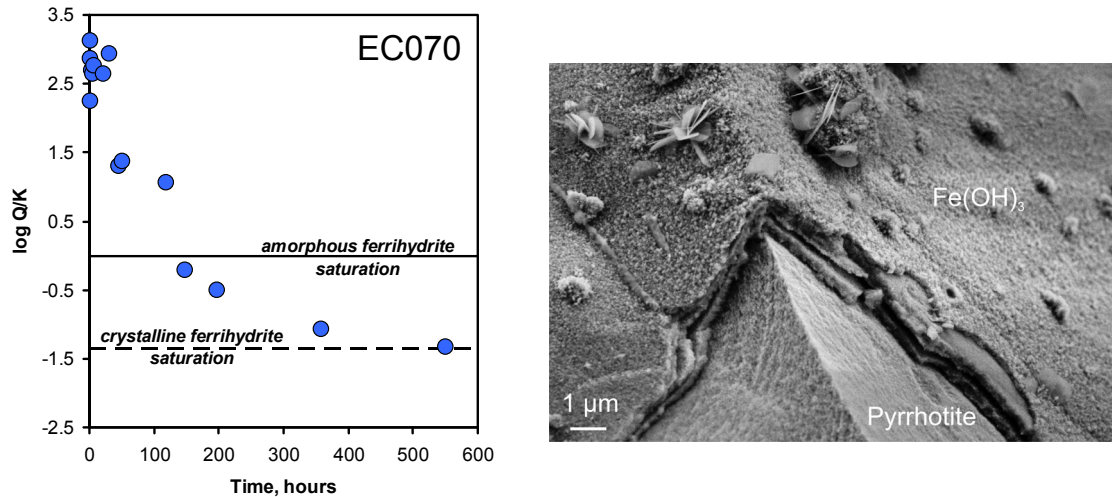
Figure 4: Left: Evolution of the saturation state of the reacting solution with respect to crystalline and amorphous ferrihydrite as a function of time during kinetic experiment EC070. Right: Fe(OH)₃ layers precipitated on pyrrhotite surface.
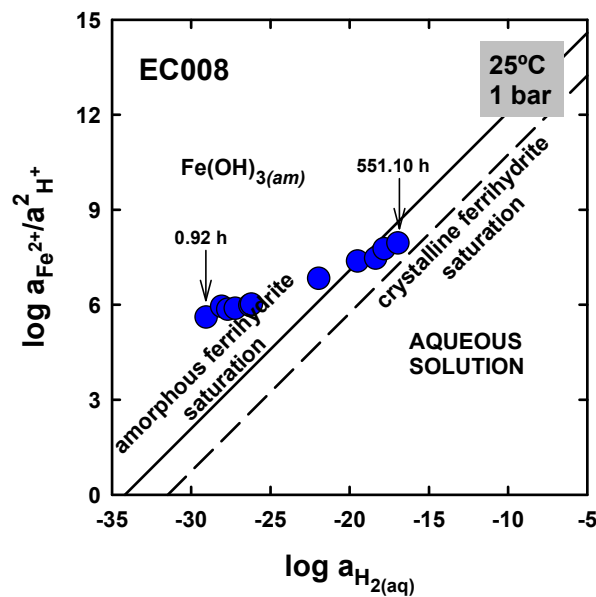
Figure 5: Activity diagram showing the reaction path followed by the solution during its interaction with pyrrhotite. The numerical values of the activities of Fe²⁺ and H₂(aq) have been computed with the PHREEQC program. The saturation lines for amorphous and crystalline ferrihydrite are consistent with the ThermoChimie database.

Kinetics

According to the evolution described in the previous sections, it seems clear that the reactions consuming oxygen in the system are the following:

$$FeS_{(c)} + 2\ O_{2(aq)} \rightarrow Fe^{2+} + SO_4^{2-}$$
$$\text{(pyrrhotite)}$$

$$Fe^{2+} + 0.25\ O_{2(aq)} + 2.5\ H_2O_{(l)} \rightarrow Fe(OH)_{3(s)} + 2\ H^+$$
$$\text{(ferrihydrite)}$$
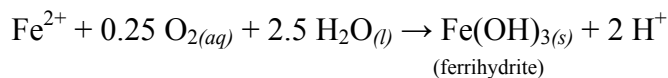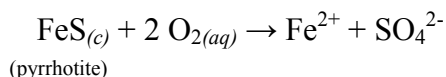
These two reactions proceed until the equilibrium is reached with respect to pyrrhotite and ferrihydrite respectively. According to the previous reactions we can expect oxygen to be consumed at a constant rate until it is exhausted or the equilibrium with at least one of the solids (pyrrhotite or ferrihydrite) is reached. If the system equilibrates first with one of the solids, then we can expect a change in the oxygen consumption rate until the equilibrium with the other solid is also achieved or oxygen is exhausted.

The evaluation of the experimental data should allow us to validate the previous conceptual model and the relative importance of the processes along the experimental time. Therefore, when looking at the oxygen evolution in the three kinetic experiments, as shown in Figure 6, we can observe that oxygen is initially consumed according to a first order rate (during the first 100 hours for experiment EC008 and the first 200 hours for experiments EC070 and EC137), and after that time a different oxygen consumption rate can be observed as a change in the slope of oxygen evolution in Figure 6.
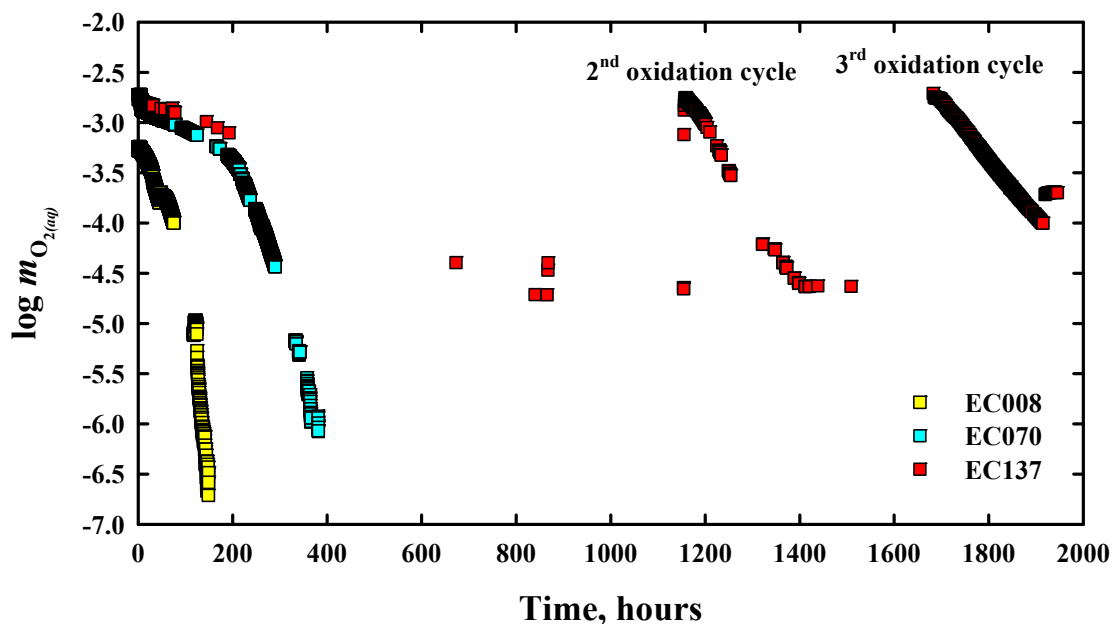
Figure 6: Oxygen evolution as a function of time in the three kinetic experiments (EC008, EC070 and EC137). Note that in experiment EC137, two additional cycles of oxidation have been forced after about 1100 and 1700 hours of reaction.

In order to clearly identify the processes responsible for the two stages of oxygen evolution (prior and after the change in oxygen consumption rate), we can examine the data for experiment EC070 (Figure 7). It can first be noted that during the first 200 hours, even though oxygen concentration decreases, pe values stay at a nearly constant

value of 7. In contrast, after 200 hours of reaction, the decrease in oxygen concentration is accompanied by a decrease in pe. It is important to note that this change in pe evolution (after the first 200 hours of experimental time) coincides with the change in slope for the oxygen consumption rate shown in Figure 6, as well as with a faster increase of iron concentration (Figure 8). However, it should be considered that measured pe under these conditions could be the result of mixed potentials due to the different redox pairs involved in the system, as $O(0)/O(-II)$, $S(-II)/S(VI)$, and $Fe(II)/Fe(III)$. Therefore, although the trends of pe could give an idea on the redox evolution, the measured values should be considered with caution.

The pe buffering effect observed during the first part of the experiment could be related to the precipitation of ferrihydrite, which has been identified in all the experiments. It would also be in agreement with the evolution of the saturation index for this mineral, which is shown in Figure 4. The incongruent dissolution of pyrrhotite and concomitant precipitation of ferrihydrite are also reflected in the concentrations of dissolved sulphur which exceed those of dissolved iron (by up to one order of magnitude in experiment EC137 – data not shown).

Once the system has reached equilibrium with ferrihydrite, which also occurs after approximately 200 hours, it can be seen in Figure 8 that iron concentration increases at a higher rate. This clearly suggests that ferrihydrite precipitation, and therefore, iron scavenging slowed down, resulting in a change in the oxygen consumption rate, as observed in Figure 6.
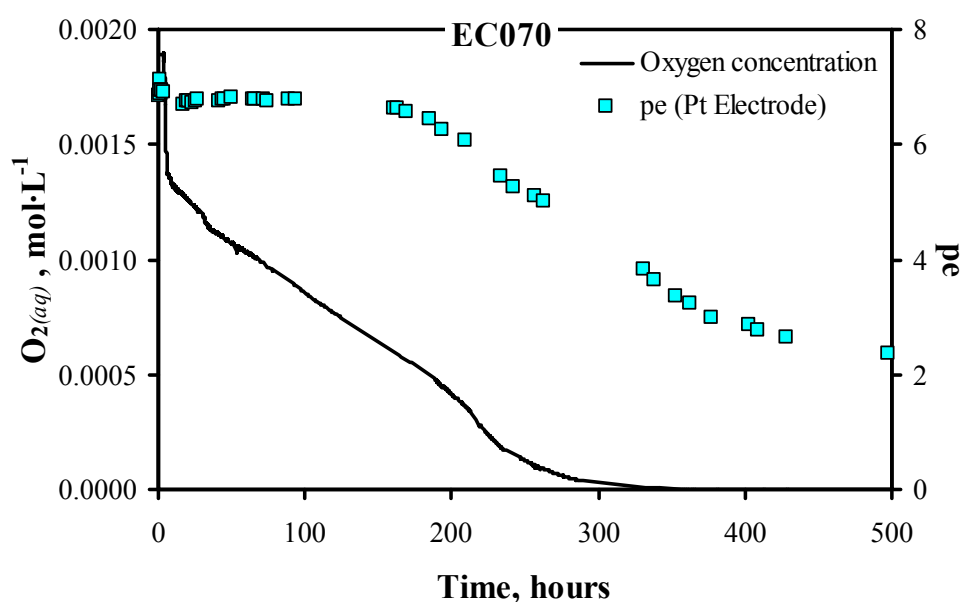
Figure 7: *Evolution of the oxygen concentration and pe in experiment EC070 for the first 500 hours.*

This change in the system behaviour has a direct impact in the pe evolution. Once the system is in equilibrium with ferrihydrite, the pe evolves towards the equilibrium with pyrrhotite as it is being dissolved, as it is shown in Figure 3. As the system approaches equilibrium with respect to pyrrhotite, the dissolution of this mineral, and hence the

oxygen consumption, slows down until it stops when the equilibrium is achieved (Figures 7 and 8).
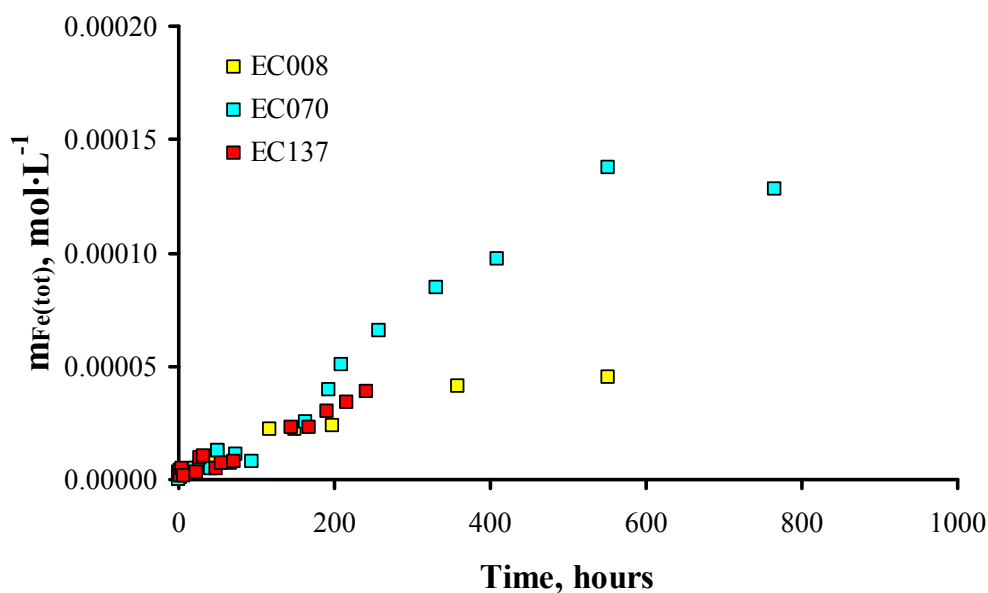
Figure 8: *Evolution of the total concentration of dissolved iron as a function of time during the first 1000 hours of the three kinetic experiments.*

Summary and Conclusions

A series of experiments has been conducted to determine the redox capacity of pyrrhotite. In the experiments, pyrrhotite has been immersed in a 0.01 M NaClO₄ solution under different initial oxidising conditions.

The results show that independently of the initial conditions, the system evolves towards the equilibrium with both pyrrhotite and Fe(III) oxyhydroxides. Moreover, the concentrations of total sulphur and iron in solution indicate an incongruent dissolution of pyrrhotite, as sulphur concentration increases faster and to higher concentrations than total iron in solution. This behaviour indicates that as pyrrhotite oxidises, the iron in solution is scavenged due to the precipitation of ferrihydrite.

However, a change in oxygen consumption rate has been observed. This change in the oxygen consumption is associated with the evolution of the system towards equilibrium with ferrihydrite first, maintaining a constant pe despite the oxygen consumption, and then to the equilibrium with pyrrhotite, where a decrease of pe together with oxygen concentration and a faster increase of iron concentration has been recorded. This second evolution stage proceeds until the system reaches equilibrium with both ferrihydrite and pyrrhotite.

A few experimental studies on pyrrhotite oxidation (bacterially mediated or abiotic) can be found in the literature, most of them conducted under acidic conditions as those expected under acid rock drainage conditions (Belzile et al., 2004, and references therein). In all cases, experimental conditions are very different to the ones considered in the present work, and therefore, their applicability for the interpretation of our results

is very limited. All these works also suggest a complex mechanism of pyrrhotite oxidation, considering the development of different oxidation product layers on pyrrhotite surface.

Our intention is to further study the pyrrhotite oxidation process and to derive a kinetic rate law for the oxidation of this mineral based on our experimental data.

References

Belzile, N., Chen, Y.-W., Cai, M.-F., Li, Y. (2004) A review on pyrrhotite oxidation. Journal of Geochemical Exploration, 84: 65-76.

Parkhurst D.L., Appelo C.A.J. (1999) User´s guide to Phreeqc (version 2) – A computer program for speciation, batch-reaction, one-dimensional transport, and inverse geochemical calculations. Water-Resources Investigations Report 99-4259. U.S. Geological Survey.

COMPARATIVE STUDY ON ELECTROCHEMICAL AND LASER-BASED FIBER-OPTIC OXYGEN MICROSENSORS APPLIED TO URANIUM CONTAMINATED BIOFILMS

Evelyn Krawczyk-Bärsch[1*], Dörte Steinbrück[2], Thuro Arnold[1], Elmar Schmälzlin[2], Michael Kumke[2]

[1] Institute of Radiochemistry, Forschungszentrum Dresden-Rossendorf e.V., P.O. Box 510119, 01314 Dresden (D)

[2] Institute of Chemistry - Physical Chemistry, University of Potsdam, Karl-Liebknecht-Str. 24-25, D-14476 Potsdam-Golm, (D)

* Corresponding author: E. Krawczyk-Baersch@fzd.de

Abstract

Dissolved oxygen is one of the key parameters in biofilm systems and may show different O_2 concentrations within the biofilm. The O_2 concentration may also be influenced by the microbial response to the exposure of heavy metals. Oxygen sensor measurements in such biofilms are a useful tool in interpreting oxygen microprofiles, which are influenced by the microbial respiratory activity. Consequently microsensors help to evaluate on redox processes in biofilms induced by heavy metals. To compare the applicability of electrochemical and laser-based fiber-optical microsensors for microbial ecology studies, oxygen microprofiling measurements in uranium free biofilms and in biofilms exposed to ecologically relevant uranium concentration were performed. The data obtained from both microsensor methods were in good agreement up to a depth of 680 and 480 μm. To avoid the risk of destroying the sensor tip, electrochemical sensor measurements had to be stopped at this depth. In contrast, laser-based sensor measurements were acquired over an additional range of 1 mm down to the biofilm/solid glass slide interface since optodes offer a high stability against consolidated materials. Thus, additional information on the oxygen concentration in lower zones of biofilms were obtained.

Introduction

The application of microsensors for microbial ecology studies to measure in situ microbial activities and microbial metabolic processes in aquatic systems has been described in recent years by a number of authors (e.g. Revsbech, 2005; Glud et al., 2000; Kühl, 2005; de Beer, 2000). Microsensors permit the measurements of fine scale chemical gradients in heterogeneous or homogeneous natural environments and are particularly useful in biofilms due to the small size of the sensor tip (few micrometers). Biofilms are populations of microorganisms that are immobilized at surfaces and are defined as matrix-enclosed bacterial populations. After the micoorganisms are attached to surfaces they excrete extracellular polymeric substances (EPS) in which the microbial cell eventually became embedded (Flemming et al., 1996. Through these water channels nutrients and possibly toxic heavy metals from the surrounding bulk solution pass through whereas metabolites and exudates of the microorganisms are transported away through these channels (Stoodley et al., 1994). Biofilms accommodate more than 99.9 % of all microorganisms on earth and can be found in soils, groundwater and surface water environments and even in extreme environments (Flemming, 1991). They are also encountered in uranium contaminated environments, e.g. associated with metal precipitates of seepage water of uranium tailings and in the acidic mine drainage water of a former uranium mine in Königstein, Saxony (Germany) as described in Arnold et al. (2010). Microorgansims in such biofilms have adapted themselves to these harsh conditions of elevated heavy metal concentrations and found a detoxification mechanism to survive and resist elevated concentrations of toxic elements without being negatively affected (Raff and S. Selenska-Pobell, 2006).

An alternative to the Clark-type oxygen microelectrodes for field applications related to aquatic biology are fiber-optic sensors. As described by Beyenal et al. (2000) fiber-optic sensors are immune to environmental changes in pH, salinity, and ionic strength and also immune to interferences caused by moisture, carbon dioxide, methane, and other substances. In comparison to microsensors they are simple to fabricate and show an improved long-term stability and storage stability. In recent years a range of fiber-optic sensor studies were carried out to measure in situ geochemical gradients in biofilms (e.g. Beyenal et al., 2000; Klimant et al., 1997; Beyenal et al., 2004; Kühl, 2005). However, there are no reported studies on optical sensors applied to biofilm samples exposed to elevated concentrations of heavy metals. In the present oxygen microprofiling study both electrochemical oxygen microsensors of the micro-Clark design (Unisense, Denmark) and fiber-optic oxygen sensors (optodes) were applied to stable multispecies biofilms grown without uranium and to the same biofilms subsequently exposed to uranium in concentrations of up to 1×10^{-6} mol/L in the nutrient solution, respectively. The aim of this study was to compare the application of fiber-optic oxygen sensors and electrochemical sensors and their suitability for environmental microbiology studies, respectively.

Experimental

The biofilms were cultivated in two rotating annular reactors. After a biofilm has been formed over a three month period, the culture medium of one of the reactors was adjusted to a uranium concentration of $1x10^{-6}$ mol/l U(VI). After three weeks the biofilm covered slides were placed in a flow cell for electrochemical and fiber-optic sensor studies as it was previously done with the biofilm of the first reactor, which was not exposed to uranium. Electrochemical microsensors of the micro-Clark design from Unisense (Denmark) were used to measure concentration profiles of oxygen in biofilms. The oxygen microsensors are based on the diffusion of oxygen through a silicone membrane to an oxygen reducing cathode which is polarized against an internal Ag/AgCl anode (Revsbech, 1989). The sensors had a sensing tip diameter of 10 µm. The stirring sensitivity with < 1 to 2% and the response time of < 1 s was specified from Unisense. The sensors were polarized and calibrated prior to each measurement series. The polarization was carried out by applying 800 mV for more than 12 hours (over night) and until the signal was stable. A two-point linear calibration was performed by measuring the electrode signal in two water samples with different oxygen concentrations. The zero reading was realized in an anoxic solution, i.e. sodium ascorbate and sodium hydroxide, both to final concentrations of 0.1 M. For the atmospheric reading, the sensors were placed in a calibration chamber, where the water had been well aerated by bubbling through a built-in bubble stone. The calibration was carried out ahead of each run since the permeability of the sensor membrane could change over time. During the measurements the sensors were fixed in a holder on a motor-driven micromanipulator stage. For automated and precise measurements at 20 µm steps along the Z-axis the micromanipulator was connected to a motor controller. The motor controller communicated with a PC via the RS-232 serial port and was controlled from the PC with the program PROFIX (Unisense, Denmark). The current was measured by an ammeter with pico-ampere sensitivity which was connected with an A/D converter for data acquisition. In the biofilms numerous oxygen microsensor profiles were measured versus depth at different points.

Microprofilings of the oxygen concentration in biofilms were also carried out by fiber-optic sensing. Compared to standard electrochemical-based detection methods optical sensing of oxygen has some advantages: i) no oxygen is consumed in the detection process, which can be crucial especially at very low oxygen concentrations and in small compartments like biological cells, where a consumption of the analyte could induce artefacts, ii) the optical method has a nearly unlimited potential for miniaturization (fiber tips with diameters < 10 µm or dye-doped polymer beads with diameters in nanometer range) allowing for highly space-resolved measurements, iii) only minor, if any, influence of the pH on the oxygen detection (see figure 2), and iv) fiber-optic sensors (optodes) are more inexpensive to replace, e.g. in the case of mechanical damage. An advantage of a laser over a light emitting diode is the high injection efficiency of coherent light into an optical fiber, which results in much increased light density at the sensor tip. An increasing of the excitation intensity is required to receive sufficient signal strength from micro- or nanoprobes. On the other hand, increased excitation intensity stimulates photo bleaching and the generation of disturbing fluorescence signals arising from the sample or from optical components within the

light path. Furthermore, residual excitation light may unintentionally reach the detector due to technical limitations. These interference signals superpose the sensor phosphorescence and generate a total signal with an altered phase shift. As long as the sensor signal is dominating and constant, the deviation may be corrected with calibration curves or even be neglected. But with decreasing sensor size, the signal-to-interference ratio degrades. While opaque sensor tip coating (Klimant et al, 1997; Kühl, 2005) is capable of insulating the setup efficiently from sample fluorescence but is without effect on interferences arising within the optical path. Furthermore, the protection layer thickens the probe tip and may be damaged during the penetration procedure.

To circumvent problems from background signals, an advanced two frequency phase modulation-technique has been applied. The basic idea of the technique is that background signals are in phase with the laser signal, since their decay times are almost zero compared to the microsecond-lifetime of the sensor's phosphorescence. Modulating the laser at two different sinusoidal frequencies simultaneously and measuring the respective phase shifts at these two different modulation frequencies simultaneously as well, allows quantifying the contribution of interfering signals in real time. Then, the unaltered sensor decay time and the corresponding oxygen concentration can be calculated. A further advantage of this technique is that it is not biased in case the signal ratios change during the measurement procedure, e.g. due to photo bleaching. A detailed description of the two-frequency phase modulation technique was given previously (Schmälzlin et al., 2005). The core of the instrument is a miniaturized 10x1x1 cm optical multiplexer, which was custom-built using optical telecommunication technique. It contains a "blue ray" 405 nm laser diode, an avalanche photo diode for detecting the red sensor signal, combinations of passive optics for a complete separation of the sensor signal from the excitation light, and an effective injection of the laser light into the fiber. When the dual-sinusoidally modulated blue laser light reaches the sensor-coated fiber tip, a fraction of the generated red sensor signal travels back through the fiber to the multiplexer, where it is separated from the excitation light and guided to the photo detector. The resulting voltage signal is routed to a dual-reference-type lock-in amplifier (EG&G, Signal Recovery 7260, Workingham, UK). This instrument is able to quantify the respective phase shifts at both modulation frequencies simultaneously (Löhmannsröben et al., 2006). Frequency synthesizers provide 5 and 9 kHz sinusoidal modulated signals, which are used to synchronize the lock-in amplifier and to generate the heterodyned modulation of the laser light. Data acquisition and evaluation of the oxygen concentrations were done online by a computer.

Results

The microsensor measurements of oxygen concentrations in biofilms were carried out by both electrochemical as well as by optode measurements. Due to the heterogeneity of biofilms numerous microprofiles were recorded starting from the biofim surface/bulk solution interface close to the biofilm/solid surface interface. Electrochemical and fiber-optic microsensor measurements were carried out in close proximity for a comparison of the measured values generated by the two different techniques. In the biofilm sample of the first reactor, which was not at all exposed to uranium, the oxygen concentration

profiles measured by electrochemical sensors showed high concentrations of oxygen almost over the total thickness of the biofilm. The average oxygen concentration ranged from 278 μmol/L at the top of the biofilm to 196 μmol/L at a biofilm depth of approximately 680 μm (see Fig. 1). This was in good agreement with the profiles obtained by fiber optic sensors. However, measurements by electrochemical sensors in deeper layers of the biofilm were avoided due to the risk of destructing the very fragile sensor tip. Microprofilings by fiber-optic sensors allow measurements in deeper regions of the biofilm, i.e. close to the biofilm/solid surface interface due to their higher stability of the optode against consolidated materials like e.g. glass slides. Consequently, the measurements were performed down to a depth of approximately 1660 μm, where the oxygen concentration was determined to be 179 μmol/L.
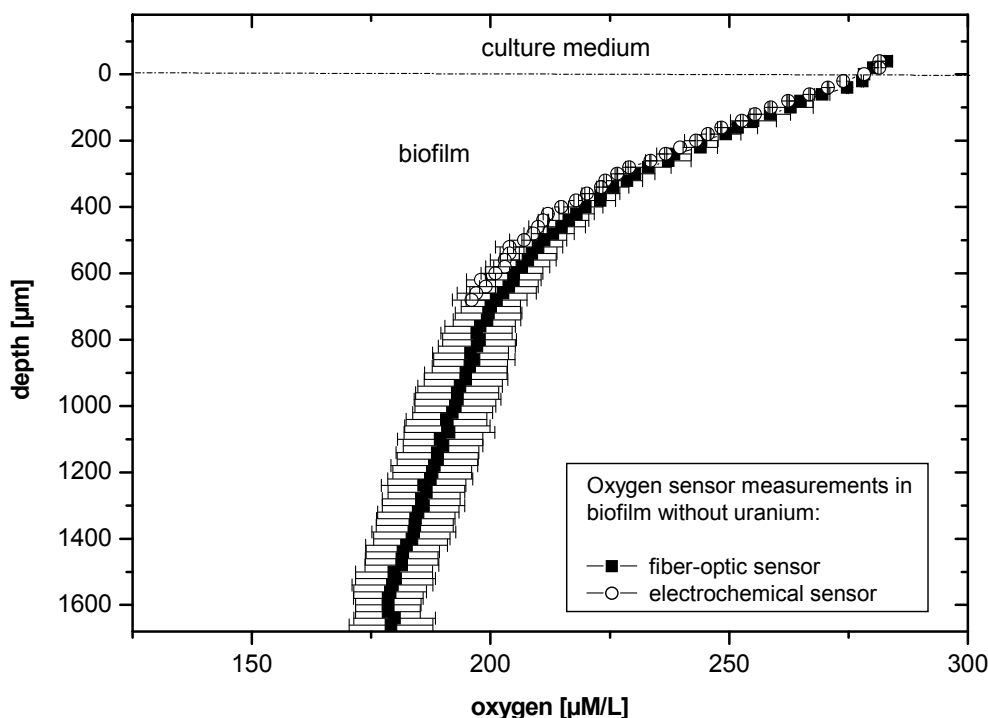
Figure 1: O₂ concentration profiles in multispecies biofilms grown without uranium measured by electrochemical and fiber-optic microsensors.

In contrast to the first biofilm, laser-based fiber-optic as well as the the electrochemical microprofilings in the biofilm, which was exposed to a uranium(VI) concentration of $1 \times 10\text{-}6$ mol/L, showed a very fast decrease of the oxygen concentrations within the biofilm from the top to the bottom of the biofilm specimens. The average concentration of the data measured at the surface of the biofilm revealed a high oxygen concentration of 278 μmol/L, which was in accordance to oxygen concentration measurements in the previously conducted uranium free biofilms. Due to the risk of destructing the very fragile tip of the electrochemical sensor the measurements were stopped at a depth of 480 μm. At this depth the oxygen concentration was determined to be 28.3 μmol/L measured by the electrochemical sensor and 24.2 μmol/L by the fiber-optic sensor, respectively (s. Fig. 2). However, measurements conducted by the laser-based fiber-optic microsensor were continued. At a depth of approximately 750 μm the oxygen

concentration dropped below the detection limit (< 1.8 μmol/L) and remained there until a biofilm depth of 1120 μm, at which the measurements were stopped.
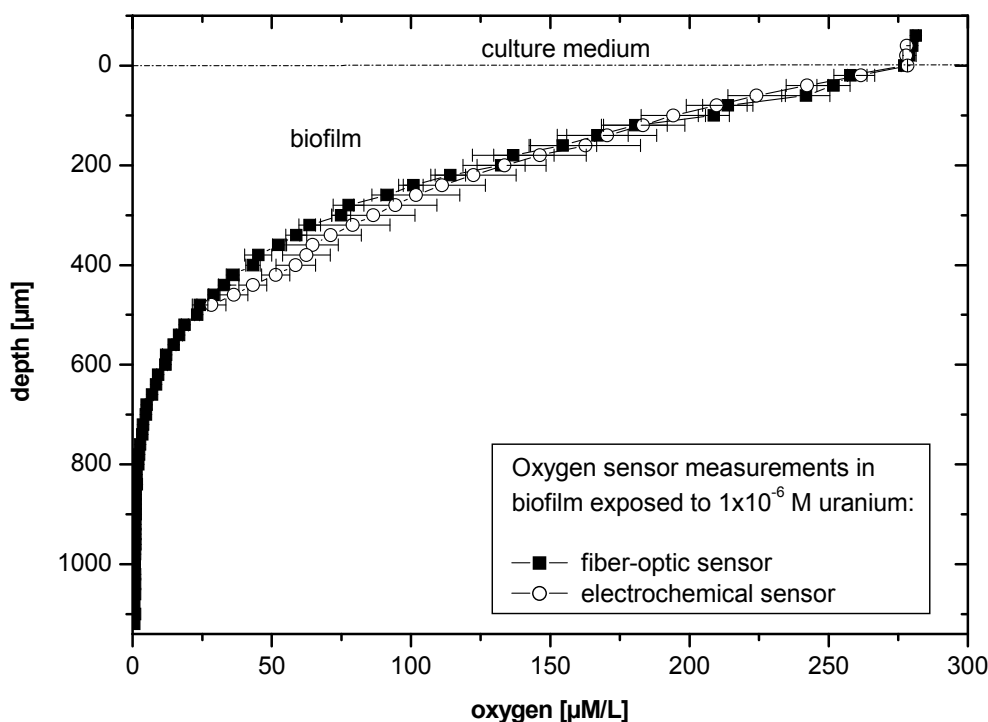
Figure 2: O₂ *concentration profiles in multispecies biofilms exposed to a uranium concentration of 1×10⁻⁶ mol/L U(VI) in the culture medium. The data were obtained by electrochemical and fiber-optic microsensor measurements.*

Discussion and conclusions

Within our research work it was shown that the application of electrochemical and laser-based fiber-optic oxygen microsensors to biological systems, e.g. multispecies biofilms exposed to environmentally relevant but elevated uranium concentration, offer two methods that allow the measurements of geochemical gradients with comparable good results. The oxygen microprofiling measurements showed independent of the two experimental techniques, that the oxygen concentration in the lower layer of the biofilms exposed to uranium is distinctively lower than the oxygen concentration determined in the lower layer of the uranium free biofilms. Krawczyk-Bärsch et al. (2008) described such a biofilm response as a prompt reaction of the microbes to the elevated concentrations of uranium. The addition of toxic heavy metals had obviously a strong effect on the stimulation of the metabolism of the microbes within the biofilm and, consequently, on their respiratory activity and oxygen consumption.

The two independent methods allow measurements of geochemical relevant gradients of oxygen in very small sample volumes and subsequently also with a high spatial resolution. In case of optode measurements, laser excitation and the two-frequency phase modulation technique allowed the use of miniaturized optodes with tip diameters < 10 μm without the need to any fluorescence-shielding opaque layer. The use of fiber-

optic oxygen microsensors in the field of environmental microbiology is a good alternative to electrochemical microelectrodes, because they can be applied in an almost non-invasive fashion, independent from pH and ionic strength. It is a general advantage of the optodes that no oxygen is consumed during measurement procedure. Particularly at measurements within micro- and nanocompartments, e.g. living cells, oxygen consumption by the probe may lead to significant interferences. In contrast to the time-consuming and expensive fabrication of electrochemical microelectrodes, optodes are produced at lower costs and with an improved long-term as well as storage stability compared to electrochemical microelectrodes. With our objective of using microsensors for field-measurement in radionuclide contaminated environments, e.g. former uranium mining sites, the fiber-optic microsensor equipments proved to be very suitable. Further improvements of the fiber-optical sensor setup, e.g. further miniaturization of the sensor equipments and simultaneously detection of additional physico-chemical parameters such as pH value are currently in progress.

Acknowledgements

References

Arnold T, Baumann N, Brockmann S, Krawczyk-Bärsch E, Zimmermann U, Jenk U, Weiß S, Wobus A (2010): Uranium speciation in subsurface acid mine drainage analysed by laser fluorescence spectroscopy. Environ. Sci. Technol. (in prep.).

Beyenal H, Lewandowski C, Yakymyshyn B, Lemley J, Wehri (2000): Fiber optic microsensors to measure back scattered light intensity in biofilms, Applied Optics 39, 3408-3412.

Beyenal H, Sani RK, Peyton BM, Dohnalkova AC, Amonette JE, Lewandowski Z (2004): Uranium immobilization immobilization by sulfate-reducing biofilms. Environ. Sci. Technol. 38, 2067–2074.

Flemming H-C (1991): Biofilme und Wassertechnologie. Teil 1: Entstehung, Aufbau, Zusammensetzung und Eigenschaften von Biofilmen. gwf-Wasser/Abwasser 132 (4), 197–207.

Flemming H-C, Schmitt J, Marshall KC (1996): Sorption Properties of Biofilms. In: Calmano W, Förstner U (ed.) Environmental behaviour of Sediments. Lewis Publishers, Chelsea, MI, 115-157.

Klimant,I, Kühl M, Glud RN, Holst G (1997): Optical measurement of oxygen and temperature in microscale: Strategies and biological applications. Sensors and Actuators B 38-39, 29-37.

Klimant I, Kühl M, Glud RN, Holst G (1997): Optical measurement of oxygen and temperature in microscale: Strategies and biological applications, Sensors and Actuators B 38-39, 29-37.

Krawczyk-Bärsch E, Grossmann K, Arnold T, Hofmann S, Wobus A (2008): Influence of uranium (VI) on the metabolic activity of stable multispecies biofilms studies by oxygen microsensors and fluorescence microscopy. Geochim. et Cosmochim. Acta 72**,** 5251-5265.

Kühl,M. (2005): Optical microsensors for analysis of microbial communities. In: Environmental Microbiology, vol. 397 (ed. J. R. Leadbetter). Methods in Enzymology, pp. 166–199.

Kühl M (2005): Optical microsensors for analysis of microbial communities. In: Environmental Microbiology, vol. 397 (ed. J. R. Leadbetter). Methods in Enzymology, pp. 166–199.

Löhmannsröben H-G, Beck M, Hildebrandt N, Schmälzlin E, van Dongen JT (2006): New challenges in biophotonics: Laser-based fluoroimmuno analysis and in-vivo optical oxygen monitoring", in: Workshop on Laser Applicationsin Europe, W. Gries, Th. Pearsall (eds.), Proc. SPIE, Vol. 6157 61570E, E-1 - E-6.

Raff J and Selenska-Pobell S (2006): Toxic avengers. Nucl. Eng. Int. 51 (619), 34–36.

Revsbech NP (1989): An oxygen microelectrode with a guard cathode, Limnology and Oceanography 34**,** 472-476.

Schmälzlin E, van Dongen JT, Klimant I, Marmodée B, Steup M, Fisahn J, Geigenberger P, Löhmannsröben H-G (2005): An optical multi-frequency phase modulation method using micro-beads for measuring intracellular oxygen concentrations in plants, Biophys. J. 89, 1339-1345.

Stoodley P, deBeer D, Lewandowski Z (1994): Liquid flow in biofilm systems, Appl. Environ. Microbiol. 60, 2711–2716.

SPECTROPHOTOMETRIC AND POTENTIOMETRIC DETERMINATION OF THE REDOX POTENTIAL IN SOLUTIONS OF HIGH IONIC STRENGTH

Tina Scharge[*], Barbara P. Bischofer, Sven Hagemann, Dagmar Schönwiese

Gesellschaft für Anlagen und Reaktorsicherheit (GRS) mbH (GER)

* Corresponding author: tina.scharge@grs.de

Abstract

The oxidation state of heavy metals and radionuclides has a considerable impact on their mobility. In an aqueous solution it can be determined by chemical speciation analysis or predicted on the basis of physical parameters of the solution, especially pH and redox potential (*Eh*).

For nuclear repositories in salt formations, potentially intruding solutions always exhibit a high ionic strength. Potentiometric measurements of *Eh* in such environments are hampered because of variable liquid junction potentials at the reference electrode. In order to maintain a relation between electrode signal and the redox potential, a model for the calculation of the medium induced bias was experimentally derived. A series of measurements was carried out for investigating the influence of different sulfate salts. From these results and other recent measurements (Bischofer et al. 2009) correction functions for the medium induced bias in sulfate and chloride media were developed.

Species analysis is another method of identifying an element specific redox potential. For this purpose the influence of saline solutions on the detection of Fe(II) and Fe$_{tot}$ with phenanthroline as well as Fe(III) with thiocyanat was analyzed by using UV/VIS spectroscopy. No salinity effect was found for the detection with phenanthroline. The complexation of Fe(III) with thiocyanate is influenced by sulfate ions and is thus not applicable for natural samples.

The two methods for determination the redox potential, the potentiometric method by using correction functions and the spectrophotometric method by species analysis were tested on different saline media. The comparison showed that both methods are in good agreement and suggests that both methods give reliable results. Furthermore the measurements demonstrated the necessity of a correction function in saline media to obtain meaningful redox potentials if redox electrodes are employed.

Introduction

Redox potentials in aqueous media are most commonly measured by determining the electric potential between a platinum electrode and a reference electrode (e.g. Ag|AgCl). In natural systems, generally more than one redox couple is present and most of the redox couples are in disequilibrium. Hence, an aqueous system has not only one redox potential but several potentials specific for each redox couple present. Unfortunately a redox electrode can only measure one potential that consequently must be regarded as a somehow mixed product of the individual redox couple potentials.

Measurements in natural media showed that the apparent electrode potential is closer to the Fe^{2+}/Fe^{3+} redox couple potential than to any other. This probably results from the relatively fast electron exchange between the two species. Another explanation could be that the platinum electrode acts as an iron specific electrode after Fe^{2+} has been oxidized to Fe^{3+} and subsequently precipitated as $Fe(OH)_3$ on the platinum surface (Doyle, 1968; Lindberg and Runnels, 1984; Runnels und Lindberg, 1990).

There is only insufficient information if and how the measured potential of the platinum electrode and the reference electrode is altered by the presence of high concentration of inorganic salts. Since the liquid junction potential at the interface between reference solution (e.g. 3 M KCl) and sample solutions cannot be regarded as constant in solutions of varying ionic strength, the conventional definition of the redox potential is no longer valid. Following the approach of a pH assessment in saline media by using the term p_{HCl}, which is the negative logarithm (base 10) of the activity product $a_H \cdot a_{Cl}$ (Knauss et al., 1990), the redox potential can be defined using the activities of $FeCl_2$ and $FeCl_3$ (cf. equation (1)).

$$Rx_0 = E^0 - 0.059 \log \frac{a_{Fe^{2+}} a_{Cl^-}^2}{a_{Fe^{3+}} a_{Cl^-}^3} \quad (1)$$

Rx represents the iron specific redox potential. The index 0 indicates the redox potential in a solution with an ionic strength of zero, thus without any influence of a varying liquid junction potential. For solutions with $I > 0$ the influence on the liquid junction potential is expressed by the term ΔRx. The measured apparent potential E is exhibited by the summation of Rx_0 and ΔRx.

$$E = Rx_0 + \Delta Rx \quad (2)$$

One method for accessing the element specific redox potential Rx_0 is by species analysis. A large number of different analytical approaches exist (Cornelis et al., 2005). In our study we concentrate on spectrophotometric techniques with the UV-VIS complexing active agents phenanthroline and thiocyanate. They are well established in water analysis but little is known whether these methods are also suitable for concentrated salt solutions. Part of this study is the examination of the influence of saline media on the iron analysis by application of these two methods. Furthermore a

transfer of the methods for solutions with low iron concentrations ($< 10^{-7}$ mol/l) by using a 5 m long pass flow cell is tested.

The activities of redox sensitive species in saline solutions can be calculated by geochemical modelling tools, if the concentrations of these species as well as the inorganic salts are determined and thermodynamic data of the redox sensitive species are available. Thereby the redox potential can be calculated with equation (1).

If a redox electrode shall be used for the determination of the redox potential, the measured E (apparent potential) can be corrected for the saline media induced bias ΔRx according to equation (2). To obtain a function for ΔRx, the potential E of known Fe(II)/Fe(III) activity ratios has to be analysed in specified saline solution. This was already done for chloride media (Bischofer et al., 2009). For sulfate systems data is shown in the publication at hand. ΔRx is determined following equation (3) by employing activities of Fe^{2+}, Fe^{3+} and Cl^- calculated by geochemical modelling tools.

$$\Delta Rx = E - E^0 + 0,059 \log \frac{a_{Fe^{2+}} a_{Cl^-}^2}{a_{Fe^{3+}} a_{Cl^-}^3} \quad (3)$$

Materials and Methods

Determination of the Fe Redox Potential

The E-Measurements were carried out at 25.0°C with a combined Pt ring electrode (Metrohm 6.0451.100) in an inert argon atmosphere to avoid oxidation of Fe(II) by oxygen. The iron containing solutions were prepared with CO_2-free water in a glove box flushed with argon. Measurements were conducted as titrations varying the salt concentrations (Na_2SO_4, K_2SO_4 and $MgSO_4$) till near saturation with 2 to 4 repetitions, respectively. In general, experiments were conducted with 0.01 M $HClO_4$, thus ensuring a constant H^+-concentration. The pH was checked with an Orion Ross-electrode (Pt/I_2, I- electrode, Orion Nr. 8102SC). The Fe(II)/Fe(III) concentration ratio was kept constant at 1 with c(Fe_{tot}) = 10^{-4} M. Additionally measurements with a varying Fe(II)/Fe(III) ratio but constant salt (NaCl) and H^+ concentration were performed.

E-Measurements were conducted after 2 minutes time of stirring and an up to 5 additional minutes equilibration time. Readings were only accepted if the signal during the measurement were within 0.1 mV in 120 sec. If this criterion was not fulfilled the measurements were repeated after a further 5 minutes.

NaCl, Na_2SO_4, and K_2SO_4 were obtained from Merck (Germany) and had the grade Suprapur®. $MgSO_4$ (purchased as heptahydrate) had the grade p. a. and was obtained from Riedel de Haen and Merck, respectively. For the preparation of Fe(II) and Fe(III) containing solutions, $FeCl_2$ and $FeCl_3$ (purity of 99,99%, respectively 99,99+%) from Sigma Aldrich were used.

UV/VIS Spectroscopy of Fe Species

For the Fe(II) determination the German DIN norm (DIN 38406 Part 1, 1983) using phenanthroline as the complexing agent was selected. Therefore the sample was spiked

with 5 vol.-% buffer solution (made up of ammonium acetate and HAc) and 0.001 g/l phenanthroline. All chemicals had the grade p. a. and were obtained from Merck. Unlike described in the DIN norm the sample was not diluted by a factor of two. With this approach also saline solutions near saturation could be studied.
Two methods were tested for analysing Fe(III) concentrations. On the one hand, the direct determination by complexation with 1 mol/l potassium thiocyanate (p. a., Merck) was used.   On the other hand, the indirect determination by analysing the total iron concentration with phenanthroline by adding a reducing agent (hydroxylamine hydrochloride, p. a., Merck) was applied, according to the German DIN method mentioned above.

The spectra were recorded between 900 and 300 nm with a double-beam UV-spectrometer (either PerkinElmer LAMBDA 20, Shimadzu UV-2450, or Varian Cary 5000) using 1 or 10 cm cuvettes. In case of low iron concentrations ($< 10^{-7}$ mol/l) an Ocean Optics S2000 fiber optic spectrophotometer coupled with a 5 m (1 m in case of absorption data for a comparison with cuvettes in figure 5) long pass flow cell was used. This spectrometer uses a capillary tube as both the sample compartment and the waveguide for light. Therefore it is also called the UV-capillary spectrometer. Here the buffer for the phenanthroline method described in the DIN method had to be replaced to avoid iron impurities from the chemicals. A buffer solution made up of a 1:8 ratio of 6.9 mol/l HCl and 5 mol/l acetic acid/ammonia solution was applied (Waterbury et al., 1997). All chemicals had the grade suprapur® and were obtained from Merck. Furthermore all samples had to be prepared in specifically purified PMP flasks (HCl leaching) by using Milli-Q water (18.3MΩ) to avoid contaminations. In addition the samples had to be filtered (pore size of 0.2 μm) to avoid particles in the capillary.

The total iron determination with phenanthroline and Fe(III) determination with thiocyanate (SCN) were tested for the influence of saline media. The methods were performed in NaCl (suprapur®, Merck) 0.01 – 5 mol/kg (maximum of 3 mol/kg for SCN), MgCl₂ (p. a., Merck) 0.01 – 4.0 mol/kg (maximum of 4.1 mol/kg for SCN), CaCl₂ (suprapur®, Merck) 0.01 – 1 mol/kg and Na₂SO₄ (suprapur®, Merck) 0.01 – 1.6 mol/kg (maximum of 1.3 mol/kg for SCN). Furthermore the phenanthroline method was transferred to the UV-capillary spectrometer and tested with saline iron solutions consisting of one or both iron oxidation states.

Results and Discussion

Method 1: Determination of the Fe Redox Potential

<u>*1. Response of the electrode in different sulfate media*</u>

In an earlier investigation (Bischofer et al., 2009) we have shown the influence of chloride media on the measured redox potential. For the current study these measurements were rerun in sulfate systems with Na₂SO₄, K₂SO₄ and MgSO₄ from 0.1 mol/kg salt till near saturation. The iron concentration (c(Fe$_{tot}$)=10^{-4} mol/l, Fe(II)/Fe(III)=1) and H⁺-concentration (10^{-2} mol/l) were kept constant. Compared to the results in chloride solutions the redox potential is already at 0.01 mol/kg sulfate about 60 mV lower. This can be explained by the presence of iron sulfato complexes, resulting in lower activities of free Fe³⁺. Apart from that similar trends in the two types

of systems are observed. K_2SO_4 has the strongest influence on the redox potential. The measured potential decreases up to 30 mV between 0.1 and 0.65 mol/kg K_2SO_4. The results of the three separate series are not in a good agreement and differ up to 11.8 mV. The weakest effect on potential was observed for $MgSO_4$. Here three series of measurements out of four are in good agreement. Between 0.1 and 0.7 mol/kg the potential decreases by less than about 20 mV, with further increasing ionic strength the electrode signal rises again. The fourth series which shows no significant change above 1 mol/kg $MgSO_4$ is due to the deviation from the other three consistent series neglected in the following. In solutions of Na_2SO_4 the measured potential is less effected than in K_2SO_4 but more than in $MgSO_4$. The two series of measurements differ at most by about 3.2 mV.
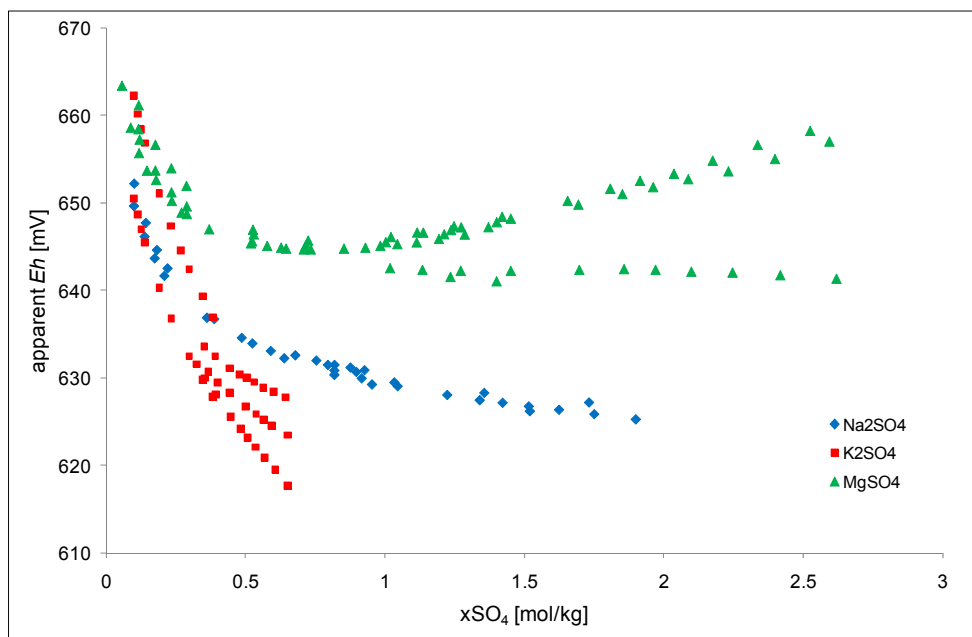
Figure 1: *Eh in relation to sulfate concentration of a redox defined system with a ratio of Fe(II)/Fe(III)=1 in 0.01 M HClO₄, c(Fe$_{tot}$)=10^{-4}.*
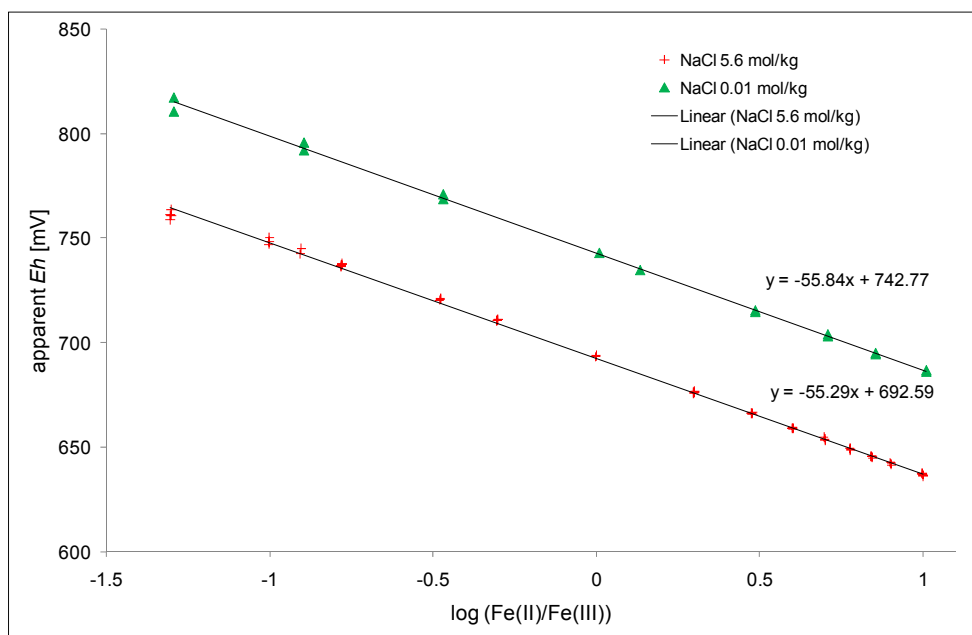
Figure 2: *Eh in relation to the Fe(II)/Fe(III) ratio with c(Fe$_{tot}$)=10^{-4} and 0.01 or 5.6 mol/kg NaCl in 0.01 M HClO$_4$.*

2. Behaviour at varying Fe(II)/Fe(III) ratio

In Bischofer et al. (2009) we presented one series of measurements with varying Fe(II)/Fe(III) ratio but constant salt (NaCl, 5.6 mol/kg) and H$^+$ concentrations (0.01 mol/l). For this study these measurements were repeated four times. Another series was conducted in a solution of low ionic strength (NaCl, 0.01 mol/kg) with two repetitions. The expected slope of the particular measurement series is the Nernst slope, i.e. -59.16 mV change of *Eh* by one log unit. In Bischofer et al. (2009) the slope differed from the theoretical value by 8.37 mV. The new measurements show a better agreement with -55.29 (high ionic strength) and -55.84 mV (low ionic strength). Furthermore differences among each other are negligible and show the failure of the previous measurements. The persisting deviation from the theoretical slope is not astonishingly. Likely the used electrode has a general deviation of the theoretical Nernst slope or other redox partners like H$^+$ have also an effect on the electrode.

3. Correction functions for the media induced bias ΔRx

The correction functions for the media induced bias Δ*Rx* were developed on the basis of the redox potential measurements in chloride (Bischofer et al., 2009) and sulfate media. The functions and their range of application are summarized in table 1. The developing of Δ*Rx* for chloride media was done according to equation (3). For sulfate media the equation had to be modified as follows:

$$\Delta Rx = E - E_0 + \tfrac{0,059}{2} \log \frac{(a_{Fe^{2+}} a_{SO_4^{2-}})^2}{a_{Fe^{3+}}^2 a_{SO_4^{2-}}^3} \quad (4)$$

The activities were calculated with EQ3/6 with Pitzer interaction parameters from Harvie et al. (1984) and Moog and Hagemann (2004). These publications include Pitzer ion interaction coefficients for the system Na,K,Mg,Ca||Cl,SO$_4$-H$_2$O, binary and ternary ion interaction parameters for Fe(II) and Fe(III) in chloride solutions, binary and ternary parameters for Fe(II) in sulfate solutions and binary parameters for Fe(III)-SO$_4$-H$_2$O. For K$_2$SO$_4$ another parameter set consisting of parameters from Harvie et al. (1984) and Christov (2004) was used. There are no parameters for the systems Fe(III)-Na-SO$_4$-H$_2$O and Fe(III)-Mg-SO$_4$-H$_2$O, hence the correction functions could not be developed yet.

Table 1: *Correction functions for the media induced bias*

Salt	Correction Function ΔRx [mV]	Range [mol/kg]
NaCl	$-28.10 \ln c_{NaCl} - 70.48$	$0.1 - 5.6$
KCl	$-32.12 \ln c_{KCl} - 75.93$	$0.1 - 4.6$
MgCl$_2$	$-25.48 \ln c_{MgCl_2} - 60.70$	$0.1 - 4.9$
K$_2$SO$_4$	$-123.61 c_{K_2SO_4}^2 - 176.69 c_{K_2SO_4} - 9.22$	$0.1 - 0.65$

Method 2: UV/VIS Spectroscopy of Fe Species

1. Influence of saline media on the colorimetric determinations

The phenanthroline method for total iron determination was tested upon the influence of NaCl, Na$_2$SO$_4$, MgCl$_2$ and CaCl$_2$ at 25°C. Samples with $2 \cdot 10^{-3}$ g/l Fe and an increasing salt concentration up to near saturation (except CaCl$_2$) were prepared and measured in 1 cm cuvettes with a regular two beam spectrometer. The iron concentration of $2 \cdot 10^{-3}$ g/l is between the upper ($2.5 \cdot 10^{-3}$ g/l) and lower ($5 \cdot 10^{-4}$ g/l) detection limit with the used optical path length and leads to an almost optimum signal-to noise-ratio. The results (figure 3) show little deviations between measured and theoretical values (maximum relative deviation within 5 %) which are in the usual range. It is obvious that the deviation is mostly positive and independent from salinity. Thus this effect is likely due to a systematic error.

It is well-known that the Fe(III) determination with thiocyanate is influenced by the delay between preparation and measurement, pH, SCN-concentration and presence of several ions like Cu, Ni, Zn, U and F (Bischofer et al., 2009; Hsu, 1967; Koch und Koch-Dedic, 1974). It was shown (Bischofer et al., 2009) that the higher concentrations of SCN (> 0.5 M) are necessary to achieve full complexation of Fe(III) in concentrated chloride solutions. Hence, for the current investigation samples with 4 mg/l Fe(III) and different salts (NaCl, Na$_2$SO$_4$, MgCl$_2$ and CaCl$_2$) up to near saturation (except CaCl$_2$) were prepared with 1 mol/l KSCN. Figure 4 shows no significant influence of chloride concentrations on the thiocyanate method even at high ionic strengths. The maximum relative deviation is less than 2 %. On the other hand a deviation of up to 30% was observed in a 1.3 m Na$_2$SO$_4$ solution. Due to the primarily presence of Na$_2$SO$_4$ in

natural samples, the other sulfates were not investigated after the result for Na_2SO_4 was found.

2. Measurements with a long pass flow cell

For low iron concentrations ($< 10^{-7}$ mol/l) the chosen determination methods had to be performed with an UV-capillary spectrometer. By using a 5 m long pass flow cell the sensitivity is raised by a factor of 500 compared to 1 cm cuvettes, respectively. This increase in sensitivity is required for analysing natural samples but implies also difficulties. Most of the purchasable chemicals necessary for the two photometric methods are contaminated with about 5 ppm Fe. Regarding the Fe(II) determination according to the German DIN method, this leads to 10^{-7} mol/l Fe in the blank. This could be improved by one order of magnitude by replacing the buffer solution as described in the chapter "materials and methods". For the direct Fe(III) determination no adequate thiocyanate was available so that this method could not be conducted with the capillary. Instead, the indirect determination by analysing the total iron concentration with phenanthroline was used.

The influence of NaCl and an Mg rich high salinity brine (IP21) on the phenanthroline method was tested with the capillary spectrometer using samples with $6.0 \cdot 10^{-6}$ g/l Fe (Fe(II)/Fe(III) = 1) and increasing NaCl concentration (0.1 – 5.0 mol/kg) or IP21 (80 %) were prepared. Already at the lowest NaCl concentration an oscillation of the base line was observed which did not change with increasing NaCl concentration. Furthermore the baseline level was declining if higher concentrated NaCl solutions or IP21 were investigated. Both effects hinder the evaluation of the maximum absorption. Therefore the determination of Fe(II) and Fe_{tot} in saline media can only be successful if the method of standard addition is applied.
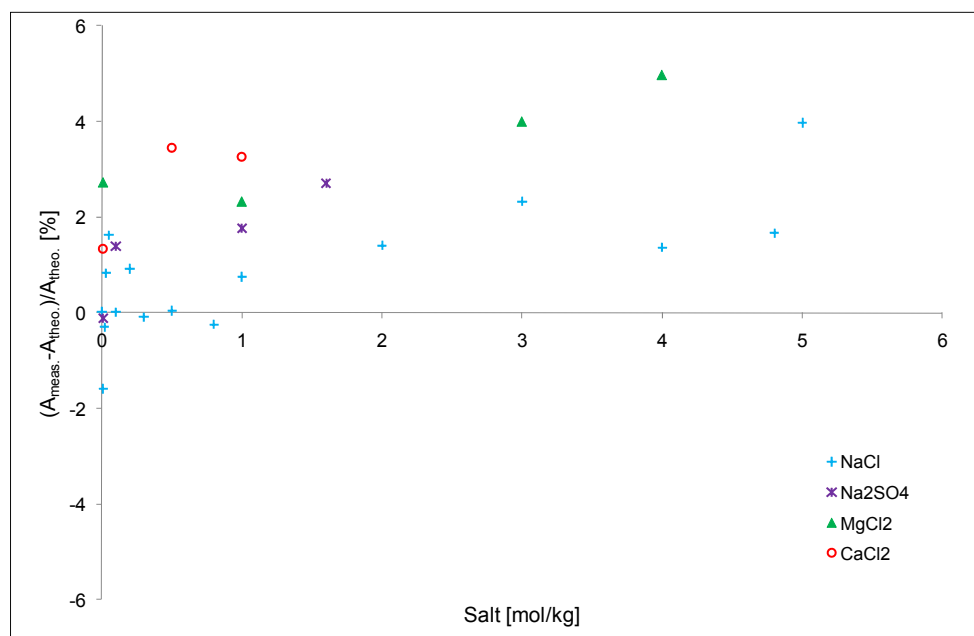
Figure 3: *Influence of different saline media on determination of total iron with phenanthroline.*
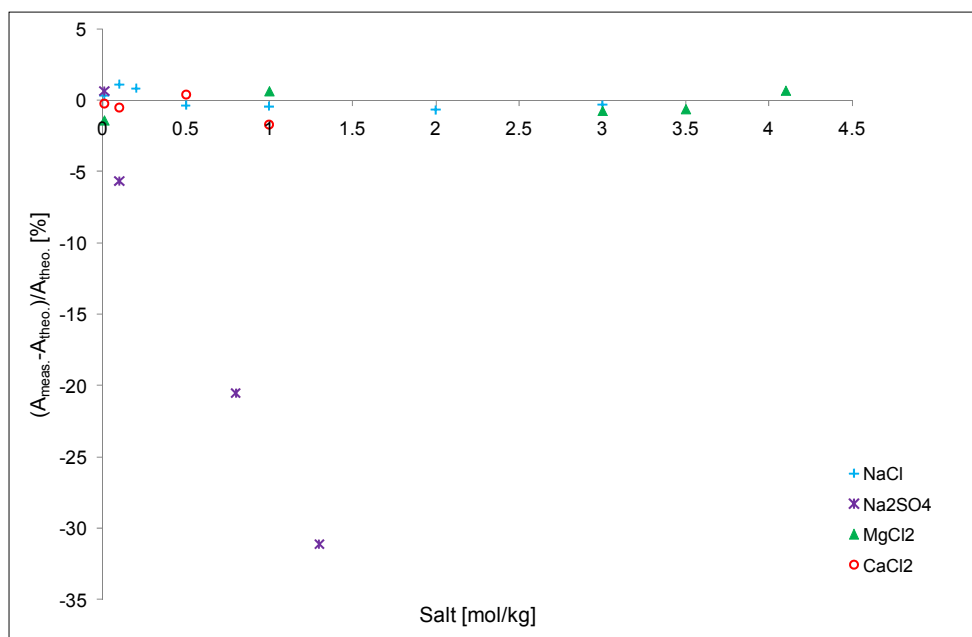
Figure 4: *Influence of different saline media on iron(III) determination with thiocyanate.*

Another observed effect was a difference between the Fe$_{tot}$ determination of Fe(II) and Fe(III) solutions. In Figure 5 the absorption of Fe(II) as well as Fe(III) solutions is shown for measurements performed with 10 cm cuvettes and with a 1 m capillary, but both normalised to the same optical path length. Whereas the absorption of Fe(II) and initial Fe(III) solution (reduced with hydroxylamine hydrochloride to Fe(II)) in a 10 cm cuvette as well as Fe(II) solution in a 1 m capillary are in good agreement the measurements of initial Fe(III) solution in the capillary lead to an irregular underestimation of the iron concentration. The determining parameter is in all samples the Fe(II)-complex with phenanthroline. It seems as if the reduction is incomplete in case of the capillary spectrometer but the rate of reduction during the sample preparation cannot be dependent of the afterwards used spectrometer. This means there has to be a so far unknown optical or photochemical phenomenon which only takes place in the capillary. Altogether it can be concluded that in solutions containing iron in both oxidation states only the Fe(II) concentration can be determined with the UV-capillary spectrometer, but not the Fe(III).
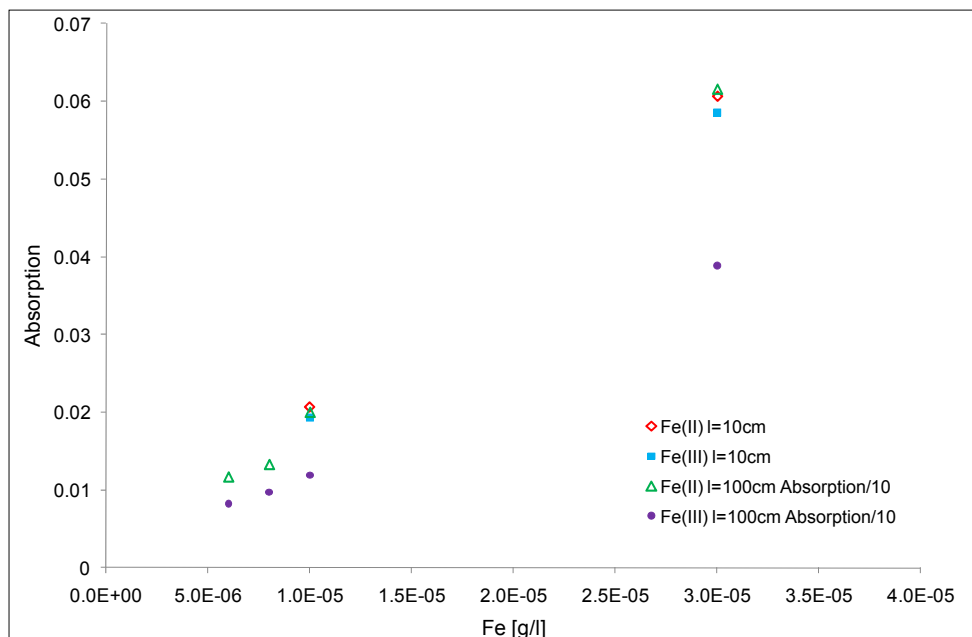
Figure 5: *Comparison of absorption data measured with a 10 cm cuvette and a 100 cm capillary. All show the total iron determination of Fe(II) and Fe(III) solutions.*

Comparison of the two methods

The two methods for determining the redox potential were compared in different saline media with low and high ionic strength at the Interlaboratory Comparison Exercise of the ReCosy Project. All samples were adjusted to a low pH (approximately pH=2) and contained $2 \cdot 10^{-4}$ mol/l Fe with Fe(II)/Fe(III)=1 except the 0.1 mol/l NaCl sample which contained $5 \cdot 10^{-4}$ mol/l Fe with Fe(II)/Fe(III)=1/4. For method 1 the potential was measured with a combined Pt ring electrode analogue to the technique described in the chapter "materials and methods". The measured values were corrected via equation (2) by using the correction functions of table 1. For the $CaCl_2$ and IP21 solutions the correction function of $MgCl_2$ were used, which is expected to have comparable characteristics. In case of method 2 the Fe(II) and Fe(III) concentrations were determined via UV/VIS-spectrometry by using phenanthroline as the complexing agent (see chapter "materials and methods"). Rx_0 was calculated following equation (1) by using Eq3/6 with Pitzer ion interaction parameters of Harvie et al. (1984) and Moog and Hagemann (2004).

The comparison of the results in table 2 shows a good agreement between the determined Rx_0 values. For solutions with low and also high ionic strength the results of the two methods differ by 16.6 mV at most. The slightest deviation is observed in case of $CaCl_2$ with 3.0 mV. In general the Rx_0 values obtained with method 1 are higher as with method 2 (except for the $CaCl_2$ sample). Nevertheless the values correspond very well and suggest that both methods give reliable results. Furthermore the comparison between *Eh* (measured apparent potential with reference to the H_2-Redox electrode) and Rx_0 values demonstrate the necessity of correction functions for media effects. The difference between these values goes up to 120 mV for the highly saline NaCl solution.

Table 2: Comparison of method 1 (redox measurements) and method 2 (Fe species analysis)

Sample	Rx_0 (method 1) [mV]	Rx_0 (method 2) [mV]	Eh (method 1) [mV]	Eh (method 2) [mV]
0.1 mol/l NaCl	720.2	711.0	714.0	704.8
5 mol/l NaCl	821.1	810.6	702.4	691.9
4.5 mol/l MgCl$_2$	794.7	778.1	692.3	675.7
2 mol/l CaCl$_2$	789.9	793.0	710.2	713.2
90 % IP21	780.4	767.8	685.6	672.9

Summary and Conclusions

In this study two methods for redox potential determination in saline media were developed and tested on solutions with low and high ionic strength. The first method is based on redox measurements with a combined Pt ring electrode in different chloride and sulfate media with a constant H^+ concentration and a constant Fe(II)/Fe(III) ratio. The results showed that sulfate media have a greater effect on the measured redox value in comparison to the calculated Eh (up to 110 mV) than chlorides (up to 60 mV). Concerning the cations a constant order was observed: potassium had the strongest impact on the redox signal followed by sodium and magnesium. Correction functions for the medium induced bias in saline solutions could be developed based on these measurements and by using geochemical modelling tools with Pitzer ion interactions coefficients.

For the second method the influence of saline media on iron species analysis with UV/VIS-spectrometry was investigated. As complexing agents phenanthroline and thiocyanate were used. It could be shown that phenanthroline according to German DIN 38406 Part 1 (1983) can be used for determining Fe^{2+} and Fe_{tot} in saline solutions with conventional cuvettes in a two beam UV/VIS spectrometer. Application of a long pass flow cell resulted in good analyses only for Fe(II) species. Determinations of Fe_{tot} and Fe(III) were not possible with the capillary spectrometer due to effects emerging by the use of a long pass flow cell. The thiocyanate method for determining Fe(III) showed influence upon time, pH, SCN^- concentration and sulfate anions. Thus, the thiocyanate method is not applicable for natural saline samples.

The comparison between the two methods during the Interlaboratory Comparison Exercise (method 1 and method 2) resulted in a good agreement of the determined redox values which suggest that both methods give reliable results. Furthermore the comparison between Eh and Rx_0 values demonstrates clearly that the apparent redox potential in saline solutions is not synonymous with the Eh in non saline solutions. For the determination of the redox potential in brines correction functions for media effects have to be applied.

Both methods were tested on acidified solutions for which a disturbance of hydroxo complexes could be excluded. For solutions with H^+ concentrations lower than 0.01 mol/l hydroxo or mixed hydroxo chloro complexes are expected. In absence of

complexing anions like chloride or sulfate hydroxo complexes are expected to be formed at even lower pH values. For these species there are no adequate interaction parameters so far. That leads to a strong limited area of application for the second method. Therefore we are developing at the moment a mathematical model valid for solutions with a higher pH. This model will be based on redox measurements in saline solution with varied pH. With this we should be able to apply method 2 till a lower limit of the H$^+$ concentration of 10^{-4} mol/l. The first method is valid independently of the pH and furthermore, is very simple practicable.

Acknowledgement

References

Bischofer B P, Hagemann S, Hühne C, Schönwiese D, Scharge T (2009): Influence of chloride concentrations on the signal of redox electrode and on UV-spectroscopic determination of Fe species, KIT Report FZKA 7466, December 2009, 83-91.

Christov C (2004): Pitzer ion-interaction patameters for Fe(II) and Fe(III) in the quinary {Na+K+Mg+Cl+SO$_4$+H$_2$O} system at T=298.5 K, J. Chem. Thermodyn (36), 223-235.

Cornelis R, Caruso J, Crews H, Heumann K (2005): Handbook of elemental speciation II – species in the environment, food, medicine and occupational health, Wiley 768 p.

DIN 38406 Part 1 (1983): German standard methods for the examination of water, waste water and sludge; cations (group E); determination of iron (E 1)), WILEY-VCH, Weinheim.

Doyle R W (1968): The origin of the ferrous ion-ferric oxide nernst potential in environments containing dissolved ferrous iron, Am. J. Sci. (266), 840-859.

Harvie C E, Moeller N, Weare J H (1984): The prediction of mineral solubilities in natural waters: The Na-K-Mg-Ca-H-Cl-SO$_4$-OH-HCO$_3$-CO$_3$-CO$_2$-H$_2$O system to high ionic strengths at 25°C, Geochim. Cosmochim. Acta (48), 723-751.

Hsu, P H (1967): Determination of iron with thiocyanate, Soil Sci. Soc. Am. J. (31), 353-355.

Knauss K G, Wolery T J, Jackson K J (1990): A new approach to measuring pH in brines and other concentrated electrolytes. Geochim. Cosmochim. Acta 54, 1519-1523.

Koch O G, Koch-Dedic G A (1974): Handbuch der Spurenanalyse, Teil 1, Springer Verlag, 750p.

Lindberg R D, Runnells D D (1984): Ground Water Redox Reactions: An Analysis of Equilibrium State Applied to Eh Measurements and Geochemical Modeling, Science (225), 925-927.

Moog H C, Hagemann S (2004): Thermodynamische Modellierung hochsalinarer Lösungen: Gewinnung von Daten für Fe(II), Fe(III) und S(-II) und Entwicklung eines

Programms zur Modellierung des reaktiven Stofftransports im Nahfeld eines Endlagers, GRS-195, 229p.

Runnels D R, Lindberg R D (1990): Selenium in aqueous solutions: The impossibility of obtaining a meaningful Eh using a platinum electrode, with implications for modeling of natural waters, Geology (18), 212-215.

Waterbury R D, Yao W, Byrne R H (1997): Long pathlength absorbance spectroscopy: trace analysis of Fe(II) using a 4.5 m liquid core waveguide. Analytica Chimica Acta, 357, 99-102.

UO₂ FUEL CORROSION – REACTIONS AT A UO₂-PALLADIUM SPENT FUEL MODEL SURFACE

Silvia Stumpf[1], Alice Seibert[1], T. Gouder[1*], F. Huber[1], T. Petersmann[1], M.A. Denecke[2], Th. Fanghänel[1,3]

[1] European Commission, JRC, Institute for Transuranium Elements, Eggenstein-Leopoldshafen, (D)

[2] Institut für Nukleare Entsorgung, KIT, Campus Nord, Eggenstein-Leopoldshafen, (D)

[3] Institut für Physikalische Chemie, Ruprecht Karls Universität, Heidelberg, (D)

*Corresponding author: thomas.gouder@ec.europa.eu

Abstract

The safety assessment of a nuclear waste repository requires the reliable prediction of the overall spent nuclear fuel (SNF) corrosion behaviour since the dissolution of the fuel matrix would result in the release of radionuclides into the groundwater and, with this, into the biosphere. The corrosion of SNF is determined by a complex interplay of oxidation and reduction processes in solution as well as at the SNF solid-aqueous interface. That is, beside the solution composition also the composition of the SNF surface itself exerts an influence on the overall redox behaviour of SNF. It becomes clear, that SNF is a redox system of high complexity. In order to understand SNF corrosion the elucidation of the involved single processes is indispensable. In this context, the impact of individual fuel components on fuel corrosion has to be clarified. In a first set of experiments, the overall redox reactivity of a SNF model surface (UO₂-Pd thin film) is investigated in cyclovoltammetric measurements and in more detail in gas adsorption experiments.

We show that in solution (at oxic conditions) the corrosion of UO₂ is inhibited when Pd is incorporated into the oxide matrix. However, secondary phase formation at the model surface disables the inhibiting effect of Pd regarding UO₂ corrosion. Furthermore, we demonstrate in gas adsorption experiments, that hyperstoichiometric UO₂₊ₓ exposed to molecular hydrogen does not result in the reduction of the oxide. By contrast, H₂ is activated at Pd doped UO₂₊ₓ surfaces leading to the reduction of the oxides. The studies allow clarifying the mechanism of SNF matrix reduction by H₂ which is directly related to the presence of Pd and with this contributes to a mechanistic process understanding

of the overall reactivity of SNF with regard to a reliable safety assessment of a nuclear waste repository.

Introduction

About 95% of spent nuclear fuel (SNF) consists of UO_2. The remainder is a mixture of radionuclides and fission products (FPs) that are heterogeneously distributed throughout the fuel assembly and that occur in a variety of phases, from gases (Xe, Kr, I) to oxides (U, Pu, Np, Am, Cm and others) and metallic precipitates, so called ε-particles (Pd, Mo, Ru etc.) [Kleykamp (1985), Bruno and Ewing (2006)]. The assessment of a nuclear waste repository depends on the calculation of the risk to humans due to the release of radionuclides into the biosphere. In this context, the alteration and dissolution of SNF represents an important source term for the mobilization of radionuclides. Corrosion studies of SNF have therefore been the focus of a number of investigations [Johnson and Shoesmith (1988), Shoesmith (2000) Buck et al. (2004), Johnson et al. (2005) and references therein]. The solubility of UO_2 in water is low with a log K°_{sp} value of -54.5 ± 1.0 for $UO_2 \cdot xH_2O(am)$ and of -60.85 ± 0.36 for $UO_2(cr)$ [Neck and Kim (2001)]. The spent fuel matrix should be therefore rather stable. However, the radiolysis of groundwater in the direct environment of SNF produces oxidants such as $^{\bullet}OH$, $^{\bullet}HO_2$ and H_2O_2. The oxidizing species react with the fuel surface, and additional oxygen atoms can enter the UO_2 structure as interstitials. The thus generated U(VI) at the fuel surface is more easily dissolved, which is facilitated by complexing ligands present in the groundwater. [Spinks and Woods (1964), King and Shoesmith (2004), Roth and Johnson (2008), Sunder et al. (1997), Rondinella et al. (2000), Wren et al. (2005), Christensen and Sunder (2000), Shoesmith et al. (2003), Poinssot et al. (2005)]

Reducing species, such as hydrogen, are also produced during water radiolysis [Spinks and Woods (1964)] and by the corrosion of the steel containment. Hydrogen is quite inert and has a low solubility in water (0.0016 g/kg). However, leaching studies in the presence of H_2 have shown it to have a very strong influence on radionuclide leaching and fuel corrosion rates [Broczkowski et al. (2005), Broczkowski et al. (2007), Spahiu et al. (2004a), Spahiu et al. (2004b), Spahiu et al.(2000), Röllin et al. (2001), Carbol et al. (2009)]: decreased rates up to four orders of magnitude in the presence of this reductant are reported. The proposed explanation is a catalytic H_2 dissociation reaction on the fuel surface resulting in the production of $^{\bullet}H$ radicals. Up to now it is not entirely clear, which SNF component drives the H_2 activation. Several authors ascribe the catalytic activation to UO_2 itself [Carbol et al. (2009), Spahiu et al. (2004a), Bunji and Zogovic (1958), Heynen et al. (1977)]. Others exclude a catalytic activity of the UO_2 matrix and claim only the ε-particles (Mo, Tc, Ru, Rh and Pd) as being responsible for the activation instead [Nilsson and Jonsson (2008a), Nilsson and Jonsson (2008b), Trummer et al. (2008), Trummer et al. (2009), Cui et al. (2004)] since the late 4d-elements and their alloys are known catalysts for redox reactions. Once H_2 has dissociated at the surface the activated hydrogen is discussed to further react in two possible ways. Either hydrogen reduces oxidized species in homogeneous reaction in solution, or in heterogeneous reaction at the fuel surface, or both of it. Homogeneous reactions can be the consumption of radiolytically produced oxidants by hydrogen resulting in the suppression of the UO_2 surface oxidation or the reduction of dissolved U(VI). For the heterogeneous case the solid phase itself is assumed to be subsequently

reduced by decomposed H_2. On the basis of kinetic considerations Trummer et al. [Trummer et al. (2008), Trummer et al. (2009)] and Nilsson and Jonsson [Nilsson and Jonsson (2008a), Nilsson and Jonsson (2008b)] argue that even if activated H_2 reacts in the homogeneous mechanism neither the consumption of dissolved oxidants nor the reduction of $U(VI)_{aq}$ by hydrogen in solution provide a sufficient explanation for the observed dissolution inhibition of UO_2. These effects are of marginal importance and cannot account for the very efficient inhibition observed in some cases. By contrast, they propose the noble metal catalyzed solid phase reduction of $U(VI)$ by H_2 as being the crucial reaction and assume if the rate of surface reduction is equal or higher to the rate of dissolution, even full dissolution inhibition can be observed. However the single steps are not observed with direct methods, and final evidence for a detailed reaction mechanism is not provided yet.

The presented study aims to investigate both: 1) the single effect of fission product incorporations (FP), such as Pd ε-particles, on the UO_2 corrosion and 2) the mechanism of H_2 activation at a UO_2-Pd surface as one possible reductive reaction path.

Experimental

Thin films of $U_xO_yPd_z$ were prepared in situ by sputter co-deposition from U (99.9%

purity) and Pd (99.9% purity) targets at an O_2 partial pressure of about $1 \cdot 10^{-6}$ mbar (the stoichiometry of the oxide was controlled by varying the O_2 pressure during the sputter process). The pressure of the sputter gas (Ar 99.9999% purity) was $1 \cdot 10^{-2}$ mbar. To generate the Ar-plasma, the Ar atoms were ionized by electrons (50-100eV) emitted from a hot W cathode. The films were deposited on single crystalline Si-wafers and piezoelectric quartz crystals coated with gold electrodes used for the electrochemical investigations. XPS spectra were recorded with a hemispherical analyzer from Omicron (EA 125 U5).

The spectra were taken using MgK$_\alpha$ (1253.6 eV) radiation with an approximate energy

resolution of 0.9 eV.

Gas adsorption experiments were conducted in the preparation chamber equipped with an atom source GenII from Tectra.

Electrochemical experiments are carried out with a electrochemical quartz microbalance system (Model 430) from CH Instruments under normal atmospheric conditions.

A commercial AFM (Topometrix, TMX 2000, Explorer, available at INE) was used for

the topographic characterization of the thin films. A series of AFM images was recorded in contact-mode using triangular cantilevers with silicon nitride tips (tip radius <50 nm).

Results and Discussion

Our scientific approach is to selectively investigate the influence of different fuel components (UO_2, Pd) on the overall redox behaviour of SNF and to clarify the

mechanism of the ongoing single redox processes, such as the activation of H_2 at the SNF surface.

The UO_2-Pd thin films prepared as model fuel interfaces by sputter co-deposition represent well the SNF surface [Cui et al. (2004), Stumpf et al. (2009), Stumpf et al. (2010)]. After a heating treatment (~ 200 °C) the films were characterized as being composed of a crystalline uranium oxide matrix doped with an agglomeration of Pd spheres in the size range of hundredth of nanometers (see Figure 1).

Electrochemical investigations

In a first set of experiments the influence of Pd on the corrosion behaviour of UO_2 was investigated by using the prepared films as working electrodes in cyclovoltammetric measurements. A detailed interpretation of such voltammograms on UO_2 and SIMFUEL has been given by Shoesmith et al. and Santos et al. [Shoesmith et al. (1994), Santos et al. (2004), Santos et al. (2006), Santos et al. (2006b),]: Generally, three stages of oxidation are observed on the anodic scan. At low potentials (region A: -1.0 to -0.4 V) a shoulder appears that can be attributed to a reversible oxidation process. Region B to region C is attributed to the oxidation of the UO_2 electrode matrix involving the incorporation of O^{2-} ions leading to a stoichiometry of the oxide close to $UO_{2.33}$.
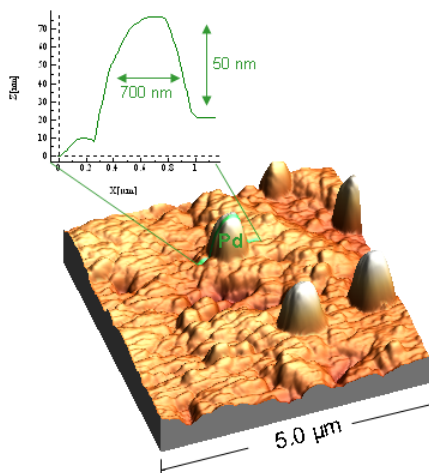
Fig. 1

Figure 1: *AFM image of a UO_2 thin film surface doped with Pd (ε-particles).*

The increasing current beyond region C is attributed to the further oxidation of the surface layer to produce soluble UO_2^{2+} species. Due to the limited solubility of UO_2^{2+} the precipitation of hydrated U(VI) solids, such as schoepite, on the fuel surface is proposed [Shoesmith (2000), Shoesmith et al. (1994)] for high anodic potentials. On the reverse scan, the feature in region E2 is attributed to the reduction of the U(VI) precipitate and the underlying $UO_{2.33}$. The redox properties of Pd are also discussed in literature [Kibler et al. (2003), Martin and Lasia (2008), Duncan and Lasia (2007), Naohara et al. (2000), Cao and Chen (2006)]. The cyclovoltammetric features are attributed to the kinetically controlled adsorption of solvent components (H_2O, O_2, H_2) onto the noble metal surface. Hereby, adsorption is described as being dissociative and the adsorbed species (H_{ads}, O_{ads}, OH_{ads}) are discussed to further undergo surface

reactions including oxidation, reduction and recombination reactions.

The normalized voltammograms of UO_2 and UO_2 doped with 2% and 16% Pd are compared in Figure 2a (0.01 M NaCl, pH ~ 5, scan rate 10 mVs^{-1}). With increasing Pd concentration new features appear in the oxidative as well as reductive path of the voltammogram (A, E1) whereas C shows a change in its intensity. Without going into more detail, we note that Pd has an impact on the overall redox behaviour of UO_2 and propose, according to literature, dissociative sorption processes at Pd sites as being responsible for such effect. In respect of feature C, we observe a decreased current with increasing Pd concentration. The current decrease indicates a less extensive oxidation of the matrix which is in good agreement with results described in Naohara et al.(2000). Assuming the adsorption and reaction of redox active species at the Pd particles as cited above, the activated components obviously couple more readily to recombination and reduction processes than to the oxidation of $UO_{2.33}$. This interpretation of experimental data is supported by theoretical studies on the recombination of OH_{ads} to form H_2O_{ads} on a Pd(111) surface performed by Cao and Chen (2000) who predict such reaction path as being very likely from an energetic point of view.
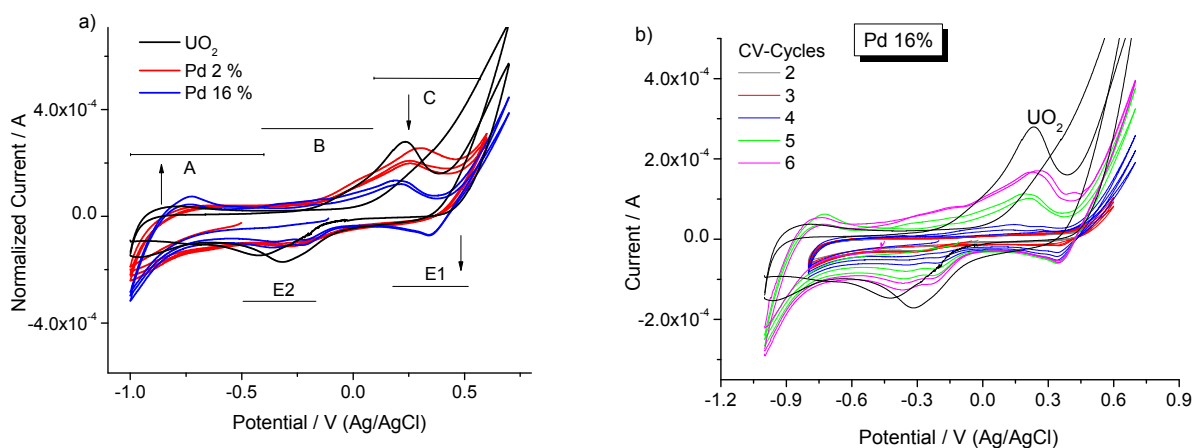
Figure 2: *Normalized voltammograms of UO_2 doped with a) 0%, 2% and 16% Pd in a comparative diagram and doped with b) 16% Pd whereas the CV is run for several cycles.*

With increasing number of voltammetric cycles (exemplarily shown for the 16% Pd sample in Figure 2b) the electrode response resembles more and more the pure UO_2 case, except the distinct feature seen in region E1. Such effect indicates the passivation of Pd particles towards dissolution inhibition. Shoesmith et al. [Shoesmith (2000), Shoesmith et al. (1994)] propose the formation of secondary phases as being responsible for the blockage of donor-acceptor sites at the UO_2 surface. In fact, the precipitation of such phases is monitored by AFM measurements shown in Figure 3. At a potential of -1 V the electrodes surface shows a structured surface composed of 100 nm sized agglomerates. The application of a potential of 0.3 V on the electrode, results in the dissolution of the surface which becomes more pronounced with a further increase up to 0.5 V. The AFM image clearly demonstrates that Pd is not dissolved during the oxidative scan since the two nanocrystalline features staying fixed to the surface can be

characterized as being Pd (SEM-EDX measurements; not shown here). The application of a negative potential induces the precipitation of secondary phases that also cover the metallic Pd particles. The precipitate is composed of hexavalent uranium as shown by XPS analysis. The following oxidative scan results in the dissolution of the barely crystalline precipitate and the structured uranium oxide surface, and the ε-particles appear again. It becomes clear, that the precipitation of these secondary phases not only leads to the coverage of Pd resulting in the blockage of the related effect. Moreover, this precipitate is the main surface component in contact with solution which takes part in oxidation/dissolution as well as reduction/precipitation processes. With this, not the matrix UO_2 but mainly the precipitate finally determines the electrochemical behaviour of the surface.

From our cyclovoltammetric results we deduce the general impact of Pd on the overall redox behaviour of UO_2. Moreover, we propose the dissociative sorption of redox active species at the UO_2-Pd surface. However, the cyclovoltammetric data does not allow clarifying the question if the "activated" species then follow a heterogeneous or homogeneous reaction path.
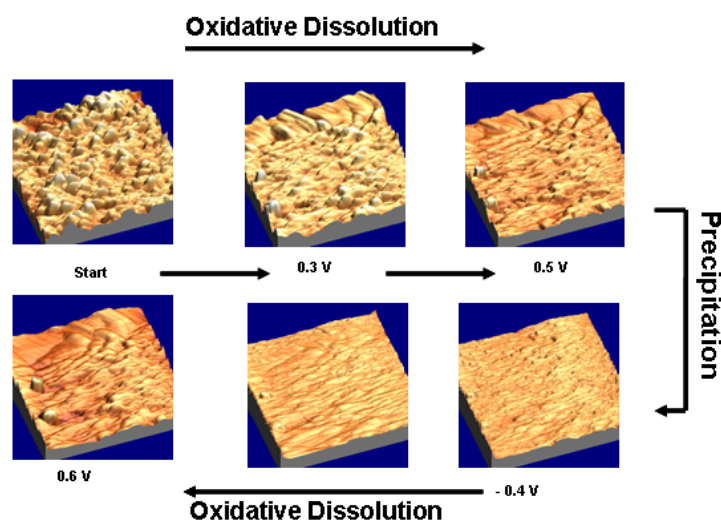
Figure 3: *AFM images of a UO_2-Pd (~16%) thin film monitored for a redox scan from -1 V up to 0.6 V.*

Gas adsorption experiments

In order to simulate one conceivable heterogeneous redox reaction, such as the oxide reduction by hydrogen, UO_2-Pd thin films are exposed to H_2 gas. The corresponding XPS spectra of a pure UO_{2+x} surface are shown in Figure 4a. The U4f spectrum of UO_{2+x} is characterized by two main peaks with peak maxima at 380 eV and 391 eV binding energy. Two satellites at 7 eV higher binding energy are characteristic for the actinide dioxides. For the hyperstoichiometric oxide these satellites are broadened. The treatment with H_2 gas does not result in a change of the U4f electronic structure and the UO_{2+x} reduction can be therefore ruled out. This changes when doping the UO_{2+x} matrix with Pd (Fig. 4b). Already at very low pressures of about $1.3 \cdot 10^{-5}$ mbar H_2 (x 5 min), the treatment of the mixed film induces a narrowing of the main peaks as well as of the satellites. The calculation of the U/O ratio from the corresponding U4f and O1s spectra after 15 minutes H_2 treatment gives a stoichiometry of UO_2. Obviously, the activation of

H_2 is solely due to the presence of Pd. We conclude as a first result, that the catalytic properties of the uranium oxide matrix can be ruled out (at least at the H_2 pressure used) and that the activating effect is exclusively attributed to the noble metal incorporation instead. The mechanism of H_2 activation is deduced from another series of experiments where pure UO_{2+x} is treated with atomic H. At comparable hydrogen pressures such treatment results in the reduction of the hyperstoichiometric oxide (not shown here). From this we conclude that the activation of H_2 is consistent with a dissociative sorption process and with the formation of atomic H at Pd active sites. The only possible reaction path to further reduce uranium oxide in the doped oxide films is the diffusion of hydrogen atoms at the UO_{2+x}-Pd surface. Such process is known in literature as spillover reaction [Teichner (1990), Gorodetskii et al. (2009)] which is defined as migration of a sorbed species, such as hydrogen, from one solid phase, such as a metal where it is easily adsorbed and dissociated, onto another solid phase, such as uranium oxide, in contact with the first. It is also reported that the spillover species may react with the oxide surface leading to the creation of surface defects and/or active sites. Further, the bulk of the oxide may react. Diffusion coefficients in the range of 10^{-3} cm^{2}s^{-1} are reported for the surface migration of the spillover hydrogen indicating that such process cannot be assumed to be rate limiting.
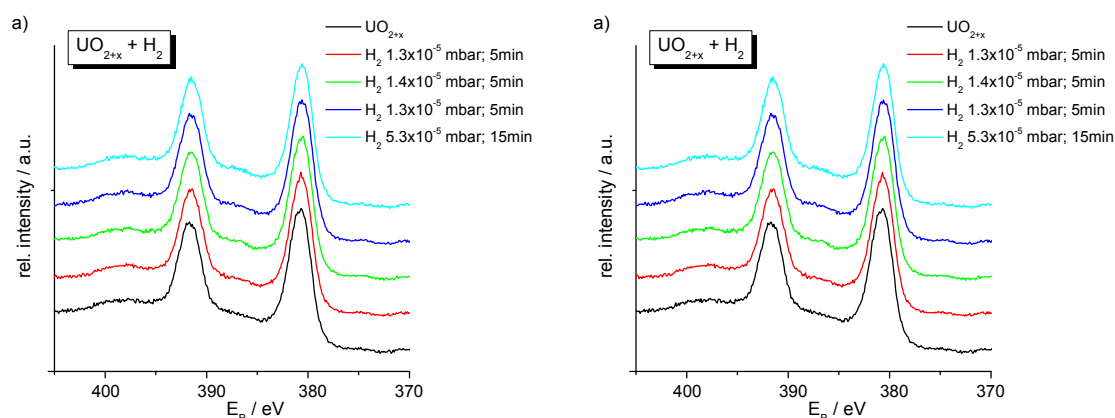
Figure 4: *U4f spectra of a) UO_{2+x} thin film, b) UO_{2+x}-Pd mixed thin film.*

In fact, this explains well our observation of UO_{2+x} solid phase reduction already at very low hydrogen pressures of about $1.3 \cdot 10^{-5}$ mbar H_2 which is eight orders of magnitude lower than reported by Nilsson and Jonsson (2008a,b) and Trummer et al. (2008, 2009). Our experimental approach allows to selectively analyze the heterogeneous reaction of H_2 with a SNF model surface. From the low H_2 pressures it becomes clear that the spillover process as an internal process is much faster than the diffusion controlled reaction observed in the above cited studies. This heterogeneous process not only delays UO_2 oxidation, but actually reverses it by converting UO_{2+x} back to UO_2.

Conclusions

Our studies clearly demonstrate that thin films are well suited for investigations of a single effect. We performed such a single effect study on the influence of Pd on the

redox behaviour of UO_2 (as SNF model). We could clarify that Pd has an inhibiting effect on the UO_2 matrix dissolution as long as the noble metal is not passivated by secondary phase formation at the solid solution interface.

One mechanism for the dissolution inhibiting effect of Pd in the presence of H_2 could be deduced from the experimental results of the surface exposure to hydrogen. A heterogeneous reaction path is directly identified: hydrogen dissociatively chemisorbs to Pd active sites, diffuses as H onto the UO_{2+x} matrix and finally reduces the hyperstoichiometric uranium oxide. The performed studies allow understanding part of the very complex redox system SNF. In fact, this is of great importance regarding the safety assessment of a nuclear waste repository.

Acknowledgement

References

M.E. Broczkowski, J.J. Noel, D.W. Shoesmith (2005): The inhibiting effects of hydrogen on the corrosion of uranium dioxide under nuclear waste disposal conditions, J. Nucl. Mater., 346, 16-23.

M.E. Broczkowski, J.J. Noel, D.W. Shoesmithn (2007): The influence of dissolved hydrogen on the surface composition of doped uranium dioxide under aqueous corrrosion conditions, J. Electroanal. Chem. 602, 8-16.

J. Bruno, R.C. Ewing (2006): Spent nuclear fuel, Elements 2, 343-349.

E.C. Buck, B.D. Hanson, B.K. McNamara (2004): The geochemical behaviour of Tc, Np and Pu in spent nuclear fuel in an oxidizing environment. In: Gieré R., Stille P. (eds) Energy, Waste and the Environment: a Geochemical Perspective. The Geological Society of London Special Publication 236, pp. 65-88.

B. Bunji, B. Zogovic (1958): Proceedings of the International Symposium on Peaceful Uses of Atomic Energy, Stockholm, pp. 350-355.

Y. Cao, Z.-X. Chen (2006): Theoretical studies on the adsorption and decomposition of H_2O on Pd(111) surface, Surf. Sci., 600, 4572-4583.

P. Carbol, P. Fors, T. Gouder, K. Spahiu (2009): Hydrogen suppresses UO_2 corrosion, Geochim Cosmochim Acta 73, 4366-4375.

H. Christensen, S. Sunder (2000) Current state of knowledge of water radiolysis effects on spent fuel corrosion, Nucl. Technol. 131, 102-123.

D. Cui, J. Low, C.J. Sjöstedt, K. Spahiu (2004): On Mo-Ru-Tc-Pd-Rh-Te alloy particles extracted from spent fuel and their leaching behaviour under Ar and H_2 atmosphere, Radiochim. Acta 92, 551-555.

H. Duncan, A. Lasia (2007): Mechanism of hydrogen adsorption/absorption at thin Pd layers on Au(111), Electrochim. Acta, 52, 6195-6205.

V.V. Gorodetskii. A.A. Sametova, A.V. Matveev, V.M. Tapilin (2009): From single crystals to supported nanoparticles in experimental and theoretical studies of H_2 oxidation over platinum metals (Pt, Pd): Intermediates, surface waves and spillover, Catalysis today, 144, 219-234.

H.W.G. Heynen, C.G.M. Camp van Berkel, H.S. van der Baan (1977): Kinetics of the reduction of uranium oxide catalysts, J. Catal.48, 386-394.

L.H. Johnson, D.W. Shoesmith (1988): Spent Fuel in Lutze W., Ewing R.C. (eds) Radioactive Waste Forms for the Future. North-Holland, Amsterdam, pp. 635-698.

L. Johnson, C. Ferry, C. Poinssot, P. Lovera (2005): Spent fuel radionuclide source-term model for assessing spent fuel performance in geological disposal. Part I: Assessment of the instant release fraction, J. Nucl. Mater. 346, 56-65.

L.A. Kibler, A.M. El-Aziz, D.M. Kolb (2003): Electrochemical behaviour of pseudomorphic overlayers: Pd on Au(111), J. Molec. Cat. A: Chemical, 199, 57-63.

F. King, D.W. Shoesmith (2004): Electrochemical studies of the effect of H_2 on UO_2 dissolution, SKB Technical Report TR-04-20.

H. Kleykamp (1985): The chemical state of the fission products in oxide fuels, J. Nucl. Mater. 131, 221-246.

M.H. Martin, A. Lasia (2008): Study of the hydrogen absorption in Pd in alkaline solution, Electrochim. Act., 53, 6317-6322.

H. Naohara, S. Ye, K. Uosaki (2000): Electrocatalytic reactivity for oxygen reduction at epitaxilly grown Pd thin layers of various thickness on Au(111) and Au(100), Electrochim. Act., 45, 3305-3309.

V. Neck, J.I. Kim (2001): Solubility and hydrolysis of tetravalent actinides. Radiochim. Acta, 89, 1-16.

S. Nilsson, M. Jonsson (2008a): On the catalytic effects of $UO_2(s)$ and $Pd(s)$ on the reaction between H_2O_2 and H_2 in aqueous solution, J. Nucl. Mater. 372, 160-163.

S. Nilsson, M. Jonsson (2008b): On the catalytic effect of $Pd(s)$ on the reduction of UO_2^{2+} with H_2 in aqueous solution, J. Nucl. Mater. 374, 290-292.

C. Poinssot, C. Ferry, P. Lovera, C. Jegou, J.M. Gras (2005): Spent fuel radionuclide source term model for assessing spent fuel performance in geological disposal. Part II: Matrix alteration model and global performance, J. Nuc. Mat. 346, 66-77.

S. Röllin, K. Spahiu, U.B. Eklund (2001): Determination of dissolution rates of spent fuel in carbonate solutions under different redox conditions with a flow-through experiment, J. Nucl. Mater., 297, 231-.

V.V. Rondinella, H. Matzke, J. Cobos, T. Wiss (2000): Leaching behaviour of UO2 containing α-emitting actinides, Radiochim. Acta 88, 527-531.

O. Roth, M. Jonsson (2008): Oxidation of $UO_2(s)$ in aqueous solution, Cent. Eur. J. Chem. 6, 1-14.

B.G. Santos, H.W. Nesbitt, J.J. Noel, D.W. Shoesmith (2004): X-ray photoelectron spectroscopy study of anodically oxidized SIMFUEL surfaces, Electrochim. Act., 49, 1863-1873.

B.G. Santos, J.J. Noel, D.W. Shoesmith (2006a): The effect of pH on the anodic dissolution of SIMFUEL (UO_2), J. Electroanal. Chem., 586, 1-11.

B.G. Santos, J.J. Noel, D.W. Shoesmith (2006b): The influence of potential on the anodic dissolution of SIMFUEL (UO_2), Electrochim. Acta, 51, 4157-4166.

D.W. Shoesmith, S. Sunder, W.H. Hocking (1994) in Electrochemistry of Novel Materials, edited by J. Lipowski and P.N. Ross, VCH Publishers, New York, pp. 297-337.

D.W. Shoesmith (2000): Fuel corrosion processes under waste disposal conditions, J. Nucl. Mater. 282, 1-31.

D.W. Shoesmith, M. Kolar, F. King (2003): A mixed-potential model to predict fuel (Uranium Dioxide) corrosion within a failed nuclear waste container, Corrosion 59, 802-816.

K. Spahiu, L. Werme, U.B. Eklund (2000): The influence of near field hydrogen on actinide solubilities and spent fuel leaching, Radiochim. Acta, 88, 507-.

K. Spahiu, J. Devoy, D. Cui, M. Lundström (2004): The reduction of U(VI) by near field hydrogen in the presence of $UO_2(s)$, Radiochim. Acta 92, 597-601.

K.Spahiu, D. Cui, M. Lundström (2004): The fate of radiolytic oxidants during spent fuel leaching in the presence of dissolved near field hydrogen, Radiochim. Acta 92, 625-629.

J.W.T. Spinks, R.J. Woods (1964) in: An Introduction to radiation chemistry, John Wiley and Sons Inc., New York, pp. 477-480.

S. Stumpf, A. Seibert, T. Gouder, F. Huber, T. Wiss, J. Römer, M.A. Denecke(2010): Development of fuel-model interfaces: Characterization of Pd containing UO_2 thin films, J. Nucl. Mater., 397, 19-26.

S. Stumpf, A. Seibert, T. Gouder, F. Huber, T. Wiss, J. Römer (2009): Development of fuel-model interfaces: Investigations by XPS, TEM, SEM and AFM, , J. Nucl. Mater., 385, 208-211.

S. Sunder, D.W. Shoesmith, N.H. Miller (1997): Oxidation and dissolution of nuclear fuel (UO_2) by the products of the alpha radiolysis of water, J. Nucl. Mater. 244, 66-74.

S.J. Teichner (1990): Recent Studies in Hydrogen and Oxygen Spillover and their Impact on Catalysis, Appl. Catalysis, 62, 1-10.

M. Trummer, S. Nilsson, M. Jonsson (2008): On the effects of fission product noble metal inclusions on the kinetics of radiation induced dissolution of spent nuclear fuel, J. Nucl. Mater. 378, 55-59.

M. Trummer, O. Roth, M. Jonsson (2009): H_2 inhibition of radiation induced dissolution of spent nuclear fuel, J. Nucl. Mater. 383, 226-230.

J.C. Wren, D.W. Shoesmith, S. Sunder (2005): Corrosion behavior of uranium dioxide in alpha radiolytically decomposed water, J. Electrochem. Soc. 152, 470-481.

DEVELOPMENT OF A SPECIATION METHOD FOR IODINE UND URANIUM IN ENVIRONMENTAL SAMPLES WITH SPECIAL FOCUS ON THE REDOX BEHAVIOUR

Bernhard Kuczewski[1,2,*], Hana Tatjana Dittrich[2], Corinna Dully[2], Markus Lagos[3], Edit Marosits[2], Christian M. Marquardt[3]

[1] Division of Nuclear Chemistry, University of Cologne (DE)

[2] Institute of Analytical Chemistry and Food Chemistry, Graz University of Technology (AT)

[3] Institute of Nuclear Waste Disposal, Forschungszentrum Karlsruhe (DE)

* Corresponding author: B.Kuczewski@uni-koeln.de

Abstract

Speciation methods for iodine and uranium were developed, to obtain additional data for the determination of groundwater's redox state. By capillary electrophoresis iodide and iodate as well as U(VI) and U(IV) were separated. The developed methods are described as well as the application for iodine species to nearly natural samples.

Introduction

The measurement of redox parameters seems to be easy but especially in systems like groundwater it can become difficult. The determination of redox potential requires equilibrium, which is seldom fulfilled due to slow kinetics of important redox reactions that have great influence on the potential. In many cases only electrochemical and optical sensors are used. Applying speciation methods additional data can be obtained. This will help to improve the reliability of the sensors data.

The use of separation techniques combined with sensitive detectors allows the determination of several redox ion pairs like FeII/III, UVI/IV or $I^-/IO_3^-/I_2$. Ion chromatography (IC) and capillary electrophoresis (CE) was verified for the determination of the iodine species. However, for uranium only CE was applied which separates the ions in an electrical field by their charge to radius ratio. In this case both -

diode array (DAD) and inductively coupled plasma mass spectrometry (ICPMS) - could be used for detection.

Method development

Iodine speciation

For the method development we have prepared solutions of the sodium salts of iodide and iodate that were stored at a dark cold place (refrigerator at +6°C). The stock solutions were diluted by different media, to prove the effects of synthetic and nearly natural sample media (e.g. high saline synthetic groundwater). While the development of the ion chromatography was up to now not completed, the CE-DAD method works well. Table 1 gives the final conditions for the separation of the iodine species by the CE-DAD system. Figure 1 shows the electropherogram of a sample containing iodide and iodate.

Table 1: *Separation conditions for iodine species with CE-DAD*

instrument	Agilent 3D CE
DAD	190-400 nm
capillary	fused silica, 50µm ID, 60 cm length
electrolyte	100 mM acetic acid
injection	30 mbar, 10 s
separation	-15 kV, 0 mbar complete in 15 min
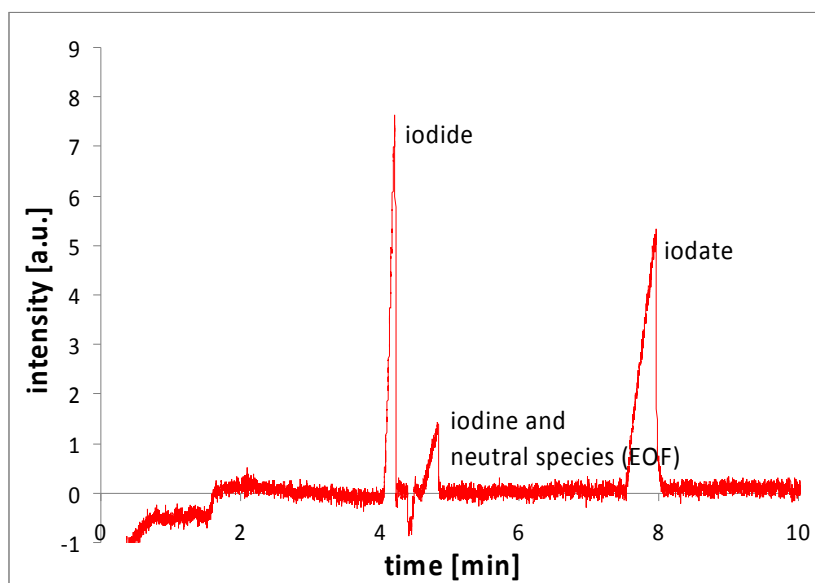
Figure 1: *Electropherogram of iodide and iodate, separated by CE-DAD*
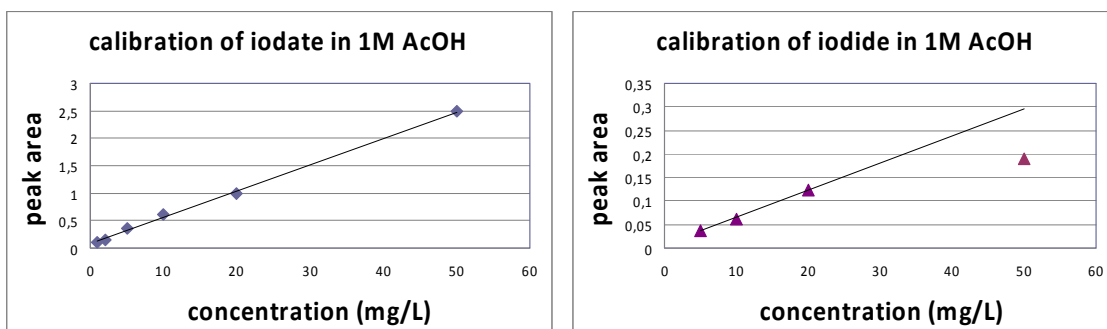
Figure 2: *Calibration of iodide and iodate obtained by CE-DAD*

The obtained calibrations for iodide and iodate in 1 M acetic acid are plotted in figure 2. The calibration has to be fitted individually, because in some cases the peak shape is strongly modified by the media. Also we have to consider that the linearity of the calibration for iodide is limited. The CE-DAD method provides information between 0.5 and 20 mg/L. Above a concentration of 20 mg/L the peak runs over into the signal of the neutral species.

Uranium speciation

The U(IV) solution was prepared by electrochemical reduction of uranyl nitrate dissolved in hydrochloric acid (~0.8 M). The U(VI) solution (25mg/L) was reduced at -10 V during 45 minutes *Delécaut (2004)*. The electrolysis cell was cooled in an ice bath. As electrodes simple platinum coils were used. To prevent the precipitation of the U(IV) the pH was kept at 0.7. The solution was checked several times by UV/Vis spectroscopy during the reduction. 5 minutes after the spectra showed a pure U(IV) solution the electrolysis was stopped and the stock solution was stored under oxygen free argon atmosphere.

Table 2: *Separation conditions for uranium species with CE-ICPMS*

CE instrument	home made
ICPMS instrument	Agilent 7500 ce
capillary	fused silica,
	50µm ID, 65 cm length
electrolyte/buffer	100 mM acetic acid
	10 mM Na_2EDTA
	pH ~ 3.5
injection	100 mbar, 10 s
separation	-25 kV, 150 mbar
	complete in 10 min

The CE was a home made system coupled to an Agilent 7500 ICPMS. The conditions are given in table 2. Figure 3 depicts the electropherogram of a sample containing U(VI) and U(IV).
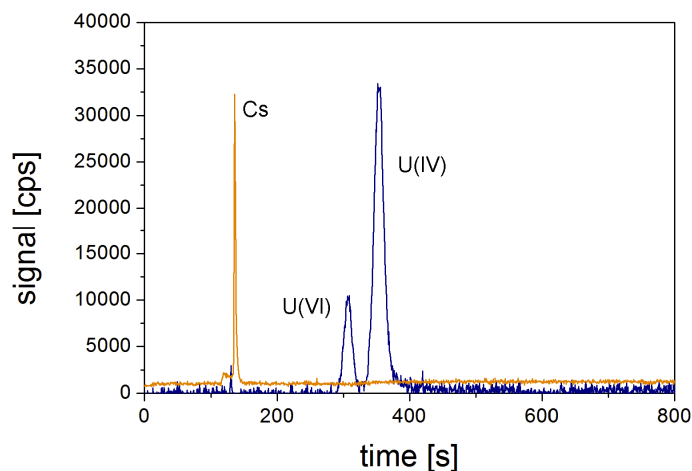
Figure 3: *Electropherogram of U(VI) and U(IV), separated by CE-ICPMS, Cs used as internal standard*

Several mixtures of U(VI) and U(IV) with different ratios were tested, to ensure the reliability of this separation. Therefore the stock solutions were mixed and instantly diluted in the buffer. To ensure that the complexation prevents the fast oxidation of U(IV) a mixture of both uranium redox species was measured after 10 and 80 minutes (storage at normal atmosphere). The effect of 1% change is within the error of the method which is around ± 5%. Details are given in table 3.

Table 3: *Time dependence of uranium species at normal atmosphere, determined with CE-ICPMS*

time	U(IV)	U(VI)
expected	83 %	17 %
10 min	81 %	19 %
80 min	80 %	20 %

Method application

While testing the calibration we have recognised that some redox reactions took place in the standard solutions. In a 0.05 M $HClO_4$ stock solution iodide and iodate were mixed and measured regularly by our method to achieve better statistics. Iodide though was reduced significantly to iodine, while iodate seemed to be more stable. The time dependence is shown in figure 4. This observation indicates the problem with the determination of the redox state. The redox equilibrium can be disturbed very easily. All

solutions have to be stored under stable conditions (inertgas box, oxygen free, dark to prevent iodine photochemistry, at constant temperature …) in order to avoid redox measurement artefacts. The method opens the possibility to determine redox reactions, but for standard measurements like calibration samples, it is necessary to avoid the contact of the different iodine species.
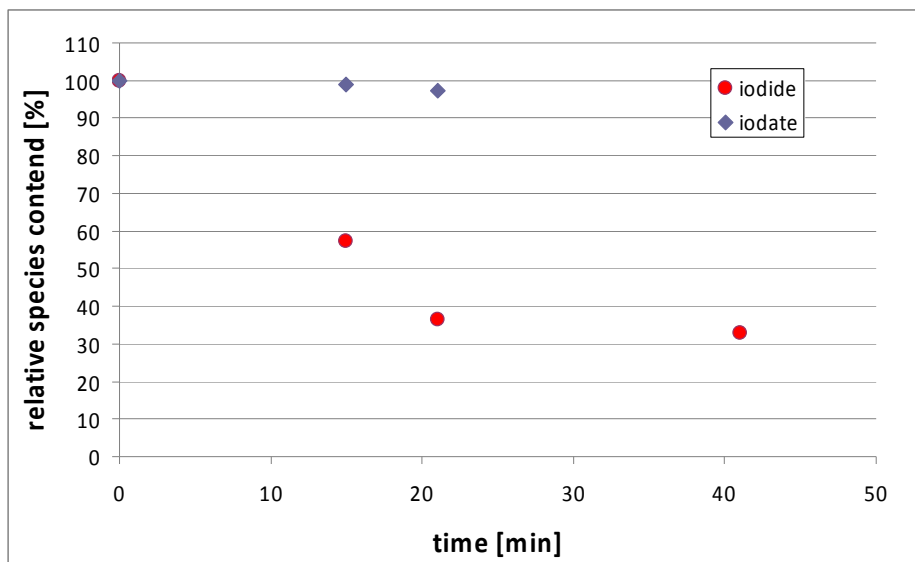
Figure 4: *Redox effects in standard solutions (mixture of iodine and iodate in 0.05 M perchloric acid*

The method was also applied to several other systems, in which the iodine species had contact with clay minerals (Opalinus clay, Wyoming kaolinite KGa1b) in a highly saline synthetic pore water *Pearson (1998)*. The details are given in table 4. The time dependent sorption of iodate is shown in figure 5. The iodine species which were not absorbed on the clay were determined by CE-DAD. In these systems no conversion of the species into each other was observed. The iodide concentrations were below the limit of detection of the CE-DAD. The determination of iodine was not possible because in the nearly natural samples too many other neutral species were present. But they don't have characteristic spectra. Therefore the DAD cannot differentiate between them.

Table 4: *Conditions for the near nature sorption experiments*

synthenic pore water	analog Pearson (1998), except SrCl
mass clay	80.5 ± 0.5 mg
volume	20 ml
initial iodine concentration (iodine in iodide and iodate)	100 mg/L
pH value (opalinus clay)	7.08 ± 0.5
pH value (KGa1b)	5.85 ± 0.7
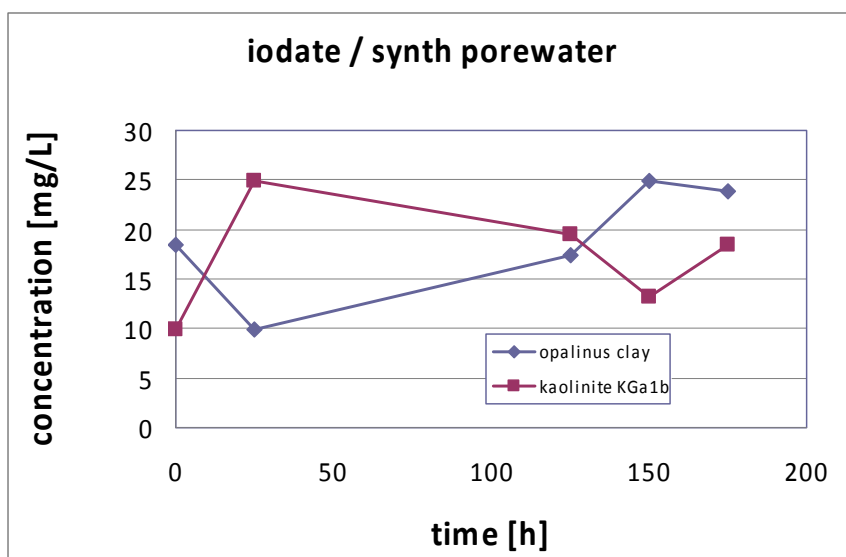
Figure 5: *Time dependent sorption of iodate onto kaolinite and Opalinus clay, determined by CE-DAD*

Summary and Conclusions

In principle the method for iodine works well, but with the sensitivity of the diode array detector is mostly insufficient for environmental conditions. Furthermore iodine can not be separated from other neutral analytes. Therefore transferring the iodine method to the CE-ICPMS would be useful, but it was not available during these experiments.

Also the samples from the Interlaboratory Comparison Exercise have to be measured by the CE-ICPMS in order to show the comparability and reliability of this method. The method for uranium works well for standard samples and has to be tested with synthetic and natural samples. For plutonium and neptunium the method is in routine operation *Bürger (2007), Ambard (2005), Kuczewski (2003).* In the future a speciation method for iron will be developed and compared to other measurement methods, too.

Acknowledgement

References

Ambard C, Delorme A., Baglan N, Aupiais J, Pointurier F, Madic C, (2005), Interfacing capillary electrophoresis with inductively coupled plasma mass spectrometry for redox speciation of plutonium. Radiochim. Acta 93**,** 665-673.

Bürger S, Banik N L, Buda R A, Kratz J V, Kuczewski B, Trautmann N, (2007), Speciation of the oxidation states of plutonium in aqueous solutions by UV/Vis spectroscopy, CE-ICP-MS and CE-RIMS Radiochim. Acta 95, 433–438.

Delécaut G, Maes N, De Cannière P, Wang L, (2004), Effect of reducing agents on the uranium concentration above uranium(IV) amorphous precipitate in Boom Clay pore water Radiochim. Acta 92, 545–550.

Kuczewski B, Marquardt, C M, Seibert, A, Geckeis, H, Kratz, J V, Trautmann, N, (2003), Separation of Plutonium and Neptunium Species by Capillary Electrophoresis - ICP - MS and Application to Natural Groundwater Samples. Anal. Chem. 75, 6769-6774.

Pearson F J, (1998), Opalinus Clay experimental water: A1 Type, Version 980318. PSI Internal report TM-44-98-07, Paul Scherrer Institut, Villigen PSI, Switzerland.

IODINE SORPTION ON KAOLINITE AND HUMIC ACID

Edit Marosits[1*], Bernhard Kuczewski[1,2], Kerstin Wenzl[1]

[1] Institute of Analytical Chemistry and Food Chemistry, Graz University of Technology, Technikerstr. 4, 8010 Graz (AT)

[2] Division of Nuclear Chemistry, University Cologne, Zülpicher Str. 45, 50674 Köln (DE)

* Corresponding author: marosits@tugraz.at

Abstract

The sorption of iodine species by the well known KG1a-b kaolinite and humic acid (HS, Sigma Aldrich) was studied in NaClO$_4$-solution within the framework of batch experiments. The sorption-behaviour of two species was examined in the pH range of 2-10. Both iodide and iodate had low sorption capacity on kaolinite: below 8% and 21%, respectively. The pH of the solutions affected the adsorbability of the species only at pH<4. The ternary systems were examined by adding HS to the already equilibrated iodine species - kaolinite systems. Compared to the binary systems, an additional sorption was observed for both species, which was higher for iodide (up to 26%) than for iodate (<14%).

Introduction

Iodine, an essential element, can be found all over in the biosphere and the environment. In order to assess the risks and long-term effects of the long-lived isotope ^{129}I produced in reactors and deposited with the nuclear waste, it is important to understand the environmental behaviour of iodine. It is a redox sensitive element with several possible oxidation states (from -1 to +7). The migration and retention behaviour of the iodine is highly dependent on its redox form. The dominating species in aqueous phases is iodide, which has a higher mobility compared to iodate.

Within this framework the sorption behaviour of iodide and iodate by kaolinite and humic acid was investigated. Several studies reported already that though iodate has a

much lower mobility than iodide, both of them have a low sorption capacity on kaolinite (Couture and Seitz (1983)), (Muramatsu et al. (1990)), Neal and Truesdale (1976)). On the contrary, organic matter seems to have an important role on iodine retention (Sheppard and Thibault (1992)). The studies about the iodine species and humic substances are very contrary. Muramatsu et al. observed considerable sorption by humic acid for both iodide and iodate (Muramatsu et al. (1990)). Other authors reported that there was no interaction between iodide and HS, while molecular I_2 reacted with humic acid without linear kinetics being observed (Ashworth et al. (2003)). The mechanism of retardation of iodine by humic substances is a hydrophilic substitution of hydrogen by iodine on a phenolic ring (Reiller et al. (2006)).

In this study the results of new batch experiments were compared to already existing data for binary systems and additionally ternary systems (iodine species – kaolinite – humic acid) were examined.

Materials and Methods

Samples

The iodide and iodate stock-solutions with a concentration of 10 g/L were prepared from NaI and NaIO$_3$, respectively. They were stored in a dark place (normal atmosphere, 22 °C).

The well-characterised KGa1-b kaolinite with a surface area of 11.7 m^2/g *(Pruett and Webb (1993))* was used for the experiments. 0.1 M NaClO$_4$ solution was prepared in one batch and used for all samples in this work. The experiments were carried out under atmospheric conditions.

For ternary systems a 10 g/L HS solution was prepared using humic acid from Sigma Aldrich cleaned and treated according to *Kim and Buckau (1988)*.

Sorption experiments

54 samples in dark glass bottles were prepared with 20 ml 0.1 M NaClO$_4$ and a kaolinite concentration of 4 g/L. These samples were divided into 6 test series each with pH values 2, 3, 4, 5, 6, 7, 8, 9, 10. The pH values were adjusted with HClO$_4$ and NaOH for two weeks until they were nearly stable. In order to have a concentration of 10 mg/L I$^-$, IO$_3^-$, respectively, the half of the solutions were spiked with 20 µl of iodide solution and the other half with 20 µl of iodate solution.

In order to calculate the loss from the pristine iodine species amount - the adsorbed quantity - "control standards" for iodide and iodate were prepared. For this reason the same bottles and same NaClO$_4$ solution spiked with the iodine species were used without the clay mineral. All samples were kept in a dark place (normal atmosphere, 22 °C) and were shaken 3 times a week by hand. After 14 days the pH of all samples was measured and 100 µl liquid near to the surface was pipetted off from each sample. These samples were diluted and the iodine content was measured by ICPMS. Then the binary systems and the "control standards" were spiked with different amounts of HS (50 mg/L, 100 mg/L, 200 mg/L) for each test series. The samples were shaken every second day and stored in the dark for another 14 days (normal atmosphere, 22 °C), after

which the pH of all samples was determined and the iodine concentration measured the same way as before.

Analytical techniques

The pH value was determined by using an Orion 3 Star pH-meter (Thermo) with a refillable Mettler Toledo In®Lab Routine pH electrode. The iodine concentration in the samples was measured by the Agilent 7500 ICPMS and the adsorbed amount was calculated as the concentration difference between the "control standards" and the particular sample.

Results

Binary systems

The sorption of iodide and iodate by kaolinite was very low (Figure 1). In the case of iodide the adsorbed amount was between 0-8%. For iodate, in most cases it was around 10% but with higher values in the acidic area (up to 21%).
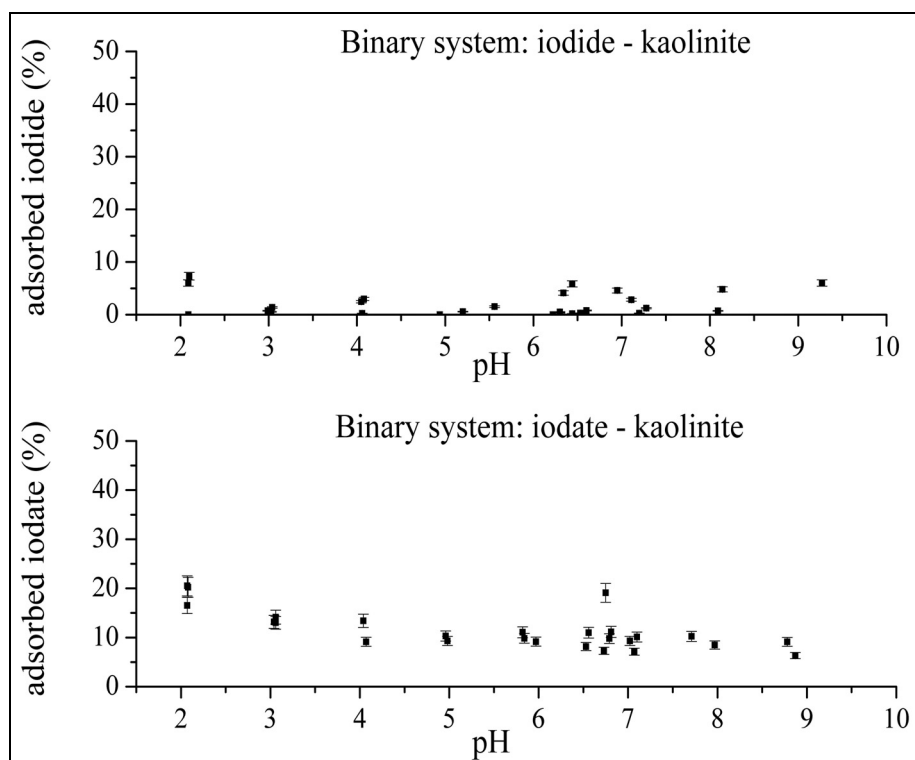
Figure 1: *Binary systems: iodine species - kaolinite. The adsorbed amount of iodine species (in %) is plotted against the pH value of the solution at the time of measurement.*

Ternary systems

Adding humic acid to the already equilibrated binary system resulted in a further loss of iodine species from the solutions attributed to additional sorption, or other chemical reactions caused by humic acid.

In the ternary systems with iodide only the samples with pH<3.5 show a correlation between the adsorbed amount and the HS concentration in the solutions. On the contrary, the iodate – kaolinite – humic acid systems seem to have a clearly recognizable positive correlation between the adsorbed iodate amount and the HS concentration of the samples.
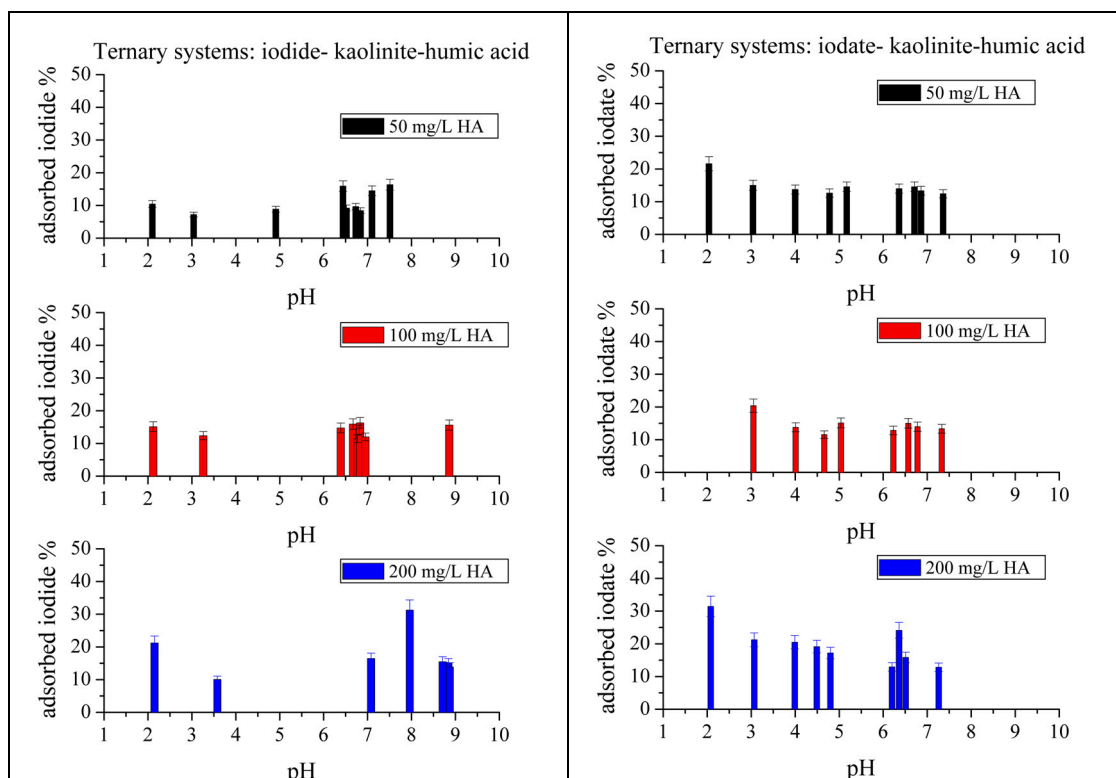
Figure 2: *Ternary systems: iodine species - kaolinite - humic acid. All test series with different iodine species and HS concentrations are presented. The iodine species totally adsorbed by kaolinite and humic acid (in %) is plotted against the pH value of the solution at the time of measurement.*

Summary and Conclusions

The results for the binary systems with little or no sorption of iodide and a low sorption capacity for iodate reinforced the data already reported by other authors *(Couture and Seitz (1983))*. The low sorption can be explained with the fact that clay minerals carrying negative charges push away anions *(Muramatsu et al. (1990))*, *(Whitehead (1984))*. This also explains the slightly higher values for iodate in the acidic area. These experiments were carried out under atmospheric conditions and Bazer-Bachi et al,

(2006) reported that the low iodide uptake on argillaceous rocks was dependent of the exposure time of the samples with atmospheric oxygen during batch experiments. The ternary systems show an additional sorption attributed to humic acid, which is contrary to some earlier results *(Reiller and Moulin (2003))*. It may occur that molecular iodine was formed in the solutions and the iodine was bound on HS in these experiments.

Further investigations with methods for structure examination like XPS or EXAFS can provide more detailed information about the sorption mechanism of iodine species in ternary systems.

Acknowledgement

References

Ashworth, D.J., Shaw, G., Butler, A.P., Ciciani, L. (2003). Soil transport and plant uptake of radio-iodine from near-surface groundwater. Journal of Environmental Radioactivity, 70(1-2), 99-114.

Bazer-Bachi, F., Tevissen, E., Descostes, M., Grenut, B., Meier, P., Simonnot, M.-O., Sardin, M. (2006). Characterization of iodide retention on Callovo-Oxfordian argillites and its influence on iodide migration. Physics and Chemistry of the Earth, 31, 517-522.

Couture, R.A., Seitz, M.G. (1983). Sorption of anions of iodine by iron oxides and kaolinite. Nuclear and Chemical Waste Management, 4(4), 301-306.

Kim, J.I., Buckau, G. (1988). Characterization of reference and site specific humic acids. RTM02188.

Muramatsu, Y., Uchida, S., Sriyotha, P., Sriyotha, K. (1990). Some considerations on the sorption and desorption phenomena of iodide and iodate on soil. Water, Air, & Soil Pollution, 49(1), 125-138.

Neal, C., Truesdale, V.W. (1976). The sorption of iodate and iodide by riverine sediments: its implications to dilution gauging and hydrochemistry of iodine. Journal of Hydrology, 31(3-4), 281-291.

Pruett, R., Webb, H. (1993). Sampling and analysis of KGa-1B well-crystallized kaolin source clay. Clays & Clay Minerals, 41(4), 514-519.

Reiller, P., Moulin, V. (2003). Influence of organic matter in the prediction of iodine migration in natural environment. in: Materials Research Society Symposium-Proceedings, 565-570.

Reiller, P., Mercier-Bion, F., Gimenez, N., Barré, N., Miserque, F. (2006). Iodination of humic acid samples from different origins. Radiochimica Acta, 94, 739-745.

Sheppard, M.I., Thibault, D.H. (1992). Chemical behaviour of iodine in organic and mineral soils. Applied Geochemistry, 7(3), 265-272.

Whitehead, D.C. (1984). The distribution and transformations of iodine in the environment. Environment International, 10(4), 321-339.

DEVELOPMENT OF AN FIBRE OPTICAL CHEMICAL SENSOR (FOCS) FOR THE DETERMINATION OF LOW OXYGEN CONCENTRATIONS

Dörte Steinbrück, Elmar Schmälzlin and Michael U. Kumke*

Institute of Chemistry, University of Potsdam (GER)

* Corresponding author: kumke@uni-potsdam.de

Abstract

Our recent developments of an improved fibre-optical chemical sensing (FOCS) system for the determination of oxygen in the ppm to ppb range are presented. A novel luminescence probe with luminescence decay time of several hundred μs was implemented. The novel dye (Weston and Patterson 2009) has an improved higher dynamic range in decay time change (gain of a factor of 10!) compared to the previously established oxygen sensor (Schmälzlin et al., 2005). For the implementation of this novel sensor in the optical detection of ultralow oxygen concentrations, a proper calibration in the ppm concentration range is indispensible and proved to be a demanding task. In a first step we have carried out calibration experiments in the low vol% range. The first results are very promising and it can be envisioned that the optical detection of oxygen at the lower ppm range is in reach.

Introduction

Fiber-optical chemical sensing (FOCS) has been proven a powerful alternative to electrochemical-based techniques for oxygen sensing. The recent availability of high quality, inexpensive optical fibers provides an exciting new direction for chemical sensor designs, because optical transduction allows a wide variety of chemical detection schemes that previously were not possible for sensor development.

Compared to electrochemical techniques optical based detection systems i) consume no analyte, which is of special importance at low oxygen concentrations and ii) are insensitive to pH variations. Moreover, optodes can be used in-situ even under harsh

conditions (e.g., presence of corrosives), have a high miniaturization potential (with sensors < 10 μm) and have fast response times. FOCS can also be used for distributed sensing applications (such as in optical time domain reflectometry) and can – even on the miniaturized level – be used in multiparameter sensing scheme.

In general, optical detection schemes can be based on measurement of luminescence intensity or luminescence decay time. While the first requires less sophisticated instrumentation, it suffers from limitations due to background signals and cross sensitivities. Luminescence decay time based FOCS can circumvent such limitations at the cost of more expensive (sophisticated) instrumentation.

In our research the development of a miniaturized multiparameter luminescence decay time based FOCS for the determination of oxygen concentration, temperature (Löhmannsröben and Schmälzlin, 2007), and pH-value is pursued. The detection scheme utilizes the phase modulation luminescence spectroscopy as its basic detection principle.

Our current research is focused on the implementation of an improved optode for the determination of oxygen concentrations in the sub-ppm range. The development of the optode for trace level oxygen measurements requires an optical sensor with a very long luminescence decay time in order to have a sufficient dynamic range at low oxygen concentrations. Technical requirements such as detection system, modulation frequencies and immobilisation matrix are further aspects that need to be adapted. In the present report the progress made addressing this topic is discussed.

Experimental

The oxygen senstive Pd(II)-tetrapentafluorophenylphorphyrin (Pd-TPFPP) was purchased from FrontierScientific, Inc and used as received. 6-Carboxyfluorescein was purchased from Sigma-Aldrich ($\geq$ 98%) and used as received. The sample solutions were prepared in Millipore water. For the pH adjustment of the solutions HCl and NaOH (both purchased from Carl Roth, Karlsruhe) were added. The tested polymers were purchased from Sigma-Aldrich as well.

The phase modulation spectroscopy in the MHz range was performed using a Lock-In Amplifier from Stanford Research Systems (model SR844).

For the fundamental characterisation of the novel Pd(II)-tetrapentafluorophenyl-phorphyrin based oxygen optode different spectroscopic methods were applied: i) frequency-domain phase modulation spectroscopy (FD-S) with a modulation frequency ν of 900 Hz, ii) dual-frequency phase modulation spectroscopy (d-FD-S) with ν_1 = 1.22 kHz and ν_2 = 513 Hz, and iii) time-domain luminescence detection using a pulsed laser source (TD-S).

The gas-mixtures containing different oxygen concentrations were prepared with a 4 channel Flowcomputer (RS232, Westphal Mess- und Regeltechnik GmbH). The ppm values of oxygen always refer to the oxygen content of the gas phase. The gas mixtures (containing N_2 and O_2) were bubbled into distilled water. The temperature of the samples was controlled using a thermostat set to T = 20°C. The optode (polymer with the embedded dye at the optical fibre tip) were immersed into the water phase. The dissolved oxygen diffuses into the oxygen permeable polymer where the oxygen

quenched the luminescence of the dye (Pd-TPFPP). The polymer is not permeable for water, only for the gas.

Characterisation of the novel oxygen sensor

In Figure 1 the absorption and emission spectra of the oxygen sensitive dye Pd-TPFPP are presented. The emission is located at $\lambda_{em} > 550$ nm with potential detection at $\lambda_{em} = 675$ nm, which is especially beneficial for applications in real-world samples since the extinction in the long wavelength region of the electromagnetic spectrum is usually decreasing in such samples. Moreover, the large separation between absorption and emission (*stokes shift*) minimizes problems arising from residual excitation light in the detection. The intensity of the emission at 680 nm is dependent on the oxygen concentration and decrease in the presence of oxygen cause of the quenching process.

A prerequisite for an ultra-sensitive detection of oxygen base on a time-resolved detection scheme is that the luminescence decay time alteration due to the presence of O_2 is large yielding a sufficient dynamic range for the determination of the analyte. Figure 2 shows the results of decay time based oxygen depended measurement of the Pd-TPFPP embedded in polymer on a sensor tip. It can be seen that for oxygen concentrations below 1 vol% (10^4 ppm gas phase, which equals at room temperature 0.0126 mmol/L of oxygen in water) a large variation ($\Delta\tau/\Delta O_2$) in the observed luminescence decay time was found. The luminescence decay times were further determined in solutions equilibrated with oxygen/nitrogen gas mixtures of different oxygen content in the concentration range up to 16 vol% O_2 (see Figure 2) yielding an overall dynamic range in τ of 200 µs $< \tau <$ 840 µs.
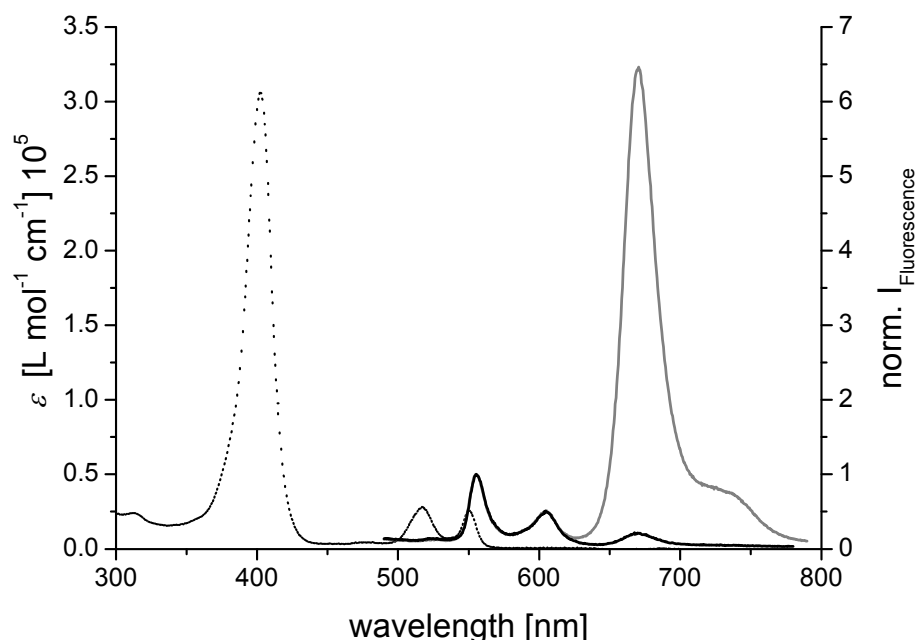
Figure 1: *Absorption coefficient ε (dotted line) and emission spectra ($\lambda_{ex} = 405$ nm) of Pd-TPFPP in EtOH bubbled with 10 vol% oxygen (black) and nitrogen (grey).*
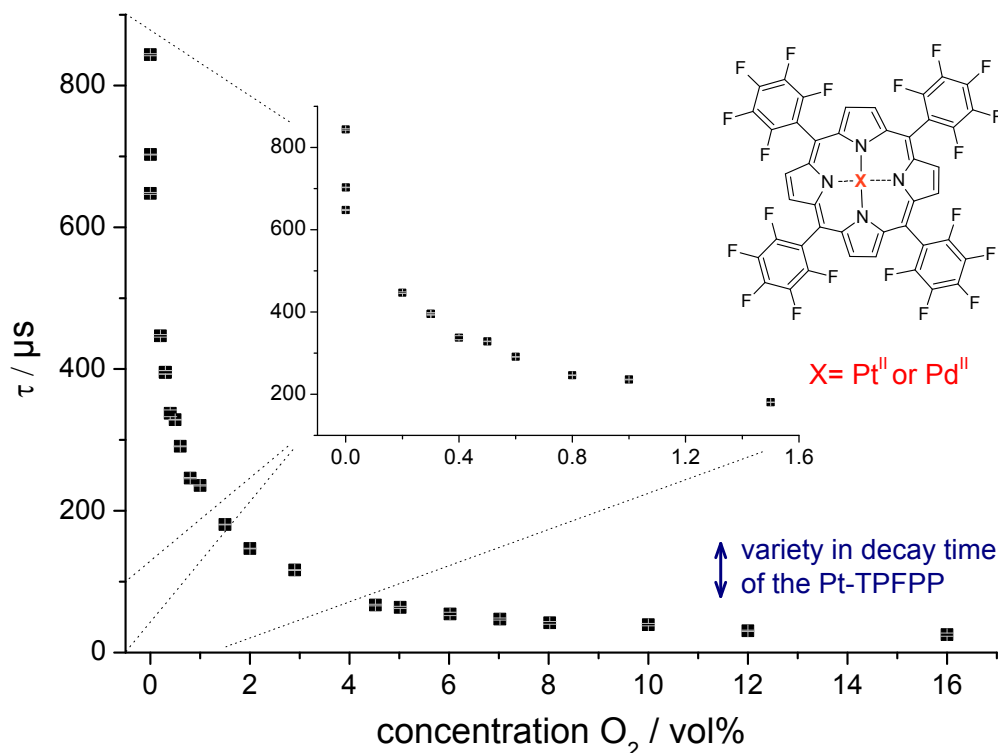
Figure 2: *Calibration curve of Pd-TPFPP immobilized in a fibre sensor tip measuring luminescence decays in dependence of the oxygen concentration in the surrounding solution. Excitation at* λ_{ex} *= 405 nm using a pulsed laser diode. The standard error of the measured luminescence decay time is one μs.*

In Figure 3 the results of the Stern-Volmer analysis for method 1 - 3 are shown and table 1 summarise the results of the analysis for different data ranges as well as methods.

Compared to measurements in solution the properties of polymer matrix, in which the dye is immobilized, have a distinct influence on the observed luminescence quenching: i) the permeability of the polymer for oxygen and ii) the thickness of the polymer will affect the performance of the sensor. The latter may cause a gradient oxygen concentration in the polymer yielding depth-dependent luminescence decay times, which can be accounted for by considering a decay time distribution in the data analysis. Therefore, a stretched exponential model was applied:

$$I(\mathrm{t}) = I_o \cdot \mathrm{e}^{-\frac{t}{\tau}^{\beta}} \qquad (1).$$

The parameter β accounts for the distribution of the luminescence decay time τ. The common evaluation of lifetime based measurements follows with the Stern-Volmer equation:

$$\frac{\tau_0}{\tau} = 1 + K_{SV}[O_2] \qquad (2).$$

From the range of zero to 1vol% of oxygen works this approach with good agreement to the data. For better data analysis over a broad oxygen concentration range the modified Stern-Volmer equation was used:

$$\frac{\tau}{\tau_0} = \frac{f}{1 + K_{SV}[O_2]} + (1 - f) \quad (3).$$

Here, the ratio f fits the non-linear behaviour of the data and according to the part of dye molecules which are quenchable (Holst et al., 1997). The unquenched lifetime τ_0 could be calculated by plot $1/\tau$ against the oxygen concentration $[O_2]$, see figure 3 and table 1 and 2.
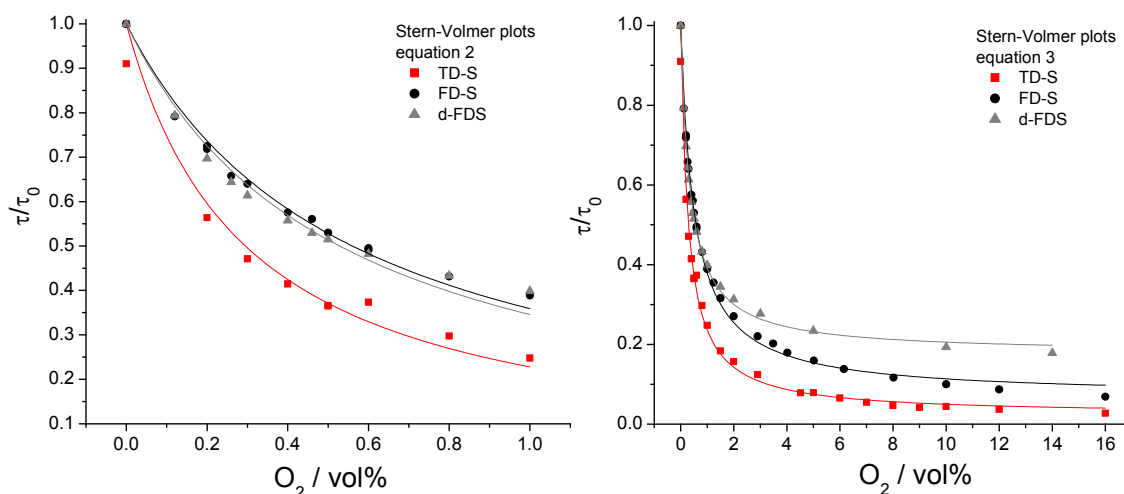
Figure 3: Stern Volmer data evaluation of the oxygen depended luminescence decay time based measurements using three different experimental methods, left: O₂ concentration up to 1 vol%, right: O₂ concentration up to 16 vol%.

The determined accuracy of the measurements was comparable. Also, the effect of the concentration range used for the calibration can be seen underlining the need for a proper calibration in the lower range of oxygen concentrations. For the sensitivity the value of k_q is very important. It was found that the reference (TD-S) and the d-DF-S yield very similar value underlining the preferred use of a dual-frequency phase modulation approach. For the two phase modulation techniques a standard error s of 0.3 µs was determined, which is comparable to the time domain measurement ($s = 1$ µs). The accuracy in table 1 was calculated according to:

$$\frac{1}{K_{SV}}\left(\frac{f}{\dfrac{\tau_0}{\tau_0-s}-(1-f)}-1\right) = x \text{ vol } \% = x \; 10^4 \text{ ppm}$$

For the application (calibration) of the optode the luminescence decay time in the absence of oxygen (τ_0) is of utmost importance. A sample containing excess Na$_2$SO$_3$ was used, which chemically removes dissolved oxygen, for the determination of τ_0. The unquenched luminescence decay time was determined to $\tau_0 = 840$ µs.

Table 1: *Results of the fits from the data in figure 3 with the modified Stern-Volmer equation (3). Given are the accuracy for the oxygen determination relative to the gas phase (in ppm) and for the corresponding concentration in the aqueous phase (in nmol/L).*

method	k_q [s ppm]$^{-1}$	f	Accuracy	
			[ppm]	nmol/L
DF	0.5	0.93	4	5.0
d-FD-S	0.5	0.82	5	6.3
TD-S	0.4	0.97	2	2.5

Table 2: *Results of the fits from the data in figure 3 with the Stern-Volmer equation (2). Given are the accuracy for the oxygen determination relative to the gas phase (in ppm) and for the corresponding concentration in the aqueous phase (in nmol/L).*

method	k_q [s ppm]$^{-1}$	accuracy	
		[ppm]	nmol/L
DF	0.3	7	8.8
d-FD-S	0.5	4	5.0
TD-S	0.5	1	1.3

From repeated measurements the accuracy of the measurement was determined to ±1 µs, which would allow to detect about 10 ppm O$_2$ under the assumption of fully diffusion controlled luminescence quenching ($k_q \sim 10^{10}$ M^{-1}s^{-1}). In the polymer matrix the diffusion of oxygen to the immobilized dye molecules may be hindered and is certainly dependent on the thickness of the actual polymer matrix.

Therefore, the calibration of the optode at trace level concentrations of oxygen is mandatory (and a crucial step because the preparation of samples with well-defined oxygen concentrations in the lower ppm level is difficult). With the current gas mixing set up, oxygen concentrations down to 0.1 vol% (1000 ppm) can be prepared with high accuracy. Work is in progress to improve the calibration set up further to much lower oxygen concentrations.

For estimating the limit of detection (LOD), two reference values (without oxygen, in a Na$_2$SO$_3$ solution and with approximately 0.2 ppm oxygen by using commercial 5.0 nitrogen for purging the water sample) and a standard error of the method of 1 µs were used. A LOD of 0.8 ppm was determined. Because the concentration of oxygen in the nitrogen is <0.2 ppm according to the manufacturer, this LOD value may be considered as an upper estimate.

Summary / Conclusions

The optical determination of oxygen was extended into the low ppm range (O$_2$ concentration > 10 pm). For an improved calibration it is necessary to perform measurements in the ultra low oxygen range which will be pursued as next step in the future. The accuracy of the used methods is already excellent meeting the required standards. It is expected that the observed error is will be even decrease further once an improved system for adjusting the oxygen concentration in the calibration set up is on hand.

Compared to conventional (electrochemical) set-ups, the optical detection scheme can be extremely miniaturized and is free of background interferences. This is especially interesting for measurements in very small volumes, where the consumption of oxygen due to the measurement (as it is the case for electrochemical detection) is crucial and may lead to wrong results. Moreover, optical detection systems offer also the advantage of multiparameter sensing. At a macroscopic scale several electrodes may be used, but for measurements which require a higher spatial resolution, an optical sensor scheme that combines several physic-chemical detection parameters is unmatched by electrochemical approaches. Currently, work is in progress to set-up such a multiparameter system using miniaturized optodes.

Acknowledgment

Reference:

Buckau G., Kienzler B., Duro L., Grivé M., Montoya V. (2009): Collaborative Project "Redox Phenomena Controlling Systems" 1st Annual Workshop Proceedings, page 103-109, Forschungszentrum Karlsruhe GmbH, Karlsruhe

Holst G., Glud R. N., Kühl M., Klimant I. (1997): A micro-optode array for fine-scale measurement of oxygen distribution, Sensors Actuators B, 38–39:122–129.

Löhmannsröben H.-G., Schmälzlin E. (2007): Minimally invasive fiber probes for optical in-vivo oxygen measurements with integrated optical thermometer Proceedings SPIE Vol. 6770, 67700V.

Schmälzlin E., van Dongen J. T., Klimant I., Marmodee B., Steup M., Fisahn J., Geigenberger P., Löhmannsröben H.-G. (2005): An optical multifrequency phase modulation method using microbeads for measuring intracellular oxygen concentrations in plants, Biophysical Journal 89 1339–1345.

Weston M. A., Patterson M. S. (2009): Using Pd-porphyrin phosphorescence and photodynamic oxygen consumption to study oxygen diffusion in cells, Proc. Of SPIE-OSA Biomedical Optics, SPIE Vol. 7368 736812-1--- 736812-9.

LACK OF REDOX RESPONSE IN SOME CASES ON BODA CLAYSTONE SAMPLES AS REFLECTED IN THE Fe^{2+}/Fe^{3+} RATIO IN MINERALS

Károly Lázár [1*], János Megyeri [1], Zoltán Máthé [2]

[1] Institute of Isotopes (HU)

[2] Mecsekérc Environmental (HU)

* Corresponding author: lazar@iki.kfki.hu

Abstract

Effects of reducing and oxidizing treatments were studied on Boda Claystone samples. A sample containing mostly ferrous ions in chlorite mineral was exposed to various oxidants in the first series. Another sample, containing dominantly ferric iron (in form of hematite and ferric ions in clay minerals) was exposed to various reducing conditions in the second series. The Fe^{2+} and Fe^{3+} contents in the samples were determined by Mössbauer spectroscopy. No significant effect of treatments was found in most of cases. An exception was the dithionite treated sample, dissolution of the hematite phase and partial re-incorporation of the dissolved ferrous ions were detected in this case.

Introduction

Boda Claystone is considered as a perspective media for disposal of high level nuclear waste in Hungary. A general description of the rock (diagenesis, compositon etc.) can be found e.g. in Árkay et al. (2000). A summary of detailed geological, geomechanical, hydrological etc. exploratory studies can be found in Szűcs et al. (2004). Effective diffusion constants of various long half life-time radionuclides have already been determined in this media in order to obtain a preliminary information on the retention capacity, namely ^{129}I, ^{85}Sr (Mell et al. (2006)), and ^{99}Tc, ^{14}C (Lázár, Megyeri et al. (2009)). Recently, study of possible influence of the redox processes taking place during the migration of species containing multivalent central ions got an emphasis.

The aptness of the rock for the redox changes has been studied on the presumption that Fe^{2+}/Fe^{3+} reversible processes may play an important role in redox responses. In

preliminary studies indirect proofs for this aptness were demonstrated, namely changes of Fe^{3+}/Fe^{2+} ratios in clay minerals due to different genesis conditions or weathering (*Lázár, Máthé et al. (2009)*).

In the present study response of Boda Claystone samples to direct redox treatments is reported. Namely, two types of samples were studied. In the first series portions from a sample containing dominantly ferrous ions were exposed to various oxidizing agents. The second series was the opposite case, a sample with the prehistory of the formation under mostly oxidizing conditions and containing thereby dominantly ferric iron ions was exposed to various reducing agents. The Fe^{2+}/Fe^{3+} contents in the respective minerals were analysed by Mössbauer spectroscopy.

Experimental

Samples selected

Two types of claystone samples were selected from drilling core of boring Delta-9. (For further geological details, location of borings, see *Szűcs et al. 2004*). In the first series a sample taken at 84.9 m distance from the start was studied. The conditions of formation here were dominantly reducing, the dominant iron bearing mineral in this sample is chlorite with iron in ferrous form. The second sample was taken from a different location of the same drilling core (at 91.9 m). In this case the conditions of formation were mostly oxidizing. Iron was present in this sample dominantly in two types of minerals, namely, in hematite, with iron exclusively in ferric form, and in layered clay minerals (chlorite, and illite-montmorillonite) containing iron in both, ferric and ferrous forms. The total iron content of the samples was 8 – 9 wt % (determined by classical titrimetry).

Treatments

800 mg of powdered samples, with average particle size 1 – 10 micron, were equilibrated in aqueous media with 5 – 7 ml of oxidizing/reducing agents used in 1 - 3 mol/L concentration. These amounts represent 4 - 5 fold excess with respect to the total amount of iron present in the sample. The oxidizing reactants were perchlorate (in acidic medium), hypochlorite (in alkaline medium) and hydrogen peroxide (in neutral medium). The reducing agents were hydroxylamine hydrochloride, formaldehyde (in acidic medium), hydrazine (in basic medium) and dithionite (in neutral medium). The standard potentials of the listed oxidizing processes vary between 1.20 and 0.89 V, the Fe^{3+} / Fe^{2+} potential is 0.77 V, and the selected reducing processes correspond to potentials from -0.25 to 0.20 V (*Inzelt (1999)*). Samples were equilibrated for 10 – 15 days, in sealed vials in the case of reducing conditions. The iron content in the clear, supernatant fluid above the slurry of the dithionite treated sample was determined by atomic absorption at the end of the treatment. It was found that ca. 10 – 15 % of the total amount of iron present originally in the sample can be found in the solution phase .

Methods of measurements

The Fe^{2+} and Fe^{3+} states in the minerals were identifyed by Mössbauer spectroscopy. To avoid the long time exposure to air (primarily in the case of samples treated under reducing condition) samples were prepared in two versions. The first version was a fast freezing by immersing the slurry of the treated rock sample in a thin sample holder to líquid nitrogen. Then, the measurement was also carried out at 77 K. In the second version the slurry was dried on air in a thin layer within a few minutes and then it was sealed in between two thin molten paraffin wax discs.

Results and discussion

Oxidizing treatments

The 77 K Mössbauer spectrum collected on the original sample taken from the ambiance of reduced character and the spectra recorded after treatments of this sample with various oxidizing agents are shown in Figure 1.
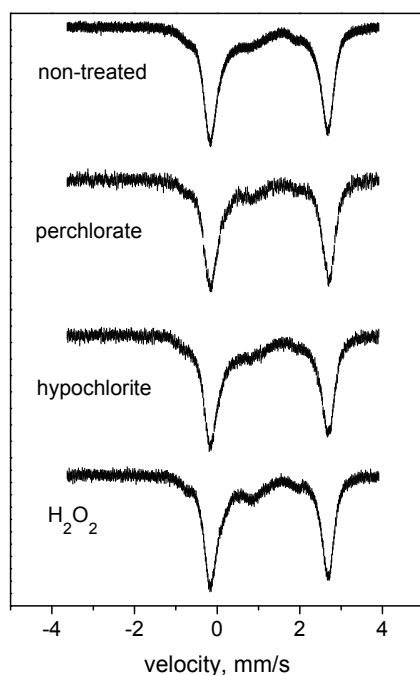
Figure 1. *77 K Mössbauer spectra of the original, non-treated sample (top), and samples treated with perchlorate (in acidic media), with hypochlorite (in alkaline media) and with hydrogen peroxide (in neutral media).*

The spectrum shown in the top is characteristic for chlorite with ferrous iron. The dominant component is a doublet with isomer shift (IS) 1.23 mm/s and with quadrupole splitting (QS) 2.84 mm/s. These data coincide well with the reported ones for chlorite with ferrous iron (*Zazzi et al. (2006)*). None of the oxidizing agents had an influence of the shape of the spectra, all spectra are practically similar to the original one. Thus it can

be deduced that the ferrous iron ions located in the sheet-like structure of chlorite are not easily accessible for oxidation, they retain the ferrous state even among strongly oxidizing conditions.

Reducing treatments

Series of 77 K spectra recorded on the original non-treated sample and on samples treated with various reducing agents are shown in Figure 2. The spectra were collected in the -/+ 4 mm/s velocity range for better resolution in the central part, thus the outer lines of the sextet of hematite are not displayed. The two central lines of the sextet are marked with "H". The spectrum of the non-treated sample can be decomposed to three components, namely, to a doublet of the Fe^{3+} components located probably in the clays (IS: 0.46 mm/s, QS: 0.56 mm/s) to another doublet of Fe^{2+} located in the chlorite (IS: 1.25 mm/s, QS: 2.88 mm/s), and to the two mentioned lines of hematite. The treatments with hydroxylamine-hydrochloride (acidic media), with formaldehyde (neutral media) and with hydrazine (alkaline media) do not result in noticeable changes in the shape of the original spectrum. Thus, it can be suggested that these treatments performed under reducing conditions, do not affect significantly the original Fe^{3+}/Fe^{2+} distribution in the minerals of the sample. (Similarly to the previous instance of the treatments performed under oxidizing conditions.)
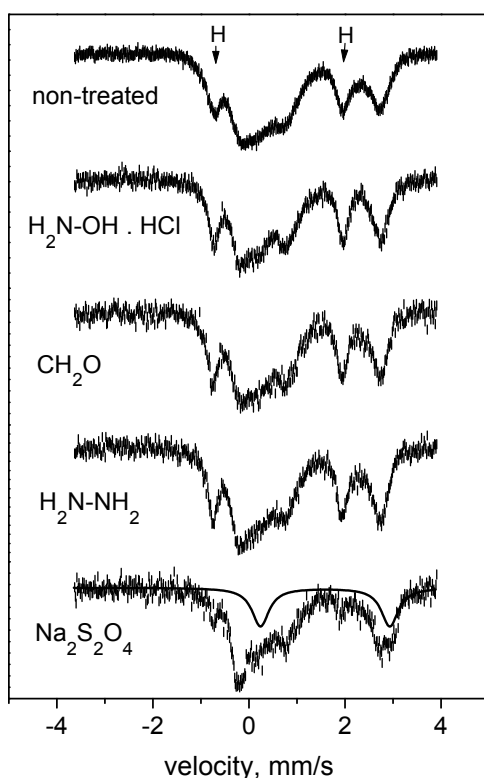
Figure 2. 77 K Mössbauer spectra of the original non-treated sample (top – H indicates the positions of the center lines of hematite), and the samples exposed to reducing reactants, namely to hydroxylamine-hydrochloride, formaldehyde, hydrazine, and sodium dithionite (from top to bottom). In the bottom spectrum the solid line displays the doublet of the novel Fe^{2+} component.

Treatment with sodium dithionite

As an exception among the treatments with strong reducing agents, the treatment with sodium dithionite results in remarkable changes. Namely, the intensities of the central lines of hematite decrease significanly, and an additional Fe^{2+} component (doublet: with IS: 1.58 mm/s QS: 2.66 mm/s) appears in the 77 K spectrum, with almost the same intensity than the Fe^{2+} component present in the chlorite (IS: 1.20 mm/s, QS: 2.93 mm/s) as shown in bottom of Figure 2.

Room temperature spectra were also recorded on this sample, to display better the phenomenon, in two velocity ranges (Figure 3.). For the interpretation, some numerical data are also collected in Table 1.
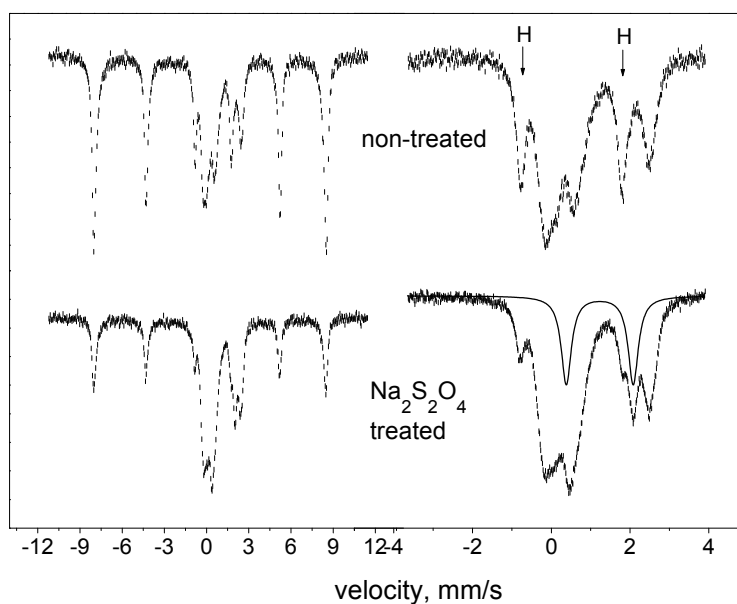
Figure 3. *Room temperature Mössbauer spectra of the non-treated (top) and the dithionite-treated (bottom) samples, recorded in two velocity ranges, -/+ 12 mm/s (full spectrum – left side), and -/+ 4 mm/s (central part only – right side.) In the right top spectrum H indicates the positions of the central lines of hematite. The solid line in the right bottom spectrum displays the doublet of the novel Fe^{2+} component*

The comparison of the spectra recorded in the full velocity range clearly demonstrates the dissolution of hematite by dithionite. After the treatment, the intensity of hematite sextet drops ca. to the half of the original value present in the non-treated sample. The dissolution is proven also by atomic absorption measurements – the solution contains 0.6 mg/ml iron which corresponds to ca. 15 – 20 % dissolved iron related to the amount present in the original sample. This phenomenon, the reducing dissolution of ferric components by reducing agents in clays, in particular with dithionite is well known (see e.g. in Cornell and Schwertmann (1996)).

However, the other observation, the presence of a second Fe^{2+} doublet upon the treatment is worth mentioning. The appearance of the new doublet is an indication of

the existence of a novel coordination site, a new location for Fe^{2+}. This new location can plausibly be attributed to incorporation of the reduced ions in a novel site, enabling to accommodate ferrous iron in the layered clay structure.

Table 1. *Distribution of iron among various states in the -/+ 12 mm spectra of Fig. 3. (IS: isomer shift, mm/s, QS: quadrupole splitting, mm/s, and RA, relative area, %.)*

Treatment			Original	Na$_2$S$_2$O$_4$
Component	*IS*	*QS*	*RA*	*RA*
Ferric iron in hematite (sextet)	0.35	0.22	64.2	29.0
Ferric iron in other clays	0.3	0.7	22.4	31.5
Ferrous iron in chlorite	1.2	2.5	13.5	23.3
Ferrous iron relocated	1.2	1.7	-	13.8

Notes: –   the   iron   contents   in   the   two   samples   are   different,
– RA and relative intensity values have different meaning.

This presumption can be proven by comparing the relative intensities of the components (the intensities related to the count number of the base line). The values of these relative intensities both for the first Fe^{2+} doublet (ferrous iron in chlorite) and for the Fe^{3+} components in the clay minerals (except the hematite) are similar (within 7 %) in the spectra of the original and the treated samples. Thus, in the first approach the positions and amounts of these components were hardly affected by the dithionite. Upon the treatment the amount of hematite decreased significantly, and simultaneously a second Fe^{2+} doublet appeared, whereas during these treatments the ferric and ferrous ions in the chlorite and other clay minerals were left in undisturbed environments.

The Mössbauer parameters for the new, second ferrous component in the 300 K spectrum are: IS 1.23 mm/s, QS is 1.66 mm/s. These parameters characterise a slightly distorted coordination – distinctly different from those sites present in the original clays.

Summary and Conclusions

Two samples taken from a Boda Claystone drilling core were exposed to reducing and oxidizing treatments, the changes of the Fe^{2+} and Fe^{3+} contents in the minerals were monitored by Mössbauer spectroscopy. Three apparent conclusions can be drawn from the presented studies, as follow.

- Single, separated iron ions were not affercted by the treatments. Neither any evidence of oxidation of the ferrous component in chlorite was observed in the first case, nor the change of proportions of ferric and ferrous components present in the clays upon reductive treatments were found in the second case.

- Effect of reduction was manifested on another constituent, in particular on hematite. In this mineral iron ions are in close vicinity to each other (linked by Fe-O-Fe chains in three dimensional structure), thus the effect of reduction can be more facilitated. However, there was only one case, the treatment with dithionite, which dissolved the hematite. This phase remained in intact state when other reductants were used.

- The third observation is the appearance of a new Fe^{2+} position in the dithionite treated sample. This slurry contained ferrous ions in large concentration – a part of these ions was swelled and incorporated reversely into the clay structure, to a distinctly different coordination than those characterising the original positions of iron in the clay.

For interpreting these results in broader aspects it should be taken into account that the Mössbauer spectroscopy is a bulk method, it is not sensitive particulary for surface processes. Fe^{2+}/Fe^{3+} redox interactions which may be important from the point of view of the transport of various radionuclides are multi-step processes, taking place mostly in the aqueous phase, in the charged (multi)layers attached to the clay. The Mössbauer technique is restricted to detect stages of processes resulting in profound changes in the solid phase. In the present study significant change has taken place only in one instance, in the dithionite treated sample where the Fe^{3+}(in solid hematite) => Fe^{2+}(in solution) => Fe^{2+}(in solid clay) process was demonstrated.

Acknowledgements

References

Árkay P, Balogh K, Demény A, Fórizs I, Nagy G, Máthé Z (2000): Composition, diagenetic and post-diagenetic alterations of a possible radioactive waste repository site: the Boda Albitic Claystone formation. Acta Geologica Hungarica, 43, 351–378.

Cornell R M, Schwertmann U (1996): The Iron Oxides, VCH, Weinheim.

Inzelt G (1999): The Contemporary Theory and Practice of the Electrochemistry, Nemzeti Tankönyvkiadó, Budapest *(in Hungarian)*

Lázár K, Megyeri J, Parneix J-C, Máthé Z, Szarvas T (2009): Diffusion of anionic species ($^{99}TcO_4^-$, $H^{14}CO_3^-$) and HTO in Boda Claystone borecore samples, in: FZKA 7461 4th Annual Workshop Proceedings – FUNMIG, Forschungszentrum Karlsruhe, 199-204.

Lázár K, Máthé Z, Földvári M, Németh T, Mell P (2009): Various stages of oxidation of chlorite as reflected in the Fe^{2+} and Fe^{3+} proportions in the minerals of Boda Claystone, Hyperfine Interactions, 190, 129-133.

Mell P, Megyeri J, Riess L, Máthé Z, Hámos G, Lázár K (2006): Diffusion of Sr, Cs, Co and I in argillaceous rock as studied by radiotracers, Journal of Radioanalitical and Nuclear Chemistry, 268, 411-417.

Szűcs I, Csicsák J, Óvári Á, Kovács L, Nagy Z (2004): Confinement performance of Boda Claystone Formation, Hungary, in: Stability and Buffering Capacity of the Geosphere for the Long-term Isolation of Radioactive Waste, "Clay-Club" Workshop Proceedings, Braunschweig, OECD 2004 NEA No. 5303, 209-224.

Zazzi A, Hirsch T K, Leonova E, Kaikkonen A, Grins J, Annersten H, Edén M (2006): Structural investigation of natural and synthetic chlorite minerals by X-ray diffraction, Mössbauer spectroscopy and solid-state nuclear magnetic resonace, Clays and Clay Minerals, 54, 252-265.

REDOX CHEMISTRY OF SULFATE AND URANIUM IN A PHOSPHOGYPSUM STACK

Fanos Papanicolaou , Stella Antoniou, Ioannis Pashalidis

Chemistry Department, University of Cyprus (Cyprus)

* Corresponding author: pspasch@ucy.ac.cy

Abstract

The present study aims to assess the effect of redox conditions existing within the stack on the stability of phosphogypsum (e.g sulfate reduction) and uranium(VI). Phosphogypsum sampling and in-situ measurements were carried out at a coastal stack in Vasiliko Cyprus, pH, E_H and solubility experiments were performed also in simulated laboratory systems. Generally, in the open stack oxidizing conditions predominate stabilizing sulfur and uranium in their hexavalent oxidation state. On the other hand, after the application of a soil/vegetative cover and in the presence of natural organic matter, anoxic conditions prevail (E_H < -70 mV) resulting in S(VI) and U(VI) reduction to S(-II) and U(IV), respectively.

Introduction

Phosphogypsum is an acidic by-product of the phosphate fertilizer industry, produced during the production of phosphoric acid from phosphate rock. Worldwide, large amounts of phosphogypsum have been produced up to now and it is estimated that if historic trends continue, production will increase to several hundred million metric tonnes annually. However, because of economic restraints (e.g. the price of the land) and pressing environmental issues the development of a safe disposal procedure is necessary. It is primarily the presence of toxic trace elements, as well as the radioactivity of radium (Ra) and uranium (U), which make this material a disposal and storage concern and have restricted its use in agriculture and construction industry (Rutherford et al. (1994); Burnett and Elzerman (2001)). Although, the best option for dealing with the PG problem appears to be the commercial use of this material in the agriculture (e.g. amelioration of acid soils) and construction industry (building/road construction), only a relative small portion of the phosphogypsum produced (14%) is

reprocessed, a significant part is dumped into water bodies (28%) and the main part of the material is accumulated in large sludge ponds and retaining stockpiles (Rutherford et al. (1994)).

Regarding the geochemistry of PG there are several studies on acidic runoff and hazardous material dispersion in the near-field of PG stacks. These studies show that in some situations groundwater pollution under a phosphogypsum stack is possible (Rutherford et al. (1994)). Modelling of the environmental radiochemistry of uranium of Florida phosphogypsum showed that within the stacks uranium exists mainly in the form of complexes with sulphate and phosphate, which are relatively mobile uncharged or negatively charged solution species. However, with increasing pH below the stack precipitation of multi-component solid phases occurs preventing large-scale migration of uranium to the underlying aquifer (Burnett and Elzerman (2001); Lysandrou and Pashalidis (2008)). Among the physicochemical parameters (e.g. pH, E_H, ionic strength, chemical composition), the redox potential (E_H) may significantly affect the chemistry and hence stability and leachability of phosphogypsum, because changes in E_H favour different oxidation states of a chemical species (e.g. sulfate or sulfide; U(VI) or U(IV)) which behave dramatically different with respect to their solubility and mobility in the geosphere. Dramatic changes in E_H within a phoshogypsum stack may occur after application of a vegetative cover on the top of the stack. Generally, an enormous drop in the redox potential takes place due to restricted oxygen diffusion within the stack, organic matter disintegration and proceeding microbial activity, which leads eventually to the reduction of sulfate (S(+VI)) to sulfide (S(-II)) (Luo et al. (2007)).

Recently, a soil/vegetative cover has been applied to an open stack in Cyprus, which has been extensively studied with respect to phosphogypsum characterisation and its radio-environmental impacts. In order to understand the impact of the redox conditions existing within the phosphogypsum stack after application of a soil/vegetative cover it is necessary to investigate the impact of possible changes of the redox potential on redox sensitive chemical species (e.g. sulfate and uranium). This study is focused on the effect of the redox potential at various pH on the redox stability of sulfate and uranium(VI), which are the stable species prior the application of a vegetative cover (oxic conditions). The paper presents experimental data obtained by chemical analysis of field and laboratory systems.

Materials and Methods

Study area and sampling description

The research reported here covers the phosphogypsum stack (about 50 000 m^2) at the Vasilikos site, which is a coastal area in front of a former fertilizer plant in Cyprus. Several observation boreholes have been drilled into the stack (to a maximum depth of 5 meters) and stack solutions were sampled from the boreholes using a submersible pump and filtered in the field immediately after collection. Sample preparation and analysis as well as data of the physico-schemical characterisation of the phospho-gypsum and the stack solution are given elsewhere (Lysandrou and Pashalidis (2008)). Since spring 2008, the stack is covered by 1-meter topsoil and dense vegetative cover, which is going to affect the redox conditions within the stack. Because the cover is

relatively young the effects due to the soil/vegetative cover are observed only close to the soil-phosphogypsum interphase. Therefore, solid material samples were obtained from phosphogypsum adjacent to the topsoil and affected by organic run-offs. The respective samples have in contrast to non-affected phosphogypsum, which is white coloured, pale-brown to dark-brown colour.

Redox Potential Measurements and Calculation

The redox potential in the stack solutions prior vegetative cover has been determined using a previously calibrated platinum E_H electrode. For the anoxic conditions (after application of the vegetative cover) the redox potential (E_H) was calculated based on the S(+VI)/S(-II) redox couple, because the redox measurements "under anoxic conditions" are strongly affect by the presence of oxygen, which enters the systems during borehole drilling and sampling.

Laboratory Experiments

The [S(-II)]/[S(+VI)] ratio in the suboxic material was determined after extraction of the sulfate and sulfide from the solid material by de-ionized water under nitrogen (N_2) atmosphere. The batch leaching procedures were performed in duplicate in 250 ml PE bottles using 20-g sample mixed with 200 ml of the extraction fluid and agitated for two days. The sulfate conentration in solution was determined by ion chromatography, whereas the sulfide concentration by potentiometric titration using sulfide ion selective electrode and a Hg(II) standard solution.

Results and Discussion

In order to assess the redox conditions existing in a phosphogypsum stack before and after the application of a soil/vegetative cover and the impact of the corresponding redox potential on the chemical behaviour of the redox sensitive species playing a key role in the phosphogypsum chemistry e.g. sulfur and uranium, experimental and calculated data are graphically correlated and discussed. Fig. 1 shows a combined E_H - pH diagram of the uranium and sulfur system, including experimental data, which correspond to the Vasiliko phosphogypsum stack and particularly to the sub-area adjacent to the sea. The redox potential data associated with aerobic conditions (open stack) have been determined on site by stack fluid analysis using a platinum electrode, whereas the suboxic data (after application of the soil/vegetative cover) have been obtained indirectly by redox potential calculations based on the S(VI)/S(IV) system according to the following redox semi-reaction Eq. (1) and the corresponding Nernst equation Eq. (2):

$$\frac{1}{8} \cdot SO_4^{2-} + \frac{5}{4} \cdot H^+ + e^- \longleftrightarrow \frac{1}{8} \cdot H_2S + \frac{1}{2} \cdot H_2O \qquad (1)$$
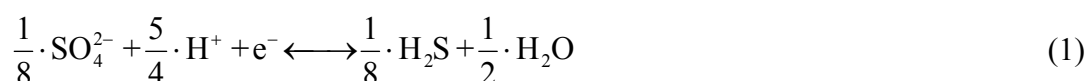
$$E_H = E_H^o - 59.2 \cdot \log\left(\frac{[H_2S]^{1/8}}{[SO_4^{2-}]^{1/8} \cdot [H^+]^{5/4}} \right) \qquad (2)$$

where $E_H{}^o$ is the standard redox potential for the above reaction and equals to 303.5 mV (Sigg (1999)). The concentration data for sulfate and sulfide determined in suboxic systems as well as the corresponding pH values are summarized in Table 1. Calculation of the redox potentials is necessary, because E_H measurements within the suboxic stack are strongly affected by oxygen that diffuses in the phosphogypsum body during borehole drilling and sampling works.
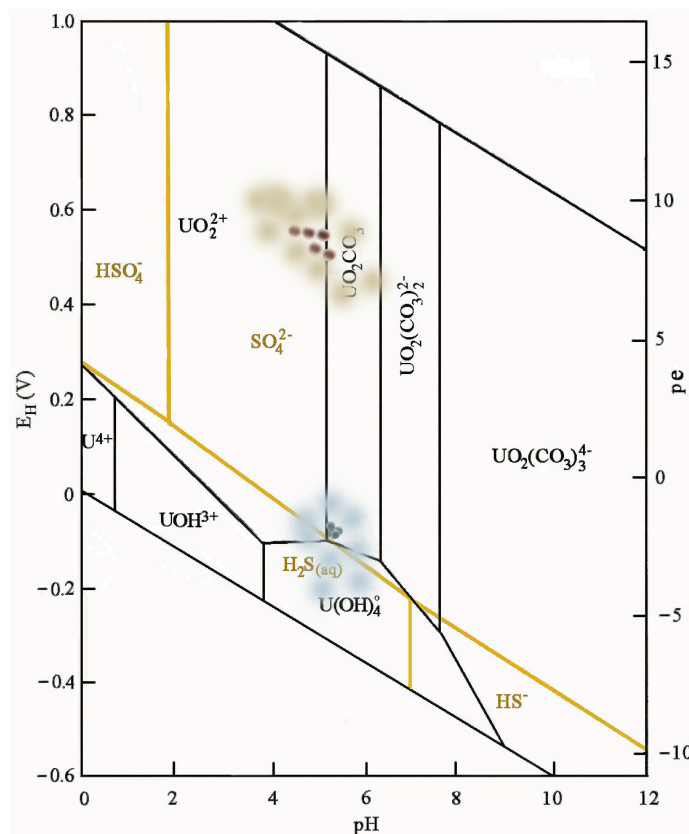
Figure 1: E_H/pH *diagram of the uranium and sulfur system. Dots represent experimental values for the redox potential corresponding to aerobic and suboxic stack conditions*

The redox potential values of the open stack vary between +500 mV and +600 mV, indicating that sulfate and uranium(VI) are the predominant species in solution for sulfur and uranium, respectively. Regarding uranium speciation in the particular pH range, the U(VI) aquo ion and the UO_2CO_3 dominate in solution. The increased redox potential values found in the open stack are attributed to the unrestricted oxygen diffusion within the stack and are in agreement with corresponding literature data (Carbonell-Barrachina, et al. (2002)).

Table 1. Eh values measured in aerobic stack solutions of the Vassiliko phosphogypsum stack and sulfate and sulfide concentration values determined in suboxic phosphogypsum lechates with the corresponding pH values

suboxic system			
pH	$E_{H(calc.)}$	$[H_2S]/(mol/l)$	$[SO_4^{2-}]/(mol/l)$
5.25	-70	0.0007	0.065
5.3	-74	0.0007	0.055
5.35	-76	0.0003	0.049
5.4	-75	0.00008	0.047

aerobic system			
pH	$E_{H(meas.)}$		
4.4	555		
4.7	550		
4.8	515		
5.0	545		
5.2	500		

On the other hand, after application of the soil/vegetative cover, the redox conditions are determined basically by runoffs containing increased natural organic matter, bacterial activity and restricted oxygen diffusion within the stack, resulting in more or less suboxic conditions below the vegetative cover. Because of the restricted oxygen diffusion and the continuous supply of natural organic matter, the redox potential decreases dramatically (down to -95 mV). At such low redox potentials (from -75 mV to – 150 mV) bacterial reduction of sulfate to sulfide begins (Luo et al. (2007); Carbonell-Barrachina, et al. (2002)). Natural organic matter acts as energy source for the bacterially assisted sulfate reaction described by following general equation:

$$SO_4^{2-} + 2 \cdot "CH_2O" \xrightarrow{\text{Bacteria}} 2 \cdot HCO_3^- + H_2S \qquad (3)$$

The consumption of protons during sulfate reduction Eq. (1) results in increased pH values in the corresponding systems. In the studied system the pH increase is about 1 pH unit, indicating the proceeding sulfate reduction. Nevertheless, the redox potential values (-70 mV < E_H < -75 mV) calculated for the studied stack are notably higher than corresponding values (-250 mV) suggested in literature (Carbonell-Barrachina, et al.

(2002)). This could be attributed basically to the fact that the measurements were performed in relatively short time (about one year) after the application of the soil/vegetative cover on the phosphogypsum stack, whereas the redox potential value of -250 mV corresponds to highly anoxic conditions. Nevertheless, in long-term (even in the real system) further decrease of the redox potential values is expected because of the continuous supply of organic matter from the top-soil cover.

Due to the activity of sulfate reducing bacteria uranium(VI) is reduced (Abdelouas et al., 2002; Gu et al., 2005) and U(OH)$_4$ becomes a predominant uranium species in the suboxic stack (Fig. 1). The reduction of U(VI) to U(IV) described by Eq. 4 is favoured under the given conditions, because of the low solubility of the U(OH)$_4$ solid phase (Guillaumont et al., 2003).

$$UO_2^{2+} + 4H^+ + 2e^- \longleftrightarrow U^{4+} + 2H_2O \tag{4}$$
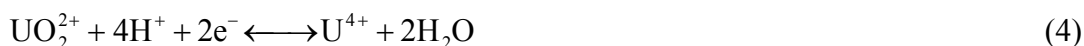
Summary and Conclusions

Experimental and theoretical results obtained from this study lead to the following conclusions: (a) The open phosphogypsum stack is characterized by redox potentials (E_H) about +500 mV whereas after application of a soil/vegetative cover results in E_H below -70 mV due to reduction processes which start upon natural organic matter supply and (b) Sulfur and uranium, which are the redox sensitive elements of particular interest in phosphogypsum, exist in the open stack in the form of SO_4^{2-}, $CaSO_4$ and $NaSO_4^-$, and UO_2^{2+}, UO_2OH^+ and UO_2SO_4 and $UO_2(SO_4)_2^{2-}$, respectively. Under suboxic conditions (covered stack) H_2S, and $U(OH)_4$ and $U(OH)_5^-$ become the predominant species of sulfur and uranium, respectively.

References

Abdelouas A., Lutze W., Gong W., Nuttall E. H., Strietelmeier B. A., Travis B. J. (2000), Biological reduction of uranium in groundwater and subsurface soil, Sci. Total Environ., 250, 21-35.

Burnett, W.C., Elzerman, A.W. (2001), Nuclide migration and the environmental radiochemistry of Florida phosphogypsum. J. Environ. Radioact., 54, 27-51.

Carbonell-Barrachina, A., DeLaune, R.D., Jugsujinda, A. (2002), Phosphogypsum chemistry under highly anoxic conditions, Waste Manage., 22, 657–665.

Gu, B., Wu, W.-M., Ginder-Vogel, M.A., Yan, H., Fields, M.W., Zhou, J., Fendorf, S., Criddle, C.S., Jardine, P.M. (2005), Bioreduction of Uranium in a Contaminated Soil Column, Environ. Sci. Technol., 39, 4841-4847.

Guillaumont R., Fanghänel Th., Fuger J., Grenthe I., Neck V., Palmer D.A., Rand M.H. (2003), Update of the Chemical Thermodynamics of Uranium, Neptunium, Plutonium, Americium, and Technetium, Elsevier, OECD-NEA, Paris, pp. 120-130.

Luo J., Weber F.-A., Cirpka O. A., Wu W.-M., Nyman J. L., Carley J., Jardine P. M., Criddle C. S., Kitanidis P. K. (2007), Modeling in-situ uranium(VI) bioreduction by sulfate-reducing bacteria, J. Contam. Hydrol., 92, 129-148.

Lysandrou M., Pashalidis I. (2008), Uranium chemistry in stack solutions and leachates of phosphogypsum disposed at a coastal area in Cyprus, J. Environ. Radioact., 99, 359-366.

Rutherford, M.J., Dudas, P.M., Samek, R.A. (1994), Environmental impacts of phosphogypsum, Sci. Total Environ., 149, 1-38.

Sigg L. (1999), Redox Potential Measurements in Natural Waters: Significance, Concepts and Problems, in J. Schüring H.D. Schulz W.R. Fischer J. Böttcher W.H.M. Duijnisveld (Eds.), Redox: Fundamentals, Processes and Applications, Springer-Verlag, New York, pp. 1-11.

EFFECT OF MICROORGANISMS ON THE PLUTONIUM OXIDATION STATES

Benedikta Lukšienė[1*], Rūta Druteikienė [1], Dalia Pečiulytė[2], Dalis Baltrūnas [1], Vidmantas Remeikis[1], Algimantas Paškevičius[2]

[1] Institute of Physics (LT)

[2] Nature Research Center (LT)

...

* Corresponding author: bena@ar.fi.lt

Abstract

Microorganisms selected from those detected at the repository in the Ignalina NPP territory were exposed to interaction with ^{239}Pu of concentration of 10^{-12} M in brine solution for 1 h and 24 h at low pH under aerobic laboratory conditions. Application of modified anion exchange chromatography following co-precipitation of reduced plutonium fraction onto neodymium fluoride allowed us to separate Pu(III) and Pu(IV) oxidation states and quantitatively evaluate them using alpha spectrometry. Averaged results of three replicates have shown that bacteria *Bacillus mycoides* and Gram-negative bacteria are able to convert up to 15% of Pu(IV) to Pu(III) in brine, while *Rhodococcus lutesus* can reduce only about 2% of plutonium (IV). Fungi *Paecillomyces* and *Lilacinus Absidia* sp. have practically no effect on the change of plutonium (IV) oxidation state. The evidences obtained in this study are useful for the assessment of radioactive waste disposal safety for the human beings and environmental ecosystems. Microorganisms tested are related to the environs of enhanced radioactivity, therefore it can be assumed that the presence of fungi of the genera *Absidia* and *Paecilomyce*s as well as Gram-positive bacteria (*Bacillus mycoides* and *Rhodococcus lutesus)* and one morphotype of Gram-negative bacterium in the far field of repositories can be possible. The results suggest that bacteria studied in the transport path of Pu(IV) are able to influence plutonium mobility at low pH under aerobic conditions because of a change in plutonium oxidation state, Pu(IV) to Pu(III).

Introduction

Performance assessment requirements include waste characteristics, facility characteristics, disposal procedures, biotic considerations, and environmental factors (Case and Otis, 1988). Radioactive waste disposal facilities must be designed, operated, and eventually closed in a manner that ensures long-term stability and protects the public health and safety. These requirements are to provide the public with reasonable assurances of limited human exposure (Kostelnik, 1991). However, sensitivity analysis of performance commonly devotes insufficient consideration to the relevance of microbial activity, although microbial activity can be attributed to the factors influencing metal/radionuclide spreading and mobility in the environment. Microorganisms because of their interaction with radionuclides affect geochemical processes, in particular radionuclide migration (Keith-Roach (2002), Pedersen (2005), Ehrlich (2006), Fomina and Gadd (2007), Levinskaitė et al. (2009). Interaction of microorganisms with transition metals/redox - active radionuclides is very often linked to a change in their oxidation states. The chemical state of actinides released to the environment, combined with the complexity and diversity of their environmental behavior, creates difficulties in modeling their behavior over the lifetime of their radioactivity (Chopin (2005). Due to a high toxicity and long half-life, fission products ^{239}Pu and ^{240}Pu are among the most important actinides to consider for the safety assessment of radioactive waste disposal. It has been indicated that the stability of the various oxidation states of plutonium has an effect on chemical processing operations, on radioactive waste storage and treatment, and the reactivity and mobility of plutonium in the environment (Lee et al. (2008). The oxidation state of the radionuclide resulting speciation, which describes both the nature and the charge of complexes formed, will influence the migration rate through geomedia (Nitsche et al. (1988). Microbial production of extracellular metabolic products, such as citric acid, and sequestering agents, such as sideropores, can affect plutonium dissolution and then enhance its environmental mobility (Francis (2001), Francis et al.(2007), Neu et al. (2005).

The reliability of different techniques for the determination of Pu oxidation states was tested. The spectrophotometric methods for a quantitative determination of the oxidation states of aqueous Pu are generally effective only at relatively high concentrations (Schramke et al. (1989), Lee et al. (2008). X-ray absorption spectroscopy (XAS) is an established technique for determination of oxidation states and speciation in transition metals and is coming into use to study actinides. The process of extracting speciation information from the XAFS occurs after the X-ray Absorption Near Edge structure (XANES) region was used to determine the average Pu valence (Ervin and Conradson (2002). A simplified model for data collection and evaluation was presented for XANES that has been recently used for the determination of Pu oxidation states at the cross section of a Pu-containing "hot" particle coming from a nuclear weapon test site (Bielewski et al. (2009). For the speciation of the plutonium oxidation states in aqueous solutions, the online coupling of capillary electrophoresis (CE) with ICP-MS has been developed, and improvement of the sensitivity of the CE method due to the offline coupling of CE to resonance ionization mass spectrometry (RIMS) has been explored (Bürger et al. (2007). Consequently, it should be recognized that some of

physical-instrumental methods are applicable to solids and liquids, they require no sample preparation, however, their employment in each institution is limited because of the technique specificity, lack of experience and appropriation-in-aid. Among the speciation technique methods listed *(Ervin and Conradson (2002), Chopin (2005)* the radiochemical trace analysis and Electron Spin Resonance (ESR) are the most advantageous methods to determine plutonium oxidation states because of their sensitivity ($10^{-8} – 10^{-12}$ M) and ($10^{-5} – 10^{-12}$ M), respectively.

The aim of this study was to investigate the ability of microorganisms selected, from those detected in dust samples at the repository in the Ignalina NPP territory, to participate in plutonium redox reactions under aerobic conditions using ion exchange chromatography.

Experimental

Isolation and identification of microorganisms

Microorganisms were isolated from dust collected at low-level radioactive waste repository in the territory of the Ignalina NPP. Bacteria were isolated and characterized using culture identification following a morphological identification, using gram staining reaction and other biochemical tests *(Holt and Bergey (1994)*. Fungi were isolated in malt extract agar (MEA, Liofilchem, Italy) and potato dextrose agar (PDA, Liofilchem, Italy), using dilutions of 10^{-2}, 10^{-3}, and 10^{-4}. Bacteria were isolated on nutrient agar (NA, Liofilchem. Italy), using the dilutions of 10^{-5}, 10^{-6}, 10^{-7}. Isolation and enumeration of actinomycetes were performed by dust dilution plate technique using Starch-casein agar. Nystatin (50 µg ml^{-1}) was added to avoid fungal contamination. Concentration of bacteria viable in dust, actinomycetes and fungi, expressed as colony forming units (CFU) in 1 g either in dust sample, was determined after 2–3, 7–14 and 7 days, respectively. Standard procedures based on colony, spore and structural morphology were followed for identification to a species level *(Gilman (1966)*, *Barnett (1967), Barron (1968), Ellis (1971), Domsch et al. (1980), Kiffer and Morelet (1999), Watanabe (2000).*

Sample preparation

Microorganism cells were collected by centrifugation at 3000 rpm for 5 min and washed thoroughly with 0.08 M brine. Pu(IV) solution of 9.2 10^{-12} M concentration was prepared using ^{239}Pu stock solution purchased from Eckert & Ziegler Isotope Products. Microorganisms (30 mg dry wt. basis) were suspended in 20 ml of 0.08 M Na brine solution with supplement of 9.2 10^{-12} M Pu(IV) solution. All reagents used were of analytical grade and solutions were prepared in deionised water (TKA LAB MICRO system, conductivity 0.055 µS/cm; TOC< 10 ppb).

At the beginning and at the end of the interaction time, solution pH was measured by WTW inoLab pH/Cond 720 using WTW Tetra Con 325 and Schott pH-electrode. Initial solution pH was kept in the range of 2.7-2.9 to reduce the influence of pH on Pu(IV) transformations because Pu(IV) hydrolysis even at pH<1 and the formation of polymeric/colloidal species *(Yun et al. (2007)* are possible. One set of experiments

included shaking of each type of microorganisms for 1 h at room temperature and the other included static microorganism-Pu(IV) interaction for 24 h at room temperature. After the elapsed interaction time, suspensions were centrifuged at 3000 rpm for 5 min. Separated aliquots, both brine solution and microorganism biomass, were prepared for plutonium oxidation state analysis.

Radiochemical oxidation state analysis

At the initial stage of the analysis the lower oxidation states of plutonium (III and IV) were separated from its higher oxidation states (V and VI) by the co-precipitation on neodymium fluoride. ^{242}Pu (III) and ^{242}Pu (IV) were added as yield tracers. The oxidized plutonium fraction retained in solution and the reduced plutonium fraction obtained by dissolution of neodymium fluoride were conditioned for Pu separation. The modified anion exchange method was employed to separate Pu (III) and Pu (IV). As it is known Pu(IV) in HNO$_3$ medium forms anion complexes with NO$_3^-$ and they show strong sorption on an anion exchange resin. Therefore, the basis for separation of Pu(IV) from Pu(III) that cannot form anionic complexes in HNO$_3$ medium relies upon the differences in sorption of these Pu oxidation states onto anion exchange resin. Thus, loading of the 8 mol·L^{-1} solution containing Pu(III) and Pu(IV) analytes onto anion exchange BiO RaD AG 1x8 resin column without valence adjustment forms conditions such that only Pu(IV) should be sorbed. Because of absence of other transuranium elements and complex matrix ingredients in the tested solution the plutonium procedure could be simplified. The steps to remove Am, U and Th by washings with 8 mol·L^{-1} and 9-12 mol·L^{-1} HCl could be omitted. Prior to loading the samples onto anion exchange column, 1 ml of saturated Al(NO$_3$)$_3$ were added to complex the fluoride and inhibit neodymium sorption on the ion exchange column. The sample solution passed through the column with plutonium (III) is loaded onto another BiO RaD AG 1x8 column but in this case valence adjustment to Pu(IV) using oxidation by nitrite is required (*Lukšienė et al. (2006)*. For elution of plutonium sorbed onto resin we used freshly prepared solution of 4mol·L^{-1} HCl with sodium sulfite. Electro-deposition was used to prepare tin layer plutonium sources for alpha spectrometric measurement. Plutonium was electrodeposited in 1 hour under direct 0.6 A/cm^2 current onto a stainless steel disc-electrode in sulphate medium.

Measurement of plutonium analytes

The electrodeposited plutonium analytes were detected using conventional α-spectrometry. The resolution of the subsequent alpha spectra of the employed Octete-Plus (Ortec) spectrometer with detectors of 600 mm^2 square was 25-27 keV at 25% counting efficiency. The counting time, depending on activity , was from 2 to 4 days.

Results and discussion

The microorganism populations isolated from dust onto wooden (WD) and cardboard (CD) surfaces at the low-level repository in the INPP territory demonstrated some differences. Four different bacteria were isolated from the WD sample and one of the morphotypes belonged to Gram⁻ bacterial group. Bacterial community isolated from the CD sample comprised 7 bacterial morphotypes and all of them belonged to Gram⁺ bacteria. Bacterial resistance under unfavorable conditions depends on the Gram⁺ and Gram⁻ characteristics. Dominance of Gram⁺ and spore forming bacteria in the dust suggests their ability to survive under the nutrient limited conditions.

Fungi belonging to the genera of *Absidia, Chrysosporium, Paecilomyces, Penicillium* and *Trichoderma* were isolated from both dust samples. Those fungi are common in soil, air, dust and they are good users of various substrates. Fungi from the genus *Chrysosporium* and one species of *Paecilomyces* genus – *Paecilomyces lilacinus* – dominated in all media plates used for fungus isolation. It can be stated that those fungi dominated in the fungus communities of investigated dust samples.

The dominating fungi of the genera *Absidia* and *Paecilomyce*s (*Absidia* sp. and *Paecilomyces lilacinus*) as well as Gram-positive bacteria (*Bacillus mycoides* and *Rhodococcus lutesus)* and one morphotype of Gram-negative bacterium were selected for the investigation of their capability to participate in the plutonium redox reactions.
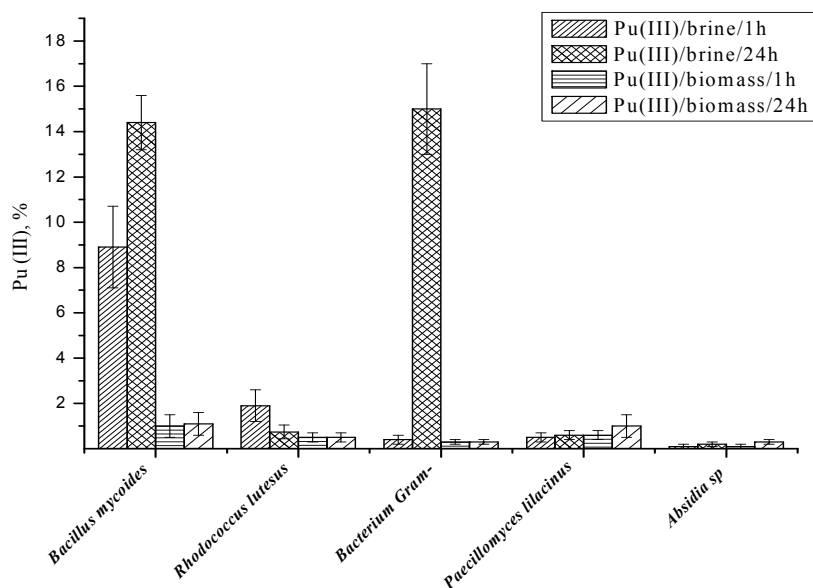
Figure 1: *Distribution of valence (III) plutonium between brine and biomass following interaction of Pu(IV) with fungi and bacteria*

Distribution of reduced Pu(III) between brine and microorganism biomass according to obtained averaged results is presented in Figure.1. The highest amount of reduced

Pu(III) after interaction of Pu(IV) with tested microorganisms was detected in brine solution of studied bacteria. Of all studied microorganisms, the largest part (8.9%) of Pu(IV) oxidation state was reduced during 1 h interaction when bacterium *Bacillus mycoides* in 0.08 mol·L^{-1} Na brine solution at pH 2.7 was affected by Pu(IV). This bacterium increased Pu(III) amount by about 5% after interaction for 24 h. The activity of Gram-negative bacterium differed from that analyzed before, it produced only about 0.4% of Pu(III) during 1 h interaction with Pu(IV) in brine solution whereas during 24 h period production of Pu(III) came up to 15%. Those two bacteria of all studied microorganisms demonstrated the highest capability to reduce Pu(IV) to Pu(III). The detected Pu(III) activity in the system Na brine-fungi *Absidia* sp. was almost at the minimum detectable activity (MDA), thus, practically this fungus has no effect on plutonium (IV) under appropriate conditions used *(Fig.1)*. Analysis of distribution of Pu of (IV) oxidation state showed that the larger amount of this oxidation state was found in liquid phase – Na brine solution at the presence of bacterium *Bacillus mycoides* and one morphotype of Gram-negative bacterium in the system (*Fig.2)*.
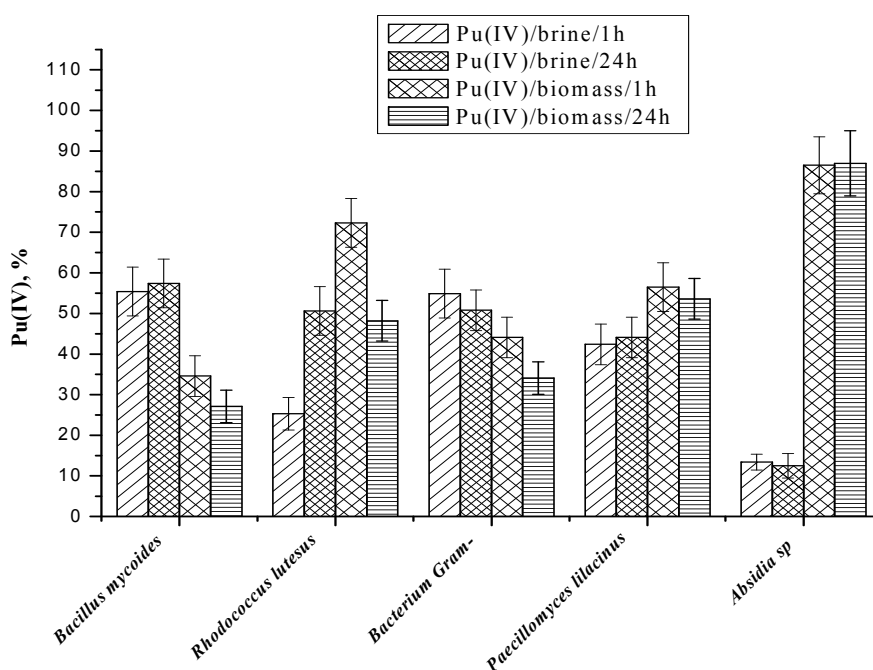
Figure 2: *Distribution of valence (IV) plutonium between brine and biomass following interaction of Pu(IV) with fungi and bacteria*

In the system with microorganisms *Absidia* sp., *Paecilomyces lilacinus* and partly *Rhodococcus lutesus,* the Pu(IV) fraction was mainly found to be distributed onto the solid phase – microorganism biomass. The enhanced amount of both Pu(III) and Pu(IV) fractions *(Figs 1, 2)* in the liquid phase of the Na brine solution - Pu(IV) - bacterium *Bacillus mycoides* or one morphotype of Gram-negative bacterium system referring to (*Neu et al. (2005)* suggests that organic acids that are extruded products of cell metabolism can solubilize plutonium and then enhance its environmental mobility. Also they indicated that bacterial membranes, proteins or redox agents can produce strongly

reducing electrochemical zones and generate molecular Pu(III/IV) species or oxide particles. On the other hand, plutonium (IV) that was bound to microorganism biomass in our experiments could interact with bacterial cellular and extracellular structures that contain metal-binding groups. Thus, the results of investigations have indicated that bacterial activity can result in different chemical species of Pu. The different Pu chemical species show differences in soil-soil solution-water partitioning and dynamics in the environment. Therefore, the models used in the sensitivity analysis of performance should consider the different chemical plutonium species as well as their biogeochemical behaviour due to the microbial activity.

Summary and Conclusions

The effect of microbial activity on plutonium oxidation states was investigated under laboratory conditions. The tested ternary systems consisted of 0.08 mol·L^{-1} sodium brine solution, Pu(IV) and appropriate microorganism in the pH range of 2.7-2.9 under aerobic conditions. Of the microorganisms detected in dust samples at the low-level radioactive waste repository in the Ignalina NPP, the fungi *Absidia* sp. and *Paecilomyces lilacinus* as well as Gram-positive bacteria (*Bacillus mycoides* and *Rhodococcus lutesus)* and one morphotype of Gram-negative bacterium were selected for the investigation of their capability to participate in the plutonium redox reactions. The results of the investigations showed usefulness of the modified anion exchange method for the plutonium oxidation state determination in the range of 10^{-12} M concentration of plutonium.

In conclusion, the following results are emphasized. The highest effect in a change of Pu(IV) to Pu(III) at low pH under aerobic conditions was demonstrated by bacteria *Bacillus mycoides* and one morphotype of Gram-negative bacterium. The amount of reduced plutonium (III) in brine solution came up to 15%. The microbial activity effect on the plutonium oxidation state (IV) conversion to Pu(III) can be attributed to the mechanism that depends on bacterial exudates because of the presence of reduced plutonium in liquid phase of the experimental system. Tested fungi *Absidia* sp. and *Paecilomyces lilacinus* practically showed no influence on the redox process in the used experimental system under aerobic conditions.

Acknowledgement

References

Barron GL. (1968). The Genera of Hyphomycetes from the Soil. Baltimore: The Williams & Wilkins Co.

Barnet H. L. (1967). Illustrated Genera of Imperfect Fungi. Princeton: Princeton University Press.

Bielewski M., Eriksson E.M., Himbert E.J., Betti E.M., Belloni E.F., Falkenberg E.G. (2009). Fast method of XANES data collection suitable for oxidation state mapping. J. of Radioanalytical and Nuclear Chemistry, 282, 355-359.

Bürger S., Banik N.L., Buda R.A., Kratz J.W., Kuczewski B., Trautmann N. (2007). Speciation of the oxidation states of plutonium in aqueous solutions by UV/Vis spectroscopy, CE-ICP-MS and CE-RIMS. Radiochimica Acta, 95, 8, 433-438.

Case M.J., Otis M.D. (1988). Guidelines for Radiological Performance Assessment of DOE Low-Level Radioactive Waste Disposal Sites, DOE/LLW42T, U.S. Department of Energy

Choppin G.R. (2005). Actinide Science: Fundamental and Environmental Aspects. Journal of Nuclear and Radiochemical Sciences, 6, 1, 1-5.

Domsch K. A., Gams W., Andesrson T. H. (1980). Compendium of Soil Fungi (Vol. I, II, III), London: Academic press

Ellis M.B. (1971). Dematiaceous Hyphomycetes. Kew, Surrey, Englad: Commonqwealth mycological Institute. Reprinted,by Aberystwyth, Dyfed, U.K.: Cambrian Printers. 608 p.

Ehrlich H.L. (2006): Geomicrobiology: relative roles of bacteria and fungi as geomicrobial agents – Fungi in Biogeochemical Cycles, (ed. Gadd G.M.), Cambridge University press.

Ervin, P.F., Conradson, S.D. (2002). Plutonium contamination valence states determination using X-RAY absorption fine structure permits concrete recycling. WM'02 Conference, February 24-28, 2002, Tuscon, AZ, 1-7.

Fomina M., Gadd G.M. (2007): Transformation of Metals and Minerals by Microorganisms. Journal of Basic Microbiology, 36(4), 269-282.

Francis A.J. (2001). Microbial transformations of plutonium and implications for its mobility. Radioactivity in the Environment, 1, 201-219.

Francis A.J., Dodge C.J., Ohnuki T. (2007). Microbial transformations of plutonium. Journal of Nuclear and Radiochemical Sciences, 8, 2, 121-126.

Gilman L.C. (1966). A Manual of Soil Fungi, Ames, Iwona: The Iwona State University Press.

Holt J.C., Bergey D.H. (1994). *Bergey's manual of determinative bacteriology* (9th ed.). Baltimore: Williams & Wilkins.

Yun J.-I., Cho H.-R., Neck V., Altmaier M., Seibert A., Marquardt C..M., Walther C., Fanghänel, Th. (2007). Investigation of the hydrolysis of plutonium (IV) by a combination of spectroscopy and redox potential measurements. Radiochimica. Acta 95, 89-95.

Keith-Roach M.J. (2002): Interactions of microorganisms with radionuclides – Radioactivity in the environment, 2, Elsevier: London

Kiffer E., Morelet M., (1999). The Deuteromycetes. Mitosporic Fungi. Classification and generic keys. USA: Science Publishers Inc., 273 p.

Kostelnik K.M. (1991). National Low-Level waste management program, MEA, EGGLLW-8843

Lee M.H., Kim J.Y., Kim W.H., Jung E.C., Jee K.Y. (2008). Investigation of the oxidation states of Pu isotopes in a hydrochloric acid solution. Applied Radiation and Isotopes, 66, 1975-1979.

Levinskaitė L.,Smirnov A., Lukšienė B., Druteikienė R., Remeikis V., Baltrūnas D. A. (2009). Pu(IV) and Fe(III) accumulation ability of heavy metal-tolerant soil fungi. Nukleonika, 54, 4, 285-290.

Lukšienė B., Druteikienė R., Gvozdaitė R., Gudelis A. (2006). Comparative analysis of ^{239,240}Pu, ^{137}Cs, ^{210}Pb and ^{40}K spatial distributions in top soil layer at the Baltic coast. J. of Environmental Radioactivity,.87, 3, 305-314.

Neu M.P., Icopini G.A., Boukhalfa H. (2005). Plutonium speciation affected by environmental bacteria. Radiochimica Acta, 93, 11, 705-714.

Nitsche H., Lee S.C., Gatti R.C. (1988). Determination of plutonium oxidation states at trace levels pertinent to nuclear waste disposal. Journal of Radioanalytical and Nuclear Chemistry, Articles, 124, 1, 171-185.

Pedersen K. (2005). Microorganisms and their influence on radionuclide migration in igneous rock environments. Journal of Nuclear and Radiochemical Sciences, 6(1),11-15.

Schramke J.A., Rai D., Fulton R.W., Choppin G.R. (1989). Determination of aqueous plutonium oxidation states by solvent extraction. J. of Radioanalytical and Nuclear Chemistry, Articles, 130, 2, 333-346.

Watanabe T. (2000). Pictorial atlas of soil and seed fungi: morphologies of cultural fungi and key to species. 2nd Edition. Boca Raton, London, New York, Washington, D.C: CRC Press.486 p.

DISTRIBUTION OF REDOX ELEMENTS AND SPECIATION-SOLUBILITY RESULTS AS A FIRST APPROACH TO THE GENERAL CHARACTERISATION OF THE REDOX SYSTEMS IN THE SWEDISH CANDIDATE SITES FOR DEEP DISPOSAL OF NUCLEAR WASTE

María J. Gimeno, [1*], Luis F. Auqué [1], Patricia Acero[1], Javier B. Gómez[1], M. Pilar Asta[1]

[1] GMG, Geochemical Modelling Group, Earth Sciences Department, Faculty of Science, University of Zaragoza, Pedro Cerbuna 12, 50009 Zaragoza (Spain)

* María J. Gimeno: mjgimeno@unizar.es

Abstract

Two sites in Sweden are being characterised within the framework of the Site Descriptive Modelling as possible candidates for hosting the proposed repository for the storage of spent nuclear fuel: Forsmark and Laxemar-Simpevarp, in the eastern coast of Sweden. This study presents the main results concerning the distribution of redox elements in groundwaters and interpret them in combination with the results from speciation-solubility and redox couples calculations in order to provide a first approach to the redox processes controlling some of the important hydrogeochemical parameters in the Swedish candidate sites. The obtained results indicate that there are not clear evolution trends with depth either for the dissolved contents of redox-sensitive elements or for the potentiometrically measured or calculated Eh values. However, the existence of very reducing conditions already in the recharge waters with very short residence time has been proven indicating an efficient redox-buffering ability of microbial and water-rock interaction processes. Moreover, at depth and in longer residence time groundwaters the main redox-controlling processes in both groundwater systems are related to the coupling between iron and sulphur systems.

Future work focussed on the integration of these results with the rest available data (mineralogical and microbial data) will allow producing an integrated conceptual model for these systems and identifying the associated uncertainties.

Introduction

Before a repository for the storage of spent nuclear fuel can be constructed or even before the candidate site can be definitively chosen, it is of paramount importance to characterize the host rock and the groundwater system in order to guarantee that, even in the event of a massive failure of the engineering barriers, the geologic environment of the repository would keep the spent fuel isolated from the surface environment.

From the hydrochemical point of view, one of the main concerns is related to the fact that, for many of the elements present in the different parts of the repository and its surroundings, their behaviour is critically determined by the redox processes and features of the storage system. Therefore, understanding the redox system is one of the most fundamental safety requirements since reducing conditions will assure that radionuclides are not transported to the biosphere in the event of canister failure and leakage (Laaksojarhu *et al.*, 2008). Unfortunately, redox systems are among the most complicated items in hydrogeochemistry. Therefore, the only way to deal with their enormous complexity is to know, understand and interpret all the information related to them (hydrochemical, mineralogical and microbiological) as a whole.

In line with this perspective and within the framework of the SKB site hydrogeochemistry programme, this study presents a first approach to the characterisation of the present undisturbed hydrogeochemical conditions in the deep geological environment considered for potentially hosting a spent fuel repository, based on the results obtained from the redox elements distribution in groundwaters, speciation-solubility calculations, and redox pair calculations (combined with the potentiometric Eh measurements). This is a first step for obtaining a general conceptual model for the system as a basis for predicting future changes.

General description of the two Swedish candidate sites

The general description of the Swedish candidate sites in crystalline rocks (Forsmark and Laxemar-Simpevarp) for the underground deep disposal of spent nuclear fuel has been extensively provided elsewhere (Laaksoharju *et al.*, 2008; Acero *et al.*, 2010) and a brief summary was already presented as an S+T contribution last year (Gimeno *et al.*, 2009a).

Hydrogeochemical characterisation of the sites and data selection

The present hydrochemistry of groundwaters in these sites is the result of a complex mixing process driven by the input of different recharge waters at least since the last glaciation. As a general trend, in both Forsmark and Laxemar-Simpevarp, there is a more or less clear trend towards more saline waters with depth from the shallowest and more dilute groundwaters to intermediate brackish groundwaters and finally to the deepest and more saline (Laaksoharju *et al.*, 2008). For both Laxemar-Simpevarp and Forsmark groundwaters, pH values range between 7.2 and 8.6 and the redox conditions are clearly reducing (Eh generally below -150 mV for both sites).

For the explorative analysis and modelling of the redox systems in Forsmark and Laxemar-Simpevarp, two types of data are considered in this work: 1) selected hydrochemical groundwater data from packed sections of core-drilled boreholes covering a wide range of depths and representative of the different hydrochemical conditions and 2) potentiometrically-measured Eh by using the sophisticated methodology developed by SKB (already presented in Auqué *et al*, 2008 and Gimeno *et al.*, 2009a, among others). The measurement and selection of both types of data and the procedures for ensuring their quality and representativity are a major concern and have already been presented elsewhere (Gimeno *et al.*, 2009b and references therein).

Results and discussion

Distribution of redox-sensitive elements and potential solubility controls

The redox-sensitive elements considered in the studied systems are mainly iron, sulphur, manganese and nitrogen. The evolution trends of their dissolved contents with depth are presented in the following subsections in combination with the results of speciation-solubility calculations (with PHREEQC code and a modified version of the WATEQ4F database; Parkhurst and Appelo, 1999, Ball and Nordstrom, 2001, Gimeno et al., 2009b) aimed at identifying some of the effective precipitation/dissolution processes in the studied systems. Dissolved CH_4 (g) and H_2 (g) distribution have also been analysed but they are not presented here due to the scarcity of available data (methane, however, will be used in the redox-pairs calculations).

Iron and sulphur systems

As will be seen below, the general redox features observed in both studied systems seem to be determined by the influence of the geochemical processes affecting the mineral phases or dissolved species of iron and sulphur. Therefore, the behaviour and evolution of dissolved Fe(II) and S(-II) are treated together here. In the groundwaters of Laxemar-Simpevarp and Forsmark, Fe(II) shows a rough decreasing trend from the surface down to 700 m (Figure 1a). Below that depth, the values are generally lower than 0.2 mg/L, reaching only occasionally values of about 1 mg/L in Forsmark.

With regard to the evolution of dissolved S(-II) contents with depth (Figure 1b), there are no clear trends either in Laxemar-Simpevarp or in Forsmark. S(-II) contents are mostly below 0.5 mg/L and in many cases below the detection limit. However, there are locally significant amounts of sulphide down to 700 or even 900 m depth (for both, Forsmark and Laxemar-Simpevarp), with maximum dissolved concentrations of 2.5 mg/L (at 700 m depth in Laxemar-Simpevarp). Due to the importance of this parameter, a very thorough monitoring program is being developed in the two sites for the last two years and the sulphide evolutions is being studied in detail.
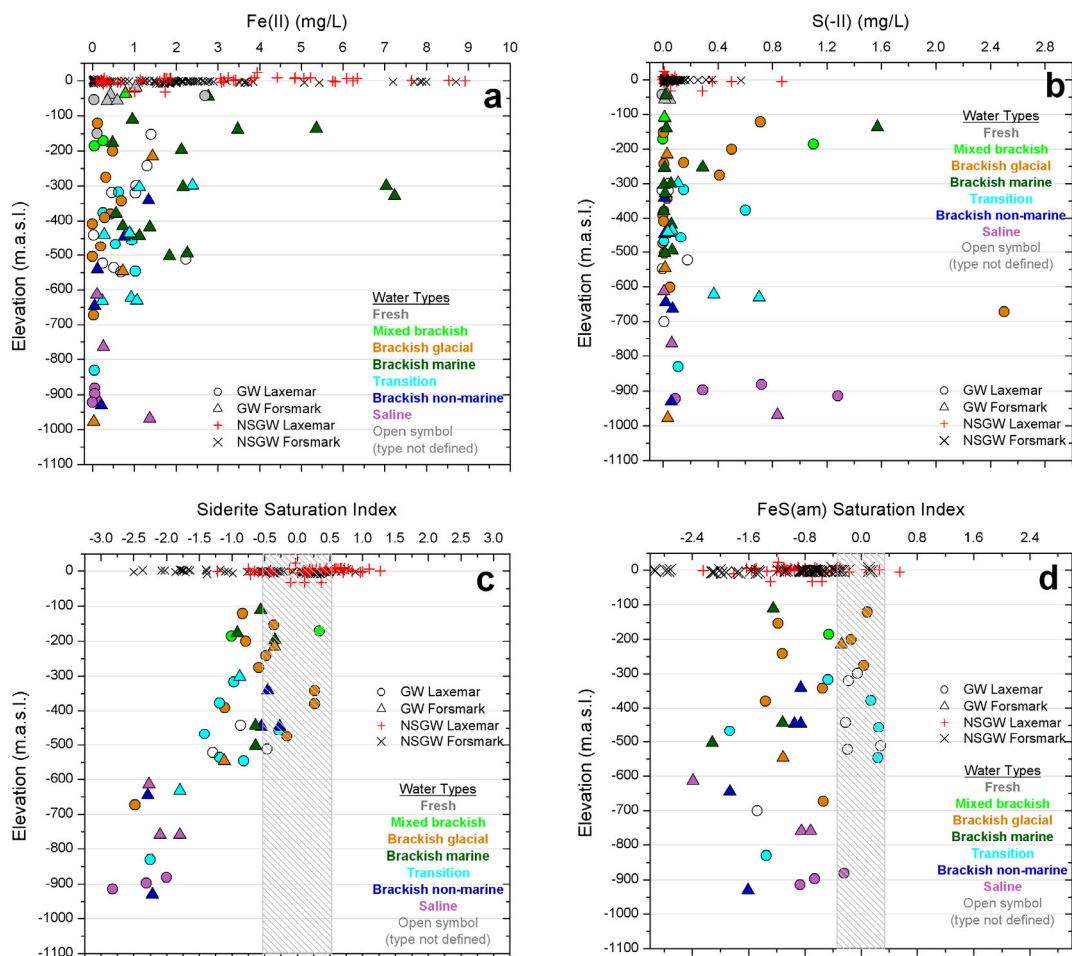
Figure 1. *Dissolved Fe(II) (a) and S(-II) (b) distribution with respect to depth and calculated saturation state of waters with respect to siderite (c) and "amorphous" FeS (d) in the Forsmark (triangles) and Laxemar-Simpevarp (circles) groundwaters. The color code used in this and the following figures is based on the water-types definition reported in Laaksoharju et al. (2009). The dashed areas in panels c and d indicate the uncertainty range for equilibrium situations.*

Speciation-solubility calculations show that the near surface groundwaters (NSGW in the plots) reach equilibrium or oversaturation states with respect to siderite ($FeCO_3$; Figure 1c) suggesting the effective precipitation of this mineral and its involvement in the control of dissolved Fe(II). However, siderite saturation indices decrease in the deep groundwaters with increasing depth and chloride contents, which indicates that this phase is not playing a controlling role on dissolved Fe(II) concentrations in this part of the system. Most of the near surface groundwaters with dissolved sulphide contents greater than 0.04 mg/L, are in equilibrium with respect to "amorphous" FeS (Figure 1d). This equilibrium situation can also be observed down to 600 m depth in many samples but it appears to be less frequent at greater depths. The equilibrium with respect to the amorphous and metastable iron monosulphides found in these groundwaters suggests a continuous and present supply of H_2S produced by Sulphate-Reducing Bacteria activity combined with the presence of an iron source.

Manganese system

The distribution of dissolved Mn concentrations with depth (Figure 2a) shows, in both sites, a similar pattern to that of dissolved Fe(II) also showing variable and high contents down to 600 m depth and very low to undetectable values at greater depths (<0.25 mg/L Mn). This suggests a "simultaneous" control of the dissolved concentrations of both elements by iron phases with traces of manganese (oxyhydroxides, clays) or by surface processes between dissolved manganese and these minerals.

However, there exists an additional control in the Mn contents as the highest values are associated with brackish groundwaters with an important marine signature. Mn contents (as well as other components such as SO_4^{2-}, Mg, SiO_2, HCO_3^-, NH_4^+, etc.) reach high values in the intruding marine waters (Littorina stage; see Gimeno *et al.*, 2008). In spite of the water-rock interaction and mixing processes of these intruding marine waters with the pre-existing groundwaters at depth, some of the resultant brackish marine groundwaters (with chloride about 5,500 mg/L; Figures 2c and 2d) still show this marine inheritance with variable and high concentrations of these components.

For the manganese system, the only mineral that reaches equilibrium in some of the studied groundwaters (the shallowest ones and those deeper but with the highest marine contribution) is rhodochrosite ($MnCO_3$), although saturation indices with respect to this mineral generally decrease towards clear undersaturation with depth (Figure 2b).

Nitrogen system

The observed evolution in the two studied sites shows the general depletion of nitrogen species usually observed in anoxic groundwater systems as residence time and/or depth increase (not shown). Thus, the higher contents and variability of NO_2^-, NO_3^- and NH_4^+ are associated with the shallowest groundwaters in the overburden, where the oxic/anoxic transition appears to occur. However, already in the shallow groundwaters with a meteoric origin, the low levels found for nitrate and nitrite indicate the presence of reducing conditions suggesting the development of an anoxic environment very soon after groundwater infiltration. Only NH_4^+ shows high and variable contents in deep groundwaters with clear marine influence also seen in other elements (Figure 2d).
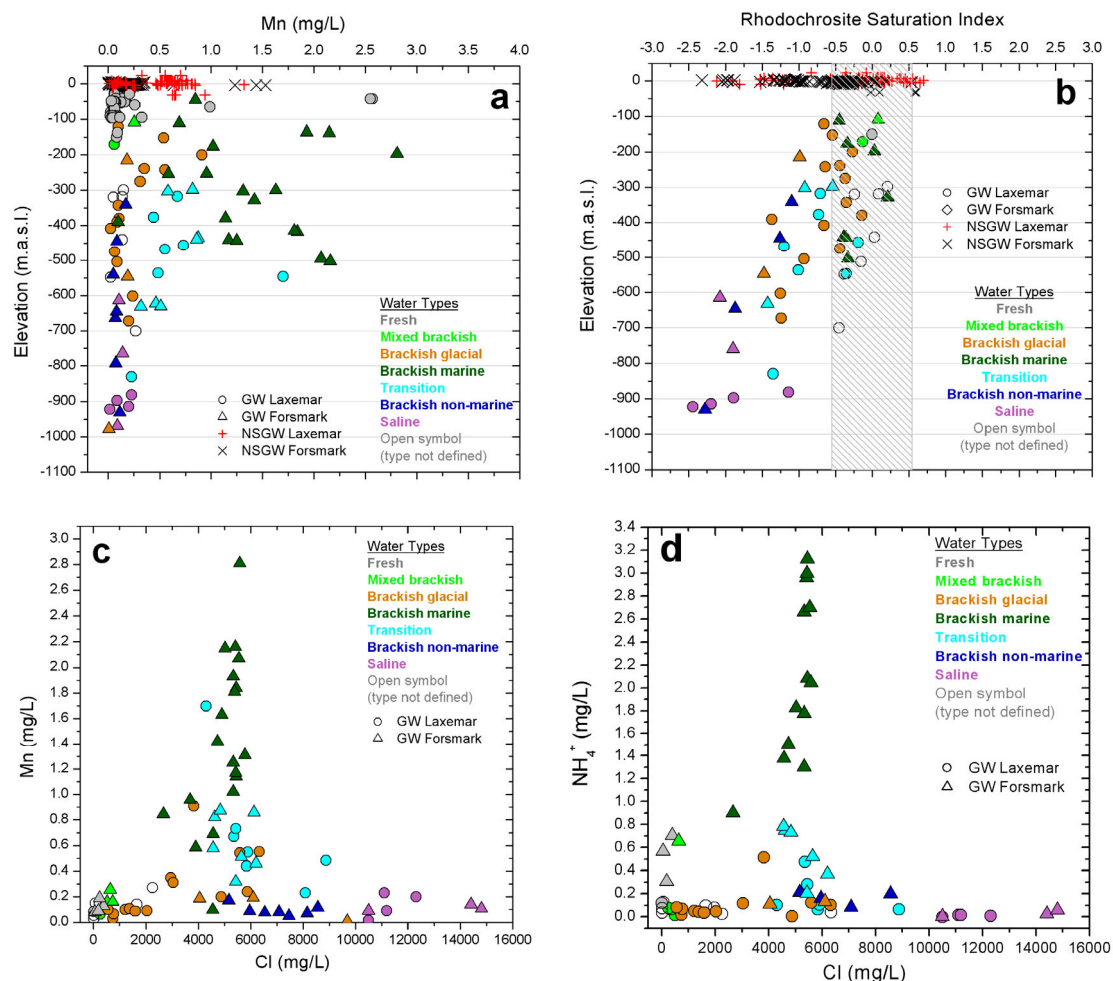
Figure 2. *Dissolved manganese (a) and calculated rhodochrosite saturation index (b) distribution with depth in the Forsmark (triangles) and Laxemar-Simpevarp (circles) groundwaters. Plots c and d show the Mn (c) and NH$_4^+$ (d) distribution with respect to chloride content.*

Eh calculations using redox pairs

As already said, all the Eh values measured in both studied sites correspond to a clearly reducing zone (−143 to −281 mV in Forsmark and -210 to -310 mV in Laxemar-Simpevarp) even for the fresh groundwater samples located in the shallowest parts of the systems, where possible perturbations of the original redox environment may have taken place during drilling and sampling activities. This would indicate an efficient redox-buffering ability of microbial and water-rock interaction processes. Moreover, most of the measured Eh values are in the range for groundwaters buffered by sulphate-reduction (Gimeno *et al.*, 2009a,b).

The distribution of Eh with depth in these waters does not show any evident trend. This behavior could be the result of a modification in the original redox state in some groundwaters (perturbation of the system). But, most probably, it can be the consequence of the complex hydrological setting and palaeohydrogeological evolution of the Forsmark and Laxemar-Simpevarp areas, where the redox-sensitive elements and

the potentials calculated from redox couples do not show a clear trend with depth either, as will be explained below.

As also described in similar systems elsewhere in the Scandinavian Shield (see Gimeno *et al.*, 2008, 2009b and references therein), the calculated redox pairs that have performed better among the many considered for Laxemar-Simpevarp and Forsmark have been the dissolved SO_4^{2-}/HS^- and CO_2/CH_4 redox pairs, and the heterogeneous couples $Fe^{2+}/Fe(OH)_3$, $HS^-/S_{(c)}$, SO_4^{2-}/FeS_{am} and $SO_4^{2-}/$ pyrite. The calculated potential for most of these pairs usually agree within a range of $\pm$ 50 mV with the potentiometrically measured Eh values (Figure 3), except for HS^-/S_c which systematically provides higher potential values (Gimeno *et al.*, 2009b) and they do not show any clear trend with depth.

$Fe^{2+}/Fe(OH)_3$ is completely reasonable as ferric oxyhydroxides (mainly hematite) have been found in the fracture fillings and it is an electroactive pair for potentiometric measurements. The calculated Eh values are generally within the range of values obtained by assuming a clearly crystalline iron oxyhydroxide (similar to goethite or hematite; Figure 3a, where the equilibrium constant proposed by Grenthe *et al.*, 1992 has been used) and assuming a low-crystallinity iron oxyhydroxide (Figure 3b, where the constant value proposed by Banwart, 1999 is used). This situation is consistent with the expected features in these clearly reducing systems, characterised by the presence of crystalline ferric oxyhydroxides under pristine conditions and long-residence time groundwaters but perturbed during the brief oxygen intrusions associated to drilling and sampling activities, which would lead to the precipitation of poorly crystalline ferric oxyhydroxides.

On the other hand, the presence of dissolved sulphide and sulphate reducing bacteria, as well as the existence of equilibrium situations with respect to amorphous ferrous iron monosulphides in the studied waters, suggest the presence of clearly sulphidic environments, consistently with the good performance of the sulphur redox couples (Figures 3c,d,e). Finally, the potentials of the redox pair CO_2/CH_4 are very similar to those obtained from the sulphur couples (Figure 3f). The surprisingly good agreement between the redox potential obtained with these two sets of non-electroactive redox pairs (sulphur and methane) and the potentiometrically measured Eh should be further studied.

Summary and Conclusions

Even though the distribution of redox parameters (mainly Eh measurements and dissolved contents of redox-sensitive elements) does not show any evident trend with depth, the existence of very reducing conditions already in the recharge waters with very short residence time has been proven indicating an efficient redox-buffering ability of microbial and water-rock interaction processes.
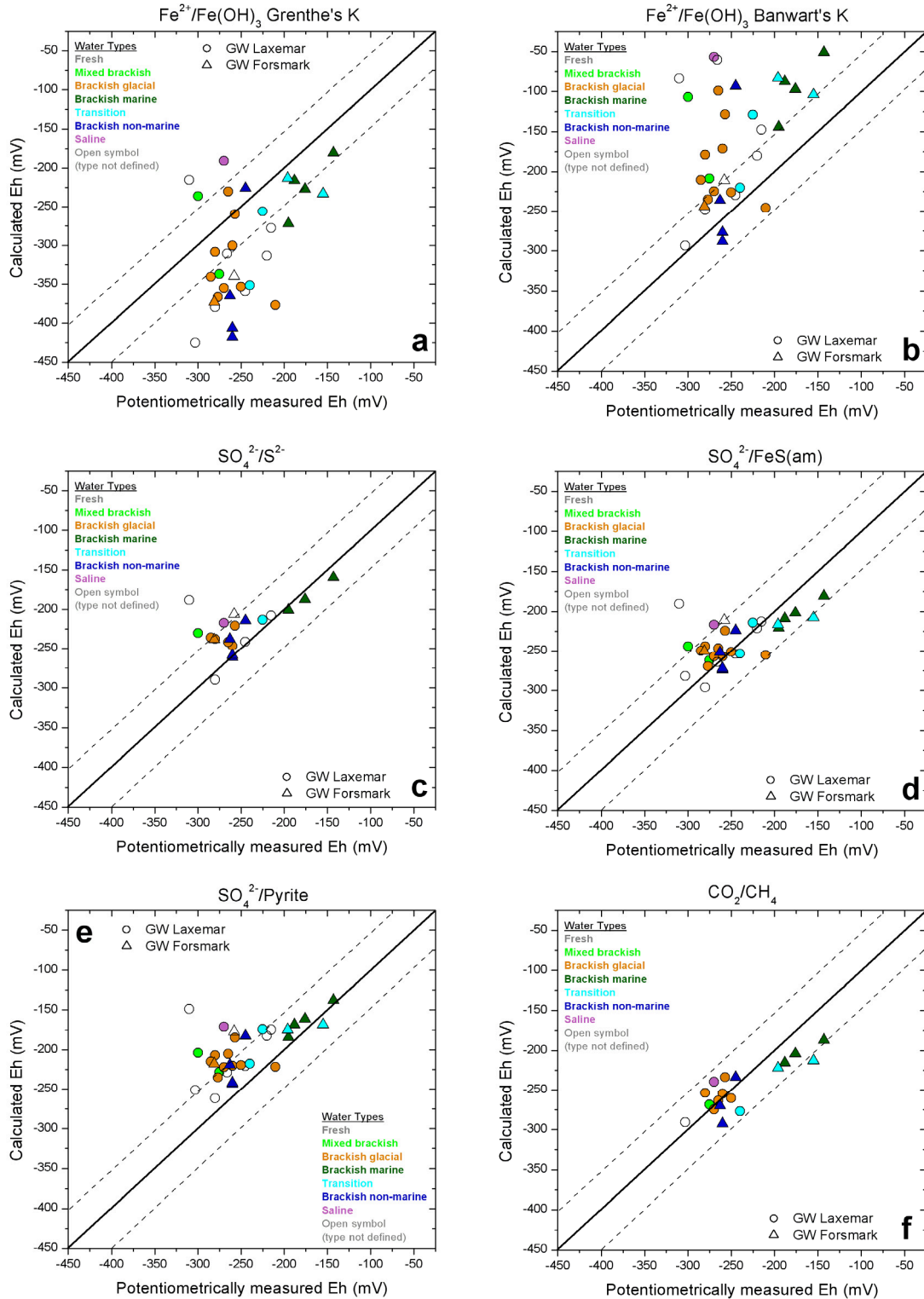
Figure 3. *Comparison of the Eh values potentiometrically measured and the Eh values calculated with different redox couples. (a) and (b) Fe^{2+}/Fe(OH)$_3$ using the equilibrium constants defined by Grenthe et al. (1992) and Banwart (1999), respectively; (c) SO$_4^{2-}$/HS$^-$; (d) SO$_4^{2-}$/FeS(am); (e) SO$_4^{2-}$/Pyrite; and (e) CO$_2$/CH$_4$. The dashed lines indicate the precision of Eh measurements around ±50 mV.*

The combined interpretation of all the available data and calculations points towards the probable existence of presently active processes of stable bacterial sulphate reduction. This is supported by the potential presence (according to speciation-solubility calculations) of metastable amorphous iron monosulphides not yet recrystallised to ordered or crystalline mackinawite or pyrite.

The existence of equilibrium situations with respect to ferrous iron monosulphides indicates the permanent supply of dissolved Fe(II), without which the concentrations of dissolved sulphide in the groundwaters would not be solubility-limited and could reach much higher values. This interpretation has important implications for performance assessment, since high sulphide concentrations are known to affect very negatively to the safety of canisters owing to corrosion processes. All these results would support the presence of clearly sulphidic environments, consistently with the good performance of the sulphur redox couples.

Acknowledgement

References

Acero, P, Auqué, LF, Gimeno, MJ and Gómez, JB (2010). Evaluation of mineral precipitation potential in a spent nuclear fuel repository. *Environmental Earth Sciences*, **59**; 1613-1628.

Auque LF, Gimeno MJ, Gomez J and Nilsson A-C (2008): Potentiometrically measured Eh in groundwaters from the Scandinavian Shield. *Applied Geochemistry*, **23**, 1820-1833.

Ball JW and Nordstrom DK (2001): *User's manual for WATEQ4F, with revised thermodynamic data base and test cases for calculating speciation of major, trace, and redox elements in natural waters*. U.S. Geological Survey, Open File Report 91-183, USA.

Banwart SA (1999): Reduction of iron (III) minerals by natural organic matter in groundwater. *Geochim. Cosmochim. Acta*, **63**, 2919-2928.

Gimeno MJ, Auqué LF, Gómez J and Acero P (2008): *Water-rock interaction modelling and uncertainties of mixing modelling*. SDM-Site Forsmark. SKB-R-08-86, 212 pp. Svensk Kärnbränslehantering AB, Stockholm, Sweden.

Gimeno MJ, Auqué LF, Gómez J, Acero P and Laaksoharju, M. (2009a): *General characterisation of the redox systems in the Swedish candidate sites for deep disposal of nuclear waste*. 1st. Annual Workshop Proceedings 7th EC FP - ReCosy CP, Barcelona 10th – 12th February 2009. pp. 49-58.

Gimeno MJ, Auqué LF, Gómez J and Acero P (2009b): *Water-rock interaction modelling and uncertainties of mixing modelling*. SDM-Site Laxemar. SKB-R-08-110, Svensk Kärnbränslehantering AB, Stockholm, Sweden.

Grenthe I, Stumm W, Laaksoharju M, Nilsson A-C and Wikberg P (1992): Redox potentials and redox reactions in deep groundwater systems. *Chemical Geology,* **98***, 131-150.

Laaksoharju M, Smellie J, Tullborg E-L, Gimeno M, Molinero J, Gurban I, Hallbeck L (2008): Hydrogeochemical evaluation and modelling performed within the Swedish site investigation programme. *Applied Geochemistry*, **23**, 1761-1795.

Laaksoharju M, Smellie J, Tullborg E-L, Wallin B, Drake H, Gascoyne M, Gimeno M, Gurban I, Hallbeck L, Molinero J, Nilsson A-C, Waber N (2009): *Bedrock hydrogeochemistry Laxemar. Site descriptive modelling SDM-Site Laxemar.* SKB R-08-93, 201 pp. Svensk Kärnbränslehantering AB, Stockholm, Sweden.

Parkhurst DL and Appelo CAJ (1999): User's guide to PHREEQC (Version 2), a computer program for speciation, batch reaction, one dimensional transport, and inverse geochemical calculations. (Science Report WRRIR 99-4259), USGS, 312 p.

STUDY OF REDOX-STATE OF U ACCUMULATED ON FRACTURE SURFACES

Juhani Suksi[*] and Susanna Salminen

University of Helsinki, Department of Chemistry, Laboratory of Radiochemistry (FIN)

* Corresponding author: juhani.suksi@helsinki.fi

Abstract

Accumulation of U on the fracture surface can take place through adsorption, specific sorption, co-precipitation and reduction. Recent mobilisation and accumulation events of U can be shown by the U series disequilibrium measurements which help to find sample material to study U accumulation in more detail. Since U is transported mainly as U(VI) the role of U(VI) reduction to U(IV) in U accumulation could be studied by analysing U oxidation states. In the ongoing work we have studied U occurrence on fracture surfaces in the groundwater infiltration area at Olkiluoto to find marks from recent U movement. We found that U has both mobilised from and deposited on fracture surface. The finding is in good agreement with the groundwater conditions in the area. Parallel to U series study we have developed the HCl extraction method to be used for studying U oxidation states. The function of the HCl extraction method in dissolving U(IV) and U(VI) was studied with a uraninite and brannerite containing rock. We found that HCl extraction dissolves all U(VI) and a large part of U(IV) from the rock. It was also found that iron dissolved during the extraction can affect the redox-state of U. Until now we have not observed U oxidation during the extraction but we have observed U reduction. It seems that extraction time is in key position in developing the method. Further experiments are in progress.

Introduction

Uranium as a redox-active element is susceptible to groundwater conditions. This can be seen if one examines U series nuclides on fracture surfaces. Depending on groundwater conditions U can either liberate from fracture surface or deposit on it. In

both cases characteristic U series disequilibrium is formed. Disequilibrium develops if U isotopes move relative to thorium which is immobile. U liberation from rock can be seen as ^{230}Th/^{238}U radioactivity ratio above unity. In the recent U deposition, i.e. when U has deposited in the time scale relative to the half-live of ^{230}Th (75.2 ky) the ^{230}Th/^{238}U radioactivity ratio should be lower than one. In radioactive equilibrium the radioactivity ratio is unity, i.e. U mobilisation has not occurred during the last 300000 years. Of course, the determination of the equilibration time depends on how accurately nuclide concentrations can be determined. As a rule of thumb one can say that the larger the deviation from the radioactivity ratio unity the more recent is the U movement event. U series disequilibrium methodology is well documented in the literature and scientific basis of the methods with numerous applications can be found *e.g.* in Osmond et al. (1983) and Ivanovich and Harmon (1992).
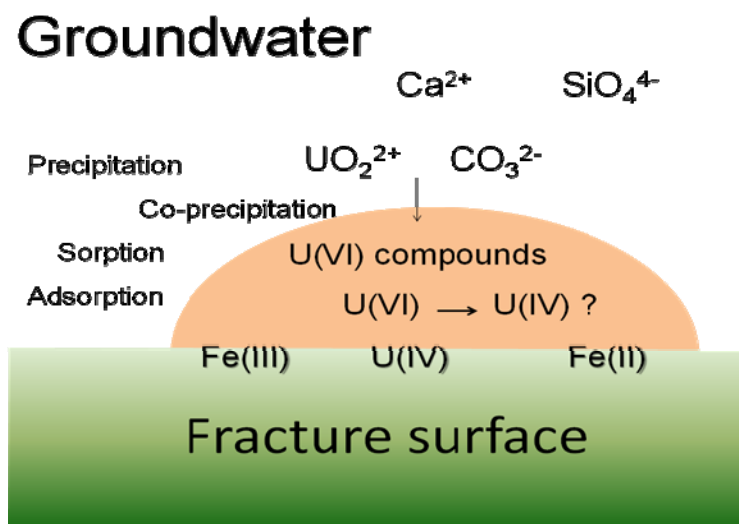
Figure 1: *Typical chemical environment in U accumulation on fracture surface. Accumulated U is selectively dissolved and the redox-state is kept until analysis.*

In the ongoing work we are interested in recent U accumulations because we want to know if the reduction of U(VI) to U(IV) plays a role. Recent accumulations on fracture surfaces have been found in Sweden and Finland. The fact that U accumulates in one place necessitates that U is leached in another place. Leaching of U certainly occurs in the groundwater infiltration area where oxidising surface waters recharge the bedrock. Significant leaching of U from fracture surfaces probably occurred also some 11000 years ago when oxygenated glacial melt water penetrated the bedrock. Dissolved U is transported practically as U(VI) which is the most mobile form of U. Accumulation of U(VI) can take place via adsorption, specific sorption, co-precipitation and reduction (cf. Fig. 1). The role of U(VI) reduction in U accumulation is unclear. One way to approach the problem is to study U redox-state in U accumulations. U concentration on fracture surfaces is generally so low that the application of the X-ray adsorption spectroscopy is often impossible. An alternative method is to dissolve accumulated U and capture U oxidation states until the oxidation states have been analysed. In the ongoing study this method is developed. We believe that the method is also of help in

studying oxidation states of U tracers deposited on ferrous minerals in laboratory experiments which are underway in the ReCoSy WPs 3-5.

Materials and methods

U series study

Drill core samples were from the groundwater infiltration area at the Olkiluoto study site, western coast of Finland. The fractures in the drill core samples were water conducting and were taken from the depths between 4 m and 53 m. Sample material that was removed from the fracture surface consisted of calcite, chlorite, and kaolinite as main minerals. U series nuclides were dissolved in *aqua regia*. U concentration and U series nuclides ^{238}U, ^{234}U and ^{230}Th were analysed using α-spectrometry.

Sample material in HCl extraction study

It is difficult to find good test material for this kind of study. Our choice was a certified reference rock DL-1a. The material has been characterized for mineralogy, elements and the ^{238}U decay series nuclides (Steger and Bowman, 1980). The material is arkose sandstone containing uraninite UO_2+x ($0<x<0.25$) and brannerite $(U,Ca,Ce)(Ti,Fe)_2O_6$ as main U minerals. U concentration is 116 ppm which is high enough to provide easily measurable amounts of U in extraction experiments. U minerals provide U in both U(IV) and U(VI) most of U occurring in U(IV), however. Natural brannerite is well known U mineral and has been intensively studied for U oxidation states in other context. Colella et al. (2005) have studied U oxidation states in brannerites and found U mostly in U(IV). DL-1a contains 0.9 % Fe providing the Fe^{2+}/Fe^{3+}-pair for studying possible redox disturbances.

Although we do not know exact U(IV)/U(VI) ratio of the material it provides an excellent test material for our purposes because Fe and U are expected to be in redox balance and the material has been studied earlier for U oxidation states (Ervanne, 2004). It is possible that some oxidation of Fe(II) and U(IV) may have occurred due to preparation and long storage time of the material.

Anoxic HCl extraction

It is well known that U(IV) and U(VI) form stable chloro complexs in anoxic conditions at high Cl⁻ concentrations. Most of U(IV) exists as positive chloro complex up to 4M HCl whereas U(VI) occurs as negative chloro complex. Opposite charges allows easy U(IV)/U(VI) separation by anion exchange. Moreover, 4M HCl facilitates dissolution of secondary U phases. The concern in U dissolution step is iron compounds which are present in rock samples creating Fe^{2+}/Fe^{3+}-pair in the extraction solution. If Fe and U are not in redox-balance U(IV)/U(VI) ratio may be modified in the extraction solution.

Our test extraction solution is 4.5 M HCl mixed with a small amount of HF (0.03 M) aimed at facilitating dissolution of UO_2. We have spiked extraction solution with

^{232}U(VI) to monitor redox-balance during the extraction. It should be mentioned here that until now we have not observed U oxidation during the extraction but we have observed U reduction.

Analysis of U oxidation states

As mentioned above U(IV) and U(VI) form stable chloro complexes ions at high Cl$^-$ concentrations. This fact has been used to separate U(IV) and U(VI) applying anion exchange chromatography (*e.g.* Hussonnois et al. 1989; Ervanne and Suksi, 1996). Sample solution is filtered (0.45 μm) and loaded in Dowex 1x4 anion exchange column regenerated with the extraction solution. U(IV) is eluted whereas U(VI) is fixed in the column and is eluted with 0.1 M HCl. To quantify U isotopes U(IV) and U(VI) fractions were spiked with the ^{236}U isotope. U isotopes were analysed using anion exchange chromatography and α-spectrometry. A typical α-spectrum of the U isotopes can be seen in Fig. 2.
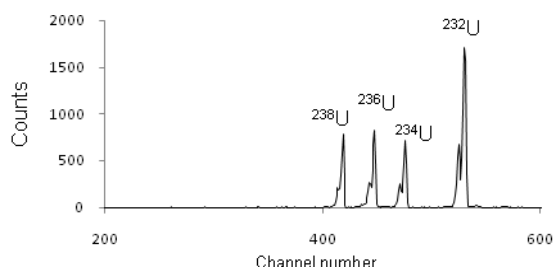
Figure 2: *α-spectrum of a U(IV) fraction. ^{236}U is a yield tracer. ^{232}U is a redox-tracer which was added as ^{232}U(VI) in the extraction solution to monitor redox-conditions. Occurrence of ^{232}U in the spectrum indicates that ^{232}U(VI) reduces to ^{232}U(IV) during the extraction.*

Results

Extraction experiments with the reference material DL-1a

The impact of dissolved Fe on the U(VI)/U(IV) ratio was studied as afunction of extraction time. Extractions were performed in the Ar-atmosphere. The solid-solution ratio was 1/10 (~500 mg of DL-1a/5 ml). Extraction times were 20 s, 60 s and 600 s. Extraction did not dissolve all U. Insoluble U occurs most probably as U(IV). If both U(IV) and U(VI) are obtained in the extraction solution one may assume that all U(VI) has been dissolved. The U(VI)/U(IV) ratio of the ^{232}U tracer and natural U is higher in short term extraction (Fig. 3). When extraction time is increased reduction of ^{232}U(VI) tracer and natural U(VI) occurs. One explanation is dissolved Fe^{2+} which increases Fe^{2+}/Fe^{3+}-ratio. Further experiments are underway. The impact of the Fe^{2+}/Fe^{3+}-pair on the U(VI)/ U(IV) ratio was studied by complexing Fe^{3+} with polyacrylic acid (PAA). PAA is known particularly as a complexing agent for trivalent metal ions (*e.g* Nicemol et al. 1998 and Peng et al. 2005). In this experiment we used extraction solution with 2 % of PAA and extraction time was 600 s. Only few tests have been done so far. Clear

observation was that U(VI) disappears from sample solution. This is explained by the reduction of ^{232}U(VI) and natural U(VI) because Fe^{3+}, which maintains higher redox potential, is captured. It seems that extraction time is in key position in developing the method. Further experiments are in progress.
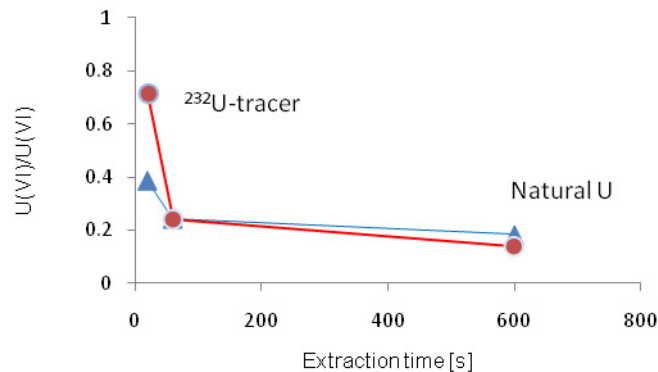
Figure 3: *U(VI)/U(IV) ratio of the ^{232}U redox-tracer and natural U formed in the extraction solution as a function of time. Results represent averages of the two independent measurements except in 20 s extraction where three independent analyses were made. U concentration increases some 30 % in the 600 s extraction.*

USD results

Over 30 drill core samples were taken from the groundwater infiltration area and some 40 fracture surface samples from them were taken to analysis. U concentrations varied between 2 ppm and 29 ppm representing normal U distribution in granitic rock. The results with the 1δ error bars have been plotted in the diagram in Fig. 6 where it can be immediately seen that U has mobilised and deposited in respective fractures. The results in Fig. 6 can be explained and understood by considering the groundwater conditions and the different mobility of the U series nuclides. Infiltrating waters derive from meteoric and surface waters typically high E_H and p_{CO2} values favour U dissolution and mobilisation. The long-term continuous infiltration removes labile U little by little. Sooner or later the more resistant minerals including hard U minerals (opposite to labile U) start to weather. Due to strong bonding of U in these minerals the decay product ^{234}U is preferentially leached. The relationship of the weathering degree and ^{234}U deficient in the rock is frequently found on fracture surfaces. The leaching of U and deposition in the down-flow side tend to produce accumulation that increases with time as the front migrates to down-flow direction. In the down-flow the waters which are not oxidising enough to dissolve reduced ^{238}U may not be reducing enough to precipitate ^{234}U which is moving further down-flow from the main accumulation of ^{238}U. Respective U concentrations on fracture surfaces can be illustrated as bell-shaped curves (Fig. 4). In the diagram ^{234}U curve appears to be shifted in the down-flow direction. The position and shape of the ^{234}U curve is constrained by the assumption that the total radioactivity of ^{234}U is equal to that of ^{238}U. The stretching ^{234}U curve illustrates enhanced mobility. ^{234}U is also decaying to ^{230}Th and in the total system the activity of ^{230}Th equals that of ^{234}U and ^{238}U. Immobile ^{230}Th is left behind as the ^{238}U and ^{234}U peaks advance causing stretching of the ^{230}Th peak. Displacement of the ^{238}U and ^{234}U peaks in a steady-state

system is caused by the enhanced mobility of ^{234}U. Of course, groundwater flow rate affects further displacements of the ^{238}U and ^{234}U peaks to the ^{230}Th peak.

The relative distribution of nuclides' radioactivity in rock seen in Fig. 4 allows one to recognise the infiltration and down-flow gradient parts and, accordingly, the position relative to the redox-front. The curve diagram has been divided into sectors from (I) to (V) which are always in the same sequence from infiltration or up-flow to down-flow provided that disequilibrium occurs in a steady-state system. In sector (I) ^{230}Th exceeds ^{238}U and ^{234}U, while ^{238}U exceeds ^{234}U. This is the far up-flow sector. U has been leached leaving ^{230}Th in rock. The rock has become deficient in ^{234}U. In sectors II and III ^{238}U exceeds ^{234}U and ^{230}Th. These sectors are considered the principal part of U deposition. Sector III differs from II in having an excess of ^{234}U relative to ^{230}Th, and is therefore further down-flow. In sector IV ^{234}U activity exceeds ^{238}U activity which indicates down-flow deposition of U. At the same time ^{238}U exceeds ^{230}Th. Sector V describes U deposition far in the down-flow where ^{234}U and ^{230}Th exceeds ^{238}U. These same relationships can be also presented in radionuclide activity ratio diagram as has been done in Fig. 5. Now, instead of five sectors (I-V) there is an extra sector between the sectors I and V which cannot be deduced from the bell-shaped curves in Fig. 4. This sector is forbidden to steady-state systems. The data plotted in this sector correspond to the situation where ^{234}U is deficient relative to ^{230}Th, *i.e.* always in infiltration or up-flow, and in excess of ^{238}U which is always the case in down-flow. Such a situation could only occur if remobilisation of deposited U occurred (for more details, see Osmond et al. 1983).
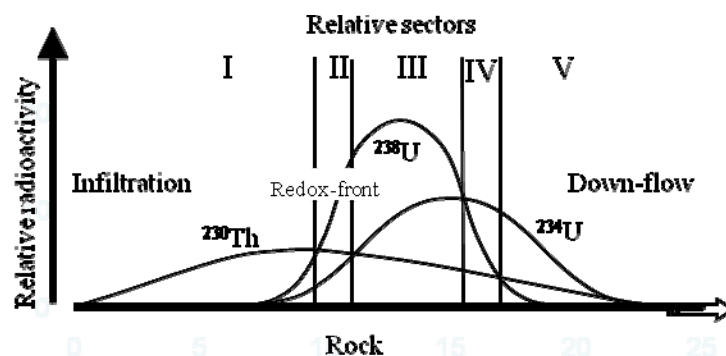
Figure 4: *Relative distribution of the three long-lived ^{238}U decay series nuclides in rock under groundwater flow. The resulting radioactivity ratios define a sequence of sectors from up-flow (I) to down-flow (V) (modified from Osmond et al. 1983).*
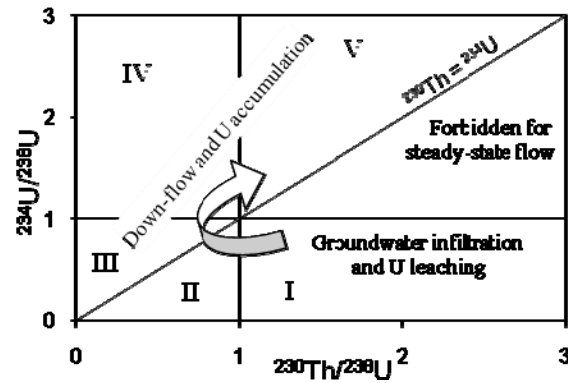
Figure 5. Characterisation of U leaching and U accumulation samples according to radionuclide activity ratios. Sectors from I to V are defined in Fig. 4.
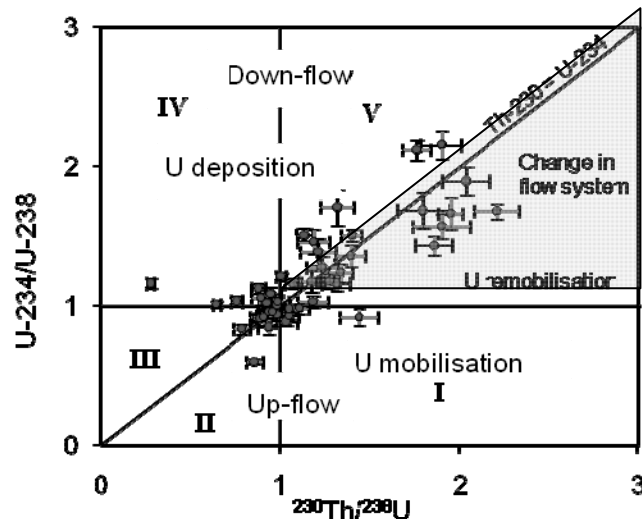
Figure 6: *USD data from Olkiluoto site. Several data points plot on U deposition sectors. N.B. Data points plot also in a gray area between sectors V and I. This sector is not allowed for steady-state flow (see text) and therefore the data points in this sector indicate that U has remobilised and that there must have been a change in groundwater flow in respective fractures.*

Summary and Conclusions

We have developed methodology to clarify the role of U reduction in U accumulation on fracture surfaces. The occurrence of U on fracture surfaces has been studied with the samples taken from the groundwater infiltration area at the Olkiluoto study site. Parallel to the fracture surface study we have developed wet chemistry to examine the U redox-state in solid U phases which is done by analysing U oxidation states.

The U series disequilibrium observations in the groundwater infiltration area show that the sampled fracture surfaces represent flow channels where groundwater has leached U and channels where U has accumulated. The U series disequilibrium results are in good agreement with the groundwater conditions in the area.

Parallel to U series study we studied the function HCl extraction to separate U oxidation states without affecting the redox-state of U. The extraction method was studied with uraninite and brannerite containing rock. The results showed that the iron dissolved from the sample material can affect U redox-state. Until now we have not observed U oxidation during the extraction but we have observed U reduction. It seems that extraction time is in key position. We believe that the redox-disturbances caused by the dissolved iron can be significantly reduced. New extraction experiments are underway.

Future prospects

Our plan is to study U occurrence and redox-state in undisturbed drill core samples. Drill cores from triple tube drilling provide the best possible material for that purpose. The sampling is presently ongoing on drill core material from one of the SFR drill cores at Forsmark, Sweden. Samples have been sealed by placing it into a dense plastic bag, using first nitrogen to fill the bag and then a vacuum pump to get rid of as much oxygen as possible and then the plastic bag is heat sealed. This is repeated once again with a new plastic bag and thereafter a third time with an aluminium foil. The sample was then been stored dark and cool until opened and sampled in the glove box (Fig. 7).

Figure 7: *Opening of the vacuum sealed samples in N2 glovebox in the laboratory of radiochemistry, University of Helsinki.*

References

Colella, M., Lumpkin, G. R., Zhang, Z., Buck, E. C. and Smith, K. L. (2005). Determination of the uranium valence state in the brannerite structure using EELS, XPS, and EDX. Phys Chem Minerals (2005) 32: 52–64

Ervanne, H. and Suksi, J. (1996). Comparison of Ion-Exchange and Coprecipitation Methods in Determining Uranium Oxidation States in Solid Phases. Radiochemistry **38**, 306-309.

Ervanne, H. (2004). Oxidation state analysis of uranium with emphasis on chemical speciation in geologic media. Academic Dissertation. Report Series in Radiochemistry 24/2004.

Hussonnois, M., Guillamont, R., Brillard, L., Fattahi, M. (1989). A method for determining the oxidation state of uranium at concentration as low as 10-10 M, in: W. Lutze and R.C. Ewing (Eds.), Mater. Res. Soc. 127, 979-984.

Ivanovich, M. and Harmon, R.S., 1992. Uranium-series disequilibrium, applications to earth, marine, and environmental sciences, Clarendon Press, Oxford (2nd ed.), 910 p.

Nicemol, S., Bini, G. and Beena, M. (1998). Metal complexes of poly(acrylic acid): Synthesis, characterization and thermogravimetric studies. Polymer Degradation and Stabilily 60 (1998) 371-375.

Osmond, J. K., Cowart, J. B. and Ivanovich, M. (1983). Uranium isotopic disequilibrium in groundwater as an indicator of anomalies. Int. J. Appl. Radiat. Isot. Vol. 34, No. 1, 282-308.

Peng, F. Li, G., Liu, X, Wu, S. and Tong, Z. (2005). Redox-Responsive Gel-Sol/Sol-Gel Transition in Poly(acrylic acid) Aqueous Solution Containing Fe(III) Ions Switched by Light. J. Am. Chem. Soc. 130, 16166–16167.

Steger, H.F. and Bowman, W.S. (1980). Reference Uranium-Thorium Ore DL-1a, Certificate of Analysis, CANMET Report 80-10E, CANMET, Energy, Mines and Resources Canada.

REACTION OF Se(IV) AND/OR Fe(II) IN PRESENCE OF CALCITE

Laurent Charlet[1], Sudipta Chakraborty[1,2], Gabriela Aurelio[1,3], Suzanne Mettler[5,6], Gabriela Roman Ross[4], Fabrizio Bardelli[1], Delphine Tisserand[1], Florian Molton[1], Urs Van Gunten[6]

[1]LGIT, Université de Grenoble-I and CNRS, BP 53X, 38041 Grenoble Cedex 9, France

[2]Department of Chemistry, Kalyani University, West Bengal, India

[3]Conicet and Centro Atómico Bariloche, S. C. de Bariloche, ARGENTINA

[4]Dept. of Chemistry, Faculty of Sciences, University of Girona, Campus Montilivi, 17071, Girona, SPAIN

[5]Swiss Federal Institute of Aquatic Science and Technology (EAWAG), Ueberlandstrasse 133, 8600 Duebendorf, Switzerland

[6]Solexperts AG, Mettlenbachstrasse 25, Postfach 122, CH-8617 Mönchaltorf, Switzerland

* Corresponding author: charlet38@gmail.com

Abstract

This contribution summarizes three papers reporting researches partly (Mettler et al., 2008; Aurelio et al., 2009) or fully (Chakraborty et al., 2010) funded by the RECOSY project.

The immobilization by calcite of Fe(II) (to be released by canister corrosion) and Se(IV) (to be released as ^{79}Se) has been investigated. The sorption and coprecipitation of each individual ion was first studied individually, with wet chemistry, and for Se, by neutron diffraction (ND), Extended X-ray Fine Structure spectroscopy (EXAFS) and ab initio modeling using the Vienna Ab-initio Simulation Package (VASP) code. Then the reaction of Se(IV) added to an Fe(II)-rich calcite suspension was investigated by X-ray Absorption Near Edge (XANES) spectroscopy.

The interaction of Fe(II) with calcite was investigated experimentally under anoxic conditions (O2 < 1 ppmv). Fe(II) sorption isotherm depicts the S-shape curve typical of

a continuum between adsorption and co-precipitation processes (Wersin et al., 1989). A Langmuir type adsorption predominates at low Fe(II) aqueous concentrations, while a surface coprecipitation process dominates at higher concentration. The incorporated Fe(II) could not after one week be remobilized by a strong complexing agent but the dissolution of surface layers of calcite particles with carbonic acid allowed its recovery. Through dynamic dissolution/reprecipitation processes, the Fe(II) ion has been incorporated in the calcite 25 nm surface layer, characterized by an Fe:Ca ratio equal to 0.04.

The coprecipitation of Se(IV) with calcite was shown to occur by substitution of the carbonate ion by the selenite oxyanion. Neutron diffraction experiments, EXAFS spectroscopy, and theoretical modeling of the crystallographic structure using VASP show the calcite unit cell volume to increase linearly with Se content in the structure. EXAFS spectroscopy, in combination with our theoretical model of the local structure surrounding the Se atom, confirms that quasi-isomorphic substitution of carbonate ions by selenite ions offer tremendous storage facilities for selenite in the various calcite-rich materials consider for the confinement of ^{79}Se rich nuclear waste.

Finally the reaction of Se(IV) with Fe(II)-rich calcite was investigated under anoxic conditions ($O_2 < 1$ ppmv) using XANES. The Se(IV) sorption on calcite increased in the presence of sorbed Fe(II) compared to that of Fe-free pure calcite. XANES spectra of Se K-edge show that nearly half of the total sorbed Se(IV) is reduced to Se(0) by Fe(II) freshly adsorbed on calcite. The extent of reduction decreases with increasing equilibration time of calcite with Fe(II) solution, before Se(IV) addition. The combined results of Field Emission Scanning Electron Microscopy (FESEM) and X-Ray Diffraction (XRD) have shown that needle shaped red monoclinic elemental Se with diameters of 30-50 nm and lengths of up to 100 nm, is precipitated on the calcite surface. In contrast, Fe(II) coprecipitated calcite does not contribute to Se(IV) reduction within 72 h. Therefore, the reduction capacity of Fe(II) linked to calcite critically depends on its location (either on the surface or in the bulk solid), and less extensively on the pre-equilibration time of calcite with Fe(II) solution. Such understanding is important to predict the transport, transformation, and attenuation of Se in subsurface and in nuclear waste repositories.

Introduction

The radioactive isotope ^{79}Se is a long-lived fission product (half-life 4.8×10^5 to 1.1×10^6 years; Jiang et al., 1997; Magill et al., 2006), which may dominate the radiation dose from high-level radioactive waste for 10^5 years, according to several national risk assessment reports. Mobility and bioavailability of Se is hence a major concern for the safe enclosure of nuclear waste. Selenium solubility is largely controlled by Se oxidation state, and therefore depends on redox conditions in soils, sediments, and aquifers. The higher oxidation states, +VI and +IV, prevail as mobile aqueous oxyanions, while the oxidation states 0, -I, and -II prevail as solids with low solubility. Along redox gradients, soluble selenate (Se(VI)) or selenite (Se(IV)) species migrate toward regions of low Eh, where they precipitate as elemental Se creating an efficient sink for Se. Speciation and mobility under storage conditions therefore control to what extent ^{79}Se is a critical radionuclide, i.e. will be a major contributor to the ultimate dose

release during the next million years from High-Level Radioactive Waste (HLRW) depository sites. Selenate is much more mobile and harder to treat than selenite. These two species are molecular ions with a three-dimensional structure of their own, and therefore their incorporation to mineral surfaces or bulk involves not only charge balance, but also the atomic-scale structure of the contaminant molecules. SeO_3^{2-} has a pyramidal trigonal shape, with a Se-O bond distance of 1.69 Å, whereas SeO_4^{2-} has tetrahedral shape, with Se-O bond lengths of 1.63/1.635 Å. In the present study, we report on the interaction of selenite ion with calcite, a major mineral component in both the near-field and far-field geological barriers.

In these two anoxic environments, ferrous iron (Fe^{2+}) is a major cation, and an important reductant. Indeed in repository engineered systems, vitrified waste will be placed in steel containers and overpacks. Under anoxic conditions, steel from containers and structural elements may react with water, i.e. corrode, and release large amounts of Fe(II),

$$Fe^0 + 2\ H_2O \rightarrow Fe^{2+} + H_2 + 2\ OH^-$$

which are themselves encased in exogenous materials (near-field engineered barrier), and buried in a clay-rich geological formation (far-field engineered barrier), both characterized by high content of calcite, a common calcium carbonate mineral.

Upon container corrosion, a variety of radionuclides, including ^{79}Se, may be released in the geological barrier and its pore water. In this work we first investigate separately the sorption (both adsorption and coprecipitation) of Fe(II) and Se(IV). We then investigate the ternary system, i.e. the electron transfer when Se(IV) is introduced in a Fe(II)-rich calcite suspension.

Interaction of Fe(II) with calcite

The interaction of Fe(II) with calcite was investigated experimentally in the absence and in presence of oxygen. After 24hr, Fe(II) sorption isotherm depicts the S-shape curve typical of a continuum between adsorption and co-precipitation processes (Wersin et al., 1989).

A Langmuir type adsorption predominates at low Fe(II) aqueous concentrations, while a surface coprecipitation process dominates at higher concentration. The curve inflection points lead to a concentration of surface functional groups of 4.0 x10^{-6} mol g^{-1}, i.e. 1.0 sites nm^{-2}, in accordance with site density values reported in various structural and spectroscopic investigations (see Wolthers et al., 2008 and references herein).
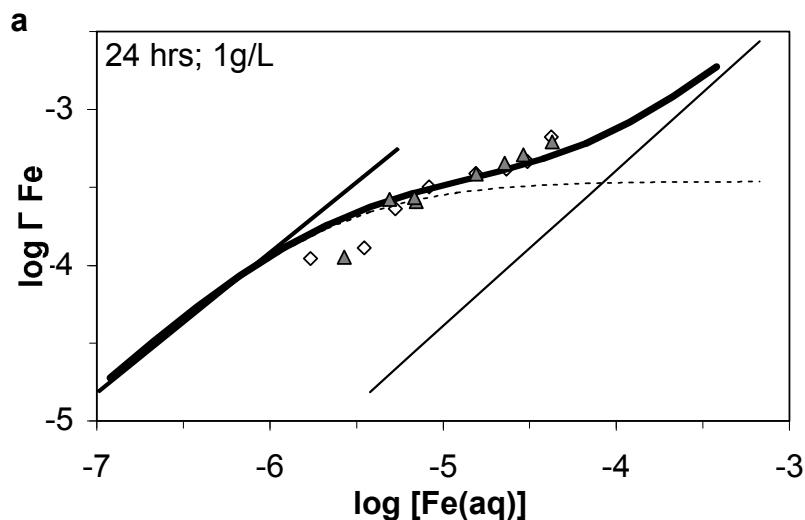
Figure 1. Sorption isotherms of Fe(II) on CaCO₃(s) for 24 hrs in a 1 g L⁻¹ suspension, Γ_Fe is the total amount of sorbed Fe(II) per mole of total calcium and [Fe(aq)] in (M), triangles and diamonds are duplicate runs (from Mettler et al., 2008).

Like for many divalent cation sorptions onto calcite (Wersin et al., 1989; Martin Garin et al., 2003), the sorption of Fe(II) occurred in two distinguishable steps: a rapid adsorption step (seconds-minutes) was followed by a slower incorporation (hours-weeks).

The incorporated Fe(II) could not be remobilized by a strong complexing agent (phenanthroline, ferrozine), but the dissolution of surface layers of calcite particles with carbonic acid allowed its recovery. Based on results of the latter dissolution experiments, the stoichiometry (Fe:Ca ratio equal to 0.04) and thickness of the mixed carbonate layer (roughly 25 nm) were estimated (Figure 2). The presence of magnesium in calcite at a similar content has been shown to correspond to the minimum value of calcite solubility product. Thus these trace amounts of divalent cations may stabilize the surface of calcite against dissolution and affect the nuclear waste repository pH buffer computations.

The effect of sorption and coprecipitation of Fe(II) with calcite on the mechanisms and kinetics of Fe(II) oxidation was investigated first using oxygen as oxidation agent.

The oxidation kinetics of Fe(II) sorbed onto/into calcite depended on the pre-equilibration time of aqueous Fe(II) with the mineral, prior to the introduction of oxygen. When the pre-equilibration lasted for >15 hours, the oxidation kinetics of Fe(II) was comparable to an oxidation kinetics in a calcite-free system. Conversely, when Fe(II) was added to an aerated calcite suspension, the rate of oxidation was higher than in the absence of calcite. This catalysis was due to the greater reactivity of adsorbed Fe(II) species.
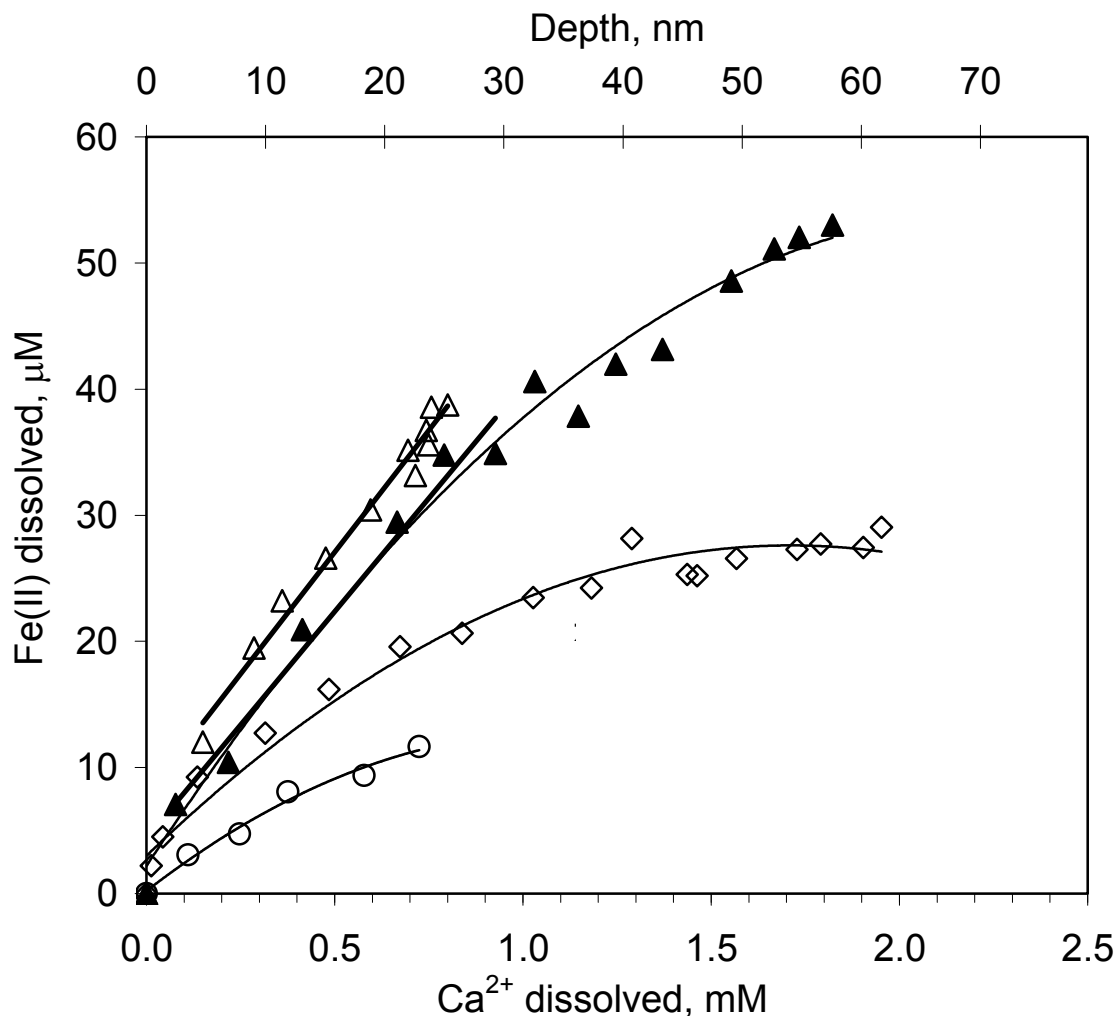
Figure 2. Dissolved Fe(II) versus dissolved Ca^{2+} of the Fe(II) equilibrated calcite. The symbols represent results after different CO_2 dissolution time and concentration: 24h (○; CO_2 20%), 48h (◊; CO_2 100%), 1 week (∆; CO_2 20%. ▲; CO_2 100%). The upper secondary X-axis, ∆r, represents an estimated thickness of the dissolved calcite layer calculated from the dissolved calcium assuming a homogeneous solid composition. A slope of 0.004 (straight line between 2 nm < ∆r < 23 nm) indicates a constant Fe(II)/Ca mole fraction of the Fe(II) equilibrated calcite surface layer (from Mettler et al., 2008).
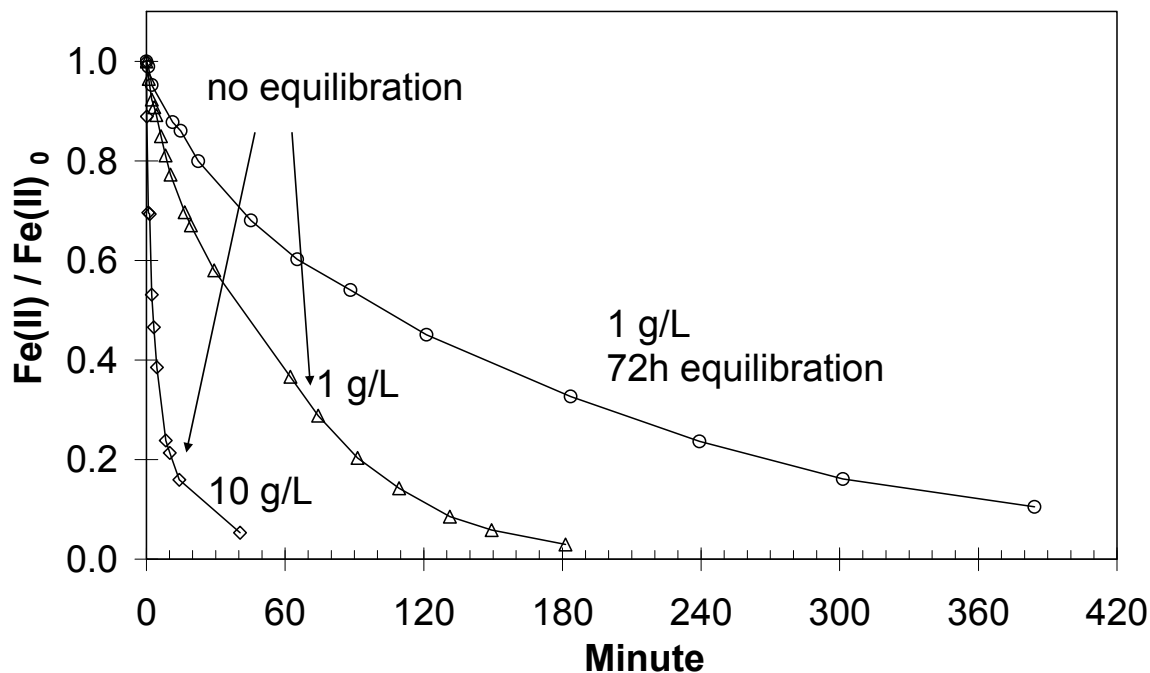
Figure 3. *Decrease of Fe(II) as a function of time due to addition of oxygen to a Fe(II) / calcite suspension, after 0h or 72h anoxic equilibration of the Fe(II)-calcite system. Data measured at 1 g L^{-1} (O and Δ) or 10 g L^{-1} calcite ($\Diamond$). Experimental conditions: Fe(II) = 1 x 10^{-5} M, O$_2$ 6.5 mg L^{-1}, pH 7.0. (from Mettler et al., 2009).*

Interaction of Se(IV) with calcite

The interaction of Se(IV) with calcite was investigated experimentally in the absence of oxygen. We investigated, both at a macroscopic and microscopic level, whether Se(IV) can be incorporated to bulk calcite by substitution at carbon sites. Neutron diffraction experiments, EXAFS spectroscopy, and a theoretical modelling of the crystallographic structure using VASP code, confirm this isomorphic substitution to be an important "sorption" mechanism for selenite oxyanion in calcite.

Combining diffraction results and VASP modelling, we have found that the calcite unit cell volume obtained from the VASP simulations increases linearly with Se content in the structure (Figure 4). This allows estimating the Se content effectively incorporated into calcite, based on volume measurements. We are able to estimate the concentration of Se(IV) coprecipitated with calcite to be 30-75 mmol/kg solid. Since neutrons penetrate deeply into calcite and probe the bulk mineral more efficiently than X-rays, we used the ND technique to confirm the macroscopic volume expansion associated to the incorporation of Se (IV) (Aurelio et al., 2009). Furthermore, our results from diffraction measurements indicate that Selenium is not present in a secondary precipitated phase.
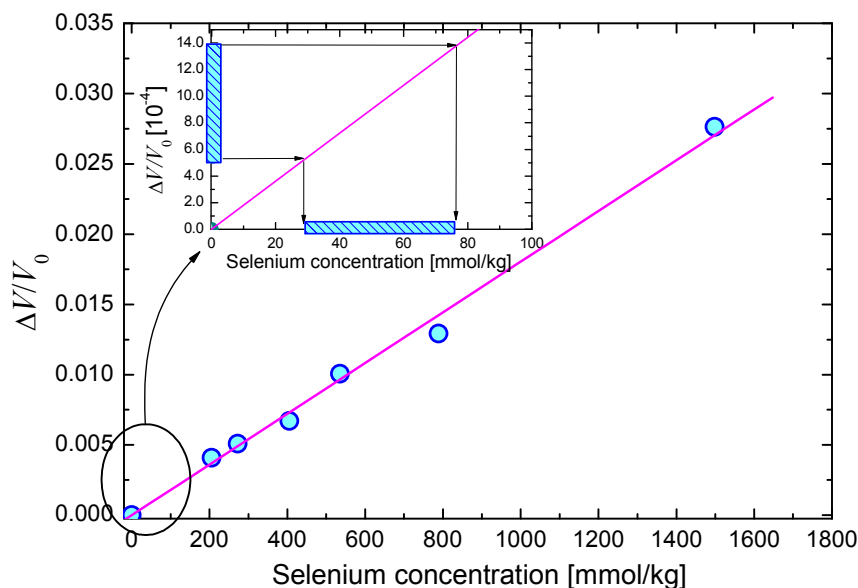
Figure 4. *Theoretical relative volume expansion as a function of selenium concentration. V_0 corresponds to the average pure calcite simulated volume. The line represents a linear fit to the data. In the inset, the low-selenium region is zoomed. The hatched area in the ordinate axis corresponds to the range of experimental $V = V_0$ values coming from neutron diffraction experiments. The hatched area in the abscissa axis corresponds to the extrapolated range of selenium concentrations incorporated into the structure in the coprecipitation experiments. (from Aurelio et al., 2009)*

Using the DFT-based simulation package VASP, we have modelled several crystallographic arrangements to evaluate the substitution of Se using different supercells and Se concentrations. The obtained theoretical model for the local structure around Se in the bulk of calcite was used to successfully analyze EXAFS spectra, confirming the incorporation of Se(IV) into calcite. EXAFS refinements demonstrate the occurrence of four atomic shells surrounding Se (table 1), an indication of highly ordered impurity incorporation into calcite.

This study shows that selenite ions may substitute for carbonate anions in the calcite structure. Therefore, in case of contamination of an anoxic aqueous phase by selenium (*e.g.* ^{79}Se), calcite represents an extremely large – near infinite – sink for selenium, due to its dynamic solubility equilibrium, even when present in trace amounts (as is the case of shists or clay rocks) and due to its ability to trap selenite ions within its structure during the dissolution/precipitation cycles, even in conditions close to equilibrium.
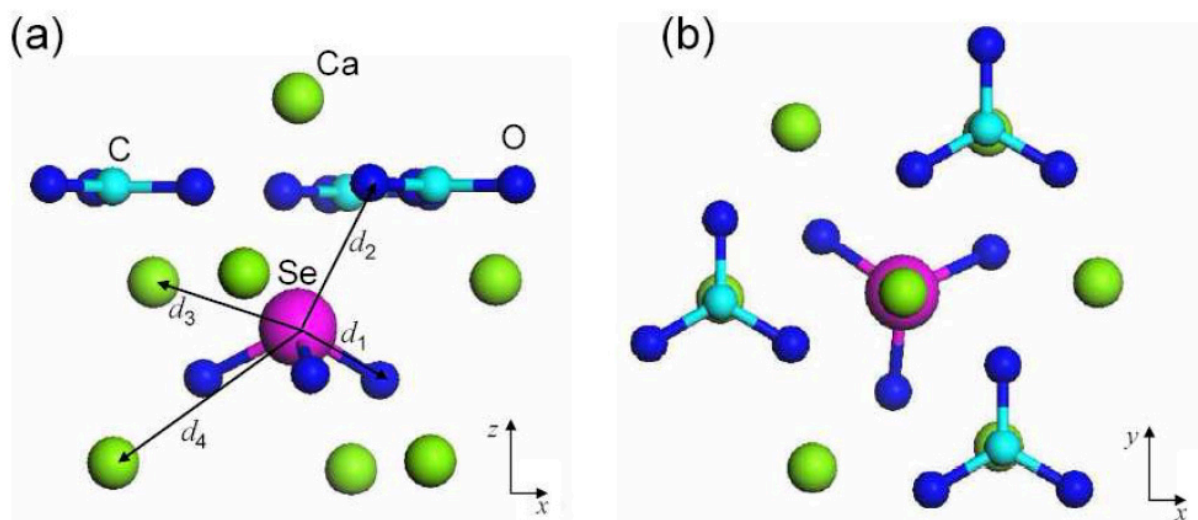
Figure 5. *Local structure around a Se(IV) atom in calcite, resulting from the VASP simulations. Panel (a) corresponds to a projection along the y direction and panel (b) to the projection along the z direction. The relevant distances to the nearest shells around the Se atoms are indicated by arrows. (Aurelio et al. 2009)*

Table 1 *Structural parameters obtained from EXAFS refinements. Distances between atoms correspond to distances indicated by arrows in figure 5.*

path	CN	R [Å]	σ^2 [Å²]	R_{vasp} [Å]
Se-O (d_1)	2.8(5)	1.67(1)	0.002(1)	1.727
Se-O (d_2)	1(1)	2.87(8)	0.002(1)	2.876
Se-Ca (d_3)	1.3(8)	3.25(3)	0.002(1)	3.202
Se-Ca (d_4)	1.7(9)	3.53(4)	0.002(1)	3.565

Reaction of Se(IV) with Fe(II) adsorbed or coprecipitated with calcite

The reductive immobilization of selenite by micron sized (100 - 200 μm) calcite containing sorbed or co-precipitated Fe(II) was investigated at pH 7 under anoxic condition (O_2 <1 ppmv) using XANES spectroscopy.

Selenite sorption on calcite increased in the order: calcite without Fe(II) ≈ Fe(II) co-precipitated calcite < Fe(II) sorbed calcite.

XANES spectra of Se K-edge show that nearly half of the total sorbed selenite was reduced to Se(0) by Fe(II) sorbed calcite within 24 hours, and the extent of reduction decreased with increase in equilibration time of calcite with Fe(II) solution before selenite addition (Figure 6). In contrast, Se K-edge normalized XANES spectra of

Se(IV) sorbed on Fe(II) coprecipitated with calcite show no evidence of reduction of selenium (Chakraborty et al., 2010). Thus coprecipitated Fe(II) cannot donate electron, neither to oxygen nor to selenium: calcite does act as a perfect insulator.
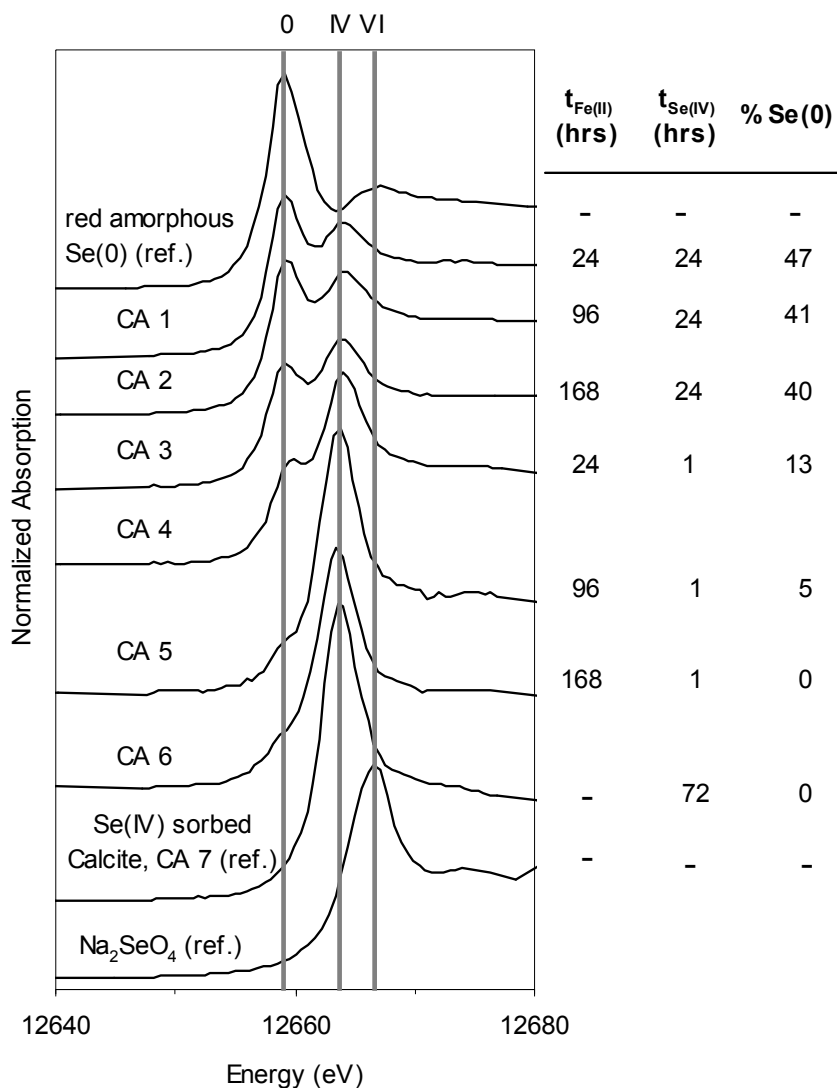
Figure 6 *Se K-edge normalized XANES spectra of Se(IV) sorbed on Fe(II) sorbed on calcite showing reduction of Se(IV) to Se(0). $t_{Fe(II)}$ = equilibration time of Fe(II) with calcite before Se(IV) addition; $t_{Se(IV)}$ = equilibration time of Se(IV) with Fe(II) sorbed on calcite (from Chakraborty et al., 2010)*

The combined results of scanning electron microscopy (SEM) (Figure 7) and X-ray Diffraction (XRD) confirmed that needle-shaped red monoclinic elemental Se with diameters of 30 – 50 nm and lengths up to 100 nm formed on the calcite surface. Fe(II) co-precipitated calcite did not contribute to selenite reduction within 72 hours
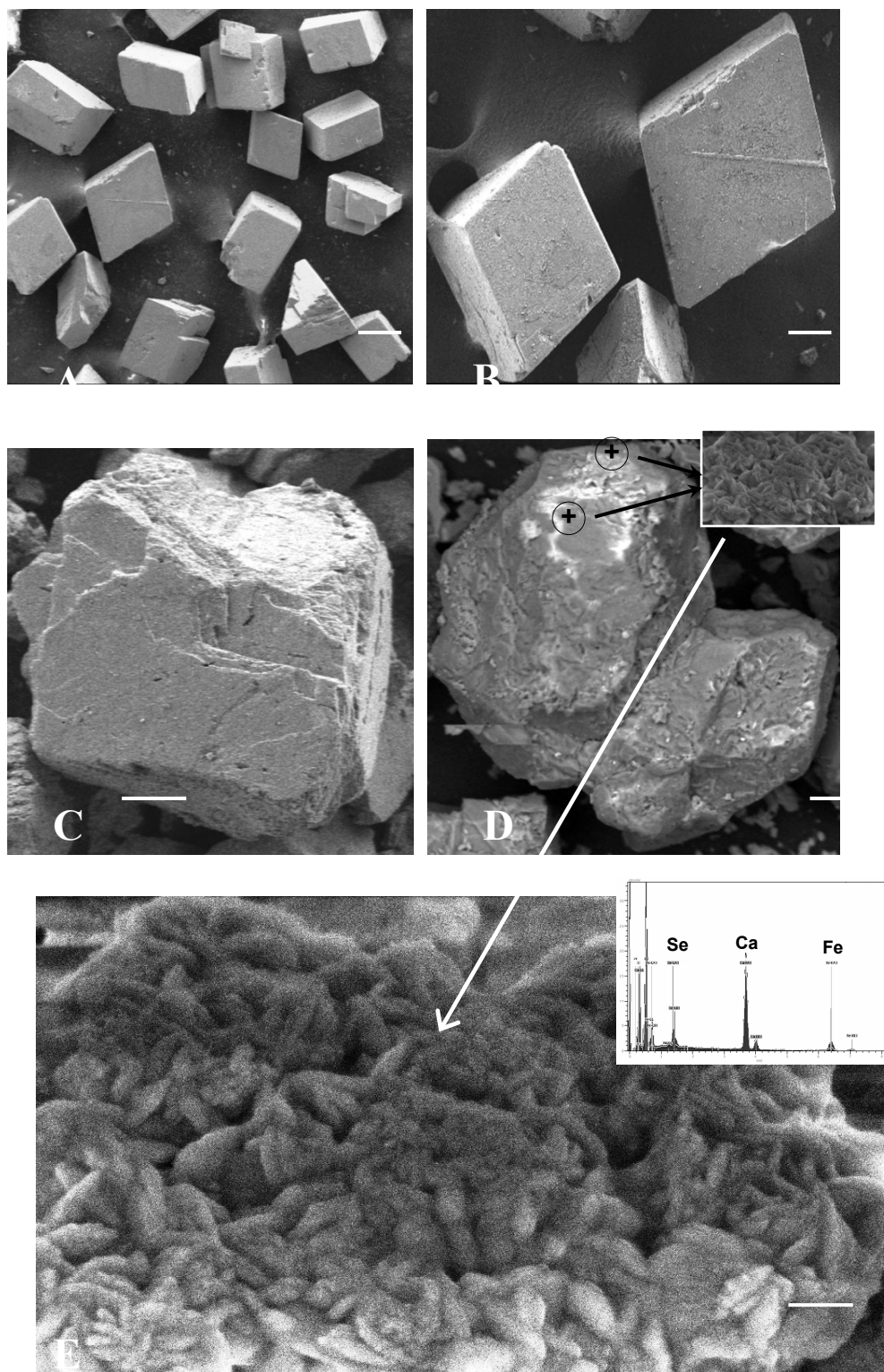
Figure 7. *Field emission scanning electron microscopic (FE-SEM) images of (A, B) crystal morphology of synthesized Fe(II) coprecipitated calcite (without Se); (C) natural calcite before and (D) after reaction with Fe(II) and Se(IV) showing formation of clustered Se(0) formation (spots encircled) on calcite; (E) magnified image of Se(0) nanoclusters (inset: EDX spectrum of the sample with backscattered peaks of Se, Ca, and Fe). (from Chakraborty et al., 2010)*

Summary and Conclusions

The present Scientific and Technical RECOSY Contribution indicates that both ions strongly interact with calcite and may be buried within calcite, a mineral characterized by a dynamic equilibrium, i.e. by fast dissolution/reprecipitation local processes.

On a short time scale, sorption of Fe^{2+} and SeO_3^{2-} is characterized at low concentration by a Langmuir-like sorption process and at higher concentration, by a coprecipitation process, the combined processes resulting in a "surface precipitation" type isotherm.

The reductive precipitation of Se critically depends on the location of the Fe(II) ion: when the ion is present as adsorbed species at the surface, the reduction to Se° is fast. In contrast, when the Fe(II) is present within the structure, where it substitutes for Ca(II) ions of calcite, the reduction does not occur. Therefore, we concluded that the reducing capacity of Fe(II) associated with calcite, is strongly influenced by its location (surface or bulk), and less extensively on the equilibration time of calcite in contact with Fe(II) solution.

Such understanding is important to predict Se transport and transformation in nuclear waste repositories.

References

Aurelio, G., A. Fernandez-Martinez, G.J. Cuello, G. Roman-Ross, I. Alliot, L. Charlet 2009 Structural study of selenium(IV) substitutions in calcite (2009) *Chem. Geol*. 270, 249-256

Chakraborty, S., Bardelli, F., Charlet, L. (2010) Reactivity of Fe(II) on calcite : Selenium reduction *Environ. Sci. Technol.* 2010**,** *44,* 1288–1294 ("highlight" paper of EST Issue)

Martin-Garin A., Van Capellen P. and Charlet L. (2003) Aqueous cadmium uptake by calcite: A stirred flow-through reactor study. *Geochim. Cosmochim. Acta* 67 (15), 2763-2774.

Mettler, S., Wolthers, M., Charlet, L., Gunten, U.v. (2009) Sorption and catalytic oxidation of Fe(II) at the surface of calcite, *Geochimica et Cosmochimica Acta*, 73:1826–1840

Scheinost, A. , Charlet, L. (2008) Selenite Reduction by Mackinawite, Magnetite and Siderite: XAS Characterization of Nanosized Redox Products, *Env. Sci. Technol.* 2008, 42, 1984–1989

Scheinost, A.C., Kirsch, R., Banerjee, D., H., Fernandez-Martinez, A., Zaenker, H., Funke, H., Charlet, L. (2008) X-ray absorption and photoelectron spectroscopy investigation of selenite reduction by FeII–bearing minerals *J. Cont. Hydr.* 102: 228–245

Wersin P., Karthein R., Charlet L. and Stumm W. (1989) From adsorption to precipitation: sorption of Mn^{2+} on $FeCO_3$(s). *Geochim. Cosmochim. Acta* 53, 2787-2796.

Wolthers M., Charlet L., Van Cappellen P. (2008) The surface chemistry of divalent metal carbonate minerals; a critical assessment of surface charge and potential data using the charge distribution multi-site ion complexation model. *American. J. Science* 308:905-941

CORROSION OF SPENT FUEL IN PRESENCE OF H$_2$

Paul Carbol[*], P. Fors

European Commission, JRC, Institute for Transuranium Elements, Eggenstein-Leopoldshafen, (D)

*Corresponding author: Paul.Carbol@ec.europa.eu

Abstract

Corrosion of the high burn-up structure (rim) of a UO$_2$ fuel irradiated to 59.1 MWd/kgHM has been studied in presence of 33 mM dissolved H$_2$, for a period of 311 days. Redox sensitive actinides (^{238}U, ^{239}Pu) and fission products (^{137}Cs, fission Mo) together with natural redox sensitive elements such as Fe, Mn, and Mo, originating from the autoclave setup, were analysed to observe the co-variation of these elements.

Low steady state concentration of U of 1.5·10^{-10} M and for Pu at a level of 3·10^{-11} M confirm that, despite radiolysis and intrusion of atmospheric O$_2$, dissolved H$_2$ inhibits radiolytically induced UO$_2$ corrosion. The redox-sensitive natural elements; Fe, Mn, Mo behave more similarly to Pu than U. The co-variation of the elements will be used as input for mass balance studies of reducing/oxidising species and for determination of the redox potential in the leachate. The redox potential is coupled to the oxidative-dissolution process at the UO$_2$-H$_2$O interface. The understanding of the redox processes occurring at the UO$_2$-H$_2$O interface is crucial for the understanding of the spent fuel corrosion and is directly applicable to the conceptual model of the spent fuel corrosion used in safety assessments.

Introduction

Corrosion of spent nuclear fuel is un-avoidable after that water has penetrated the safety barriers in a nuclear waste repository. Despite the fact, that in general, reducing conditions prevail in a deep granitic repository, α-radiolysis due to the presence of actinides, at the spent fuel surface will create local oxidising environment. Presence of oxidants at the fuel surface will oxidise the rather non-soluble U(IV)O$_2$, the main constituent of spent fuel, to U(VI) oxides that finally dissolves. During the dissolution process the fission products present in the UO$_{2+x}$ matrix will be released. On the other

hand, it has been shown that presence of hydrogen, above 1 bar H_2, suppresses the UO_2 dissolution and, indirectly expressed, the oxidation of U(IV) to U(VI). The hydrogen is produced through anoxic corrosion of the iron canister encapsulating the fuel [Bonin et al., 2000].

Due to this duality: α-radiolysis producing an oxidising environment and the H_2 suppression of UO_2 corrosion creating reducing conditions at the fuel surface, it is important to study which effect is dominating and which are the boundary conditions.

The corrosion experiments of the high burn-up structure zone of commercial spent nuclear fuel in presence of 4.1 MPa hydrogen gas pressure, i.e., a dissolved H_2 concentration of 33 mM, has continued as planned during 2009. A detailed description of the fuel, the inventory and the initial corrosion results for the first 60 days is given in the 1st annual ReCosy workshop proceedings [Buchau 2009]. In the following sections more details are given concerning the sampling, analysis procedures and the results obtained in the period 0 to 316 days. The detailed information of the experiment can be found in reference [Fors 2009].

Experimental

Preparation of the autoclave in the hot cell
A 600 cm^3 titanium autoclave (Parr Instruments Co, USA) was modified for work on active material and hot cell manipulation. The entire setup, i.e., the autoclave itself, valves, tubing, magnetic stirrer, was manufactured of quality grade II-weldable titanium (99.3 wt-% Ti, 0.3 wt-% Fe, and trace elements C, N, O and H). To avoid titanium abrasion due to stirring, the Ti-coated magnetic stirrer was placed in a small PEEK cup. Graphite seals and gaskets were used for all connections, to avoid foreign metal surfaces. ´
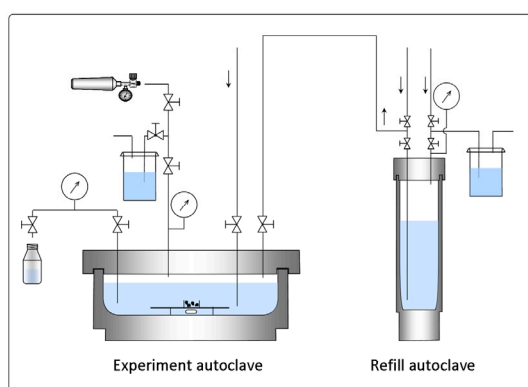
Figure 1:   *The corrosion autoclave setup (left) and a photograph of the autoclave vessel (right).*

The setup was equipped with electrical and mechanical pressure gauges, electrochemical sensors for measurement of oxygen and hydrogen concentrations, possibilities for gas and solution sampling, and with an in-stream E_h-sensor for redox potential measurement during sampling. The setup allows filling, purging and sampling

of solutions and gases, without intrusion of external air oxygen into the autoclave, and was certified for H_2-pressures up to 60 bars. A schematic of the setup and a picture of the autoclave are shown in Fig. 1.

Preparation and inventory determination of the fuel

A high burn-up UO_2 fuel rod irradiated under normal conditions (without ramping) in a pressurized water reactor to an average burn-up of 59.1 MWd/(kg HM) was used for the experiment. The rod was cut into 20 mm long segment. The segment was drilled with a core drill to separate the centre of the pellet from its radial periphery, in order to single out the rim-structure containing outer part of the fuel, see Fig 2.

The rim containing part was detached from the Zircaloy cladding. The thickness of the rim-containing part resulting from the drilling was 725 µm, while the thickness of the rim-structure was approximately 75-100 µm. The de-cladded fuel fragments (~millimeter-sized) were stored under dry N_2 atmosphere during one year before the start of the corrosion experiment. Of those fragments, 20 pieces, with a total mass of 0.26 gram, were selected for the corrosion study. The surface to volume ratio at the experiment start was approximately 0.2 m^{-1}.
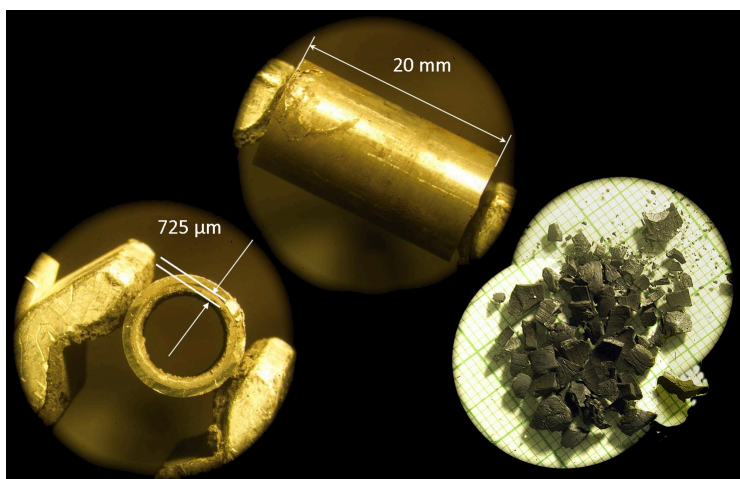
Figure 2:   *The cut segment (upper part), the core drilled fuel (left) and the obtained rim structure containing fuel fragments on a millimeter paper (right).*

Some fuel fragments were used for total dissolution with subsequent ICP-MS analysis to determine the content of actinides, lanthanides and lighter fission products. The U, Pu and Cs vectors together with the ^{148}Nd and the in-pile history were used as input into the ORIGEN code calculation to obtain the complete fuel inventory. After some iteration it could be settled that the average burn-up for this fuel fraction, of the outer 750µm of the 16N03 fuel pin, was 67 MWd/kg HM.

Corrosion experiment

The experiment was carried out in a simplified groundwater consisting of 10 mM NaCl (suprapur, Merck) and 2 mM $NaHCO_3$ (suprapur, Merck) dissolved in ultra pure Milli-Q H_2O (>18 MΩ/m, UHQ ELGASTAR). The pH of the initial solution, 8.1, was measured with a combined KCl pH-electrode (WTW SenTic Mic, and WTW pH340/ION analysator). Gas was supplied to the autoclave in welded tubes from a gas bottle.

At the start of the experiment the fuel fragments were placed into the fuel holder which was then loaded into the autoclave. The autoclave was closed and tightened. The volume in the autoclave was purged for 15 minutes with H_2 gas to removed oxygen. The autoclave was pressurized to 20 bar H_2 and 15 consecutive batches of 38 cm^3 leachant were transferred to the autoclave until it contained 520 cm^3 leachant. Subsequent to the filling the autoclave was pressurized to 4.1 MPa H_2 gas. The experiment was run under 4.1 MPa pure H_2 gas (grade 6.0, Linde GmbH) corresponding to 33 mM dissolved H_2.

Sampling

Leachates were sampled 10 times throughout the corrosion experiment; during filling (5 hours after wetting the fuel), and after 1, 7, 62, 63, 138, 265, 313, 316 and 319 days. The sampling sequence consisted of one rinse and two samples. The rinse served to collect all old, stagnant solution in the tubes leading from the reactor autoclave to the sampling outlet. The stagnant volume was estimated to ~5 cm^3, the volumes of the rinse samples ranged from 10 to 20 cm^3. The two (~10 cm^3) samples, taken after the rinse, were both considered as representative for the autoclave solution.

ICP-MS and γ-spectrometry analysis

Inductively coupled plasma mass spectrometry, ICP-MS (Thermo Element2, Thermo Electron Corporation, Germany), measurements were made on all samples to determine the concentration of the elements shown in Table 1.

Table 1: *Elements analysed by ICP-MS.*

	Elements
Natural elements	Ti, V, Cr, Mn, Fe, Ni, Cu, Zn, Mo
Fission products	Rb, Sr, Zr, Mo, Tc, Ru, Ag, Cd, Sn, Te, Cs, Ba
Lanthanides	La, Ce, Pr, Nd, Sm, Eu, Gd, Tb, Dy
Actinides	U, Np, Pu, Am, Cm

All samples were analysed in duplicates, one with and one without internal standard addition. The elements Sc, Co, In and Ho, and the isotope ^{236}U were used as internal standards. All samples were acidified to 1 M HNO$_3$. At the start of each measurement, a multi-element calibration was made using certified standards (Agilent Life Sciences/Chemical Analysis GmbH, Germany). Calibration standards with the concentrations 0, 50, 200, 1000, 5000 and 20000 ppt were prepared. Two quality-check (QC) solutions, each containing 0.5 ppb of one of the multi-element standards plus 1 ppb of the internal standard, were run to examine the ICP-MS performance. The limit of detection for actinides was approximately $1.0 \cdot 10^{-12}$ M whereas the transition elements and lanthanides had a limit of detection of $1.0 \cdot 10^{-11}$ M. The fission Mo, originating from the fission of ^{235}U and ^{239}Pu, could be distinguished from the natural Mo through the difference in isotopic abundance/cumulative fission yield profiles.

The concentration of the γ-emitters in the leachates were measured using γ-spectrometry. Measurements of leachates and backgrounds were made using a high-purity Ge-detector in 2π-geometry (EG&G Ortec Inc., USA). The detector was energy and efficiency calibrated using a certified mixed nuclide γ-source (PD954, AEA Technology QSA GmbH, Germany). The reference date was 28 February 2007.

Results

The main concern of these results, in relevance to the ReCosy project, are the behavior of redox sensitive actinides (U and Pu), fission product (^{137}Cs, fission Mo) and natural elements (Ti, Cr, Mn, Fe, Ni, Cu and Mo) existing in the leachate in contact with the rim structure of the spent UO$_2$ fuel, during the period 0-313 days, the wash-out action during the days 313-314 and the sampling after this on day 319. The pH is in the range of 7.2-8.5 and the temperature 23±4 °C.

The wash-out action was carried out to lower the Cs concentration in the leachate. Before it was started the H$_2$ gas bottle was exchanged for a bottle containing H$_2$/0.03 vol.% CO$_2$ to minimise the loss of carbonates during purging of the leachant. The wash-out action consisted of seven stepwise dilutions of the stagnant 140 cm^3 leachate, which always remains below the dip tube (used to siphon out the leachate) in the autoclave after emptying. Batches of 216 cm^3 leachant were added to, and subsequently removed from, the autoclave giving a theoretical dilution in each step of 3.2. A break for the night was made before emptying the fourth refill leachate. Each refill cycle lasted 40 minutes; however, most of this time was spent on sparging the refill leachant to remove dissolved O$_2$ before transfer to the experiment autoclave. The actual residence time in the experiment autoclave between solution transfer and draining was less than 5 minutes. After the wash-out, the autoclave was refilled and left with 500 cm^3 leachant.

^{238}U and ^{137}Cs

The measured concentrations of ^{238}U and ^{137}Cs are plotted as a function of corrosion time in Fig. 1. The concentration changes of ^{137}Cs are taken as the reference for UO$_2$ corrosion. The figure can be divided into three regions representing a change of the conditions in the autoclave.
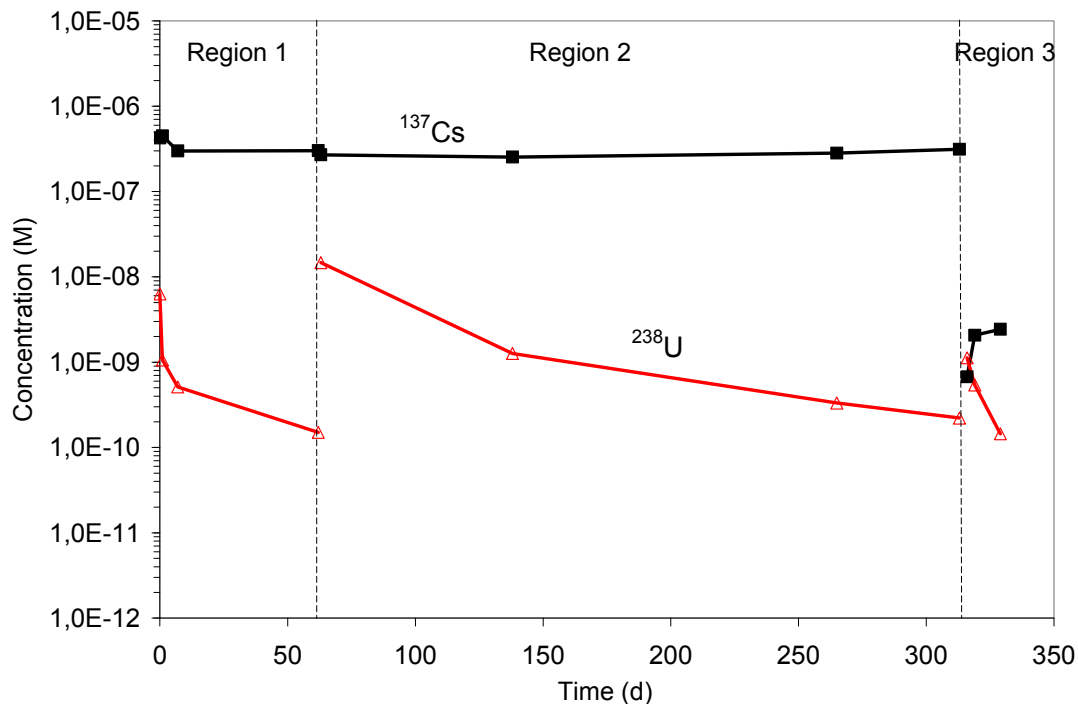
Figure 1:   *Concentration of ^{238}U (Δ) and ^{137}Cs ($\blacksquare$) as a function of corrosion time in autoclave.*

The first region shows the initial 62 days of the experiment, including the start-up. A decreasing ^{238}U concentration is seen in the leachate throughout this region. The second region starts with addition of new HCO_3^- rich leachant into the autoclave on day 63 and ends before the wash-out action on day 313. This region is characterized by decreasing ^{238}U concentration and a stable concentration of ^{137}Cs. The third region corresponds to the wash-out action during the days 313-319 (performed as described above).

Region 1 shows a fast instant release of ^{137}Cs from the fuel fragments and results in an instantaneous ^{137}Cs concentration of $9.7 \cdot 10^{-7}$ M in the first leachate. The subsequent leachates contain lower Cs concentrations as a result of additional filling of the autoclave. The amount of dissolved ^{137}Cs remains constant at a level of $3.75 \cdot 10^{-7}$ mol during the time period 7-62 days. On the other hand, the concentration of ^{238}U in the leachate decreases by a factor of 40, from $6.3 \cdot 10^{-9}$ M to $1.5 \cdot 10^{-10}$ M, during the initial 62 days.

The sharp increase in the ^{238}U concentration observed at the beginning of region 2 is a response to oxidation of the fuel surface. This can be deduced from the increased amount of dissolved Cs in the leachate, not possible to see in the figure, but observable when recalculated to total amount of dissolved ^{137}Cs. Oxygen must have intruded into the autoclave during the refill of the autoclave, with 37 ml of a solution containing 10 mM NaCl + 30 mM HCO_3^- leachant. The apparent lowering in ^{137}Cs concentration between region 1 and 2 is a result of the dilution caused by the solution transfer. After the initial increase and within the uncertainties of the measurements, the amount of ^{137}Cs released stays constant for the remaining part of region 2. The ^{238}U concentration

decreases throughout region 2. It can be noted that it takes 250 days to get back to a concentration of $2 \cdot 10^{-10}$ M.

Region 3 describes the wash-out action (day 313-319) and ends with a ^{238}U concentration of $1.5 \cdot 10^{-9}$ M in the first leachate, a similar concentration as the last leachate collected before the wash-out action ($2.5 \cdot 10^{-9}$ M).

The concentration of Cs was lowered by three orders of magnitude during the wash-out action; but, as can be seen for the last sampling started to increases towards a new stable concentration at $2.4 \cdot 10^{-9}$ M, an increase by a factor of 4 compared to lowest value.

^{239}Pu

The concentration of the redox sensitive element ^{239}Pu, with ^{238}U as reference, is shown as a function of corrosion time in Figure 2. Owing to the dissolution of the pre-oxidized surface layer, the ^{239}Pu concentration shows a correlated increase with the ^{238}U in the beginning of the experiment. The first sampling shows the expected Pu/U ratio of 0.015.
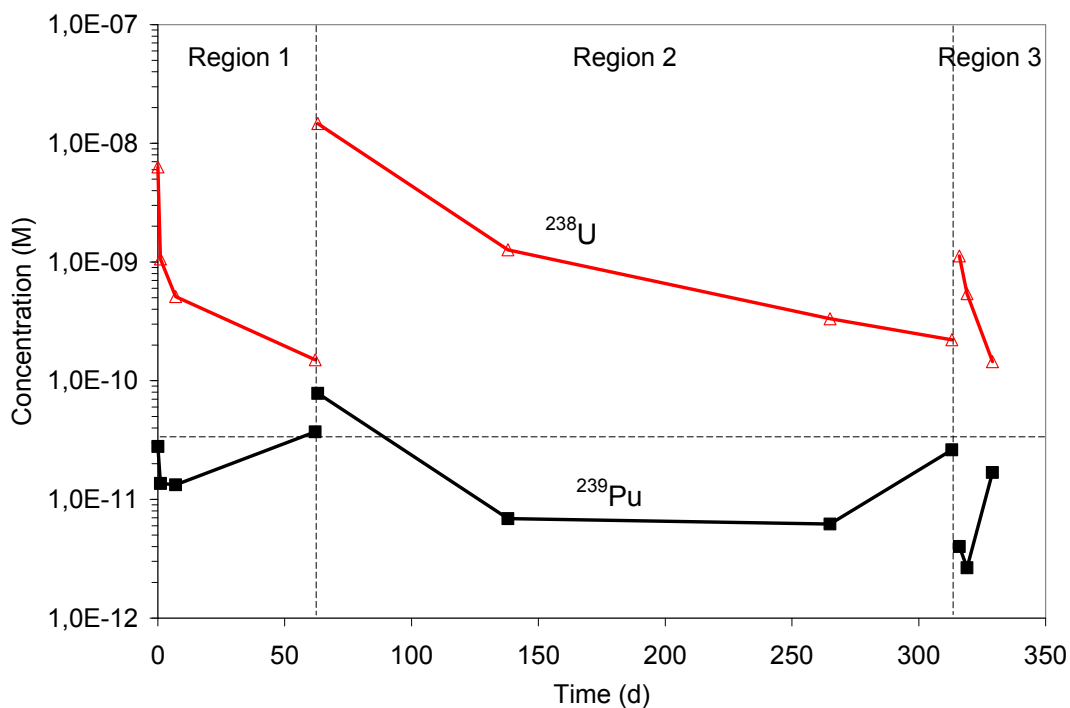
Figure 2:   *Concentration of ^{238}U (Δ) and ^{239}Pu ($\blacksquare$) as a function of corrosion time in autoclave.*

After this initial increase both ^{238}U and ^{239}Pu decreases, only at the last sampling in this region ^{239}Pu increase, a behaviour that is repeated also in region 2 and 3. Between region 1 and 2 (day 63) the autoclave refill causes oxidation and dissolution of already reduced U but also fresh fuel is oxidised as can be seen on the stepwise increase of ^{238}U, ^{239}Pu and ^{137}Cs (Figure 1).

In region 2 the almost parallel decrease in ^{239}Pu and ^{238}U concentrations, indicate that ^{239}Pu is very probably co-reduced with the ^{238}U. During this co-reduction part of the

experiment, the ^{239}Pu concentration passes through a minimum and then starts to increase towards a concentration of $\sim 3 \cdot 10^{-11}$ M.

This concentration is reached at the end of both region 1 and 2 and is marked in Figure 2 as a horizontal dashed line. In region 3, this increase in Pu concentration is especially apparent as it starts very low (due to the preceding wash-out action) is lowered even further in the first sample (due to co-precipitation), to thereafter increase towards $1 \cdot 10^{-11}$ M at the end of the region. The Pu/U ratio at the end of each region is in the range between 0.24 and 0.50, i.e., far from the Pu/U ratio in the fuel of 0.015.

The behaviour of U and Pu is well correlated in the first part of each region, see Fig. 2. However, at the end of the regions, the Pu concentration increases while U reaches a steady-state. This is not expected to occur in a system, where a solid solution is created by slow precipitation of dissolved species from the aqueous phase, since equilibrium is expected to be formed between the phases. The low U concentration at $1.5 \cdot 10^{-10}$ M shows that reducing conditions prevail in the system. The increase in Pu concentration can, therefore, not be explained by a fuel surface oxidation. However, it is possible that a further reduction of the Pu(IV) to Pu(III) occurs on the surface. Such a reduction of Pu takes place if the E_h is below -300 mV (SHE) [Vitorge 2002]. This would lead to an increased solution concentration of Pu due to the higher solubility of Pu(III) oxide [Felmy 1989] as compared to Pu(IV) oxide [Neck 2007] and is tentatively proposed as a possible explanation. The reasoning made above can possibly be resolved by observing the behaviour of the natural redox-sensitive element iron (see section *Fe, Mn and Mo*).

Fe, Mn and Mo

The natural redox sensitive elements, such as Fe, Mn and Mo, originating from the inner surfaces of the autoclave is of interest to study since they contribute to the understanding of the redox processes inside the autoclave. The concentration of natural redox sensitive elements and ^{239}Pu as reference is given in Figure 3.

The correlation between the elements Fe, Mn and ^{239}Pu is relatively strong. At the occasion of leachate refilling (day 63) the ^{239}Pu concentration increases due to dissolution of re-precipitated ^{239}Pu and fresh fuel while the concentration of Fe and Mn decreases, as expected due to dilution. No correlation was found between natural Mo and ^{239}Pu, the changes that occur are related to the dilution of the leachate during refill of the autoclave. The general conclusion is that the redox processes occurring in the autoclave affects all redox-sensitive elements.

With the reference an identical setup, run under the same conditions but with ^{233}U-doped UO_2 [Carbol 2009], in which a redox potential of -300 to -350 mV of the leachate was measured, it is possible to make a coarse speciation (using HYDRA/MEDUSA). The calculations show that under the specified conditions; Mo will mainly exist as $MoO_2(s)$ in equilibrium with MoO_4^{2-}, while Mn will exist as Mn^{2+} and $MnCO_3$ and is not solubility limited within the measured Mn concentration range. Applying the same methodology it can shown that the iron in the system can exist as Fe^{2+} in equilibrium with $Fe(OH)_{2.7}Cl_{0.3}(s)$.
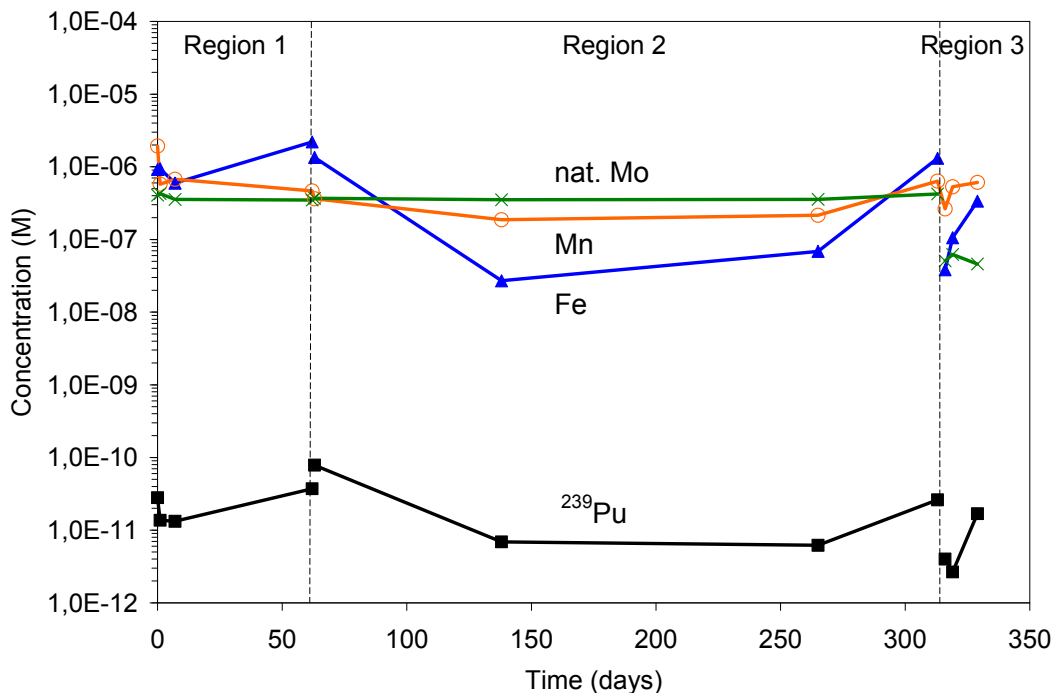
Figure 3: *Concentrations of the natural elements Fe (Δ), Mn (○), and Mo (x) together with* ^{239}*Pu (■) as determined in the leachate.*

Coming back to the discussion on the reduction of Pu(IV) to Pu(III). An interesting observation is that at the end of each in each region (1-3) when the U concentration decreases to a minimum of $1.5 \cdot 10^{-10}$ M then Pu starts to repeatedly increase, from its minimum concentration of $3-6 \cdot 10^{-12}$ M, to $\sim 3 \cdot 10^{-11}$ M. The Pu-concentration increase is almost one-order of magnitude and it is interesting to observe that the corresponding concentration values for Fe also increases by one-order of magnitude. A plausible explanation is given above (see section ^{239}*Pu*) suggesting highly reducing condition (-300 mV SHE) at the UO_2 surface which could lead to reduction of co-precipitated Fe(III) oxides/hydroxides, formed during oxygen intrusion into the autoclave, to Fe(II). Since the solubility of Fe(II) is high in oxygen-free solution this would explain the increased Fe-concentration at the end of region 1-3.

Summarizing the corrosion of high burn-up structure of a UO_2 fuel shows that the iron concentration is linked to the changes of Pu, which, in its turn is correlated to the ^{238}U concentration changes. It can also be concluded that while Fe varies within a relatively small concentration range (factor of two) the changes related to ^{238}U are more significant, more in the range of two orders of magnitude (see intrusion of O_2 at day 63 in Fig. 1). On the other hand, the number of oxidised moles of Fe is much larger (two orders of magnitude) than the moles of U.

Results of the wash-out action

From Figure 4 it is seen that an oxidation and dissolution occurred during the first day (samples 2-4). The fuel oxidation occurred due to air intrusion into the gas line when

the gas bottle was changed from H_2 to $H_2/0.03$ vol.% CO_2 (as described above). The oxidation of the fuel surface caused an increase in the concentration of the redox sensitive elements ^{238}U and ^{239}Pu. Oxidation of U appears to be strongly favoured in samples 1-4. This is verified in the third and fourth samples, which show a Pu/U ratio lower than the average fuel inventory.

It can be speculated if U is the only element which is oxidized in the system while Pu is probably released to the solution when the surrounding U atoms are dissolved. The each wash, i.e., close to the expected dilution. This indicates that the oxidation concentration of redox-insensitive Cs in the samples 2-7 is lowered by a factor of 3.1 in seen in the first dilutions occurred on the precipitated U-phase. Nevertheless, due to the large amount of Cs in the first leachates a minor Cs release from pristine fuel could potentially have occurred without being detectable.
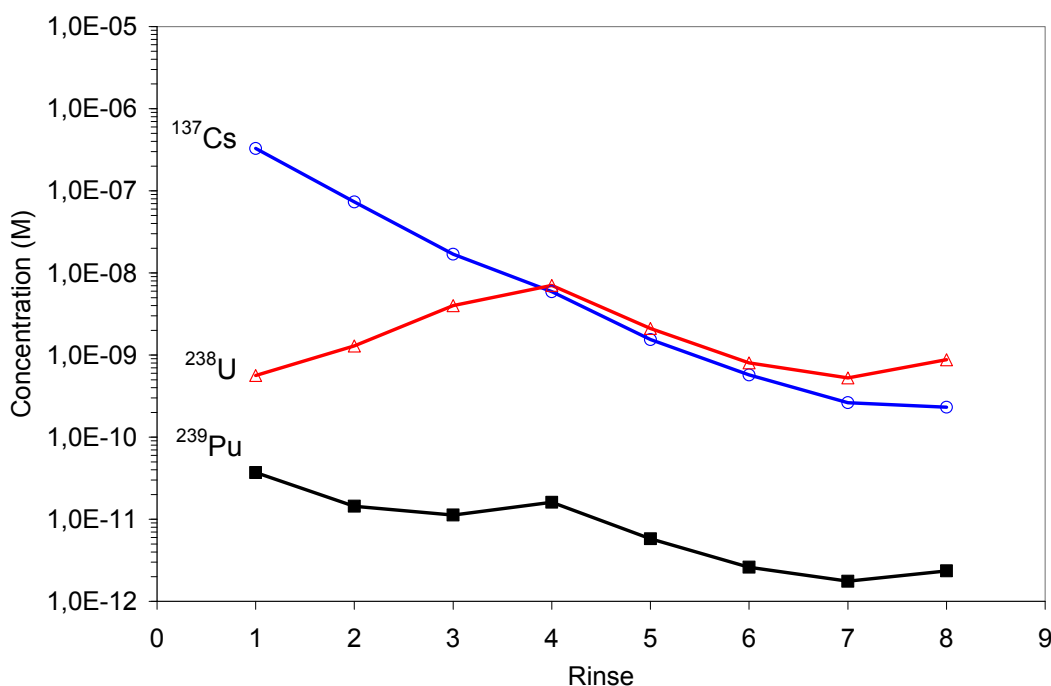
Figure 4: *Concentration of ^{137}Cs (○), ^{238}U (Δ) and ^{239}Pu (■) during the wash-out action.*

A comparison of the natural elements Fe, Mn and fission Mo with the ^{238}U and the ^{239}Pu wash-out profiles shows (Figure 5) that these elements mainly behave as ^{239}Pu. Manganese varies only slightly during the leachant changes (a factor of three) indicating an internal Mn source somewhere inside the autoclave setup. The iron profile decreases two orders of magnitude during the four first leachant almost a factor of 3 as expected from the dilution. After this initial decrease of Fe it fluctuates around a concentration of $3 \cdot 10^{-7}$ M. The Fe-profile does neither resemble the one U nor Pu. On the contrary, the fission Mo profile (rinses 1-8) imitates strongly the Pu-profile. This indicates an oxidation and dissolution of small amounts of virgin fuel leading to a congruent release of fission Mo and Pu.
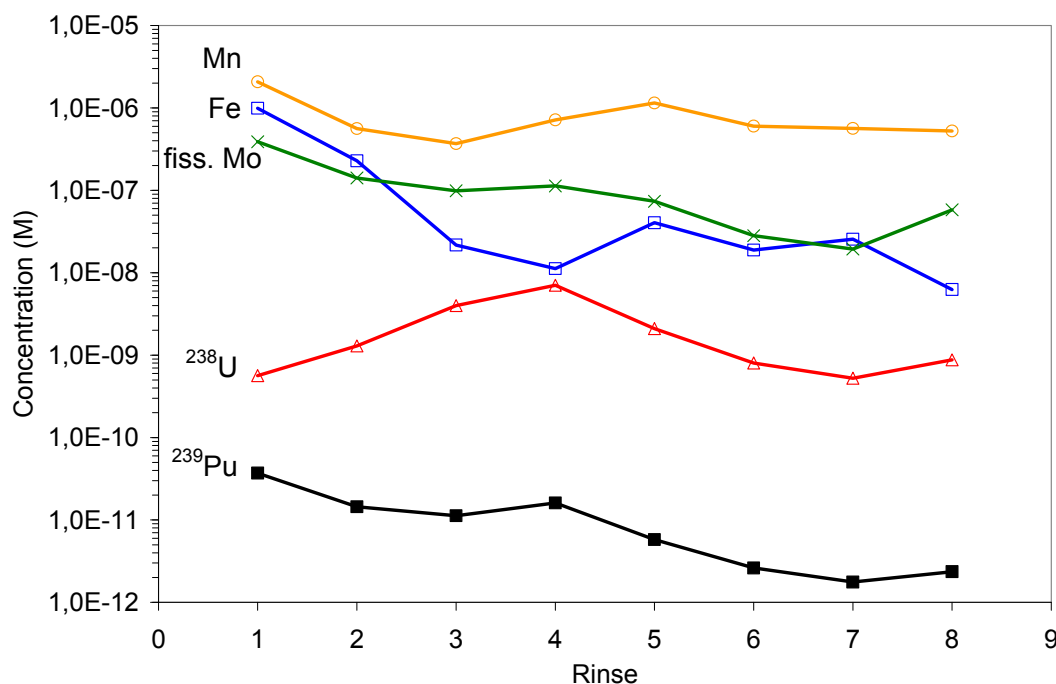
Figure 5:   *Concentration changes of Fe (□), Mn (○), fission Mo (x) and ^{238}U (Δ) in comparison to ^{239}Pu (■) during the wash-out action.*

Conclusions

Despite the fact that 0.23 mol of atmospheric O_2 intruded the autoclave on day 63 [Fors 2009] and additional O_2 was produced in the autoclave during the period of 0-311 days, as a result of α-radiolysis of water, low steady state concentration levels were reached for U and Pu of $1.5 \cdot 10^{-10}$ M and $3 \cdot 10^{-11}$ M, respectively. The release of Cs almost stopped which indicate an almost insignificant corrosion of grain boundaries and the UO_2 matrix (which contains 97 wt.% of the total Cs [Johnson 1997], [Walker 2009]). The results confirms that 33 mM dissolved H_2 inhibits radiolytically induced UO_2 corrosion in the studied UO_2-H_2-H_2O system and that the high burn-up structure in the 59.1 GWd/tHM fuel did not enhance fuel dissolution.

The redox-sensitive natural elements; Fe, Mn, Mo behave more similarly to Pu than U. For the first time, to the knowledge of the authors, the variation of redox sensitive natural elements, present in the leachate as contaminants from the autoclave setup, are studied in order to confirm the redox state of redox sensitive actinides and fission products. Knowledge of the concentration of natural redox sensitive elements makes it possible to make mass balance calculations of reducing and oxidising species during the corrosion experiment. Additionally, the co-variation of redox sensitive natural elements with redox elements originating from the fuel will be used to determine the redox potential in the bulk leachate which is coupled to the oxidative-dissolution process at the UO_2-H_2O interface. The understanding of the redox processes occurring at the UO_2-H_2O interface are crucial for the understanding of the spent fuel corrosion and are

directly applicable to the conceptual model of the spent fuel corrosion used in safety assessments.

Acknowledgement

References

G. Buckau, B. Kiensler, L. Duro, M. Grivé, V. Montoya (2009): Euratom EC 7th Framework program "Collaborative project "Redox phenomena controlling systems", 1st annual workshop proceedings. Institut für Nukleare Entsorgung, Forschungzentrum Karlsruhe, Germany, Report FZKA 7466 (2009).

P. Fors, P. Carbol, S. Van Winckel, K. Spahiu (2009): Corrosion of high burn-up structured UO_2 fuel in presence of dissolved H_2. J. Nucl. Mater. 394 (2009) 1-8.

P. Carbol, P. Fors, T. Gouder, K. Spahiu (2009): Hydrogen suppresses UO_2 corrosion. Geochim. et Cosmochim. Acta 73 (2009) 4366-4375.

B. Bonin, M. Colin, A. Dutfoy. Pressure building during the early stages of gas production in a radioactive waste repository. J. Nucl. Mater. 281 (2000) 1-14.

L.H. Johnson, J.C. Tait. Release of segregated nuclides from spent fuel. SKB technical report TR-97-18, Swedish Nuclear Fuel and Waste Management Co., Stockholm, Sweden.

C. T. Walker, S. Bremier, S. Portier, R. Hasnaoui, W. Goll. SIMS analysis of an UO_2 fuel irradiated at low temperature to 65 MWd/kgHM. J. Nucl. Mater. 393 (2009) 212-223.

P. Vitorge, H. Capdevila, S. Maillard, M.-H. Faure, T. Vercouter, J. Nucl. Sci. Technol. Suppl. 3 (2002) 713–716.

A. Felmy, D. Rai, J. Schramke, J. Ryan, Radiochim. Acta 48 (1989) 29–35.

V. Neck, M. Altmaier, T. Fanghänel, J. Alloy. Compd. 444–445 (2007) 464–469.

ADDITIONAL CONTRIBUTIONS

List of additional contributions

INTERCOMPARISON EXERCISE FOR THE DETERMINATION OF REDOX STATE OF DESIGNED AND NATURAL SYSTEMS

Marcus Altmaier[*] and Gunnar Buckau

Institut für Nukleare Entsorgung, KIT, Campus North,

Herrmann-von-Helmholtz-Platz 1, 76344 Eggenstein-Leopoldshafen, DE

* Corresponding author: Marcus.Altmaier@kit.edu

Abstract

Determination of the redox state of designed and natural systems is required at different points within the nuclear waste disposal Safety Case. The correct determination of the redox conditions is needed for site characterization and real system analysis/natural analogues/chemical homologues associated with site data, determination of basic thermodynamic data from designed solutions to near-natural conditions in the lab, as well as description of response to changes in conditions at the candidate site as part of the Safety Analysis long-term predictions. The theoretical basis for the redox conditions and processes has been established. Contrary to this, practical determination of the redox state of different types of systems is associated with great uncertainties. In response to this practical limitations and uncertainties, an Intercomparison Exercise (ICE) was conducted. The ICE is implemented as part of the activities within the EURATOM FP7 Collaborative Project "Redox Phenomena Controlling Systems" (CP ReCosy). The ICE was held 16-20 November 2009, in Karlsruhe, hosted by KIT-INE.

The aim of the ICE was to compare different methods and handling protocols, making use of a series of different samples. The preliminary outcome verifies the overall concerns, namely that the redox conditions reported from different groups by different methods vary widely. Various preliminary conclusions were drawn already during the ICE. The full report is still under preparation, and thus final conclusions are not yet available and future actions still need to be decided. It is expected that the detailed evaluation will lead to a more homogeneous picture than the picture given by the present very preliminary evaluation.

Objectives of the Intercomparison Exercise (ICE)

The objectives of the Intercomparison Exercise (ICE) is to compare different redox determination methods in order to (i) identify critical redox determination issues, (ii) provide the basis for more confidence in redox determinations for the individual groups, and (iii) identify future activities that could contribute to further progress in determination of the redox state of nuclear waste disposal Safety Case relevant systems and conditions. ICE is a key element in ReCosy, tackling the central question of how the redox state can be determined, what different redox determination methods register and if differences in the protocols between different groups/organizations is the reason for considerable differences in results reported by different groups.

It should be noted that, contrary to some intercomparison exercises, that it is not a prime objective to provide the best estimates for the redox state of the samples used. It is also not the objective to provide a recommended protocol for redox determination.

Key features

The key features of the ICE are:

i   A large number of organizations get together at one place and measure the redox state on a limited number of samples under well defined conditions avoiding transportation of redox sensitive samples whenever possible. The conditions include that storing the samples and conducting the investigations/measurements was done in inert gas boxes.

ii Three different principle approaches were used, namely electrochemical measurements, thermodynamic evaluation of chemical and physico-chemical data, and optodes.

iii The reference and (near-) natural samples are prepared and stored under inert-gas. Two natural samples have been conditioned since more than 15 years, in sealed vessels under inert gas in a fridge. The microbial samples were prepared by MICANS, sent to the host, and stored and treated under inert gas.

iii Where organizations have immobile equipment, samples were sent to them by the host.

iv The outcome is documented in a report, communicated, disseminated and brought forward for future development.

Samples

Reflecting different purposes, the samples can be divided into the following three types/groups:

1. Well defined reference systems expected to have very stable redox conditions. They are of major importance for evaluating the different techniques and handling protocols and assessing the correctness of the redox reading. They also cover different pH conditions and include:

    • Fe-system at low ionic strength.

    • Fe-system at high salinity/brine conditions.

    • System with "simple" organics (e.g. Hydroquinone).

    • System under hyperalkaline conditions.

2. A set of near-natural groundwater samples with varying redox stability. Samples include:

    • Groundwater with humic substances (Gorleben, Germany).

    • Clay-rock system (COX, France).

    • Granitic groundwater (Grimsel, Switzerland).

    • High salinity brines (Asse and Gorleben, Germany).

3. Homogenous systems with microbiological activity

The samples under points 1 and 2 were prepared at the hosting organization with help from ReCosy partners and made available for ICE participants. As mentioned above, the microbial samples were prepared by MICANS, and sent to KIT-INE.

A list of the different samples is given in Appendix I. The analytical data are not yet available (in progress).

Participation

There were 19 organizations participating in the exercise. Out of these organizations, 15 participated on-site by direct measurements on the samples during the exercise. One of the organizations taking part in the on-site exercise, also had sampled transferred to their own institute for measurements (ITU). Three organizations (ARMINES, CTH and IPL) did not take part in the on-site exercise, but had samples sent to them for analysis in their home-institutions. One organization contributed by preparing and sending the microbial samples. An overview of the participation is shown in Appendix II.

Each contribution is summarized by a "summary outcome report". These reports are found at the project WEB space. Studies where the summary outcome report is still pending are shown by fields marked in light red in the table in Appendix II.

Preliminary on-site assessment

The outcome of the ICE cannot be finally assessed until the different results and reports have been obtained, brought together and evaluated by the participants of ICE. The different results, including timely evolvement of the reading signals, are still being gathered. The final report is about to be established. For this purpose, the complete set of data from the different samples and groups are being gathered.

At the end of the ICE, the complete data sets were not available. Nevertheless, a preliminary assessment on few selected samples was done on the last day of the ICE. The assessment documented merely the "final outcome" of individual measurements but not the time function of approaching this reported value. The outcome of this preliminary assessment is given in Table 1 (at the end of the paper). Several observations can be made from only this preliminary assessment, including:

- Different groups are reporting party very different values, verifying the basis for the exercise, namely that reported values will need to be taken with care,

- Values determined with standard combined Pt electrodes, might fall outside a general range of values by other methods and longer contact times,

- There are considerable differences between values in redox determining suspensions, and in the supernatant,

- Stirring of the samples leads to different readings that not stirring.

Outcome of the general discussion

The outcome of the ICE cannot be finally assessed until the different results and reports have been obtained and brought together. Nevertheless, a general discussion was held on the last day of the ICE. For this purpose two questions were formulated. These were:

a. Do you feel confident that you can determine the redox state of a system correctly?

b. Can we identify preliminary conclusions on any topics?

With respect to the first question, there was general agreement that the redox state can be determined, however, with a very low level of confidence.

With respect to the second question, there was some agreement on the following points:

i. There is a slow conversion of the surfaces of the active electrode materials, leading to the partially very long drift observed. A follow-up study should be considered analyzing this conversion of the active surfaces along with drift and equilibration.

ii. Stirring the samples prior to measurement may decrease the drift time.

iii. pH should be monitored simultaneously with the Eh.

General conclusions and outlook

The general conclusions are that the basic concerns remain with respect to determination of the redox conditions of designed and near-natural samples. Eh values are determined in different situations and for different purposes. The numbers obtained by different methods (type of electrodes, contact time, stirring/not stirring, in suspension/in supernatant, contact time, ….) vary considerably. The preliminary assessment does not allow for conclusions concerning the reasons for these strongly varying values. Consequently, the confidence in these numbers is very low.

Based on these findings it becomes clear that additional efforts will be required in order to resolve this topic. The outcome and final evaluation and assessment of the ICE will be published as a KIT report. This report will be important for communicating the overall issue and design future activities.

Acknowledgement

Table 1: *On-site preliminary assessment of the individual redox determinations by the used of different electrodes. The very diverse results from this preliminary on-site assessment at the end of the InterComparison Exercise is expected to become less diverse in the more elaborate still on-going data evaluation.*

Sample (pH)	Organization/Group	Eh	Comment
Ref1Fe(a), Fe Powder, ~ 100 mg Fe-powder, pH not fixed (~9)			
pH 8.5	INE/MB	-392	Pt combination electrode, 15 minutes
	MSU	-280 ± 60	
	AMPHOS/KAIST	-250 (-370)	In Fe suspension (after cleaning the electrode)
pH 8.6 ->	PSI	-460 ± 50	In Fe suspension
	ITU/DF+CNRS/RK	-350 / -75	In suspension / suspension separated
pH 8.0 ->	BRGM	-190	After 15 minutes with Au, Pt and CG
	ITU/??	400	
Ref1(II/III)(a), FeCl$_2$, FeCl$_3$, 1:1-buffer, 10^{-4} M each, pH 5-6 fixed with MES			

pH 5.3	INE/MB	-12	Pt combination electrode, 15 minutes
	ITU/DF+CNRS/RK	42, 250	First value in suspension, second in supernatant
	PSI	360	Suspension
	INE/CW	300	
	ITU/??	365	
	AMPHOS/KAIST	300	Stable after 4 min.
pH 5.0 ->	BRGM	340	
	CNRS/MP	297, 72	Potentiometric , Amperemetric
Ref2C(b), FeCl$_2$, FeCl$_3$, 2 M CaCl$_2$, 10^{-4} M Fe(II), Fe(III)-chloride each, pH 12 fixed with Ca(OH)$_2$(s)			
pH$_c$ ≈12	INE/MB	-261	Pt combination electrode, 15 minutes
	MSU	18	As above, but stirring
(pH 10 ->)	BRGM	-85	
	ULOUGH	20	Stable after 20 min.
	AMPHOS/KAIST	85	Stable after 2 minutes
	PSI	100	
Ref3HC(a), Hydroquinone, 10^{-3} M Hydroquinone, pH 5-6 fixed with MES buffer			
	INE/MB	120	Pt combination electrode, 15 minutes
	FZD	255	
	ITU/DF+CNRS/RK	308	Pt
	ITU/DF+CNRS/RK	311	Au
	PSI	190	
Ref4MQ1, Na-dithionite, [Ca] = 1E^{-4} M; [Si] = 1E^{-2} M			
pH 9.55	INE/MB	-370	Pt combination electrode, 15 minutes
	BRGM	-512	After 10 minutes response, then stable 30 min.
	ULOUGH	-785	
	PSI	-560	
Nat1(a), Gorleben Sediment S-102 with low salinity groundwater Gohy-2227, conditioned since 03/071991			
pH 8.6	INE/MB	230	Pt combination electrode, 15 minutes
	MSU	330 ± 40	
	FZD	160	
	ULOUGH	-148	After 24 h (strong drift in beginning)
	INE/CW	210	
	PSI	190	Stable after 15 min stirring
	INE/FH	163	Pt, 16 h
	INE/FH	130	Au, 16 h
	INE/FH	170	CG, 16 h

	AMPHOS/KAIST	28	Very stable from beginning to over 1 h
Nat2, Crushed COX Material equilibrated with artificial COX pore water (Prepared at KIT-INE)			
pH 7.87	INE/MB	120	Pt combination electrode, 15 minutes
	INE/CW	270	
pH 8.38	ULOUGH	81	10 h until stable
	FZD	240	
	AMPHOS/KAIST	100	Strong variations
	PSI	250	Stable after 10 min stirring
	BRGM	260	Stable after 2 h, remains stable 24 h
Nat3, Crushed Grimsel material equilibrated with artificial Grimsel water (Prepared at KIT-INE)			
	INE/MB	224	Pt combination electrode, 15 minutes
	ITU/DF+CNRS/RK	70	Pt
	ITU/DF+CNRS/RK	296	Au
	FZD	156	
	INE/CW	230	
	ULOUGH	12	2 hours contact time
	INE/FH	298	Pt, 17 h, still drifting
	INE/FH	187	Au, 17 h, still drifting
	INE/FH	160	CG, 17 h, still drifting
	PSI	260, 140	Parallel samples, 15 min stirring
	AMPHOS/KAIST	-30	1 h
Nat4, Magnesium rich high salinity brine, (IP21 Solution), 10% dilution factor			
pH 0.5	INE/MB	408	Pt combination electrode, 15 minutes
	ULOUGH	490	Stable for 20 min.
pH$_c$ 3.0	INE/CW	640	
	GRS/BB	677 (760)	In brackets, corrected for salinity
	GRS/TS	680	Fe-analytics
	FZD	635	After 45 min., still drifting
	PSI	580	
	AMPHOS/KAIST	660	

THERMOCHIMIE, THE ANDRA THERMODYNAMIC DATABASE

Lara Duro[1], Mireia Grivé[1] and Eric Giffaut[2]

[1]Amphos 21

P. de Garcia I Faria 49-51, 1-1, E-08019 Barcelona, Spain

[2]ANDRA

1/7 rue Jean Monnet - 92298 Chatenay Malabry cedex – France

* Corresponding author: Lara.duro@amphos21.com

Abstract

ThermoChimie is the thermodynamic data base initially created by ANDRA in 1996, especially designed and qualified for systems of interest for the repository concept designed by ANDRA. This database is supported by an experimental program on actinides and fission products and also on major components of the systems of interest, and it has been continuously updated since its creation to undertake geochemical calculations related to the performance assessment of different backfill/buffer materials and/or geological formations. ThermoChimie contains data on major elements, a long list of radioelements, such as actinides and lanthanides, chemotoxic metals and organic and inorganic ligands.

In this paper, the main characteristics of ThermoChimie are presented and a brief summary of the methodology followed for its main development is described.

Introduction

Thermodynamic databases are a substantial part of the models and submodels used in the Performance Assessment of Nuclear Waste repositories. They are mainly used in assessing the geochemical evolution of the repository both in terms of performance of the engineering barrier system as well as the migration/retention behaviour of radionuclides.

ThermoChimie is the thermodynamic data base initially created by ANDRA in 1996, especially designed and qualified for systems of interest for repository concept designed by ANDRA. It is supported by an experimental program on actinides and fission

products and it has been continuously updated to undertake geochemical calculations related to the performance assessment of different backfill/buffer materials and/or geological formations.

ThermoChimie contains data on major elements, a long list of radioelements, such as actinides and lanthanides, and chemotoxic metals.

The ThermoChimie project especially deals with six tasks, in consistency with PA requirements and with specific conditions in the Callovo-Oxfordian formation or inside the disposal cells:

- Determination of radioelement and chemotoxic element aqueous speciation and solubility,

- Study of geochemical evolution of both the near- and the far-field of the repository, covering the stability of the constituents of clay minerals and bentonite clays, and secondary minerals of the aluminosilicate systems

- Assessment of the process of cement degradation to account for the stability of cementitious phases and considering a broad composition range with respect to formula,

- Assessment of the process of canister corrosion;

- Assessment of the role of ligands derived from the degradation of Natural Organic Matter (NOM) present in the Callovian-Oxfordian argillite >(about 1% mass) as well as the impact of its degradation simple organic ligands on the mobilization of radionuclides

- Tools and applications of the thermochemical database under different storage scenarios

Prior to the development of Thermochimie it was important to define the range of validity of the database. On the basis of the conditions of interest of ANDRA, the range of main geochemical variables affecting the behaviour of the radioelements of interest was defined as:

- pH range of 5 to 14, i.e, from mildly acidic to hyperalkaline systems

- Eh range of water stability

- T range of 15° to 90°C, i.e., in the low geochemical temperature range

- Ionic strength up to 3 mol/kg

It is important to highlight that the selection of the data must consider both, temperature and ionic strength corrections. On the basis of data availability and range of conditions, it was decided to follow i) for temperature corrections assume temperature independent enthalpy (Van't Hoff equation), unless data on Cp was available and ii) for ionic strength corrections the Specific Interaction Theory (SIT) when possible.

History of the development of ThermoChimie

The development of ThermoChimie has been achieved in four different stages:

- 1995-1999: Data acquisition period through experimental programs and reviews. Production of version s 1 to 3 of ThermoChimie. Introduction of thermodynamic data for radionuclides but not consistency checks implemented. Selection of SUPCRT as basic source of data for major element systems.

- 2000-2002: Version 4 of ThermoChimie, development of consistent database and ORACLE application on the ANDRA intranet.

- 2003-2005: Version 5 of ThermoChimie, basis of the calculations presented in the Dossier 2005 document. It constituted a consistent database, submitted to external expert review.

- 2006-2010: Versions 6 and 7 of ThermoChimie, submitted to external expert review.

Experimental data acquisition is continuous through different specific research projects and Ph.D developments.

Since 2000, data for the elements shown in Figure 1 have been reviewed in ThermoChimie.

Figure 1. *Periodic table showing the elements for which themodynamic data have been reviewed and introduced in ThermoChimie*

Data selection procedure

Primary data in Thermochimie include:

- Equilibrium constants

- Reaction or formation Gibbs free energies, enthalpies and entropies

- Specific interaction coefficients for activity corrections

- Uncertainties in all thermodynamic parameters when possible

In general, the updating process of ThermoChimie has been focused on:

- ensuring the self-consistency of the database by checking that all thermodynamic principles are obeyed ;

- extending ThermoChimie to cover all the radionuclides and processes of interest;

- making ThermoChimie traceable by citation of the original source;

- updating the "old" values and introducing new values in the ThermoChimie ACCESS© file.

The description presented here highlights the selection process for equilibrium constants and enthalpy data, although the process also applies to all parameters included in the TermoChimie database.

The main sources of thermodynamic data are:

- Previous Thermodynamic data compilations

- Open scientific literature

- Specific experimental programmes

- Estimations

The selection process includes a compilation of the thermodynamic data reported in previous databases such as SUPCRT92 (Johnson et al. 1992), NBS (Wagman et al., 1982), USGS Database (Robby and Hemingway, 1995) for major elements.

The main data sources for U, Np, Pu, Am, Se, Ni and Zr and auxiliary species are the OECD NEA TDB Project compilations (Grenthe et al, 1002; Lemire et al., 2001; Guillaumont et al., 2003; Brown et al., 2005; Hummel et al., 2005; Gamsjäger et al., 2005;Olin et al., 2005; Rand et al., 2009.

Data extracted from scientific literature are analysed and tested in front of independent data when possible.

In some cases, data gaps exist and good quality data are not available in previous compilations or in open literature. In this case, estimations can be conducted to solve this problem. More detailed information about some of the methodologies used for data estimation can be found in Bruno et al. (2001) and Duro et al. (2002).

Data included in ThermoChimie can be classified into three different types according to the data selection process:

1. The first selection procedure is based on thermodynamic stability, i.e., aqueous stability constants and solubility equilibria are selected as main data. In some cases these data allow the calculation of Gibbs free energy of formation of the species as far as the free energy of formation of the basic components is available. Therefore, $\log K_r^o$ and ΔG_r° are the first parameters selected and ΔG_f° are calculated accordingly.

2. The second set of data selected considers temperature effects, i.e., enthalpies and entropies. In some cases Gibbs free energies are calculated from ΔH_f° and S_f° data but this is not always possible. There are not many sources for enthalpy data in the literature and in some cases enthalpy must be calculated from Gibbs free energy and entropy data when available. The selection of ΔH_r° and ΔS_r° allows the calculation of ΔH_f° and S_f° when enthalpy and entropy data for the basic components are available.

3. The third set of data is related to ionic strength corrections. ThermoChimie primes the SIT to correct to infinite dilution and provides interaction coefficients for anion and cations in NaCl medium. Data for these coefficients are either taken from the published literature or estimated based on chemical analogies.

Figure 2 aims at showing the general procedure used in the selection or update of Thermodynamic equilibrium constants in ThermoChimie.
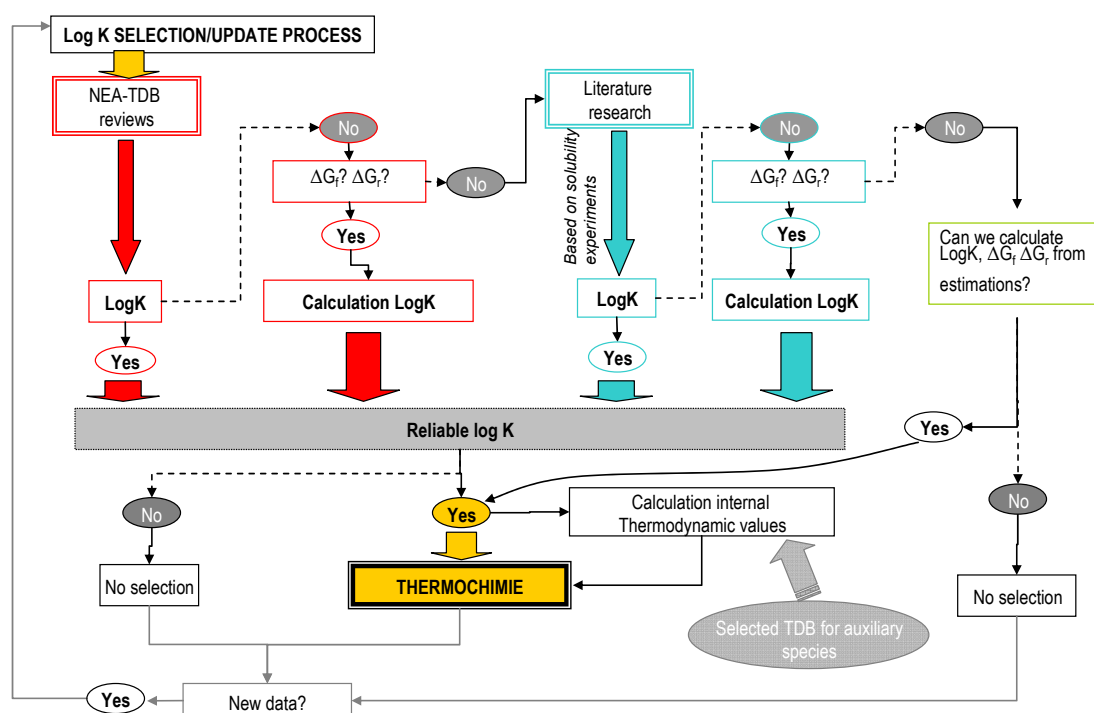
Figure 2. *Overview of the general data selection process followed in ThermoChimie for radionuclides*

Several efforts have been done in comparing ThermoChimie with other databases, such as JAEA, HATCHES, NAGRA-PSI, MINTEQ or the LLNL TDB. This has allowed identification in some cases of important gaps in data, redundancies and/or discrepant values. It is relevant to account for a non insignificant number of errors introduced in databases due to mistypos of data. This comparison with other peers may, in some cases, help in the process of error identification.

The structure of ThermoChimie

For each element in ThermoChimie a basic component is defined. Aqueous, solid and gaseous species are defined in terms of the basic components.

<u>Basic components.</u> The basic components are usually free cations or anions (for example Sr^{2+}), oxycations (for example UO_2^{2+}) or oxyanions (for example MoO_4^-) of the element of interest. They constitute the building blocks for the construction of the formation reactions of all other species in the database.

Besides, e^- and H^+ are included as building blocks.

Data included in ThermoChimie for basic components are:

ΔG_f^0, ΔH_f^0, S_f^0 at 25ºC and I = 0 and,

SIT activity coefficients ($\varepsilon_{Na+,anion}$ or $\varepsilon_{cation,Cl-}$) at 25˚C

<u>Aqueous species, solids and gases</u>. Both aqueous species and solid and gases compounds are defined in ThermoChimie by chemical reactions of the basic components. The fields to fill in ThermoChimie for all these species are:

$logK_r^0$, ΔG_f^0 and ΔG_r^0, ΔH_f^0 and ΔH_r^0 and S_f^0 and ΔS_r^0, Cp_f, Cp_r at 25ºC and I = 0

SIT activity coefficients ($\varepsilon_{Na^+,anion}$ or $\varepsilon_{cation,Cl^-}$ or $\varepsilon_{cation,ClO4^-}$) at 25˚C

All the magnitudes included in ThermoChimie have associated uncertainties, when possible, and are accompanied by a bibliographic reference of the source from where the datum has been adapted.

Uncertainty assignment

The uncertainty assignment is not straightforward. In some cases a simple error propagation approach has been followed, while in other cases the procedure is much more complex due to the fact that estimations and/or extrapolation from different conditions have been done.

As a general rule, when assigning uncertainties the following approaches have been followed:

When the data is derived from one of the NEA TDB compilations, the uncertainty is normally given

When the data is derived from other compilations, a review of the selection process and also of the original sources has been conducted

When the data is obtained from original sources, independent tests in front of data and other independent publications (when possible) has been conducted and unless very clear indications of the quality of one single publication versus the others, the uncertainty range has been selected to include all the data range in the literature

When the data is obtained from an estimation method, the uncertainty has been assigned by comparing estimations in front of available experimental data and calculating observed deviations.

For values internally calculated, error propagation calculations have been done.

The current version of ThermoChimie has been issued together with the last release of PHREEQC, with SIT application (PHREEQC 2.17.0 and PhreeqcI 2.17.0).

Consultation interface

The current consultation interface is supported by and ACCESS application in the ANDRA intranet. It will be open to public consultation in a near future. The application contains specific supporting material on the selection of each single datum, so that the selection process, including uncertainty assignment can be tracked. Original sources or references have been preferred and are included unless the datum has been selected from a general accepted review publication such as the ones originated by the NEA-TDB review team.

Conclusions and further work

ThermoChimie constitutes one of the most complete and developed thermodynamic databases with application to the modelling related with performance assessment of geological repositories of nuclear waste. The database is consistent, traceable and extensive. The process of data selection is transparent and the aim is that the database is used as extensively as possible in order to identify possible gaps and mishaps in data. The development of this database is continuous and it is supported by several experimental projects for data acquisition as well as geochemical model applications that allow the validation of the database. Further works are focused on the use of ThermoChimie for model application and continuous development.

Acknowledgements

project for contributing to the dissemination of the status of ThermoChimie among the nuclear scientific community.

References

Brown, P., Curti, E., Grambow, B. (with a collaboration from Ekberg, C.) (2005) Chemical Thermodynamics 8. Chemical Thermodynamics of Zirconium. NEA Data bank, OECD. North Holland Elsevier Science Publishers B.V., Amsterdam, Netherlands;

Bruno, J., Duro, L., Cera, E., Grivé, M., El Aamrani, F., Rovira, M. (2001b) Revision of the ThermoChimie Thermodynamic Database for radioelements. Version A. ANDRA report C.RP. 0ENQ.01.002 211 pp.

Duro, L., Cera, E. and Bruno, J. (2002) Revision of the thermodynamic database for radioelements. Version B. Final report. ANDRA report C.RP.0ENQ.02-001. 352 pp.

Fuger, J. and Oetting, F.L. (1976) The chemical thermodynamics of actinide elements and compounds: Part 2. The actinide aqueous ions, Vienna: International Atomic Energy Agency, 1976, 65p.

Gamsjäger, H., Bugajski, J., Gajda, T., Lemire, R.J. and Preis, W. (2005). Chemical Thermodynamics 6: Chemical Thermodynamics of Nickel. NEA OECD, Elsevier

Grenthe, I., Fuger, J., Konings, R.J.M., Lemire, R.J., Muller, A.B., Nguyen-Trung, C., Wanner, H. (1992): Chemical Thermodynamics 1; Chemical Thermodynamics of Uranium. NEA OECD, Elsevier;

Guillaumont, R., Fanghänel, J., Neck, V., Fuger, J., Palmer, D.A., Grenthe, I., Rand, M.H. (2003) Chemical Thermodynamics 5. Update on the Chemical Thermodynamics of Uranium, Neptunium, Plutonium, Americium and Technetium. NEA OECD, Elsevier;

Hummel, W., Anderegg, G., Rao, L., Puigdomènech, I., Tochiyama, O., (2005). Chemical Thermodynamics 9: Chemical Thermodynamics of Compounds and Complexes of U, Np, Pu, Am, Tc, Se, Ni and Zr with Selected Organic Ligands. NEA OECD. Elsevier.

Johnson, J.W., Oelkers, E.H. and Helgeson, H.C. (1992) SUPCRT92: A software package for calculating the standard molal thermodynamic properties of minerals, gases, aqueous species, and reactions from 1 to 5000 bar and 0 to 1000 ºC; Computers and Geosciences,18, pp. 899-947.

Lemire, R.J., Fuger, J., Nitsche, H., Potter, P., Rand, M.H., Rydberg, J., Spahiu, K., Sullivan, J.C., Ullman, W.J., Vitorge, P., Wanner, H. (2001) Chemical Thermodynamics 4. Chemical thermodynamics of neptunium and plutonium. NEA OECD, Elsevier;

Olin, A., Noläng, B., Osadchii, E.G., Öhman, L.O. and Rosén, E. (2005). Chemical Thermodynamics 7: Chemical Thermodynamics of Selenium. NEA OECD, Elsevier

Rand, M. H., J. Fuger, I. Grenthe, V. Neck and D. Rai.   (2009) Chemical Thermodynamics of Thorium. Chemical Thermodynamics 11. NEA OECD. Issy-les-Moulineaux, France

Wagman, D.D., Evans, W.H., Parker, V.B., Schumm, R.H., Halow, I., Bailey, S.M.,Churney, K.L. and Nuttall, R.L., (1982), The NBS tables of chemical thermodynamic properties, selected values for inorganic and c1 and c2 organic substances in SI units. J. Phys. Chem. Ref. Data, V. 11, supp. 2, 392p.Robby and Hemingway, 1995